ISSN 2542-1565

Vol. 15 2022 No. 01

GEOGRAPHY ENVIRONMENT SUSTAINABILITY

«The journal GEOGRAPHY, ENVIRONMENT, SUSTAINABILITY was founded in 2008 by Russian Geographical Society, the Lomonosov Moscow State University Geography Department, and the Russian Academy of Sciences Institute of Geography. Since that time the journal publishes **4 issues per year**, containing original research papers and reviews. The journal issues are open source and distributed through subscriptions, library exchanges of leading universities, and via the website through the world»

FOUNDERS OF THE JOURNAL: Russian Geographical Society, Faculty of Geography, Lomonosov Moscow State University and Institute of Geography of the Russian Academy of Sciences

The journal is published with financial support of the Russian Geographical Society.

The journal is registered in Federal service on supervision of observance of the legislation in sphere of mass communications and protection of a cultural heritage. The certificate of registration: ПИ № ФС77-67752, 2016, December 21.

PUBLISHER
Russian Geographical Society
Moscow, 109012 Russia
Novaya ploshchad, 10, korp. 2
Phone 8-800-700-18-45
E-mail: press@rgo.ru
www.rgo.ru/en

EDITORIAL OFFICE
Lomonosov Moscow State University
Moscow 119991 Russia
Leninskie Gory, 1,
Faculty of Geography, 1806a
Phone 7-495-9391552
Fax 7-495-9391552
E-mail: ges-journal@geogr.msu.ru
www.ges.rgo.ru

DESIGN
Layout designer: Tereshkin Anton
Moscow, 115088,
26 Simonovsky Val str., bldg. One
Phone: +7 (903) 108-04-44
E-mail: smile.tai@gmail.com

DOI prefix: 10.24057

Format A4 (210x297mm)

"GEOGRAPHY, ENVIRONMENT, SUSTAINABILITY" is the only original English-language journal in the field of geography and environmental sciences published in Russia. It is supposed to be an outlet from the Russian-speaking countries to Europe and an inlet from Europe to the Russian-speaking countries regarding environmental and Earth sciences, geography and sustainability. The main sections of the journal are the theory of geography and ecology, the theory of sustainable development, use of natural resources, natural resources assessment, global and regional changes of environment and climate, social-economical geography, ecological regional planning, sustainable regional development, applied aspects of geography and ecology, geoinformatics and ecological cartography, ecological problems of oil and gas sector, nature conservations, health and environment, and education for sustainable development.

OPEN ACCESS POLICY. "GEOGRAPHY, ENVIRONMENT, SUSTAINABILITY" is an open access journal. All articles are made freely available to readers immediately upon publication. Our open access policy is in accordance with the Budapest Open Access Initiative (BOAI) definition - it means that articles have free availability on the public internet, permitting any users to read, download, copy, distribute, print, search, or link to the full texts of these articles, crawl them for indexing, pass them as data to software, or use them for any other lawful purpose, without financial, legal, or technical barriers other than those inseparable from gaining access to the internet itself.

Date of publication: March 31st, 2022.

EDITORIAL BOARD

EDITORIAL OFFICE

CONTENTS

RESEARCH PAPER

WASTE MANAGEMENT REFORM IN REGIONS OF THE RUSSIAN FEDERATION: IMPLEMENTATION ISSUES ON THE WAY TO SUSTAINABLE DEVELOPMENT

Andrei M. Dregulo[1,2*], Alexander M. Khodachek[1]

[1]National research University «Higher School of Economics», Pechatnikov str. 16, 198099 Saint- Petersburg, Russia

[2]Saint-Petersburg Federal Research Center of the Russian Academy of Sciences, 18 Korpusnaya str.,197110, Saint- Petersburg, Russia

***Corresponding author:** amdregulo@edu.hse.ru; a.m.dregulo@ecosafety-spb.ru

Received: July 4th, 2021 / Accepted: February 15th, 2022 / Published: March 31st, 2022

https://DOI-10.24057/2071-9388-2021-078

ABSTRACT. Disposal of production and consumption waste is a worldwide problem. Despite the experience of foreign countries, waste disposal practice in the Russian Federation remains at the level of the 1970s. The method of waste burial at landfill sites prevails, leading to a loss of secondary resources and the appearance of sites of accumulated environmental damage, which is connected with the lack of a clear legal framework for waste management activities. Analysis of waste accumulation standards for apartment buildings in 20 regions of the Russian Federation showed that the difference in accumulation standards can vary by 2.32 times (from 0.125 m^3 in the Kursk region to 0.279 m^3 in the Voronezh region). At the same time, the difference in the cost of solid waste removal services can be varied by 2.74 times from 51.55 rubles in the Altai Territory (on average in the region) to 141.45 rubles in the Tyumen region. At the same time, the share of the population with incomes below the subsistence minimum in different regions reaches 7 - 36%. This is largely due to the critically low recovery of secondary materials (about 7%). The capacity of landfills in the regions of the European part of Russia (where more than 2/3 of the population lives) is almost exhausted. Many landfills of solid waste are objects of accumulated environmental damage. The decision to introduce the «institute» of "regional environmental operators", which was adopted at the level of the Russian Federation to implement the waste management reform, has not, yet had any positive effect. Given the constant deficit of the consolidated budgets of most regions, the high level of poverty and the lack of state support, the prospects for waste management reform indicate the need for additional efforts on the part of the state, business and society.

KEY WORDS: waste management reform, regions, investments, tariffs, socioeconomic factors

CITATION: Dregulo A.M., Khodachek A.M. (2022). Waste Management Reform in Regions of the Russian Federation: Implementation Issues on the Way to Sustainable Development. Vol.15, № 1. Geography, Environment, Sustainability, p. 6-13 https://DOI-10.24057/2071-9388-2021-078

Conflict of interests: The authors reported no potential conflict of interest.

INTRODUCTION

The issue of production and consumption waste disposal[1] in the Russian Federation ranks among the most significant problems (Agiamoh, 2020). As the industrialisation and urbanisation of the last decades have shown, all the regions obviously need a comprehensive solution to the waste disposal problem (Kholienchinova et. al. 2020; Ferronato and Torretta, 2019; Skorupskaite and Yunevicius 2017; World Bank Group, 2014). Waste burial facilities (landfill sites), most of which were initially located outside of cities, have gradually been pushed close to residential areas due to intensive growth in housing construction. People have 'got used to' mass media references to an adverse impact of municipal solid waste (MSW) landfills (land pollution, declining investment appeal of polluted and adjacent territories and negative effect on public health) (Wilke, 2020; Njoku et al. 2019; Florin, 2013; Dregulo and Bobylev 2021). One of the reasons for it is the lack of an effective legal regulation of the waste management system (Federal Law No. 89-FZ, 1993) as well as the 'incomplete and unarticulated conceptual framework' in the fundamental Federal Law No. 89 (Waste of production and consumption, 2009). Officially, this FZ No. 89 was passed in 1998. Since then, 40 amendments have been made to it; however, legal relations in waste management have not been fully put in order until the present. The applicable legal and regulatory framework for waste management activities has been recognised as insufficient (Morozov et. al. 2020). The situation is influenced

[1]Suffice it to recall MSW landfills in the Moscow region (24 out of 39 ones are closed), the re-cultivation of which will require 20 billion roubles (i.e. 0.83 bn per landfill on average in terms of prices as of 2018) https://mosreg.ru/gubernator/press-slujba/obzori-smi/okolo-20-mlrd-rub-privlekut-dlya-rekultivacii-poligonov-tbo-v-podmoskove-4885

by different (in many aspects depressed) social and economic situation in the Russian regions and the absence of regulatory mechanisms for regional waste collection and recycling markets (Ponomarev 2014; Fedotkina et. al 2019).

The goal of this article was to analyse the socio-economic reasons that exert an adverse impact on the implementation of the waste management reform in the Russian Federation. Public data of statistical surveys by Rosstat, regulatory documents were used as major information sources, periodicals and scientific literature were analysed as well.

MATERIALS AND METHODS

The methodological apparatus of the research was based on the method of expert evaluation (Fig. 1), including the analysis of open statistical data of the Russian Federation, regulatory documents in the period from 2019-2021 (Federal State Statistics Service) as well as periodical and scientific literature. Expert evaluation is based on several methods:

• Associative. It consists in studying an object that has similar properties.

• Paired comparisons. Compares the alternatives of one solution in order to study the most preferred options for the future.

The authors of the article attempted to link the seemingly disjoint aspects of the designated problem, which, on closer examination, form a single chain of mutually dependent factors. Another important consideration, which was valid at the time of writing, was financing. Expert assessments are qualitative in nature, in contrast to quantitative assessments, and their purpose is to obtain statistically significant results when the identified problem and the available data are evaluated by a small group of experts.

The advantages of this approach are that it provides fast and cost-effective results, as opposed to more expensive types of qualitative user research, which require more experts to reflect a representative result and correspondingly increased funding. The expert evaluation method is proposed as one of the possible ways to solve the problem under discussion. The idea is not just to summarize documents or analytical data of statistical observations, but to characterize the geospatial organization of economic activities for waste management and the accompanying ecological and socio-economic processes.

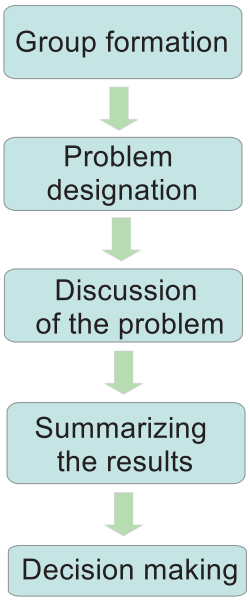

Fig. 1. The main stages of expert evaluation

The experts were assigned the following tasks:

1. Analyze the implementation of the control targets of the federal comprehensive program for waste management and elimination/reclamation of MSW waste disposal (deposit) objects according to state statistics and research materials;
2. Evaluate the prospects for recycling returnable containers and packaging for their separate collection;
3. Identify the main problems in the pricing of the MSW disposal services;
4. Describe the impact of the MSW disposal tariffs imbalance on the problems of poverty;
5. Describe how waste management activities will develop in the future? From your point of view, will the economy of the country and households benefit or lose from introducing the institution of "Regional Environmental Operators" compared to the previous practice of waste disposal?
6. Determine which key problems need to be solved first? Are there any technical, technological or methodological limitations that prevent research in this field from developing further?
7. What is the potential for further research on this topic?

The interpretation of the obtained data is presented in this article.

RESULTS

Amendments made to FZ No. 89 over the last few years launched the modernisation of the waste management system, which has drastically changed waste collection and recycling processes.

On 14 January 2019, the President of the Russian Federation signed Decree No. 8 'On the establishment of a public company for building a comprehensive system for solid municipal waste management called Russian Ecological Operator' (REO) (Decree of the President of the Russian Federation No 8., 2019). The functions and powers of the company's founder on behalf of the Russian Federation are exercised by the Ministry of Natural Resources and Environment of the Russian Federation.

The foundation of the REO public company was connected with the fact that for the last 30 years, waste management was mainly part of the 'shadow' state economy. An attempt of the REO public company to bring local enterprises engaged in waste collection, transportation, disposal and burial under control via regional operators revealed that the regions are not prepared to carry out the waste management reform as such. In many aspects, this is a result of a waste treatment/sorting infrastructure shortage and, subsequently, the appearance of illegal MSW dumps.

The implementation of the waste management reform in the regions made it obvious that the introduction of the territorial waste management scheme (TWMS) enables regulation of waste generation and collection standards as well as of tariffs for waste collection, transportation, and disposal services, and makes it possible to form a separate collection system. At the federal level, a number of bylaws were adopted to modify the rules for MSW management in individual constituent entities of the Russian Federation, including the rules for development, public discussion and adoption of territorial waste management schemes. The most significant changes included the following:

1) Territorial scheme indicators should be taken into account when determining cap tariffs[2] for the MSW management;
2) By Decree of the Government of the Russian Federation "List of production and consumption waste types that include useful ingredients and that may not be buried" (Decree No 1589-p, 2017)[3].

The changes introduced in 2017 are supposed to make sure that by 2024 targets of the Comprehensive Programme for Waste Management will be achieved, namely 50 % of waste in the country will be collected separately. But the achievement of these targets within this period raises doubts among the expert community. Waste of hazard classes III, IV, V, except for MSW, is not included in the Ecology national project, while the placement of this particular waste (oils, electronics, tires, rechargeable and other batteries, glass etc.) at landfills has been consistently prohibited from 2016 to 2021; in particular, liability for disposal of these types of waste was imposed on manufacturers and importers. In addition, these waste types are subject to separate collection and sorting in the course of building an MSW management system.

The absence of waste of hazard classes III, IV, V in the Ecology national project is a technical flaw that impedes the achievement of the national project's goals and objectives. If this issue is not resolved, economic and administrative incentive measures will not apply to a considerable part of the waste generated from the use of goods, including waste that may not be placed at landfills. At the same time, the share of MSW sent for treatment is expected to account for at least 10 % of the overall MSW mass (Fig. 2).

An important element of assisting the regions in the implementation of targets of the Ecology national project is allocation of subsidies from the federal budget in the form of an asset contribution (Government of the Russian Federation Resolution No. 1727 (2019), which is crucial given the deficit in consolidated budgets of many regions of the Russian Federation.

The regions can receive this type of subsidy if the REO issues mandatory recommendations, and if a regional programme for waste management is approved or adjusted or the MSW accumulation standards are corrected (The Government of the Russian Federation Resolution No. 1815, 2019).

The performance indicator on which a decision to grant the subsidy depends is the attraction of private investments, including those in the form of proprietary funds and borrowed (loan) funds, for projects in the amount of at least 2.46 roubles per 1 rouble of the subsidy allocated (The Government of the Russian Federation Resolution No. 1815, 2019). Private investments raised for investment projects can be essential for the reform's implementation.

If the regions lack additional capacities for waste recycling and burial within the next two years, private investments might be attracted for the re-cultivation of old waste disposal landfills and construction of new ones. Fig. 3 demonstrates data on landfills in 32 Russian regions, whose capacity will be exhausted within five years, as of 1 January 2019.

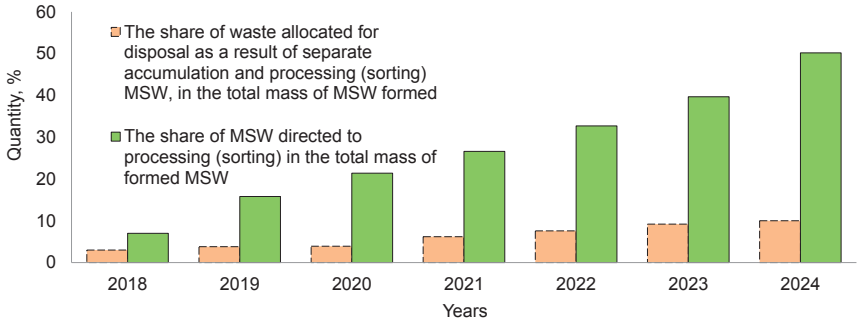

Fig. 2. Individual indicators of the Comprehensive Programme for Waste Management under the implementation of the Ecology national project

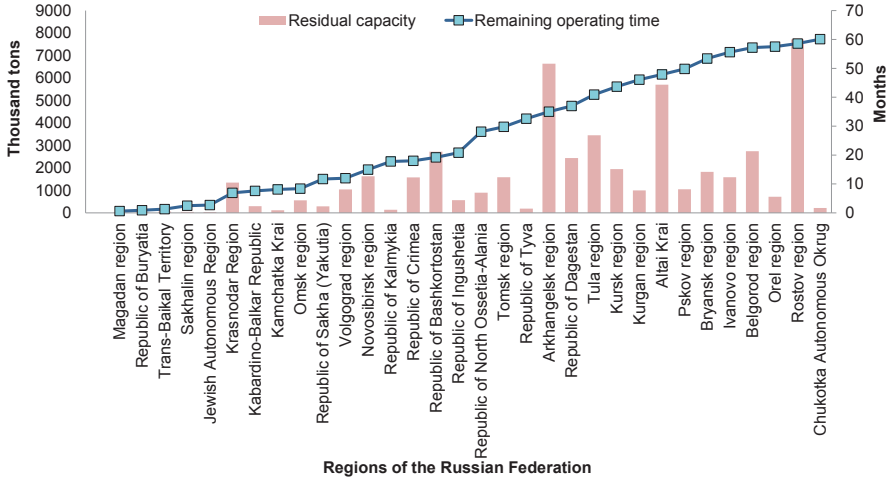

Fig. 3. Data on the residual capacity of MSW placement facilities

[2]It should be noted that the tariff policy (a tax applicable since 1996) in respect of waste burial in England, Wales, Scotland has become the only compulsory (and effective) tool used for encouraging businesses and consumers to lower waste production [The Landfill Tax Regulations 1996 http://adlib.everysite.co.uk/adlib/defra/content.aspx?doc=18602&id=18604]. Similar mechanisms, namely the management of a waste burial tax, are applied in France and Italy. The Netherlands, for instance, draw on another practice; they focus on voluntary agreements between state structures, businesses and the population [Buclet N., Godard O. The Evolution of Municipal Waste Management in Europe: how Different are National Regimes. Journal of Environmental Policy and Planning, Taylor & Francis (Routledge), 2001, 3, 303-317].

[3]Swedish Ambassador Peter Ericson says in his interview to Interfax: 'Russia is lagging 40-50 years behind Sweden in terms of waste recycling issues', https://www.interfax.ru/interview/673785

The biggest problem in reducing the capacity of landfills is the lack of a separate waste collection system, especially for packaging. In Russia, about 7-15% of waste comes from containers and packaging made of plastic, paper, aluminum, etc. The rest of the waste is deposited in landfills. (Ryabov and Tugov 2020).

The capacity of the plastic waste market in 2017 amounted to 461 thousand tons, despite the fact that more than 3.5 million tons were generated. According to the data of 2018, the production of items belonging to the category of plastic containers and packaging amounted to 110 billion pieces.

This is 6.9% more than in 2017, and 108.9% more compared to the data of 2010 (i.e. twice as much as 10 years ago). In 2018, Moscow occupied the first place among the Russian regions in terms of the import of plastic containers and packaging in value terms with 28.8 thousand tons of goods worth 124.2 million dollars (~7.8 billion rubles based on the average exchange rate in 2018) (Volkova, 2018). The production of PET (polyethylene terephthalate) containers in the near future may grow by 2.4% and reach around 112.6 billion pieces. In 2019, the production of plastics reached 8.76 million tons, over 5 years it increased by 64.2%, which means that the need for the development of the "extended producer responsibility" system and the infrastructure of separate collection based on it will significantly increase (Dregulo and Khodachek 2021).

However, the legislative consolidation of the environmental collection norms, as well as the requirement of self-collection (removal) of manufactured products from manufacturers with ineffective control over the subjects of extended producer responsibility (EPR) and a lack of necessary infrastructure, have not yet produced the expected effect. To a large extent, this is due to the distrust of producers (subjects of EPR) to this reform. Waste generation in the Russian Federation rose from ~2.8 to ~7.9 bn tonnes on average within the last 15 years, while disposal and neutralisation increased from ~1.4 to ~3.9 bn tonnes (Fig. 4).

Although the achievement of five main targets of the Comprehensive Programme for Management of Solid Municipal Waste is supported financially (Report on the results of the expert-analytical event 2020), only three out of these targets were partially accomplished in 2019 (data for 2020 was not available at the time of carrying out this research):

• The establishment of an electronic federal scheme for MSW management (Modernisation of the Unified State Information System for keeping records on product waste) was only 48 % complete in 2019;

• The development of regulations concerning activities of the Russian Ecological Operator public company for building the comprehensive system for solid municipal waste management was only 22 % complete in 2019;

• Ensuring of operation of the Russian Ecological Operator public company for building the comprehensive system for solid municipal waste management was only 48 % complete in 2019.

Other two targets were not accomplished:

• The asset contribution of the Russian Federation to the REO public company for building the comprehensive system for MSW management to finance projects aimed at putting facilities for solid municipal waste treatment into commercial operation (0 % complete);

• The asset contribution of the Russian Federation to the REO public company for building the comprehensive system for MSW management to finance projects aimed at putting facilities for waste and fraction disposal after MSW treatment into commercial operation (0 % complete %). This implies the unpreparedness of regional authorities and regional businesses for the implementation of the waste management programme. Apart from that, one should pay attention to the problem of development and approval of reasonable MSW disposal tariffs.

DISCUSSION

The analysis of MSW accumulation standards for apartment buildings in 19 Russian regions revealed that the accumulation volume can vary by a factor of 2.32 (ranging from 0.125 m3 in Kursk region to 0.279 m3 in Voronezh region. At the same time, the cost of MSW removal services can vary by a factor of nearly 2.74, ranging from 51.55 roubles in Altai region (the average regional indicator) to 146.21 roubles in Tyumen region (Fig. 5).

The MSW disposal tariff is frequently set too high without due grounds. In 2019, the Federal Antimonopoly Service of Russia detected breaches of the legislation in the state tariff regulation in 16 regions, where, in particular, cap tariffs incorporated unreasonable costs of regional MSW management operators. Following the results of the proceedings, tariffs were cut by 16.8% - 30.85%. As per clause 148 of Decree No. 354 of the Government of the Russian Federation dated 06.05.2011 (The resolution of the RF Government N 354, 2011), calculation of the utility payment for MSW management in a conventional dwelling is based on the number of permanent and temporary residents of the dwelling, MSW accumulation standards or the total area of the dwelling, as regulated by a decision of a region.

For example, in St. Petersburg, the utility fee for MSW management is calculated and charged with the total area of the residential premises taken into account, although Order No. 30-p of St. Petersburg's Tariff Committee dated 14.04.2017 provided for MSW accumulation standards per person living in an apartment building or detached house. At the same time, MSW generation

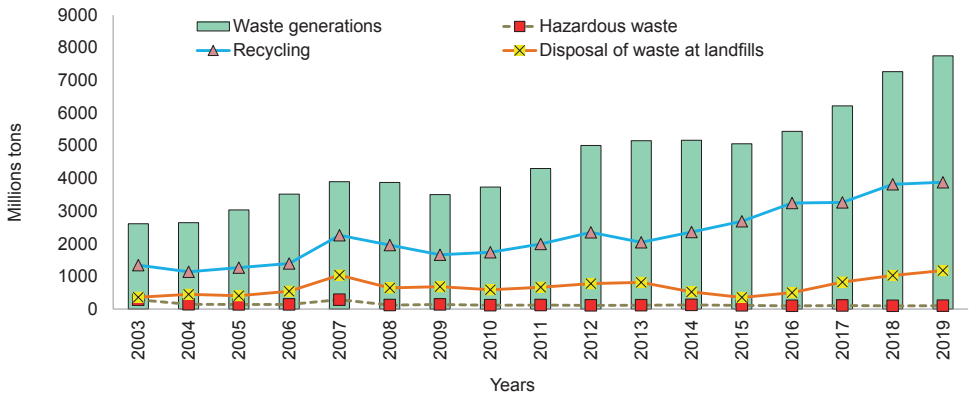

Fig. 4. Waste generation, disposal and neutralisation in the Russian Federation

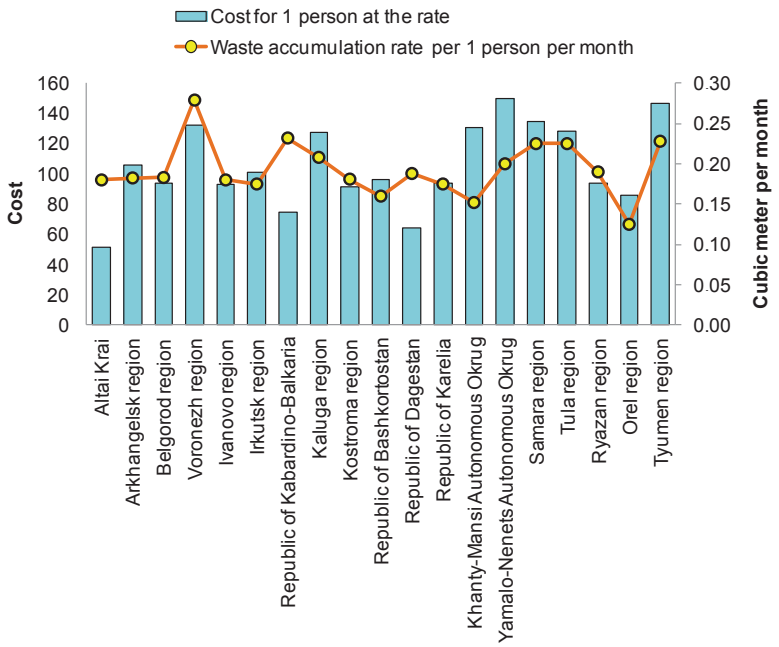

Fig. 5. Standards for the accumulation of MSW and the cost of services for the export of MSW for apartment buildings (per 1 person) in the regions of the Russian Federation

standards per resident of an apartment building differ drastically in the regions.

The service fee is distributed in equal shares based on the cost (an approved price for the service in the current year) for 12 months. The utility price for MSW management, determined in accordance with the properly approved and unified tariff of the regional MSW management operator, is a key indicator for the formation of the MSW disposal tariff. A new MSW management system suggested under the reform comprises several stages: sorting, recycling, neutralisation, and burial of waste. These particular services of the regional operator should be paid for. As far as foreign experience is concerned, a study of qualitative and quantitative characteristics of domestic waste of 144 households from 11 main quarters of the city of Dehradun, India, has demonstrated that the waste weight ranged from 24.5 to 4147.1 g/day and varied considerably among miscellaneous social groups of the city's population. Food waste was the major component, representing ≥80% of the aggregate weight; polyethylene and plastic waste accounted for 7%, paper for 6%, clothes and rubber waste for 4%, cardboard for 2%, and glass 1% (Suthar and Singh 2015).

The findings prove that a rational approach to separate waste collection can massively augment the positive effect of the MSW management reform. Basically, the share of waste recycling and generation of secondary raw materials will rise, and the share of waste placed at landfills will shrink, which, in its turn, will cause a decrease in MSW disposal tariffs.

To make the assessment of the MSW management reform implementation 'transparent', this expenditure item of the population should be specified in utility bills in detail, with a breakdown of payment into elements: waste collection, transportation, separate collection, recycling etc. Such notification of the population will scale up separate MSW collection. Order No. 43 of the Ministry of Construction, Housing and Utilities of the Russian Federation dated 26 January 2018 suggests that such the wording as 'management of solid municipal waste' (Order of the Ministry of Construction of the Russian Federation N 43/pr, 2018) should be used for this type of services when filling in a utility bill. Although this wording is rather advisory in nature, in accordance with order No. 43, the notion of 'management' may mean both all the aforementioned MSW management stages in total combined and any of these stages. This expenditure item is of particular relevance for single elderly people in case of an unfortunate concatenation of circumstances: e.g., when a spouse died, children left, and payment has to be made for the entire area of residential premises.

The loss of income due to stagnation of the economy and liquidation of many small and medium-sized enterprises during the COVID-19 infection period have resulted in the population's rising debt for utility services. According to a report of the REO public company (Annual report of PPK "Russian Ecological Operator" 2019 year, 2020), the accounts owed by the population

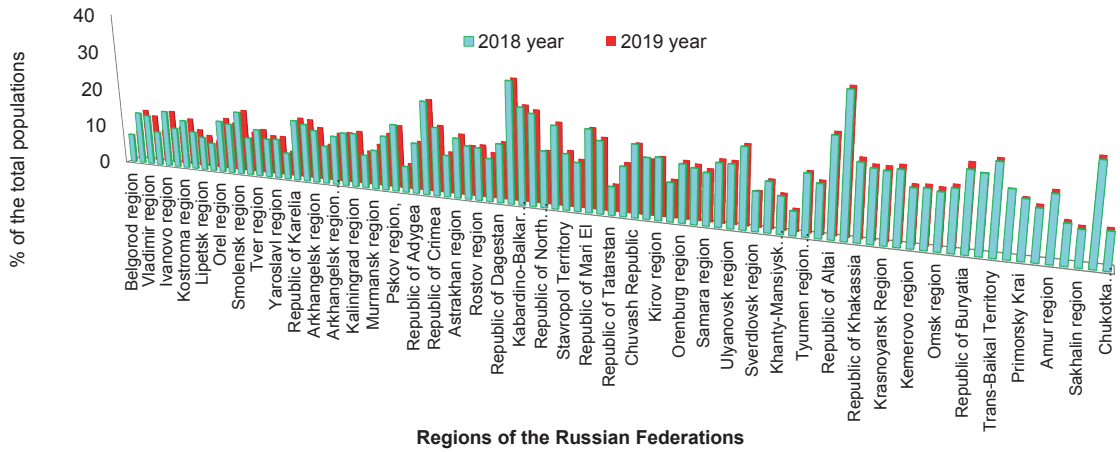

Fig. 6. The share of the population with monetary income below the subsistence minimum

to regional REOs for utility services as of 01.01.2020 exceeded 39 billion roubles. This is probably due to the lack of income to pay for utilities. The share of the population with income below the subsistence minimum in different regions varies from 7 to 36% (Fig. 6). All these factors undermine positive public perception of the reform.

According to an opinion poll conducted in the city of Arkhangelsk (Larionova, 2018), two-thirds of the pollees consider the reform to be centred around the need to sort waste and recycle it properly, and others believe that it is aimed at augmenting tariffs, which enhances social discontent with the reform. Moreover, the negative view of the population of Arkhangelsk region on the reform is attributable to an attempt to build a landfill in the Shies settlement of Arkhangelsk region, which is probably due to the residual filling of landfills in Arkhangelsk region with waste, see Fig. 2). Investments were supposed to be raised by placing waste generated in the city of Moscow. Placement of waste generated in constituent entities of the Russian Federation in other regions violates[4] Decree N 641 of the Government of the Russian Federation dated 25 August 2008 (with amendments as of 15 December 2018) (Decree of the Government of the Russian Federation No 641, 2008) and necessitates the adjustment of the territorial waste management scheme and supplementary financial costs. Amid growing unemployment and the population's debts for utility services, this will lead to a decrease in tax revenues for the regional budget in many regions.

The unemployment rate went up from 1 to 4.2 % from March to November 2020. In the second quarter of 2020, the proprietary income of the consolidated regional budgets fell by 20% (–567 bn roubles), inter alia, corporate income tax revenues dropped by 27% (–243 bn roubles), and personal income tax revenues by 10% (– 99 bn roubles) compared to the similar period of 2019 (Zubarevich, 2021). Another crucial factor of the waste management reform implementation is the issue of demolition of accumulated environmental damage (AED) sites[5], in particular, of MSW landfills. Regular references of mass media to MSW landfill sites in Moscow region, where, due to half-baked measures for shrinking landfill gas emissions, the hydrogen sulphide concentration in the air of surrounding areas exceeded the maximum allowable concentration (MAC) by 625 times, were a vivid example of AED. Far from being an isolated incident, this is a systemic issue for all regions. According to official data of the Ministry of Natural Resources and Environment, in Russia, 121 facilities were classified as AED sites (the real number can be considerably higher). As many as 1500 unauthorised dumps were detected. Their negative impact results in environmental degradation and the appearance of AED sites, which is why additional resources are required for their demolition. Given rough estimates of the cost of eliminating an AED site (by simplified analogy with landfills in Moscow region, where demolition of one landfill site as an AED facility costs 1 bn roubles on average), no less than 500 bn roubles will be required by 2024 for demolition of 500 AED sites besides expenses on the destruction of unauthorised dumps. In accordance with targets of the Ecology national project, the number of destructed unauthorised dumps is supposed to reach at least 180 by 2024, with at least 75 extremely hazardous AED sites to be eliminated (Fig. 7).

Apart from required finance for demolition of AED sites, the problem in many aspects is attributed to:

- legal uncertainty concerning the liability of officials for infliction of environmental damage;
- lack of mechanisms for compensating the population for the damage inflicted;
- inefficient taxation system for enterprises involved in waste disposal (payment for an adverse impact on the environment) (Federal Law No. 7-FZ, 2002; Vypkhanova, Zhavoronkova 2018; Ignatieva, 2017).

In the EU countries, the problem of mitigation of AED is regulated by Directive 2004/35/CE. The Directive is based on the 'polluter pays' principle (Directive 2004/35/ EC, 2004). Nevertheless, the Directive does not provide for any measures compensating the population for harm to health resulting from AED.

Another socially-oriented example of state policy aimed at solving the AED problem was the adoption of the Comprehensive Environmental Response, Compensation, and Liability Act of 1980 (CERCLA) as well as amendments and additions (SARA) introduced thereto in 1986, which made it possible to identify performance problems of the Superfund programme (The Law on amendments to the Superfund and Reauthorization (SARA, 1986).

The Superfund programme solved only part of the problems related to restoration of the ecologically damaged natural environment. The way from identification of environmental harm to cleaning (re-cultivation / restoration) and reuse of territories is highly challenging and does not lead to rapid elimination of AED's repercussions and risks for public health (Lioy and Burke, 2010).

The US Environmental Protection Agency reported in 2009 that facilities listed as AED sites over 20 years ago were still undergoing various stages of demolition. As of December 2009, only 340 out of 1270 sites were excluded from the list (demolished), and 63 new sites were added (National Priorities List (NPL) Sites - by Stat, 2021).

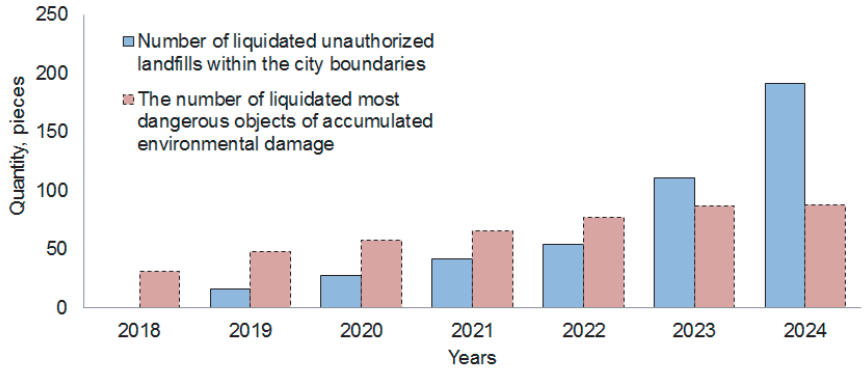

Fig. 7. Separate indicators of the Ecology national project implementation in terms of demolition of AED sites

[4]Clause 5 of the Decree: 'The contract for the provision of solid municipal waste management services shall be concluded between the consumer and regional operator in whose operation area solid municipal waste is generated, and facilities (sites) for their accumulation are located, as prescribed by section 1 of these Rules.'

[5]Official website of the Ministry of Natural Resources and Environment of the Russian Federation. Data on sites of accumulated environmental damage https://www.mnr.gov.ru/activity/directions/likvidatsiya_nakoplennogo_ekologicheskogo_ushcherba/

Thus, residents of areas within the programme-covered territory had lived amid possible adverse risks to health and life quality for several generations.

In the Russian Federation, geoecological features of a technology-related effect of regional AED sites have not been thoroughly explored (Potravny et. al. 2018). The existing methodological concepts make allowances only for elimination costs of AED sites (Economic efficiency of elimination of accumulated environmental damage and restoration of degraded lands 2016) and fail to consider external effects, in particular, compensation to people living in areas that suffered from environmental damage (Kotta 2020).

Obviously, the situation will deteriorate with each passing year; nevertheless, forecasts for real externalities caused by the implementation of the waste management reform in the Russian Federation are virtually impossible to give due to absent or sketchy details.

CONCLUSION

Given the economically challenging situation in the Russian Federation, there is little likelihood that 50 % treatment of MSW waste will be ensured, and no less than 75 extremely hazardous AED sites will be eliminated by 2024. The key grounds for the severe situation in waste management in Russia include socioeconomic conditions, particularly a decline in the population's real disposable income, and the absence of regulatory mechanisms for the MSW collection and recycling market in the regions. The activities of regional ecological operators are difficult to appraise yet.

A number of negative developments in the Russian Federation have not been overcome, such as:

- high share of people with income below a minimum subsistence level;
- high and unbalanced MSW disposal tariffs;
- reduction in the real income of the population (in particular, due to the coronavirus infection);
- social discontent and public misapprehension of the objectives of the waste management reform;
- low efficiency of the use of budgetary funds under the comprehensive MSW management programme;
- lack of methodology for identification and ecological diagnostics of AED;
- imperfect environmental assessment and underdevelopment of environmental insurance.

All of the above indicates that the waste management reform in the Russian Federation is associated with multi-factor socioeconomic conditions that necessitate awareness-raising work among the population and effective governmental control, drawing on the experience of foreign countries.

REFERENCES

Agiamoh R.G. (2020). From Bureaucracy to Market? Ongoing Reform and Performance Challenges of Solid Waste Administration in Moscow. Public Administration Issues, no 5, (Special Issue I, electronic edition), 149-170, DOI: 10.17323/1999-5431-2020-0-5-149-170. (in English)

Annual report of PPK «Russian Ecological Operator» 2019 year (2020). [online] Available at: https://reo.ru/media/documents/2021/Godovoi_otchet_PPK_REO_NS_ot_09.02.2021.pdf [accessed 21.02.2021] (in Russian).

Decree of the President of the Russian Federation No 8. (2019). «On the creation of a public law company for the formation of a comprehensive system for the management of solid municipal waste» Russian Environmental Operator» [online] Available at: URL: https://base.garant.ru/72146514/ [Accessed: 22.01.2021]

Decree N 1589-p of the Government of the Russian Federation (2017). On approval of the list of types of production and consumption waste, which include useful components, the disposal of which is prohibited [online] Available at: URL: http://www.consultant.ru/document/cons_doc_LAW_221683/ [accessed 21.02.2021] (in Russian)

Decree of the Government of the Russian Federation No 641 (2008). «On municipal solid waste management and modification» (amended on 15 December 2018) [online] Available at: URL: http://docs.cntd.ru/document/420382731 [Accessed 27.02.2021] (in Russian).

Dregulo A. M., Shapkin V. M., & Kichko A. A. (2021). Microbial analysis of sewage sludge shows closer monitoring needed for landfill waste. Proceedings of the Institution of Civil Engineers - Waste and Resource Management, 1–7. DOI: 10.1680/jwarm.21.00023

Dregulo A.M., Khodachek A.M. (2021). International and Russian practice in the field of containers and packaging waste management. Innovations, 2(268), 16-23, DOI: 10.26310/2071-3010.2021.268.2.003.

Directive 2004/35/ EC (2004). of the European Parliament and of the Council of the European Union on environmental responsibility for the prevention of environmental damage and the elimination of its consequences. (with amendments and additions). from 23.04.2009). [online] Available at: URL: http://docs.pravo.ru/document/view/22337326/21744131 [Accessed 27.02.2021].

Economic efficiency of elimination of accumulated environmental damage and restoration of degraded lands (2016). Monograph ed.: S.I. Nosov. Moscow: Prospekt, 208 (in Russian).

Fedotkina O., Gorbashko E., Vatolkina N. (2019). Circular Economy in Russia: Drivers and Barriers for Waste Management Development. Sustainability, 11(20), 5837, DOI 10.3390/su11205837

Ferronato N., Torretta V. (2019). Mismanagement of waste in developing countries: An overview of global challenges. International Journal of Environmental Research and Public Health, 16(6), 1060, DOI: 10.3390/ijerph16061060.

Federal Law No. 89-FZ (1999). «On Production and Consumption Waste» (version effective from June 14, 2020) [online] Available at: URL: http://docs.cntd.ru/document/901711591: [Accessed 03.03.2021] (in Russian).

Federal Law No. 7-FZ (2002). «On Environmental Protection» System GARANT: [online] Available at: URL: http://base.garant.ru/12125350/#ixzz6pp0hzWxC [Accessed 11.03.2021] (in Russian).

Federal State Statistics Service (2021). [online] Available at: URL: https://rosstat.gov.ru/folder/11194 [Accessed 13.03.2021] (in Russian).

Florin M. (2013). The impact of tourism on local waste management. Case study: Neamc County, Romania.Modern Environment and Sustainable Development, de Gruyter open, 7(1), 214-221.

Ignatieva I.A. (2017). Legal support for the elimination of accumulated harm to the environment, 2, 164-177. (in Russian)

Government of the Russian Federation Resolution No. 1727 (2019) On approval of the rules for granting subsidies from the federal budget in the form of a property contribution of the Russian Federation to the public law company for the formation of a comprehensive system for the management of solid municipal waste «Russian Environmental Operator» [online] Available at: URL: https://reo.ru/media/documents/2020/Postanovlenie_Pravitelstva_Rossiiskoi_Federatsii_ot_20.12.2019__1727_.pdf [Accessed 21.02.2021] (in Russian).

Government of the Russian Federation Resolution No. 1815 (2019) «On Approval of the Rules for Sending to the Subjects of the Russian Federation and their Consideration of the Recommendations of the Russian Environmental operator when Approving or Adjusting the regional program in the field of waste management, including solid municipal waste, as well as when establishing or adjusting the standards for the accumulation of solid municipal waste» [online] Available at: URL: https://reo.ru/media/documents/2020/postanovlenie_Pravitelstva_Rossiiskoi_Federatsii_ot_25.12.2019__1815.pdf [Accessed 21.02.2021] (in Russian).

Kotta B. (2020). What is happening, is happening? Access and distribution issues in the global North–South waste trade. Environmental Agreements 20, 255-269, DOI: 10.1007/s10784-020-09479-3.

Kholienchinova M., Nagyova L., Holota T. (2020). The impact of environmental responsibility on changing consumer behavior – a sustainable market in Slovakia. Economics and Sociology, 13, 84-96, DOI: 10.14254/2071-789X.2020/13-3/6.

Larionova N.S. (2020). The attitude of the residents of Arkhangelsk to the garbage reform (results of a sociological study). Russian Economic Bulletin, 3(1), 254-258 (in Russian).

Law on amendments to the Superfund and Reauthorization (SARA) [Electronic resource]: URL: [online] Available at: https://www.epa.gov/superfund/superfund-amendments-and-reauthorization-act-sara [Accessed 25.11.2020].

Lioy P.J., Burke T. (2010) Superfund: Is it safe to go home? Journal of exposure science & environmental epidemiology, 2, 113-114, DOI: 10.1038/jes.2009.69.

Order of the Committee on Tariffs of St. Petersburg No. 30-r of 14.04.2017 [online] Available at: https://www.gov.spb.ru/gov/otrasl/energ_kom/documents/npa/7118 [Accessed 21.02.2021] (in Russian).

Morozov V.V., Kurbatova Z.I., Kurbatova E.P. (2020). Problems of handling solid household waste and environmental disaster zones. Natural sciences, 1, 9-13 (in Russian).

National Priorities List (NPL) Sites – by Stat (2021). [online] Available at: URL: https://www.epa.gov/superfund/national-priorities-list-npl-sites-state [Accessed 25.05.2021].

Njoku P.O., Edokpayi J.N. & Odiyo J.O. (2019). Health and environmental risks to residents living near the landfill: A case study of the Tohoyandu landfill, Limpopo Province, South Africa. International Journal of Environmental Research and Public Health, 16(12), 2125, DOI: 10.3390/ijerph16122125.

Order of the Ministry of Construction of the Russian Federation N 43/pr (2018). «On approval of the approximate form of a payment document for making payments for the maintenance and repair of residential premises and the provision of public services» (Registered with the Ministry of Justice of the Russian Federation on 14.05.2018 N 51074) [online] Available at: URL: http://www.consultant.ru/document/cons_doc_LAW_297915/2ff7a8c72de3994f30496a0ccbb1ddafdaddf518/ [Accessed 01.03.2021] (in Russian).

Potravny I.M., Novoselov A.L., Novoselova I.Yu. (2018). Development of methods of economic assessment of damage from environmental pollution and their practical application. Economic Science of modern Russia, 3(82), 35-48 (in Russian).

Ponomarev M.V. (2014). Trends and prospects for improving legislation in the field of waste management of production and consumption. Journal of Russian Law, 4, 22-32 (in Russian).

Report on the results of the expert-analytical event (2020). «Analysis of the implementation of measures that ensure the environmental safety of the Russian Federation, in terms of the elimination of objects of accumulated harm and the formation of a comprehensive system for the management of solid municipal waste». 2019 [online] Available at: URL: .https://ach.gov.ru/upload/iblock/41b/41b02dc50697e6fc57ec2f389a8b68f0.pdf (in Russian).

Resolution of the Regional Energy Commission of the Sverdlovsk Region of 30.08.2017 No. 77-PC (ed. of 28.06.2018) « On approval of standards for the accumulation of solid municipal waste in the territory of the Sverdlovsk region(with the exception of the municipal formation «city of Yekaterinburg»)» [online] Available at: URL: https://docs.cntd.ru/document/446475627 [accessed 11.03.2021] (in Russian).

Resolution of the Cabinet of Ministers of the Republic of Tatarstan № 922 (2016). «About the approval of standards of accumulation of solid municipal waste in the Republic of Tatarstan» [online] Available at: URL: https://kt.tatarstan.ru/obrashchenie-s-tverdimi-kommunal-othodami-2659677.htm [Accessed 11.03.2021] (in Russian).

Resolution of the RF Government N 354 (2011). «On the provision of public services to owners and users of rooms in apartment houses and homes» (along with «the Rules for the provision of utilities to owners and users of premises in apartment buildings and houses») (ed. by 02.03.2021) [online] Available at: URL: http://www.consultant.ru/document/cons_doc_LAW_114247 [Accessed 12.04.2021] (in Russian).

Ryabov G., Tugov A. (2020). Energy recovery of solid waste disposal in Russia, State of the Art and operation experience. Waste Disposal & Sustainable Energy, 2, 265-273, DOI: 10.1007/s42768-020-00050-z.

Skorupskaite K. and Yunevicius A. (2017). Waste management policy development in Lithuania using the Circular Economy model. Public Policy and Management, 16(1), 91-107, DOI: 10.5755/j01.ppaa.16.1.1801.

Suthar S., & Singh P. (2015). Solid waste generation and composition in different-sized families and socio-economic groups: a case study. Sustainable Cities and Society, 14, 56-63, DOI: 10.1016/j.scs.2014.07.004.

Volkova A.V. (2018). Waste disposal market [online] Available at: URL: https://dcenter.hse.ru/data/2018/07/11/1151608260/%D0%A0%D1%8B%D0%BD%D0%BE%D0%BA%20%D1%83%D1%82%D0%B8%D0%BB%D0%B8%D0%B7%D0%B0%D1%86%D0%B8%D0%B8%20%D0%BE%D1%82%D1%85%D0%BE%D0%B4%D0%BE%D0%B2%202018.pdf [Accessed 01.03.2021] (in Russian).

Vypkhanova G.V., Zhavoronkova N.G. (2018). Legal regulation of environmental damage compensation in modern realities. Environmental law, 5, 5-12. (in Russian).

Waste of production and consumption (2009). [online] Available at: URL: http://council.gov.ru/activity/activities/parliamentary/29679 [Accessed 09.01.2021] (in Russian).

Wilke R. (2020). Cooperation between government and Agribusiness in Biogas Production: Balanced Development of Public Policy and Rural Sustainability Management, 19(2), 298-313, DOI: 10.13165/VPA-20-19-2-11.

World Bank Group (2014). Waste in Russia: garbage or valuable resource? Scenarios for developing the municipal solid waste management sector [online] Available at: URL: https://documents1.worldbank.org/curated/pt/702251549554831489/pdf/Waste-in-Russia-Garbage-or-Valuable-Resource.pdf [Accessed 31.09.2021].

RESEARCH PAPER

GIS-ANALYSIS OF THE URAL POWER GRID VULNERABILITY TO THE IMPACT OF SLEET AND WIND

Andrey M. Karpachevskiy[1*], Oksana G. Filippova[1], Pavel E. Kargashin[1]

[1]Lomonosov Moscow State University, Geography faculty, department of cartography and geoinformatics, Leninskie Gory 1, 119991, Moscow, Russia

***Corresponding author:** karpach-am@yandex.ru

Received: July 20th, 2021 / Accepted: February 15th, 2022 / Published: March 31st, 2022

https://DOI-10.24057/2071-9388-2021-082

ABSTRACT. In this paper, we describe an experiment of complex power grid structure and wind and sleet mapping of territory using two different network indices: standard edge betweenness centrality and new author's index – electrical grid centrality. Such analysis of the network allows to identify power lines with high load which could be vulnerable elements of the power grid. It is very important for strategic planning of power grids to reduce the risk of accidents by distributing loads across several lines so that they will be able to reserve each other. As a case territory for this research, we took the Ural united power system in Russia which is greatly exposed to different sleet and wind according to the statistics of the power grid operator. The degree of natural hazard consequences could be compensated by the network structure through alternative paths of energy supply or vice versa – increased if they are absent. At the same time, in this paper we consider that power grids have their own features from the graph theory point of view, for example multiple (parallel) edges, branches, different types of vertices. The existing index of edge betweenness centrality does not perfectly cope with them. We compare two indices characterizing power line importance within the system – betweenness centrality and electrical grid centrality and analyze the network structure features together with the spatial distribution of sleet and wind. As a result, we could identify bottlenecks in the study network. According to this study the most vulnerable power lines were detected, for example 500 kV Iriklinskaya CHP – Gazovaya and 500 kV Yuzhnouralskaya CHP-2 – Shagol power lines, that supply big cities such as Chelyabinsk and Orenburg and a bunch of industries around them.

KEY WORDS: GIS-mapping; graph centrality; network analysis; power grid structure; sustainable power supply

CITATION: Karpachevskiy A.M., Filippova O.G., Kargashin P.E. (2022). GIS-Analysis of the Ural Power Grid Vulnerability to the Impact of Sleet and Wind. Vol.15, № 1. Geography, Environment, Sustainability, p 14-25
https://DOI-10.24057/2071-9388-2021-082

ACKNOWLEDGEMENTS: This study was conducted within the framework of the state-ordered research theme of the Lomonosov Moscow State University, Cartography and Geoinformatics department, no. 121051400061-9 «Development of methods and technologies of cartography, geoinformatics and aerospace sensing in the research of nature and society».

Conflict of interests: The authors reported no potential conflict of interest.

INTRODUCTION

Structural vulnerability of geographical networks

Power grids are complex geographical objects that supply consumers with electricity. Sustainability of energy supply is necessary for the efficient functioning of the economy. The sustainability of any transport network is primarily determined by its configuration and structure (Bugromenko 1987; Tarkhov 2005). The sustainability of a network is its specific property, which allows to identify «bottlenecks» in the power grid, particularly the elements that are most prone to emergency situations. Environmental conditions of a network are equally important because they can cause great damage to the infrastructure. Some natural hazards can lead to emergency situations of local or even national scale. The consequences may become even more threatening when the supplied territory covers multiple settlements, important facilities, etc. However, the degree of damage depends not only on the impact of wind and sleet but also on the spatial structure of the network. For example, an isolated power system of Sakhalin is highly susceptible to cascading failures. It means that the failure of one network element will inevitably lead to the failure of another due to the predominantly dendritic network structure. On August 24, 2016, a short circuit occurred on the 220 kV power transmission line Yuzhno-Sakhalinskaya power plant – Kholmsk due to strong winds and heavy rainfall. As a result, 12 out of 18 municipalities of the island (the central and northern parts) were left without electricity.

GIS tools allow to carry out spatial analysis of the power grid sustainability taking into account natural hazards data. Network analysis methods help to model emergency blackouts and predict their consequences. This article discusses the experience of GIS analysis of the sustainability of the power grid in the Ural united power system (UPS) using network centrality measures and spatial data on natural hazards.

The analysis of the sustainability of transport systems began with an attempt to formalize their representation in a machine-readable form and apply mathematical

modelling methods to such data. Sustainability analysis is based on the methods of studying the network structure using graph theory. The analysis of complex networks originated in the early 2000s and has become the new stage of network analysis theory development.

A complex network is a system that has a certain non-trivial relationship of elements (Pagani and Aiello 2013). This direction emerged from narrow research related to the concepts of the random graph, scale-free network and «small world» models. The «random» graph model, or the Erdős-Rényi model, describes the equal probability distribution of graph parameters (Erdős and Rényi 1959). In scale-free networks the number of edges between nodes follows the power-law distribution, thus it is uneven. In «small-world» models the typical distance between two randomly selected vertices grows proportionally to the logarithm of the vertex number in the network (Watts and Strogatz 1998). A schematic representation of the most common network models is shown, for example, in the paper (Hines and Blumsack 2008).

The geographical study and mapping of network structure are more common for road and railroad transport. In 1974 U.S. Federal highways were first studied using the graph model (Garrison 1974). The vertices of that graph were represented by settlements, and the edges by the roads connecting them. Indicators such as Koenig number and topological accessibility were calculated for each vertex. In addition, the characteristics describing the whole graph were calculated – topological diameter and degree of connectivity. The well-known PhD thesis of Kansky contains the transformation principles of the cartographic representation to the graph model. He also developed several indices, known as Kansky indices. These indices characterize the level of network development. In the Soviet Union, graph theory found its application in the Carpathian Ukraine railway network analysis. For example, Shabliy (1976) calculated indices characterizing the network configuration based on graph theory. Also, researchers proposed an index of integral transport accessibility characterizing the efficiency of roads based on graph theory (Bugromenko 1987). The PhD thesis (Chibryakov 2015) presents a method of mapping structural indices for the railway networks study. The author calculated the β index characterizing connectivity of transport networks and mapped it. In addition, the author proposed a topological approach to the generalization of transport networks, which considers topological models of different complexity levels at different mapping scales.

The work (Guimer and Amaral 2014) was devoted to the analysis of more than 3 thousand airports and air transport networks around the world. They were the first who found out that degree centrality values determine connectivity and sustainability to a lesser degree than betweenness centrality, i.e. the number of routes passing through the edge or node.

Only at the end of the twentieth century similar methods were used for power grids. One of the first studies in which graph theory was applied to the analysis of the structure and sustainability of power grids was devoted to the case study of Italy (Crucitti et al. 2005). The authors used a weighted graph in which the weight of edges corresponded to the ratio of its power to load. The main concept in this paper was betweenness centrality. The authors simulated the removal of random edges and analyzed changes in betweenness centrality of the remaining elements.

In another study (Chaitanya et al. 2011), the authors considered topological properties of the Eastern India power grid. As in most other works, the graph was considered exclusively from a mathematical point of view and had no spatial reference. The authors created three types of origin-destination matrices: the incidence matrix, the Laplace matrix, and the adjacency matrix, and then calculated the clustering coefficients, Pearson correlation coefficient, average degree and other indices for graph vertices.

Rosas-Casals et al. (2007) studied different characteristics of the power grid in 23 European countries. They divided network accidents into those that occur randomly and intentionally. By simulating these actions, they calculated the critical probability of disconnecting for a particular vertex in the network. The main concept used by the authors was the node degree. In this kind of work, the results were usually presented in the form of tables. Information about the studied network is presented in the form of a schematic image or a small-scale map that shows the location of network elements and occasionally its parameters. For example, in the study (Rosas-Casals et al. 2007) the color of a vertex corresponds to its degree. Since 2010 many similar studies in which authors simulated blackout of a power grid and determined its impact on the state of the whole network through changes in the values of some theoretic and probabilistic indicators have been conducted (Hines and Blumsack 2008; Nasiruzzaman and Pota 2018).

Northwestern University in the USA conducted an interesting research (Yang et al. 2017). The authors previously constructed an anamorphic map of electric networks so that the density of the network vertices became uniform throughout the territory. Then, using maximum capacity data and the actual length of the network, they calculated the percentage of transmission lines that are most critical in terms of the occurrence of an accident. As a result, the lines with considerable length and capacity made up 10.8% of the total lines number.

The first power grid structure mapping was carried out in (Faddeev 2016). The author studied the structural sustainability of power grids in Russia and other countries of the former Soviet Union. The main concept used in this work was betweenness centrality, which determines the load of a network vertex. An algorithm for removing random vertices was close to those described above. The author created maps of the power grid sustainability based on the obtained results. Sustainability was expressed in terms of the percentage of vertices, the removal of which will lead to cascade failures. The resulting values were aggregated within the united power systems.

A new approach to the analysis of structural characteristics of the power grid as a resource for long-term development was presented in the PhD thesis (Karpachevskiy 2018). The author considered centrality, alternativeness (number of supplying power lines) and topological distance to be the main structural characteristics. Also, he described the content of the electric network structure maps and proposed some visualization methods.

Thus, the study of power grids from the graph theory point of view has begun quite recently. Initially, graph theory methods were used to analyze road and rail networks, later they were applied to power grids. Mapping the structure and sustainability of power grids is a new and poorly developed field in thematic cartography. In our study, we propose a new centrality measure that corresponds to the power grid features and is more representative.

Natural hazards affecting power networks

Power systems are influenced by a variety of natural hazards that are taken into account during the design and construction of electric power lines. The main and the most frequent natural hazards that are studied in this paper are wind and sleet.

The danger of wind lies in the dynamic impact on objects. Strong winds include a wide range of wind meteorological phenomena: typhoons, storms, tornadoes, squalls, etc. The danger of sleet load is associated with significant damage due to the accumulation of ice with a diameter of more than 20 mm on the wires (Atlas of natural… 2012).

According to statistics, these natural hazards cause the most accidents in power systems. The main documents regulating the construction of power lines in Russia are the following:

• The standard of the organization of Federal Grid Company of the Unified Energy System, Norms for the Technological Design of Overhead Power Transmission Lines with Voltage of 35 – 750 kV (FSK-EES.ru, 2014);
• Wiring regulations (PUE7.ru, 2006);
• Building norms 2.01.07-85 «Loads and impacts» (docs.cntd.ru, 2010);

These documents present the zoning of Russia by wind and sleet loads. Each zone has its own value of wind/sleet load impact (Table 1, Table 2).

So, these maps represent the only available and official data about the spatial spread of maximum wind and sleet loads with a probability of 0.04 (one time per 25 years). They are often used to study the natural conditions of a power system operation and development.

We assume that joint analysis of electric networks and maps of natural hazards is necessary for the accurate identification of «bottlenecks» in power grids and determining the degree of their vulnerability. GIS is the most appropriate and efficient method for conducting spatial analysis of natural hazards along with the network structure analysis.

MATERIALS AND METHODS

The study area

A preliminary study based on the actual data about failures has revealed the power systems for which the assessment of sustainability is most relevant (Karpachevsky and Filippova 2018). The Ural united power system (Fig. 1) consists of nine regional power systems: the Republic of Bashkortostan, Kirov region, Kurgan region, Orenburg region, Perm Krai, Sverdlovsk region, Tyumen region, Khanty-Mansi and Yamalo-Nenets Autonomous districts, Udmurt Republic, Chelyabinsk region. The combination of complex and sometimes irrational configurations of the power grid and difficult environmental conditions (mountain terrain often leads to considerable wind and sleet loads) causes the maximum number of failures among all power systems, including high voltage power grids. According to the Ministry of energy data on emergency shutdowns at electric power facilities in the Ural UPS (minenergo.gov 2019), there were 245 failures on power lines with a voltage of 110 kV and above. A third part of the failures was caused by wind and sleet loads.

Power grid graph

In the power grid graph, power plants and substations act as vertices, and power lines act as edges. Electric network, however, has its own features (Karpachevsky and Novakovsky 2019):

• Different functional types of vertices: sources (power plants) and consumers (electrical substations);

Table 1. Maximum wind pressure for different zones with a return period of 25 years

Zone	Wind pressure, Pa
I	Less 400
II	400-500
III	500-650
IV	650-800
V	800-1000
VI	1000-1250
VII	1250-1500

Table 2. Maximum sleet load on wires for different zones with a return period of 25 years

Zone	Sleet thickness on wires, mm
I	Less 10
II	10-15
III	15-20
IV	20-25
V	25-30
VI	30-35
VII	35-40

Fig. 1. Schematic map of the main power transits in the Ural UPS

• One-direction flow at one point in time: electricity moves from sources to consumers in general, but the direction could be changed;
• The presence of multiple edges (parallel edges connecting same vertices);
• The presence of branches – edges connecting three or more vertices, which are named hyperedges in the graph theory terminology (Karpachevsky and Novakovsky 2019; Newman 2018);
• The graph is non-planar – there are no vertices at intersections of power lines, flow switching is possible only at the vertices of the graph;
• The hierarchy of the graph edges depends on the power line voltage;
• The weight of an edge is determined by the capacity of the power line.

We collected the initial data using visual identification of the power grid objects. We used mosaics of high-resolution space images (Bing, QuickBird, GeoEye, etc.) available on map services. Identification of power lines was based on a topological approach. According to this approach, the unit of mapping is a power line circuit (not the power line itself, because it can consist of several circuits), so that we could trace a line along the circuit as a graph edge. On a space image we could recognize power lines using single pylons and the composition of pylon species. We defined the pylon species composition as a regular stable combination of anchor and intermediate pylons on the line (Kargashin et al. 2016). The composition of pylons species depends on the geographic features of the territory, climatic loads, current typical pylon design, number of circuits and nominal voltage. In addition, various topomorphological relations – a set of repeating spatial configurations such as branches, cuts, furcations, etc. – were taken into account during the identification of power lines (Karpachevsky 2018). We carried out image interpretation using the Google Earth application, which provides free access to the mosaic of space images. The results of interpretation were assessed using some existing schemas, documents and maps. It was concluded that the accuracy of the resulting network is sufficient for spatial and network analysis (Karpachevskiy et al. 2020).

To minimize the effect of boundary on the modelling (Tikunov 1997) we expanded the network: in addition to the network of the studied territory, we included power lines crossing the boundary of the power system and some linking lines, which provide inter-system communication, as well as adjacent vertices.

Identified objects were topologically corrected. Below is a formalized list of topology rules that must be followed when constructing a power grid graph:
• The graph should be non-planar;
• There should be no hanging vertices – each power line should start at a point (power plant/substation) and end at a point;
• Self-intersections are not allowed;
• «Stand-alone» nodes are not allowed – each power plant/substation must have connected power lines.

A weighted graph should be used to perform the analysis. In this case, the weight of the edges corresponds to the inverse value of the power lines capacity which depends on the voltage (Table 3) (Faybisovich 2012).

Network analysis

Centrality measures from the graph theory are popular tools for assessing the edge significance (load) in graphs. In the case of transport networks, betweenness centrality is often used. For calculating the edge betweenness centrality, it is convenient to use the NetworkX library in the Python programming language. This function is rather simple and takes the graph itself and the weight attribute as input parameters. Betweenness centrality for a vertex or an edge is determined as the number of shortest routes passing through this element. The experience of using betweenness centrality has shown high efficiency in investigating not only geographical networks (Rosas-Casals et al. 2007; Faddev 2016), but also social ones (Scott and Carrington 2011).

However, as we can see from the previous section, this approach does not take into account some features of the power grid graph. For power grids it is much more reasonable to use centrality that we call electrical grid centrality. We have developed a programming code for its calculation (Fig. 2). The features of this index are listed below:

1) Shortest paths are calculated only between generation points and substations, paths between two substations are not taken into account;

2) For the generation points subset we considered only power plants with an installed capacity of 200 MW and higher – this corresponds to the power which typically requires transportation using power transmission lines with a voltage of 220 kV and higher;

3) Betweenness centrality for an edge is calculated as the sum of the fraction of all-pairs shortest paths that pass through the edge. For power grids the number of shortest paths between two points is usually determined by the number of multiple edges, so that there is no need for the calculation of fractions.

4) Normalization of indicators for ordinary graphs is performed by division by n(n - 1), where n – number of vertices. This expression corresponds to the number of edges in the complete graph. In a power grid graph it does not make sense to take into account complete graph because there is no need to link all generation points with each other. Thus, the number of possible edges between generation points is subtracted from the number of possible edges in the complete graph;

5) Lines with branches (hyper-edges) in NetworkX are deconstructed to simple edges, new vertices adjacent to these simple edges are included in the graph. These vertices become involved in ordinary centrality calculation. In the case of electrical grid centrality, these vertices are excluded from short paths calculation.

6) Ordinary function for reading shapefiles in NetworkX creates a simple graph object. We have developed a function for reading the power grid shapefile as a multigraph.

7) Multiple (parallel) edge values have no difference from ordinary edges in the case of betweenness centrality. In the case of electrical grid centrality, these values are distributed equally (divided by the number of multiple edges) to reflect the load decrease.

Table 3. Capacity of power lines

Nominal voltage, kV	Capacity (average value), MW	Weight, (1/MW)*100
35	10	10
110	37.5	2.6
220	150	0.6
500	900	0.1

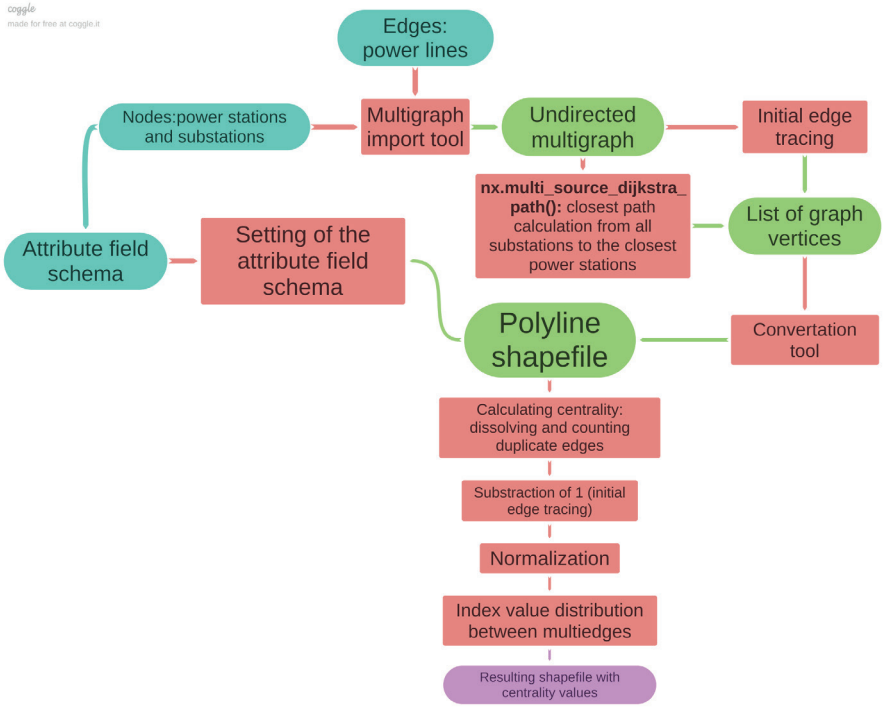

Fig. 2. Algorithm of the electrical grid centrality calculation

Natural hazards data

We used maps of wind and sleet loads impact from Wiring Regulations. We georeferenced and digitized them, obtaining vector layers for the joint analysis with the results of network analysis (Fig. 3, Fig. 4).

The zones of wind impact in this territory have sublatitudinal boundaries and almost coincide with the boundaries of natural zones due to the flat topography and the large extent of the territory from west to east. The central part of the study area (almost 50%) lies within the wind zone II. It covers Kirov, Sverdlovsk, Tyumen, Perm regions and Khanty-Mansi Autonomous Okrug. Wind pressure increases when moving north and south. In the northern part (Khanty-Mansiysk and Yamal-Nenets Autonomous Okrugs) it is caused by the absence of a natural barrier and the drift of cold air masses from the Arctic Ocean. Continentality increases from north to south (Chelyabinsk and Orenburg regions). Moreover, wind speed increases here due to the treeless territories of the steppe. Almost the entire plain territory lies in zone II of sleet load. The northwest of Kirov region is characterized by minimal values of ice thickness (less than 10 mm). Sleet thickness is higher in the mountains (zone IV and V) beginning from the foothills of the Urals. The foothills (at an altitude of 300-500 meters) and the hills adjacent to the Ural Mountains correspond to the sleet load zone III.

RESULTS

We calculated both edge betweenness centrality and electrical grid centrality for the Ural UPS network. We took lines not only within the Ural UPS, but also lines from bordering power systems that form cycles with lines from the Ural UPS and lines connected to big power stations. After that, we overlaid output shapefiles with sleet thickness and wind pressure layers.

The analysis of the power lines location in various sleet thickness and wind pressure zones showed that many of them are located in the most dangerous areas. Moreover, it is necessary to take into account the age of lines. So, the 500 kV lines Kropachevo – Ufimskaya, Kropachevo – Privalovskaya, Privalovskaya – Zlatoust and Zlatoust – Chelyabinsk pass through the area with the maximum sleet load and through the zone II of wind load. This transit was built in the 1950s-1960s. Listed lines have low relative centrality values of 1.44%, 0.007%, 1.44% and 5.7%, which means that their outage would lead to redistribution of the load without cascade failures.

The same situation is observed for the 220 kV lines from Kama hydroelectric power plant (HPP) to the power substations of Yekaterinburg. These lines were built in the 1950s-1960s and are located on the western foothills of the Urals. This territory combines severe sleet and wind conditions. The centrality of these lines is very low (less than 1%), which does not allow us to speak about the critical level of consequences due to emergency situations.

Fig. 3. The main power transits in the Ural UPS overlaid with the sleet load zones

Fig. 4. The main power transits in the Ural UPS overlaid with the wind pressure zones

In the 1970s-1990s, several power lines were built linking the regional power systems and crossing the Ural Mountains. They are located in heavy sleet zones. For example, the 500 kV Kalino – Tagil line passes through the zone IV of sleet thickness, however, its centrality is zero. Among all the other lines built after 1990, the most critical are the 220 kV lines located in the wind pressure zone III: Urengoy – Nadym (centrality 0.5%), Urengoy – Pangody (centrality 0.1%) and Urengoy CHP power plant – Tarko-Sale (centrality 0%). In the southern part of the power system, several lines are located in the wind pressure zone III: the 500 kV Iriklinskaya CHP power plant – Magnitogorskaya (centrality 40%) and the 500 kV Iriklinskaya CHP – Gasovaya (centrality 53%). Thus, among all the transmission lines of the Ural UPS, the most unfavorable conditions are observed for the lines crossing the Ural Mountains, because mountainous areas are characterized by the thickest sleet.

In addition, there are several lines with large centrality values (more than 50% of the maximum value). Such lines make up less than 1% of the total number of lines. Emergencies on them can be dangerous due to the lack of backup power transmission routes. All these lines have a power plant as a feeding centre, i.e. they are the initial link of further electricity transmission. Also, two of those lines connect the Surgut CHP-1 with substations. This indicates that this power plant in the network is a local centre and there are no alternative energy sources in the territory of its service.

Joint analysis of the network location and natural hazards may help to identify bottlenecks in the system. We took the results of network analysis and created a table of bottlenecks of the Ural UPS (only 500 kV). A bottleneck is an edge of the network that has high betweenness centrality (>50 % of the maximum value), is located in high wind pressure and/or ice thickness zone (zone III and above) or was built in the 1960s and earlier. These lines are the most critical parts of the power system which should be carefully serviced (Table 4).

Thus, there are two lines that have several critical factors. The 500 kV Yuzhnouralskaya CHP-2 – Shagol power line has the maximum value of the modified centrality in the entire graph. This line serves the Chelyabinsk industrial hub and is part of the intersystem transit of electricity between the Urals and the Volga UPS. An outage of the line will lead to a failure in the power supply, first, in the city of Chelyabinsk and its agglomeration with a total population of more than 1.5 million people, and second, in the largest enterprises of the Southern Urals: Chelyabinsk Metallurgical Plant, Zinc Plant, and Chelyabinsk Electrometallurgical Plant.

The 500 kV Iriklinskaya CHP – Gazovaya power line (Fig. 5) mainly serves the largest plants of Orenburg region (Ural Steel Plant, Mednogorsk Copper-Sulfur Plant), and also provides electricity to the railway, the cities of Orenburg, Mednogorsk, Kuvandyk, Orsk, Novotroitsk and a number of settlements with a population of about 800 thousand people. In general, the Iriklinskaya CHP is the most powerful in the Southern Urals: its capacity is almost 2500 MW, which allows it to provide power to almost the entire Orenburg region. In addition, part of the electricity is exported to Kazakhstan, which makes the line a geopolitically important object.

Table 4. Bottlenecks of the Ural UPS (most critical factors are highlighted in red)

Power line	Electrical grid centrality, % of maximum value	Wind pressure zone	Ice thickness zone	Year of construction
500 kV Yuzhno-Uralskaya CHP-2 – Shagol	100.0	2-3	3	1964
500 kV Iriklinskaya CHP – Gazovaya	53.0	3	2-3	1992
500 kV Iriklinskaya CHP – Magnitogorskaya	40.0	2-3	3	1976
500 kV Surgutskaya CHP-1 – Pyt-Yakh	85.0	1	1	1976
500 kV Surgutskaya CHP – Holmogorskaya	85.0	1	1	1985
500 kV Karmanovskaya CHP – Udmurtskaya	71.0	2	2	1968
500 kV Votkinskaya HPP – Vyatka	66.0	1	2	1976
500 kv Kropachevo – Ufimskaya	1.4	2	3	1961
500 kV Kropachevo – Privalovskaya	<1.0	2	3-4	1961
500 kV Privalovskaya – Zlatoust	1.4	2	3	1961
500 kV Zlatoust – Chelyabinsk	5.7	2	3	1961
220 kV Kamskaya HPP – Kalino	<1.0	1	3	1965
500 kV Kalino – Tagil	<1.0	1	3	1974
220 kV Urengoy – Nadym	<1.0	2-3	1	1980
220 kV Urengoy – Pangody	<1.0	3	1	1985
220 kV Urengoy CHP power plant – Tarko-Sale	<1.0	2-3	1	1982

Fig. 5. Most critical lines in the Ural UPS (highlighted in pink)

DISCUSSION

We wanted to compare the network model with the real geographical distribution of natural hazards, supplementing this comparison with data on the age of the infrastructure. This is the first fundamental difference from the previously considered works, where networks without a real geographical reference were used for modelling.

In Fig. 6 and Fig. 7 we can see an example comparison of calculation results obtained using different methods. Calculated values were additionally normalized by their range since the calculation algorithms in both instruments generate results in different scales.

For both methods, several corridors are clearly distinguished, representing the sequence of the most loaded power lines: the 500 kV Karmanovskaya CHP – Udmurtskaya and Votkinskaya HPP – Emelino (both with centrality values of 0.50 or higher). Considered lines are not connected to each other with an adjacent line in both calculation results: when using the usual centrality, the connecting line with a close value is the 500 kV Karmanovskaya CHP – Votkinskaya HPP, when using a modified tool, there is a cascade of lines forming a loop and passing through the Vyatka substation (near Kirov). Because of this, in the case of modified centrality, the centrality of the 500 kV Votkinskaya HPP – Vyatka line is greatly increased. The second corridor includes the 500 kV Demyanskaya – Pyt-Yakh power line. This is because these lines are connecting subgraphs of regional power systems and account for the main share of the interregional capacity flow transit. Both corridors are connected to the largest generating capacities: the first corridor is directly connected to Karmanovskaya CHP and Votkinskaya HPP, as well as to Reftinskaya CHP. However, in the second case, when using a modified tool, this relationship is not clearly traced since the centrality is distributed over multiple edges proportionally to avoid overloading of the lines. Similarly, the 500 kV Demyanskaya – Pyt-Yakh line is connected to the Surgutskaya CHP cascade by neighbouring lines.

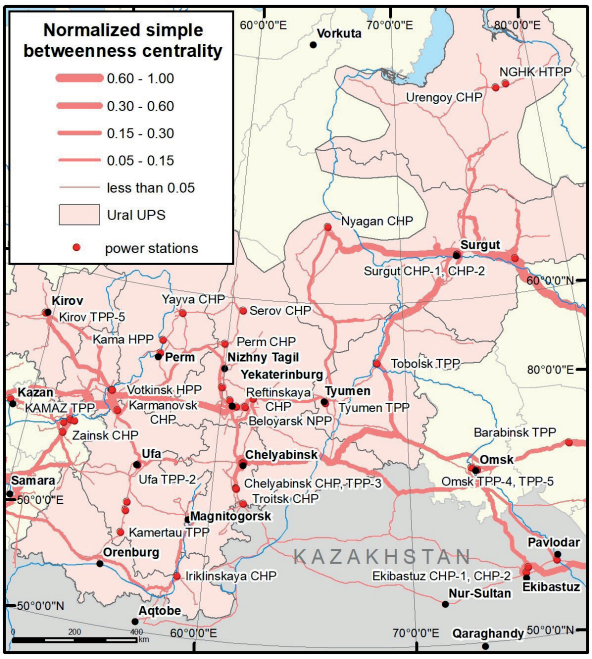

Fig. 6. Betweenness centrality calculated in NetworkX using standard function

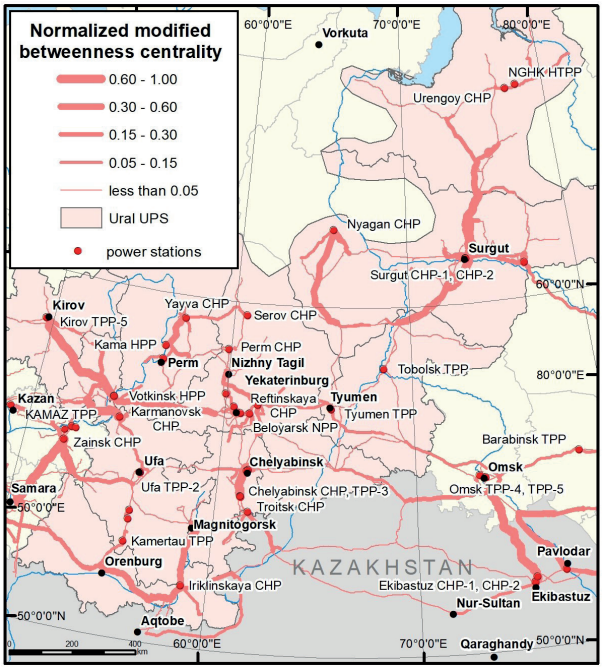

Fig. 7. Electrical grid centrality calculated using author's script

Visualization of the results clearly shows that the use of a modified tool for calculating the power grid centrality is more objective. When using the classic centrality calculation tool, routes are built between all nodes of the network, regardless of their functional purpose. Because of this, the resulting centrality values are inadequately overestimated. The flow of capacity is in the direction from the power plant to the substations, which is taken into account in the modified tool. Therefore, in the second method, the concentration of the most loaded lines is observed mainly near power plants. For example, let us consider the site to the east of Chelyabinsk. Here the power lines form a cycle that consists of the following 500 kV overhead lines: Kurgan – Vityaz, Voskhod – Vityaz, Voskhod – Barabinskaya, Kurgan – Aurora and Tavrichesky – Aurora. This cycle closes in Omsk through a corridor of several 220 kV power lines. When calculating the classic centrality, the normalized values on these edges of the graph are biased, since the traditional algorithm uses not only power plants, but also substations to calculate centrality. In this cycle, there are power plants only in Omsk. They were used for the calculation when using the modified tool (Fig. 8, 9).

As mentioned above, the classical centrality calculation tool does not consider multiple edges. In power systems, the presence of multiple edges is a standard solution for improving the reliability of energy supply: in the case of outage of one line a backup is used. When using the classic routing tool, only one of multiple edges is randomly selected and the entire load is distributed to it. In the modified tool, the resulting centrality value is distributed proportionally to the number of edges. This approach gives a more objective picture of the distribution of centrality values in the network. So, Fig. 10 and 11 show the 500 kV Reftinskaya CHP – Tyumen 1 and 2 lines. When using the classical centrality tool, only the 500 kV Reftinskaya CHP – Tyumen 2 participates in the calculation. In reality, the transit of electricity is carried out on both lines equally, so the results obtained using the modified tool are more accurate.

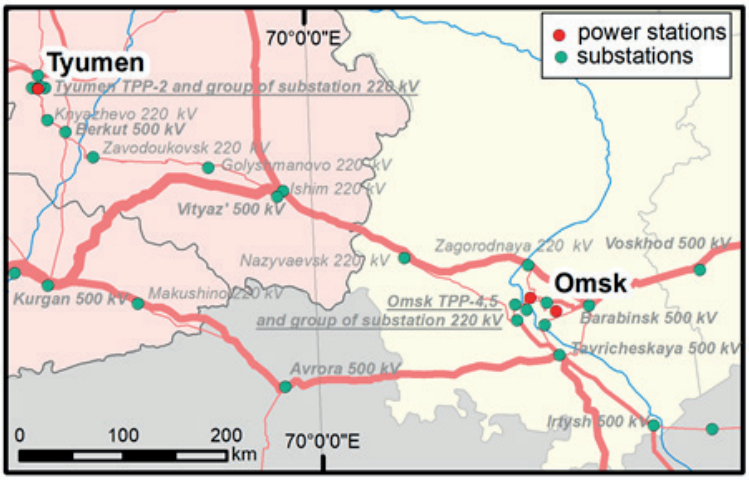

Fig. 8. Enlarged fragment of the territory of Omsk – visualization of betweenness centrality

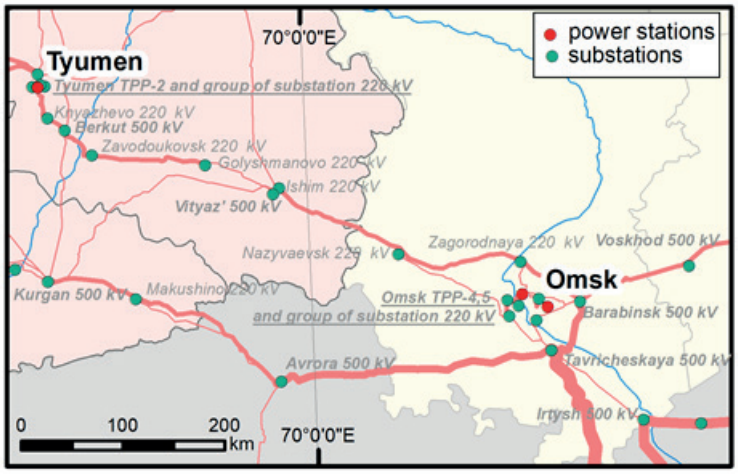

Fig. 9. Enlarged fragment of the territory of Omsk – visualization of electrical grid centrality

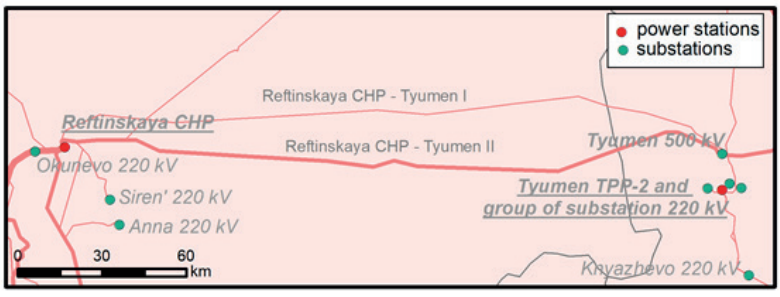

Fig. 10. Enlarged fragment of the territory of Tyumen – visualization of betweenness centrality

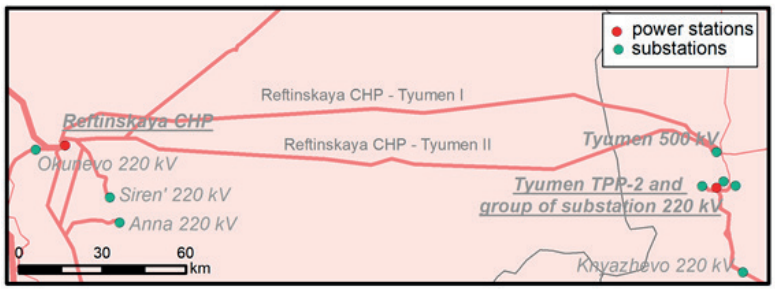

Fig. 11. Enlarged fragment of the territory of Tyumen – visualization of electrical grid centrality

Another aspect of power grids that affects the accuracy of calculations is the presence of hyperedges, that is, edges connecting three or more vertices. When using the classical centrality tool, the points for the calculation will also be used for branching along with power plants and substations, which may lead to incorrect centrality values. In a modified tool, branch points are not taken into account in the calculation.

It was found that the use of standard betweenness centrality is limited due to the characteristics of the grid graph: the presence of multiple edges, specific topomorphological relations, different functional types of vertices and some other features. Thus, the use of this index does not allow one to divide the nodes into sources and consumers and regulate the direction of the electricity flow. The vertices of branches are perceived by the algorithm as independent vertices and they also participate in the calculation of indices, distorting the results. Regulation of multiple edges usage in centrality calculations and interpretation of the received results is not obvious. Usage of electrical grid centrality allows to separate vertices and edges by functional types/hierarchy and assign them different roles in the network, as well as to manage topological relationships in the graph depending on the type of transport network. It is also recommended to topologically simplify the places of branching to avoid inaccuracies in the calculations and exaggeration of the centrality of power lines.

CONCLUSIONS

As a result, the calculation of centrality indices for power line networks allows to visualize some aspects of the spatial distribution of power grid sustainability. The less even distribution reflects the higher vulnerability of the power grid towards sleet and wind.

Firstly, the choice of network analysis index depends on the purpose of the work, quality and completeness of the initial data, and availability of special skills of the user. At the same time, it is very important to understand the difference in centrality measures in relation to power grids. Betweenness centrality is an illustrative index for any geographic network, but it does not consider some features of power grids. Suggested in this study electrical grid centrality index is more appropriate for analysis.

Secondly, we analyzed the spatial distribution of natural hazards, particularly sleet load and wind pressure, in the study area together with the results of network analysis. Additionally, we took into account the age of lines. Such analysis showed that joint use of knowledge about network features and natural hazards may help to identify bottlenecks in the power grid. A bottleneck is a «thin» element of a network that has very high betweenness centrality (>50% of maximum value), is located in zones of severe natural hazards impact (zoned 4 and 4) and/or has worn-out infrastructure.

Thus, using the electrical grid centrality and methods of geoinformation analysis, we identified a list of lines that are vulnerable to a particular factor. Special attention should be paid to lines that have a combination of these critical factors. It was found that two such lines are located in the southern part of the power system. They serve the largest enterprises of the Southern Urals and provide electricity to about 3.5 million people, as well as export electricity to Kazakhstan. Disconnecting these lines can cause serious damage to the population and economy of the entire Ural UPS.

Moreover, we could see that complicated sleet and wind conditions are connected with Ural Mountains, at the same time Ural is an old industrial region with many plants and populated cities, thus the power grid network began to develop quite a long time ago. So that, we have a set of aged power lines with high centrality vulnerable to strong wind and sleet.

REFERENCES

Atlas of natural and man-made hazards and emergency risks (2012). Moscow, Russia: Feoria Pub (in Russian).

Bugromenko V. N. (1987). Transport in territorial systems. (in Russian). Moscow: Nauka.

Chaitanya V.V.R.V., Mohanta D.K. and Reddy M.J.B. (2011). Topological analysis of eastern region of Indian power grid. In 10th International Conference on Environment and Electrical Engineering. 8-11 May 2011, Rome. Rome: IEEE, 449-453.

Chibryakov Ya.Yu. (2015). The development of cartographic methods for studies of the Russian railway network. Thesis (PhD). Moscow state university of Geodesy and Cartography (In Russian).

Crucitti P., Latora V. and Marchiori M. (2005). Locating critical lines in high-voltage electrical power grids. Fluctuation and Noise Letters, 2(5), 201-208.

Docs.cntd.ru (2015). Building acts 2.01.07-85 «Loads and impacts» [online] Available at: https://docs.cntd.ru/document/5200280 [Accessed 30 Apr. 2020] (in Russian).

Erdős P., Rényi A. (1959). On Random Graphs. I. Publicationes Mathematicae, 6, 290-297.

Faddeev A. (2016). Assessment of vulnerability of power systems of Russia, CIS countries and Europe to cascade accidents. Bulletin of Moscow University. Series 5: Geography, 1, 46-53 (in Russian).

Faybisovich D.L. (2012). Handbook of power systems design. Moscow: ENAS (in Russian).

FSK-EES.ru (2014). Standards of organization. [online] Available at: https://www.fsk-ees.ru/about/standards_organization [Accessed 20 Apr. 2020] (in Russian)

Garrison W.L. (1974). Connectivity of the Interstate Highway System. In: M.E. Eliot Hurst ed. Transportation Geography: Comments and Reading, New York: McGraw-Hill, 81-92.

Guimer R. and Amaral L.A.N. (2004). Modeling the world-wide airport network. The European Physical Journal B – Condensed Matter, 38(2), 381-385.

Hines P. and Blumsack S. (2008). A centrality measure for electrical networks. In: 41st Hawaii International Conference on Systems Science, 7-10 January 2008 Waikoloa, Big Island, HI, USA.

Kargashin P.E. Novakovskiy B.A., Prasolova A.I. and Karpachevskiy A.M. (2016). Study of the spatial configuration of power grids from satellite images. Geodesy and cartography, 3, 50-55. (In Russian).

Karpachevskiy A.M. and Filippova O.G. (2018). Mapping of emergency power systems based on open data. In: InterCarto/InterGIS 24, 19-22 July 2018, Petrozavodsk: Carelia science centre, 1, 202-211. (In Russian).

Karpachevskiy A.M. and Novakovskiy B.A. (2019). Opportunities of ArcGIS GIS tools usage for structural analysis of electrical networks. Geoinformatics, 2, 4-11. (In Russian).

Karpachevskiy A.M., Moskalev A.V. and Viktorov V.N. (2020). Classification and possible consequences of errors in vector mapping of power line routes in the Federal Grid Company's geoinformation system. Energy of united grid, 3(52), 42-49. (In Russian).

Karpachevskiy A.M. (2018). Cartographic support of planning of development of regional electric networks. Thesis (PhD). Lomonosov Moscow state university. (In Russian).

Minenergo.gov. Blackouts. [online] Available at: https://minenergo.gov.ru/node/267 [Accessed 09 Sept. 2021] (in Russian).

Nasiruzzaman A.B.M., Akter M., Nahida M., Md Apel and Pota H.R. (2018). Network theory based power grid criticality assessment. In PEDES 2018: Proceedings of the 2018 IEEE International Conference on Power Electronics, Drives and Energy Systems, Institute of Electrical and Electronics Engineers, Piscataway, N.J., 1-5.

Newman M. Networks. 2nd ed. Oxford: Oxford University Press.

Pagani A. and Aiello M. (2013). The power grid as a complex network: A survey. Physica A, 392(2013), 2688-2700.

PUE7.ru (2006). Wiring regulations [online] Available at: http://pue7.ru/pue7/sod.php [Accessed 25 Apr. 2020] (in Russian)

Rosas-Casals M., Valverde S. and Solé R.V. (2007). Topological vulnerability of the European power grid under errors and attacks. International Journal of Bifurcation and Chaos in Applied Sciences and Engineering, 17(7), 2465-2475.

Scott J. and Carrington P.J. (2011). The SAGE Handbook of Social Network Analysis. Los-Angeles: SAGE publications.

Shabliy O.I. (1976). Intersectoral territorial systems (problems of methodology and theory). Lviv: Higher school. (In Russian).

Tarkhov S.A. (2005). Evolutionary morphology of transport networks. Smolensk-Moscow:Universum. (In Russian).

Tikunov V.S. (1997). Modelling in cartography. Moscow: Moscow University Publishing. (In Russian).

Watts D.J. and Strogatz S.H. (1998). Collective dynamics of «small-world» networks. Nature. 393 (6684), 440-442.

Yang Y., Nishikawa T., and Motter A.E. (2017). Small vulnerable sets determine large network cascades in power grid. In: Science, 358(6365), DOI: 10.1126/science.aan3184.

RESEARCH PAPER

FORMATION CONDITIONS AND DEBRIS FLOW REGIME IN JIANGJIA RAVINE, YUNNAN, CHINA – APPLICABILITY OF RUSSIAN METHODOLOGY

Mingtao Ding[1], Aleksandr L. Shnyparkov[2], Pavel B. Grebennikov[2], Timur I. Khismatullin[2], Sergey A. Sokratov[2]*

[1]Southwest Jiaotong University, Faculty of Geosciences and Environment Engineering, The Western Park of the Hi-Tech Industrial Development Zone (Xipu Town), Chengdu, Sichuan, 611756, China

[2]Lomonosov Moscow State University, Faculty of Geography, Leninskie gory 1, Moscow, 119991, Russia

***Corresponding author:** sokratov@geogr.msu.ru

Received: September 20th, 2020 / Accepted: February 15th, 2022 / Published: March 31st, 2022

https://DOI-10.24057/2071-9388-2020-156

ABSTRACT. The requirements of the debris flows' parameters assessments vary from country to country. They are based on different theoretical and empirical constructions and are validated by data from different regions. This makes difficult comparison of the reported results on estimated debris flows activity and extent. The Russian normative documents for the debris flows' parameters calculations are based on empirically-measured parameters in wide range of geological and climatic conditions at the territory of former USSR, but still not cover all the possible conditions of debris flow formation. An attempt was made to check applicability of the Russian empirical constructions for the conditions of the debris flows formation in Yunnan, China, where unique long-term dataset of debris flows characteristics is collected by the Dongchuan Debris Flow Observation and Research Station. The results show, that in general the accepted in Russia methodology of calculation of the parameters of debris flows of certain probability corresponded well to the observed in Dongchuan debris flows characteristics. Some discrepancies (in the average debris flow depth) can be explained by unknown exact return period of the actually observed debris flows. This allowed to conclude that the presently adopted empirical dependencies based on country-wide (USSR) empirical data can be extrapolated up to the monsoon climate and geological conditions of Yunnan province.

KEY WORDS: debris flow, probability, formation, regime, Yunnan, China, normative documents

CITATION: Ding M., Shnyparkov A.L., Grebennikov P.L., Khismatullin T.I., Sokratov S.A. (2022). Formation Conditions and Debris Flow Regime in Jiangjia Ravine, Yunnan, China – Applicability of Russian Methodology. Vol.15, № 1. Geography, Environment, Sustainability, p 26-34 https://DOI-10.24057/2071-9388-2020-156

ACKNOWLEDGEMENTS: This study was concluded as a part of the research on the BRICS project "Improving risk management of landslide and debris flow hazards in mountainous area" with financial support of the Ministry of Science and Higher Education of the Russian Federation grant (BRICS2019-104, UI RFMEFI61319X0097).

Conflict of interests: The authors reported no potential conflict of interest.

INTRODUCTION

The study of debris flow activity in China has longstanding history. Research is actively conducted in such provinces as Sichuan, Yunnan, Gansu, Shaanxi, etc. In 1961, a unique Dongchuan Debris Flow Observation and Research Station (DDFORS) was organized in the north of Yunnan province. The station is positioned in the valley of the Jiangjia creek and is the right-hand tributary of the larger river Xiaojiang, being part of the Upper Yangtze River basin. Continuous year-round observations have been conducted at this station with automatic fixation of the main parameters of debris flows since 1987 (Fig. 1). Since 2000, the station was authorized to be the State Key Field Observation Station.

Differently from also unique Soviet (Vinogradova & Vinogradov 2017) or Swiss (Rickenmann et al. 2006) full-scale experimental cites, the station was originally focused on observing naturally-released debris flows. Such approach was also adopted in other regions later (i.e.: Comiti et al. 2014; Hürlimann et al. 2014; Marchi et al. 2002; etc.) and should be able to provide comparable with DDFORS's one datasets with time.

The station was registering timing of the first waves of released debris flows and the ends of the events. Also, the duration of the releases and quantity of waves in each case were recorded. The velocity of the debris flows was calculated based on stopwatch timer records of a wave passing two 200-m apart positions in the torrent. The height and the width of a debris flow had expert estimation in the beginning of the observations at the station. Later they were provided by specially-installed equipment. The debris flow discharge was calculated from the height, the width and the velocity. Sampling from the moving debris flows by volume-calibrated electronic sampling instrument was used for estimation of the flow density and the bulk concentration of the flows (Guo et al. 2020).

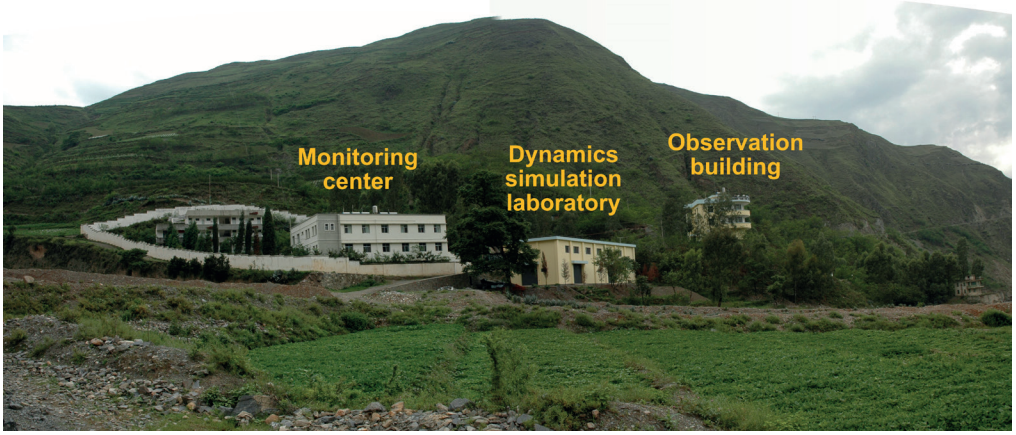

Fig. 1. Dongchuan Debris Flow Observation and Research Station, Institute of Mountain Hazards and Environment, Chinese Academy of Science

The debris flows investigations at DDFORS were covering various aspects: mechanism of debris flow formation (Cui et al. 2005; Chen et al. 2017; Kang & Hu 1990), debris flow movement (Chen et al. 2007; Guo et al. 2020; Li et al. 2003; Shu et al. 2007), debris flow deposition (Wang et al. 2007), analysis of various parameters of the debris flows, such as velocity (Li et al. 2012) and relation between the dimensions of the granular material and the characteristics of the released debris flows (Li et al. 2003), effects of topography, landslides and erosion, precipitation on debris flows formation (Chen et al. 2005; Guo et al. 2013; Tian 1987; Tian et al. 2020), debris flow forecasting (Hu et al. 2011; Liu et al. 2012), debris flow mitigation engineering (Lin et al. 2007), disaster evaluation and management of debris flow (Liu et al. 2009; Liu et al. 2002), direct observations of formation of debris flow (Cui et al. 2007; Huang et al. 2015; Fu et al. 2006; Li et al. 1983; Tian et al. 2007), direct observation of debris flow dynamics (Kang & Hu 1990), statics and rheology of debris flows (Chou 2007; Li et al. 1983), hazard and risk assessment of debris flows (Cui et al. 2013; Wei et al. 2010; Zhu & Tang 1996).

Assessment of the debris flow danger and risk, as well as planning of mitigation measures and building of defense infrastructure, require quantitative estimation of height, volumes and discharge rates of the debris flows. Long-term observational data on such parameters is preferable for construction of the probability curves and calculation of these values for a required probability. However, extensive observational data is absent in 99.9% of debris flows basins. As a substitute, numerous studies are directed to finding statistical relationships between the debris flows volumes and their repeatability (Gao et al. 2019; Helsen et al. 2002; Hungr et al. 2008; Jakob & Friele 2010; Johnson et al. 1991; Liu et al. 2008; Stoffel 2010; van Steijn 1996; etc.). Another approach to statistical methods of determination of characteristics of debris flows of certain probability is mathematical modeling of such characteristics (O'Brien et al. 1993; Rickenmann et al. 2006; Shieh et al. 1996; etc.). The studies show that the dependence between frequency and magnitude of debris flows follows the power law, with strong dependence on the area of a debris flow basin. The dependencies vary from region to region and cannot be directly transferred from one region to another. Additionally, more and more common become physical models of debris flows dynamics (RAMMS; Geobrugg, FLO-2D; etc.). For any approach the large amount of collected data on debris flow activity in the Jiangjia Valley is of much use for verification of the adopted methods of estimation of the conditions of formation and regimes of the debris flow of required probability. The Russian normative documents suggest methodology and require calculation of the parameters of debris flows for 1% probability. Extensive DDFORS dataset is much closer to such probability than most of other published empirical data. The other matter of interest is applicability of the Russian normative methodology for wider than used for construction of presently adopted in Russia dependencies range of possible conditions of debris flow formation (at least the Yunnan province, and possibly the territory of the People's Republic of China).

Area of investigation

Analysis of debris flows hazard, vulnerability and risk suggests that the regions of China with different extent of debris flow phenomena can be divided on five categories: extremely high-risk regions cover the area of 104 km^2, high risk regions – 283008 km^2, moderate risk regions – 3161815 km^2, low risk regions – 3299604 km^2, and extremely low risk regions covering the area of 2 681 709 km^2 (Liu et al. 2012). Maximum debris flow activity is registered in the west, south-west and north-east provinces of mainland China. More than 50 000 debris flow catchments documented there, covering around 48% of these territories (Cui et al. 2005).

The Jiangjia debris flow catchment is located in the northern part of Yunnan province, in the basin of Xiaojiang River (Fig. 2). The climate is of a monsoon type. Heavy rainfall occurs mainly from May till November. The morphology of the catchment is characterized by steep exposed slopes with intense erosion and landslide activity, which contributes to intensive debris flow activity. The catchment's area is 47.1 km^2. Weighted mean slope angle of debris flow channel – 141‰. The length of the channel up to the estimated target №1 – 12.1 km, target №2 – 12.1 km.

Conditions of the formation of the debris flows

Relief: The debris flow catchment of Jiangjia is a U-shaped steeply inclined ravine. Absolute altitude varies from 2880 to 1100 m. The elevation of the slopes above the bottom of the ravine is 400–500 m. Mean absolute altitude of the catchment is 2045 m a.s.l. The inclination of the slopes varies between 600 and 700‰. The slopes are complicated by a large number of erosion-denudation funnels, in which intense erosion activity with a large number of fans occurs. This material, supplied from erosion-denudation funnels to the mainstream, is an additional potential debris flow material. The inclination of the debris flow channel in the upper part of the basin reaches 500‰, in the middle part about 110–120‰ and decrease down to 70‰ in the estuary of the catchment. The width of the bottom of the ravine varies from the first tens of meters to 170 m at the

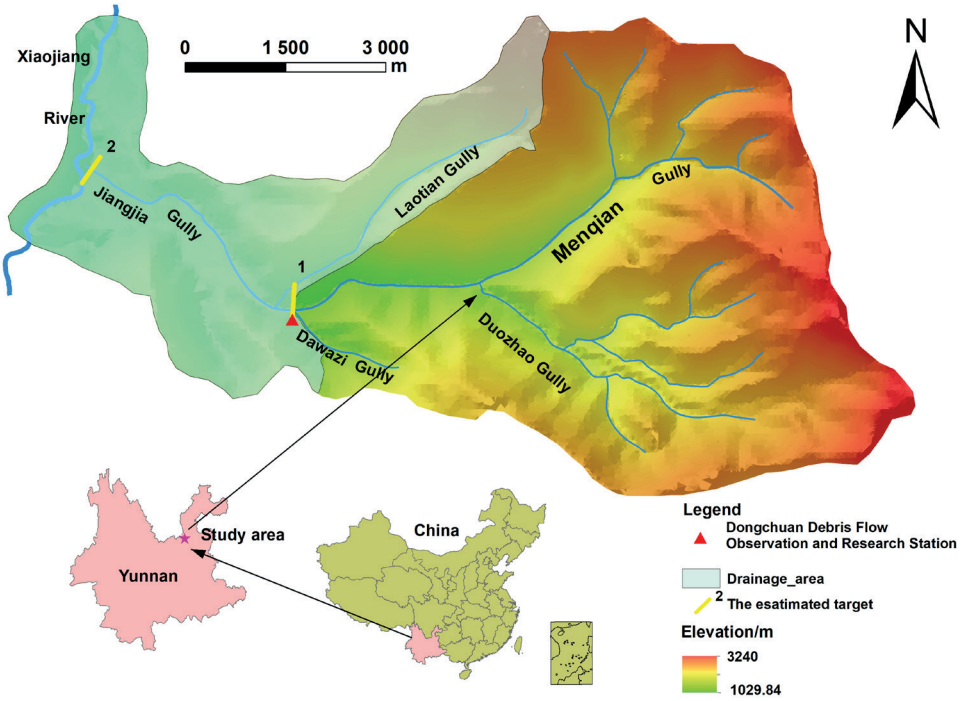

Fig. 2. Research area location and location of the target control points in Jiangjia

widest point near the Dongchuan Debris Flow Observation and Research Station.

Geology: The Jiangjia valley lays along seismic faults and frequent earthquakes result in bedrock destruction and fragmentation. The outcrops are dominated by pre-Cambrian epimetamorphic rocks, such as slate, phyllite, and shale, all being easily weathered. Accordingly, quaternary diluvium and colluvium are widely distributed on slopes (Tian et al. 2020). About 80% of exposed bedrocks are crumbling and weakly metamorphosed. The main sources of the solid material for debris flows are landslides and debris flows' deposits at torrents' beds (Tian et al. 2020). The volume of loose deposits of landslides sites which are material for potential debris flows is estimated as 1.23×109 м^3 (Du et al. 1987) and at torrents' beds of about 7.5×108 m^3 (Yang 1997). The thickness of the loose deposits on the slopes reaches several tens of meters (Huang et al. 2015). Loose material is represented mainly by debris particles up to 10–15 cm in diameter. The filler consists of sands, loams and clay particles with the prevalence of the former. It is important that the content of the clay particles is high – 10–15% (Tian et al. 2020), which provides conditions for formation of mud-stone and mud flows.

Climate: The region lay in monsoon climate zone. The climatic conditions of the formation of the debris flows can be provided by the data of the closest to the Jiangjia site Huize weather station. Huize is situated 25 km NNW from the debris flow basin of interest. The absolute altitude of its position is 2114 m a.s.l., which is close to the mean absolute altitude of the debris flow basin. The meteorological observation at Huize were started in 1957. The published rows of data start from 1980.

Throughout the year, the air temperatures are above 0°C with maximum values in the summer period (Table 1).

Precipitation falls in liquid form throughout the year. Most of the precipitation falls in the summer–autumn period – about 80–90% of the totals for year (Huang et al. 2015).

According to the Huize weather station data, the average annual precipitation is 784.4 mm (Table 2). The maximum amount is in June–August – 57% of annual precipitation.

Vegetation: Vegetation cover is spread over only 39.5% of the debris flow catchment area, and only 4.2% of it is occupied by forests (Cui et al. 2005; Zhuang et al. 2015; Huang et al. 2015). Currently, there is an increasing degradation of vegetation as a result of intensification of economic activity. The distribution and nature of vegetation in the Jiangjia Ravine does not prevent origination of debris flows. Most of the slopes in the ravine are not covered in forest or sod. Only on the right side of the valley, higher than 2000 m above sea level, there is forest vegetation, which sharply decreases the activity of erosion processes in place (Fig. 3).

Seismic conditions are favorable for the formation of solid debris material, due to the fact that the study area is located in active seismic zone. In the Yunnan province, earthquakes of magnitude higher than 5 points on the Richter scale have been repeatedly registered (Daniell 2010; Zhao et al. 2013):

Table 1. Mean monthly and annual air temperatures, °C, Huize weather station (https://en.tutiempo.net/climate/ws-566840.html)

I	II	III	IV	V	VI	VII	VIII	IX	X	XI	XII	Annual
12.0	14.4	19.0	21.7	23.0	23.3	23.6	23.4	21.0	18.0	14.8	12.0	18.9

Table 2. Monthly and annual average amount of precipitation, mm, Huize weather station (https://en.tutiempo.net/climate/ws-566840.html)

I	II	III	IV	V	VI	VII	VIII	IX	X	XI	XII	Annual
11.8	11.2	20.7	32.5	77.6	143.3	161.8	144.4	95.9	53.8	25.8	5.6	784.4

Fig. 3. The right side (the slope is of northern exposition) of the Jiangjia Ravine, with forest vegetation above 2000 m (Google Earth image 04.01.2020)

1. On January 5, 1970, an earthquake occurred in Yunnan Province with a magnitude of 7.7 on the Richter scale. 15621 people were killed, 32431 were injured.
2. On July 22, 2006, an earthquake occurred in Yunnan, 90 kilometers from Zhaotong City, with a magnitude of 5.1 on the Richter scale. 13 people were killed and 41 more were injured. 56 buildings were destroyed.
3. On February 25, 2010, an earthquake occurred 90 km northwest of Anning and its suburbs Lianzhang, with a magnitude of 5.2 on the Richter scale. 35 people were injured, residential buildings were damaged. Economic damage amounted to about 52 million US dollars.
4. August 29, 2010, on the border of the provinces of Yunnan, Sichuan and Guizhou, an earthquake of 4.9 on the Richter scale occurred. The epicenter of the earthquake was located 71.6 km west of the city of Zhaotong (Yunnan Province). 14 people were injured, more than 1000 houses were destroyed. Economic damage amounted to about 13 million US dollars.

An analysis of the conditions of the relief, vegetation, seismic, climate and lithology showed that there are favorable conditions for the formation of debris flows in the Jiangjia valley.

Sources of data and methodology of calculations

The research involved wide list of scientific publications about the debris flow hazards and activity in Yunnan province of China, as well as on information collected from the Internet. Data collected in the Dongchuan Debris Flow Observation and Research Station in Jiangjia Ravine during years 1966–1967, 1974–1975, and 1982–2001 was used for the analysis of regime of debris flows. These data regarding registered debris flow include: date of a debris flow event, duration of event, maximum flow height, density of the solid material and density of debris flow mixture, the debris flow discharge, volume of the debris flow – overall and of its solid part, velocity of the debris flow.

Statistical processing of the data allowed to determine the period of the formation of debris flows, the duration of the debris flow hazard period, the duration of the debris flow main and maximum dangerous periods, the frequency of the debris flow events, the genetic types of debris flows, the type by the ratio of the solid and liquid components of the debris flow, the long-term average and maximal debris flow volumes, average and maximum values of debris flow velocity, debris flow depth.

The debris flow hazard period is the period between the first and the last date of debris flow occurrence during a calendar year; the debris flow main danger period is determined by a time when 90% of debris flow events occur, and the maximum danger period – when 50% of the events take place (Perov 2014). A methodology is developed in Russian Federation to determine the duration of these periods (Belaya 2005). The methodology is based on precipitation and temperature regimes over year. The research area belongs to the type № 18. This type is characterized by several dry months in a year, with excessive moisture, and a monsoon type of climate. According to this methodology, a month refers to the main debris flow danger period if the ratio of the amount of precipitation for this month is greater than or equal to 60% of the amount of precipitation for the month with the maximum value. The debris flow maximum danger period includes months with the same ratio of more than or equal to 80%.

The equations for determining the debris flow volume of 1% probability are as the following (VSN 03-76):

Maximum debris flow discharge of 1% probability in the Jiangjia Ravine is calculated by equation 1:

$$Q_{cp} = q_{1\%} m_a \lambda'_p \left(\frac{1}{W_{otP}} \right)^{1.08} F \qquad (1)$$

where $q_{1\%}$ is a module of maximum rainfall run-off with probability of exceeding P=1%, m^3 ($s \times km^2$), determined from (VSN 03-76: Table 9). It depends on attain time of a debris flow to an estimated target and on the hydrological area. The latter was taken as № 2 in accordance ещ (VSN 03-76: Table 10). The climatic conditions of the Jiangjia debris flow catchment are closest to that;

m_a – coefficient depending on hydrological area, where the catchment is situated, determined according to (VSN 003-76: Table 10) and by equation: $m_a = H_{1\%}/250$. The maximal daily precipitation of 1% probability is equal to 109 mm, thus: $m_a = 109/250 = 0.43$. The value of m_a should be in the range 0.75–1.25, which makes it 0.75 for presented calculations;

λ'_p – transition coefficient from debris flow discharge with P = 1% to discharge of another probability, determined according to (VSN 03-76: Table 11) and it is 1 for $P = 1\%$;

W_{otP} – The coefficient of fluidity of the debris flow material for the peak phase and is determined by equations 3 and 4 below;

F – debris flow catchment area above a target, km^2.

Assessment of the volumetric concentration and discharge of a debris flow requires estimation volumetric concentration of the solid constituent (So) of the debris flow. It depends on the mean bed slope and the coefficient of the debris flows activity μ. The latter is calculated by:

$$\mu = \frac{\sum F_i \times Z_i}{F} \quad (2)$$

where F_i – areas of individual sections of the debris flow catchment, that are characterized by their specific coefficients of debris flow activity z_i, that are determined by (VSN 03-76: Table 1).

The sections with different landscape conditions in Jiangjia basin were identified at Google Earth Pro-provided image and corresponded to different debris flow activity according to (VSN 03-76: Table 1). The coefficients are varying from 0.7 to 1.0, for heavy erosion cuttings filled by thick layer of loose material, to 0.005–0.01 for forested and matted areas with no erosion. The calculations by (2) gave the following results: For target I the coefficient of the debris flows activity is 0.73, for target II – 0.66.

Debris mass fluidity factor (W_{otP}) for the peak phase of debris flow and as average ($\overline{W}_{otP}$) are, respectively:

$$W_{otP} = 1 - S_{oP} / S_{pt}, \quad (3)$$

$$\overline{W}_{otP} = 1 - S_{oP} / S_{pt}, \quad (4)$$

where S_{oP} and $\overline{S}_{oP}$ are the volumetric concentrations of the solid debris flow component for the peak phase (VSN 03-76: Table 5) and the average during the event (VSN 03-76: Table 6) respectively with a given probability of exceeding 1%;

S_{pt} – the maximal volumetric concentration of solid material in a debris flow, at which it loses its fluidity properties, in this particular case assumed to be 0.705.

Debris flow volume (both solid and liquid components) $W_{c1\%}$, corresponding to maximal discharge depending on the volume of rainfall flood $W_{b1\%}$ and debris saturation coefficient φw:

$$W_{c1\%} = W_{b1\%} \varphi_w, \quad (5)$$

where:

$$W_{b1\%} = q_{1\%} m_a \lambda'_{1\%} F C_{1\%} 10^3 \quad (6)$$

$$\varphi_w = 1 / W_{otP}, \quad (7)$$

$C_{1\%}$ – debris flood coefficient, that depends on the duration of the run-up time (τ) and the probability of an annual excess of 1% of the maximum debris flow discharge, determined from (VSN 03-76: Table 12) by interpolation.

The volume of sediment transport of solid material (as a solid component) for calculated wave of a debris flood ($W_{\tau P}$) should be determined as:

$$W_{\tau 1\%} = \overline{S}_{oP} W_{c1\%} \quad (8)$$

The volume of debris flow deposit (in a friable body) at a target control point, corresponding to the estimated discharge with 1% of exceeding probability is determined by (VSN 03-76: p. 16, Eq. 27):

$$W_{fr1\%} = W_{\tau 1\%} \left(1 + \varepsilon_{dep}\right) I_y^{2/3} / \left(5 + I_y^{2/3}\right) \quad (9)$$

where: $W_{\tau 1\%}$ – the volume of loss of solid material (in a dense body) for the calculated wave of the debris flood;

I_y – average slope of the debris channel within the estimated runoff, ‰;

ε_{dep} – porosity coefficient of fresh debris flow deposits (VSN 03-76: Table 8).

The velocity of debris flow V_{df} is calculated as (VSN 03-76: Equation 33):

$$V_{df} = 0.56 Q_c^{0.2} I^{0.3} W_{dep1\%}^{0.2} \quad (10)$$

And its average depth h_{av} (VSN 03-76: Equation 34):

$$H_{av} = 0.245 Q_{c1\%}^{0.4} / I_y^{1/15} W_{otP}^{4/15} \quad (11)$$

Maximum debris channel depth before erosion is calculated as (VSN 03-76: part 4.4, Equation 41):

$$h_{\max} = 1.5 h_{av}, \quad (12)$$

Conditional width B_y (m) of debris flow channel in its top corresponding to the estimated debris flow discharge rate $Q_{c1\%}$ is calculated as (VSN 03-76: Equation 28):

$$B_y = 7.1 Q_{c1\%}^{0.4} W_{ot1\%}^{0.067} / I_y^{0.23} \quad (13)$$

RESULTS

Calculations of debris flow parameters of 1% probability were carried out for two target control points (Fig. 2).

Studies of debris flows at the Dongchuan Debris Flow Observation and Research Station have shown, that the main genetic type of debris flows in the Jiangjia Ravine are rain debris flows, the origination of which corresponds with a period of intense monsoon rains. Seismogenic debris flows can also form here, due to intense seismic activity.

Powerful earthquakes and heavy rainfall can lead to the formation of landslides that block the channels of watercourses. The formation of landslide dams and their subsequent breaching and rapid erosion can also lead to the formation of debris flows. Thus, in addition to the erosion-shear mechanism of the formation, breaching mechanism can also occur.

The average slurry density according to the observed data is 2022 kg/m^3. The average density of debris/mud flow is 1680 kg/m^3, varying from 1140 to 2044 kg/m^3 (Data… 1997; 2006; 2007).

According to the recorded data from the Dongchuan Debris Flow Observation and Research Station, the debris flow hazard period lasts from early May to the first of September, its duration – 4 months. Table 3 presents the duration of different debris flow danger periods, obtained by the methodology of N.L. Belaya and from the recorded data. According to V.F. Perov (2014) the debris flow principal danger period corresponds to the time period of 90% of all the debris flows releases, while the maximal danger period corresponds to 50% releases time period.

Table 3. Comparison of duration of different types of debris flow danger periods according to N.L. Belaya (2005) and the actual data, months (Data… 1997; 2006; 2007)

Type of dangerous period	Methodology	
	according to N.L. Belaya (2005)	from recorded data*
Debris flow hazard period	V–IX	V–IX
Debris flow principal danger period	VI–VIII	VI–VIII
Debris flow maximal danger period	VI–VII	VII–VIII

* based on the data of the Dongchuan Debris Flow Observation and Research Station.

Analysis of the comparison of the obtained durations of different types of the debris flow danger period shows that the durations of the debris flow hazard period and the main danger period completely coincide. The duration of debris flow maximum danger period is 2 months in both cases, but according to the calculations this period is shifted a month earlier, which is obviously due to very large precipitation in June (see Table 1).

According to the actual long-term data, the duration of debris flow hazard period varies from 3 (1993) to 122 (1989) days, with an average value of 58 days. The earliest date of debris flow event is May 3, the latest is September (Data… 1997; 2006; 2007).

The occurrence of debris flow is observed annually, on average up to 10 times per season (Zhuang et al. 2011) In some years, with a small amount of liquid precipitation, from 2 (1993) to 4 (1988) events during the hazard period. In years of high humidity, the number of the events reaches 22 cases (1991) (Data… 1997; 2006; 2007).

The parameters of the recorded debris flows (Data… 1997; 2006; 2007) are as the following:

The flowing duration changes from half a minute to 16.5 minutes (Data… 1997; 2006; 2007);

The average debris flow discharge for all recorded events is 722 m^3/s, and its maximal value reaches 4687.5 m^3/s (Data… 1997; 2006; 2007).

The change in maximal daily precipitation amount from 1980 till 2020 is shown at Fig. 4. There is slight positive trend in this parameter starting from 1990th.

The registered maximal daily amount of precipitation was 98.7 mm (in 1998). To estimate the maximal daily precipitation amount of 1% probability the existent raw of data was used (Fig. 4) and provided 109 mm (Fig. 5).

The volume of debris flows averages 327 876 m^3, ranging from 1 000 to 2 025 400 m^3. The average volume of the slurry component in the debris flow is 215 579 m^3, reaching up to a maximum of 1 266 334 m^3 (Data… 1997; 2006; 2007).

The average velocity of the observed debris flows is 9.5 m/s, with a maximum value of 14.4 m/s (Data… 1997; 2006; 2007).

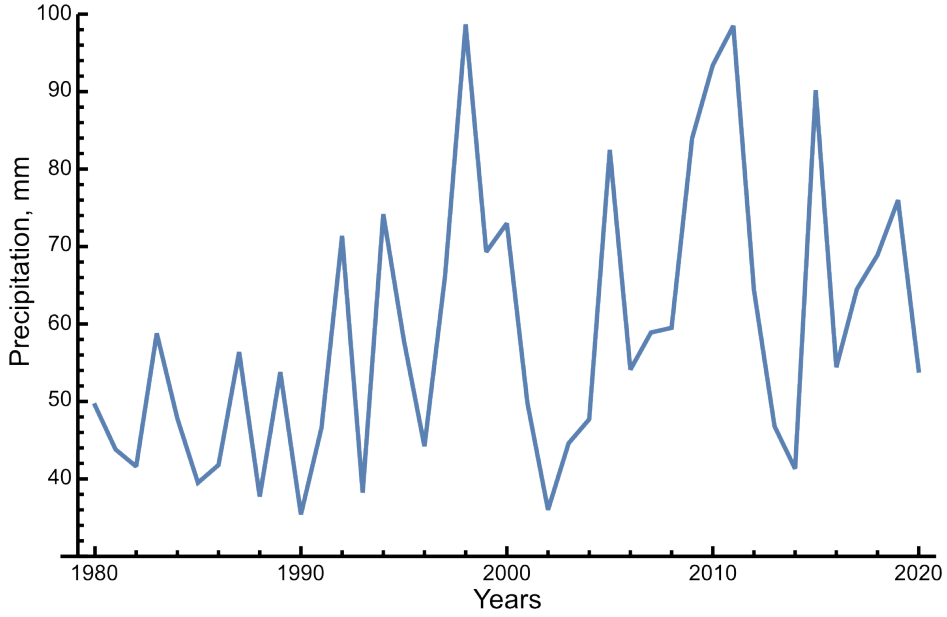

Fig. 4. Variation in maximum daily precipitation values for the time period from 1980 to 2020

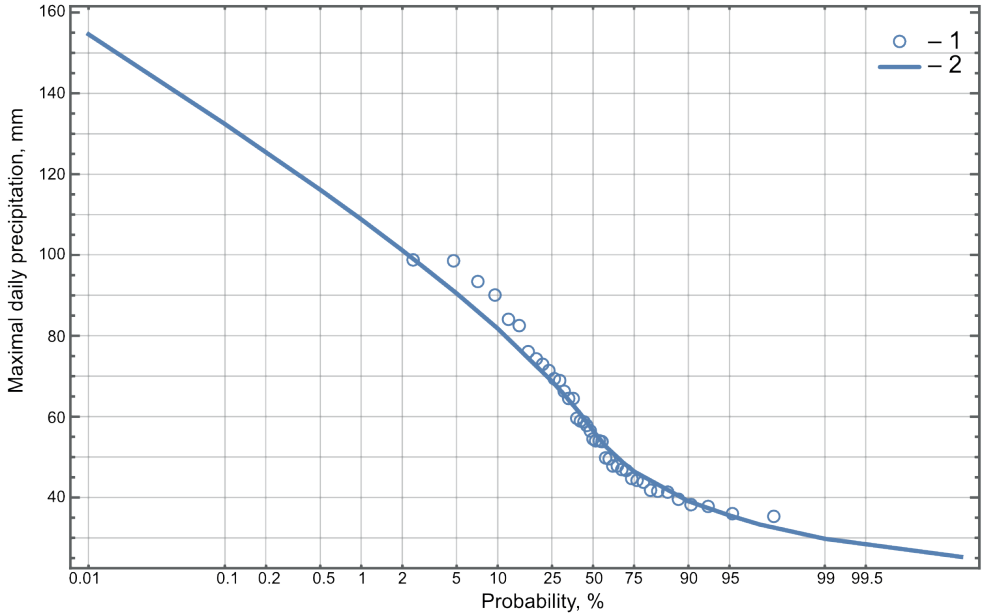

Fig. 5. The probability curve for maximum daily precipitation at the Huize weather station: 1 – the distributed registered values; 2 – the Pearson probability curve of type III, $C_s/C_v=3$

The average flow depth of debris flows is 1.88 m, with a maximum value of 6.49 m (Data… 1997; 2006; 2007).

To compare the observed parameters of debris flows with the ones calculated according to (VSN 03-76), a probability curves of the debris flow parameters were constructed based on the data from the Dongchuan Debris Flow Observation and Research Station (Data… 1997; 2006; 2007). According to such calculations, the volume of a debris flow with the probability of occurrence equal to 1% at target No. 1 (Fig. 2) is 2 667 028 m^3. The debris flow discharge of 1% probability was found to be 5105.5 m^3/s (Fig. 6).

DISCUSSION

An analysis of the results of comparing the calculated and recorded parameters of the debris flows shows that the results of calculations by the method proposed in (VSN 03-76) are close enough to the actual data: For peak discharge the error was 5.3%, for the debris flow volume it was 17.2%, for the volume of solid component the error was 1.2%, for the debris flow velocity the error was 5.6%.

Comparison of the calculated parameters of the debris flows for 1% probability with the values provided by the probability curves based on the recorded data can be interpreted as 10–15% underestimation. The exceptions are the velocity of a debris flow (56.4% lower) and the debris flow depth (7.3% overestimation). The latter has up limits. In Russia it is accepted that the maximal debris flow velocities are 15–16 m/s (Perov 2014). So, the comparison of the calculated data with the curves is not correct. Same as a construction of a probability curve for the debris flows velocities. Since the target position for the debris flow characteristics observation is not rigid, there is possibility both for underestimation and overestimation of the debris flows parameters.

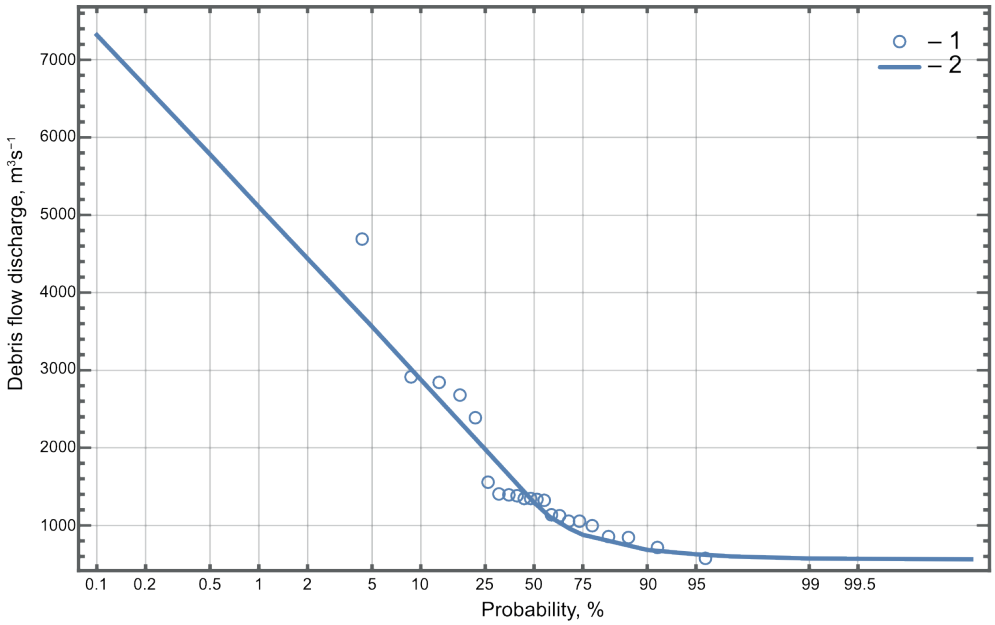

Fig. 6. The probability curve for the debris flow discharge: 1 – the distributed registered values; 2 – the Pearson probability curve of type III, $C_s/C_v=3$

Table 4. Calculated and observed parameters of debris flows with 1% probability of occurrence in the Jiangjia Ravine

	Target (Fig. 2)	Q_c, m^3/s	$W_{c1\%}$, m^3	$W_{т1\%}$, m^3	V_{sel}, m/s	h_{cp}, m	h_{max}, m	B_y, m
Based on (VSN 03-76)	1	4429.8	2375248	1282634	8.4	7.3	11.0	56.7
	2	6072.7	3068498	1521975	8.7	7.5	11.3	71.6
	1 (probability curves)	5105.5	2667028	1602199	19.3	6.8	–	–
Actual maximal data	1	4678.0	2025400	1266324	8.9	6.5	–	–
The ratio of (VSN 03-76)-provided to the actual data, %	1	–5.3	17.2	1.2	–5.6	12.3	–	
The ratio of (VSN 03-76)-provided tothe actual data for 1% probability, %	1	–13.2	–10.9	–15.7	–56.4	7.3	–	

Q_c – peak discharge debris flow, m^3/s;
$W_{c1\%}$ – debris flow volume (both slurry and fluid components), m^3;
$W_{т1\%}$ – the volume of sediment transport of solid material (in a slurry component) for calculated wave of the debris flood, m^3;
V_{sel} – debris flood velocity, m/s;
h_{cp} – average debris flow depth, m;
h_{max} – maximum debris flow depth, m;
B_y – debris flow width, m, м.

CONCLUSIONS

The observational data from the Dongchuan Debris Flow Observation and Research Station is suitable for testing new methodologies for debris flow parameters estimating and for testing the existent ones. Based on the long-term accepted and used in Russia methodology the parameters of debris flow regime, in particular, the duration of the debris flow hazard period and number of parameters of debris flows, could be estimated for considerably different geological and climatic conditions. The obtained values are in good agreement with the results of actual observations. The observed maximal parameters of debris flows, required for territorial planning and engineering construction also agree well with the values calculated by the Russian normative documents, with the estimated error of 10–15%.

Considering the above, the Russian methodology for determining the parameters of debris flows with various probability of occurrence, and the methodology for determining the duration of the debris flow hazard period, can be used in the regions of People's Republic of China.

REFERENCES

Belaya N.L. (2005). Modeling of intra–annual distribution of rainstorms in mountain regions of the world. Diss. on the degree of Candidate of geographical Sciences. Moscow, 187 (in Russian).

Chen J., He Y.P., Wei F.Q. (2005). Debris flow erosion and deposition in Jiangjia Gully, Yunnan, China. Environmental Geology, 48(6), 771–777, DOI: 10.1007/s00254–005–0017–z.

Chen N.S., Zhu Y.H., Huang Q. (2017). Mechanisms involved in triggering debris flows within a cohesive gravel soil mass on a slope: A case in SW China. Journal of Mountain Science, 14(4), 611-620, DOI: 10.1007/s11629-016-3882-x.

Chen S.C., Wu H.Y., Peng S.H. (2007). Experimental and numerical comparison of the density current movement induced by instantaneous inflow on steep slope. In: C.-L. Cheng & J.J. Major, eds., Proceeding Debris–flow hazards mitigation. Chengdu. Mechanics, Prediction, and Assessment. Rotterdam: Millpress Science Publishers, 241-250.

Chou H.T., Cheung Y.L., Zhang S.C. (2007). Calibration of infrasound monitoring system and acoustic characteristics of debris–flow movement by field studies. In: C.-L. Cheng & J.J. Major, eds., Proceeding Debris–flow hazards mitigation. Chengdu. Mechanics, Prediction, and Assessment. Rotterdam: Millpress Science Publishers, 571-580.

Comiti F., Marchi L., Macconi P., Arattano M., Bertoldi G., Borga M., Brardinoni F., Cavalli M., D'Agostino V., Penna D., Theule J. (2014). A new monitoring station for debris flows in the European Alps: first observations in the Gadria basin. Natural Hazards, 73(3), 1175-1198, DOI: 10.1007/s11069-014-1088-5.

Cui P., Chen X.P., Wang Y.Y., Hu K.H., Li Y. (2005). Jiangjia Ravine debris flows in the southwestern China. In: M. Jakob & O. Hungr, eds., Debris flow hazards and related phenomena. Berlin Heidelberg: Springer-Verlag, 565-594, DOI: 10.1007/3-540-27129-5_22.

Cui P., Zhu Y.Y., Chen J., Han Y.S., Liu H.J. (2007). Relationships between antecedent rainfall and debris flows in Jiangjia Ravine, China. In: C.-L. Cheng & J.J. Major, eds., Proceeding Debris–flow hazards mitigation. Chengdu. Mechanics, Prediction, and Assessment. Rotterdam: Millpress Science Publishers, 3-10.

Cui P., Zou Q., Xiang L.-z., Zeng Ch. (2013). Risk assessment of simultaneous debris flows in mountain townships. Progress in Physical Geography, 37(4), 516-542, DOI: 10.1177/0309133313491445.

Daniell J. (2010). Damaging Earthquakes Database. 2010 – The Year in Review. Australian Earthquake Engineering Society; «M 5.2 – Yunnan, China». www.earthquake.usgs.gov. [Accessed January 3, 2020].

Data collection of Dongchuan debris flow observation and research station Chinese Academy of Sciences (1961–1984). (2006). Z. Jun, X. Gang, eds. Science Press. (in Chinese).

Data collection of Dongchuan debris flow observation and research station Chinese Academy of Sciences (1995–2000). (2007). Z. Jun, X. Gang, eds. Science Press. (in Chinese).

Data collection of kinematic observation of debris flows in Jiangjia Ravine, Dongchuan, Yunnan (1987–1994). (1997). Z. Jun, X. Gang, eds. Science Press. (in Chinese).

Du R.H., Kang Z.C., Chen X.Q. (1987). Investigation and prevention planning of debris flows in Xiaojiang River, Yunnan. Chongqing: Chongqing Branch of Science and Technology Literature Press. (In Chinese).

Fu X.D., Wang G.Q., Kang Z.C., Fei X.J. (2006). Planar velocity distribution of viscous debris flow at Jiangjia Ravine, Yunnan, China: A field measurement with two radar velocimeters. Wuhan University Journal of Natural Sciences, 12(4), 531-538, DOI: 10.1007/s11859-006-0297-5.

Gao Y.C, Chen N.S, Hu G.S, Deng M.F. (2019). Magnitude–frequency relationship of debris flows in the Jiangjia Gully, China. Journal of Mountain Science, 16(6), 1289-1299, DOI: 10.1007/s11629–018–4877–6.

Guo X., Lia Y., Cuia P., Yana H., Zhuang J. (2020). Intermittent viscous debris flow formation in Jiangjia Gully from the perspectives of hydrological processes and material supply. Journal of Hydrology, 589, 125-184, DOI: 10.1016/j.jhydrol.2020.125184.

Guo X.J., Cui P., Li Y. (2013). Debris flow warning threshold based on antecedent rainfall: a case study in Jiangjia Ravine, Yunnan, China. Journal of Mountain Science, 10(2), 305-314, DOI: 10.1007/s11629-013-2521-z.

Helsen M., Koop P., Van Steijn H. (2002). Magnitude–frequency relationship for debris flows on the fan of the Chalance torrent, Valgaudemar (French Alps). Earth Surface Processes and Landforms, 27(12), 1299-1307, DOI: 10.1002/esp.412.

Hu M., Wang R., Shen J. (2011). Rainfall, landslide and debris flow intergrowth relationship in Jiangjia Ravine. Journal of Mountain Science, 8(4), 603-610, DOI: 10.1007/s11629-011-2131-6.

Huang Y., Ding M., Miao Ch., Wang J., Zhou P. (2015). Characteristics and evolution of debris flow motion in Jiangjia gully in Yunnan province. Resources and Environment in the Yangtze Basin, 24(8), 1434-1442. (in Chinese).

Hungr O., McDougall S., Wise M., Cullen M. (2008). Magnitude–frequency relationships of debris flows and debris avalanches in relation to slope relief. Geomorphology, 96(3), 355-365, DOI: 10.1016/j.geomorph.2007.03.020.

Hürlimann M., Abancó C., Moya J., Vilajosana I. (2014). Results and experiences gathered at the Rebaixader debris-flow monitoring site, Central Pyrenees, Spain. Landslides, 11(6), 939-953, DOI: 10.1007/s10346-013-0452-y.

Jakob M, Friele P. (2010). Frequency and magnitude of debris flows on Cheekye River, British Columbia. Geomorphology, 114(3), 382-395, DOI: 10.1016/j.geomorph.2009.08.013.

Johnson P.A, McCuen R.H, Hromadka T.V. (1991). Magnitude and frequency of debris flows. Journal of Hydrology, 123(1-2), 69-82, DOI: 10.1016/0022-1694(91)90069-T.

Kang Z.C., Hu P.H. (1990). Measurements for kinematic parameters of debris flows in Jiangjia Gully. In: J.S. Wu, Z.C. Kang, L.Q. Tian, eds., Observation and study of debris flows in Jiangjia Gully, Yunnan. Beijing: Science Press, 99-140. (in Chinese).

Li J., Yuan J., Bi Ch., Luo D.F. (1983). The main features of the mudflow in Jiangjia Ravine. Zeitschrift für Geomorphologie, 27(3), 325-341, DOI: 10.1127/zfg/27/1983/325.

Li Y., Kang Z.C., Yue Z.Q., Tham L.G., Lee C.F., Law K.T. (2003). Surge waves of debris flow in Jiangjia Gully, Kunming, China. In: L. Picarelli, ed., Fast slope movements prediction and prevention for risk mitigation, Naples, May 11-13, 1. Bologna: Patron Italy, 303–307.

Li Y., Liu J.J., Hu K.H., Su P.C. (2012). Probability distribution of measured debris–flow velocity in Jiangjia Gully, Yunnan Province, China. Natural Hazards, 60(2), 689-701, DOI: 10.1007/s11069-011-0033-0.

Li Y., Yao S.F., Hu K.H., Chen X.Q., Cui P. (2003). Surges and deposits of debris flow in Jiangjia Gully. Journal of Mountain Science, 21(6), 712-715. (in Chinese).

Lin P.S., Lin J.Y., Chan K.F., Chou W.H. (2007). An experimental study of the impact force of debris flows on slit dams. In: C.-L. Cheng & J.J. Major, eds., Proceeding Debris–flow hazards mitigation. Chengdu. Mechanics, Prediction, and Assessment. Rotterdam: Millpress Science Publishers, 647-658.

Liu J.J., Li Y., Su P.C., Cheng Z.L. (2008). Magnitude–frequency relations in debris flow. Environmental Geology, 2008, 55(6), 1345-1354, DOI: 10.1007/s00254-007-1083-1.

Liu K.F., Li H.C., Hsu Y.C. (2009). Debris flow hazard assessment with numerical simulation. Natural Hazards, 49(1), 137-161, DOI: 10.1007/s11069-008-9285-8.

Liu X., Yu Ch., Shi P., Fang W. (2012). Debris flow and landslide hazard mapping and risk analysis in China. Frontiers of Earth Science, 6(3), 306-313, DOI: 10.1007/s11707-012-0328-9.

Liu X., Yue Z.O., Tham L.G., Lee C.F. (2002). Empirical assessment of debris flow risk on a regional scale in Yunnan Province, Southwestern China. Environmental Management, 30(2), 249-264, DOI: 10.1007/s00267-001-2658-3.

Marchi L., Arattano M., Deganutti A.M. (2002). Ten years of debris-flow monitoring in the Moscardo Torrent (Italian Alps). Geomorphology, 46(1-2), 1-17, DOI: 10.1016/S0169-555X(01)00162-3.

O'Brien J.S., Julien P.Y., Fullerton W.T. (1993). Two–dimensional water flood and mudflow simulation //Journal of Hydraulic Engineering, 119(2), 244-259, DOI: 10.1061/(ASCE)0733-9429(1993)119:2(244)

Perov V.F. (2014). Debris flows phenomena. Terminological dictionary. 2nd ed. Moscow: Moscow University Publishing House. (in Russian).

Rickenmann D., Laigle D., McArdell B.W., Hubl J. (2006). Comparison of 2D debris–flow simulation models with field events. Computational Geosciences, 10(2), 241-264, DOI: 10.1007/s10596-005-9021-3.

Shieh C.L, Jan C.D, Tsai Y.F (1996). A numerical simulation of debris flow and its application. Natural Hazards, 13(1), 39-54, DOI: 10.1007/BF00156505.

Shu A.P., Fei X.J., Feng Y. (2007). A preliminary study on energy dissipating mechanism for viscous debris flow. In: C.-L. Cheng & J.J. Major, eds., Proceeding Debris–flow hazards mitigation. Chengdu. Mechanics, Prediction, and Assessment. Rotterdam: Millpress Science Publishers, 131-140.

Stoffel M. (2010). Magnitude–frequency relationships of debris flows—A case study based on field surveys and tree–ring records. Geomorphology, 116(1), 67-76, DOI: 10.1016/j.geomorph.2009.10.009.

Tian B., Wang Y.Y. (2007). Experimental study on the thixotropy of viscous debris flows. In: C.-L. Cheng & J.J. Major, eds., Proceeding Debris–flow hazards mitigation. Chengdu. Mechanics, Prediction, and Assessment. Rotterdam: Millpress Science Publishers, 111-120.

Tian L.Q. (1987). Geomorphology and debris flow of Jiangjia Gully. Journal of Mountain Science, 5(4), 203-212 (In Chinese).

Tian X., Su F., Guo X., Liu J., Li Y. (2020). Material sources supplying debris flows in Jiangjia Gully. Environmental Earth Sciences, 79(13), 318, DOI: 10.1007/s12665-020-09020-4.

van Steijn H. (1996). Debris–flow magnitude—frequency relationships for mountainous regions of Central and Northwest Europe. Geomorphology, 15(3-4), 259-273, DOI: 10.1016/0169-555X(95)00074-F.

Vinogradova T.A., Vinogradov A.Yu. (2017). The experimental debris flows in the Chemolgan river basin. Natural Hazards, 88(S1), S190-S198, DOI: 10.1007/s11069-017-2853-z.

VSN 03–76 (1976). «Instructions for determining the calculated characteristics of rain debris flows». Leningrad: Hydrometeoizdat (in Russian).

Wang D.J., Cui P., Su F.H., Zhu Y.Y. (2007). Sediment properties of hyperconcentrated flow and the potential for agricultural improvement of debris flow deposits – A case study on the Jiangjia Ravine, Yunnan Province, China. In: C.-L. Cheng & J.J. Major, eds., Proceeding Debris–flow hazards mitigation. Chengdu. Mechanics, Prediction, and Assessment. Rotterdam: Millpress Science Publishers, 725-734.

Wei F., Jiang Y., Zhao Y., Xu A., Gardner J.S. (2010). The distribution of debris flows and debris flow hazards in Southeast China. WIT Transactions on Engineering Sciences, 67, 137-147, DOI: 10.2495/DEB100121.

Yang R.W. (1997). Solid material supplied volume to debris flow in Jiangjia ravine, Yunnan province. Journal of Mountain Research, 15(4), 305-307.

Zhao L., Luo Y., Liu T.-Y., Luo Y.-J. (2013). Earthquake Focal Mechanisms in Yunnan and their Inference on the Regional Stress Field. Bulletin of the Seismological Society of America, 103(4), 2498-2507, DOI: 10.1785/0120120309.

Zhu J., Tang C. (1996). A study on the risk regionalization of debris flow hazard in Yunnan province. Chinese Journal of Geological Hazard and Control, 7(2), 86-93 (in Chinese).

Zhuang J.Q., Cui P., Ge Y. (2011). Debris flow annual frequency and sediment delivery variations compared to rainfall changes over the last 40 years (Jiangjia Gully, China). In: International Conference on Debris–Flow Hazards Mitigation: Mechanics, Prediction, and Assessment, Proceedings (Italian Journal of Engineering Geology and Environment – Book). Casa Editrice Università La Sapienza, 173-179, DOI: 10.4408/IJEGE.2011-03.B-021.

Zhuang J.Q., Cui P., Wang G., Chen X., Iqbal J., Guo X. (2015). Rainfall thresholds for the occurrence of debris flows in the Jiangjia Gully, Yunnan Province, China. Engineering Geology, 195, 335-346, DOI: 10.1016/j.enggeo.2015.06.006.

RESEARCH PAPER

CONTRIBUTION ANALYSIS OF PERMANENT AND SPORADIC CONTROLS OF CO_2 EFFLUX FROM CHERNOZEMS OVER FOUR SEASONS

Dmitry V. Karelin*[1], Olga E. Sukhoveeva[1]
[1]Institute of Geography RAS, Staromonetny Lane, 29, 119017, Moscow, Russia
***Corresponding author:** dkarelin7@gmail.com
Received: April 17th, 2021 / Accepted: February 15th, 2022 / Published: March 31st, 2022
https://DOI-10.24057/2071-9388-2021-042

ABSTRACT. We analyzed four years field observations (2017–2020) of soil CO_2 efflux from Chernozems of arable and forest-steppe ecosystems of Kursk region (Russia), which correspond to the period of the maximal current warming. Three well-known simulation models of different structure and variable sets (DNDC, RothC, T&P) and nonparametric regression analysis were used to estimate annual CO_2 emission from soil and contributions of constant and sporadic controls. The applied models satisfactorily predict both the rate of annual soil CO_2 emission and its seasonal dynamics on arable Chernozems. However, while RothC is suitable for the whole set of crops considered, DNDC is most suitable for cereals and T&R for bare soils only. A comparison of the contributions of permanent and sporadic factors to soil respiration showed that on an inter-annual scale soil temperature and moisture are less important than yearly crop rotation in Chernozem plowlands, making the latter the most important predictor apart from general land-use type. Although the combination of significant permanent and sporadic factors is able to explain 41% of the soil CO_2 emission variance, the leading involvement of spatial controls prevents the construction of quantitative regression models that are able to make forecasts, requiring the use of more sophisticated simulation models (i.e. RothC) in this case. However, the use of the latter does not yet solve the problem of predicting soil CO_2 emission and its net balance in forest-covered or steppe areas of Chernozem forest-steppe landscape.

KEYWORDS: Haplic Chernozems, Luvic Chernozems, soil respiration, carbon dioxide emission, natural and anthropogenic controls, simulation and regression modelling

CITATION: Karelin D.V., Sukhoveeva O.E. (2022). Contribution Analysis of Permanent and Sporadic Controls of CO_2 Efflux from Chernozems over Four Seasons. Vol.15, № 1. Geography, Environment, Sustainability, p 35-45
https://DOI-10.24057/2071-9388-2021-042

ACKNOWLEDGEMENTS: This work was supported by RFBR grant no. 19-29-05025 (field research in 2019), and RSF grant no. 20-76-00023 (field research in 2020-2021 and simulation modeling). Dmitry Karelin was working under the State Assignment for the Institute of Geography RAS (IG RAS) no. 0148-2019-0006 (observations of 2017–2018 processing) and Olga Sukhoveeva was working under the State Assignment no. 0148-2019-0007 (weather data processing) for IG RAS. The authors are grateful to A.A. Vlasov, Director of the Alekhine Central Chernozem Reserve, PhD, and O.V. Ryzhkov, Deputy Director of the Reserve, PhD, for providing the opportunity to collect field data on the territory of the Reserve, and for logistical support. The authors are deeply grateful to A.N. Zolotukhin, MA student at Kursk University, V.N. Lunin, PhD, Head of the Kursk Biosphere Station of IG RAS and A.V. Kudikov, Senior Engineer at IG RAS for invaluable assistance in field data collection and to A.I. Azovsky, PhD, professor of Biology, Lomonosov Moscow State University for participation in statistical data processing and useful comments.

Conflict of interests: The authors reported no potential conflict of interest.

INTRODUCTION

The problem of identifying and quantifying permanent factors of CO_2 emission from various types of soils has now been elaborated in sufficient detail (Zavarzin and Kudeyarov 2006; Kuzyakov 2006; Luo and Zhou 2006; Kudeyarov et al. 2007; Naumov 2009; Stepanov 2011; Chen et al. 2014; Karelin et al. 2014, 2020 a,b; Kurganova et al. 2020) and might be considered close to final solution. Importantly, the results of these studies have been «digitized» in the form of simulation mathematical models at various scales (Jenkinson et al. 1987; Li et al. 1992; McGuire et al. 2001; Raich et al. 2002; Chertov and Komarov 2013). This is of great importance for calculations of the carbon balance and assessment of greenhouse gas contributions to climate change and prediction of their dynamics from individual ecosystems to the biosphere (Tian et al. 2016). In addition to improving existing models, the attention of researchers in this field is now shifting to more specific issues. These include the identification and assessment of the relative contribution of short-term (impulse, sporadic) or highly localized environmental drivers. These are likely to include factors whose marked effects are infrequent, only when they reach a certain degree of severity or threshold. The increased attention to such sporadic or locally acting CO_2 emission controls is due to the fact that

their contribution to the annual carbon budget can often be significant (Kuzyakov and Blagodatskaya 2015; Leon et al. 2014; Ohashi et al. 2007; Karelin et al. 2017).

The latter is particularly important under conditions of ongoing warming, increasing frequency of droughts and storm events in Russia (Zolotokrylin et al. 2007; The second Roshydromet assessment 2014; Kurganova et al. 2020; Leskinen et al. 2020). In forests, the most significant are sporadic soil CO_2 emission and C-balance drivers associated with tree stand mortality caused by fires, logging and phytophages (Leskinen et al. 2020; Karelin et al. 2020b).

In agro-landscapes, these controls include, in particular, horizontal wind speed creating lower surface pressure, which leads to the so-called «pressure pumping effect» (Takle et al. 2004), i.e., additional degassing of soil, including CO_2, into the atmosphere, which greatly enhances the no-wind diffusion rate. This effect is particularly noticeable when wind intensifies in arid flat or mountainous ecosystems with low vegetation canopy, such as steppes (Roland et al. 2015; Sánchez-Cañete et al. 2013) or agro-ecosystems (Smagin and Karelin 2021).

Another well-known sporadic emission factor in soil ecology is the so-called «Birch effect»[1], in the understanding of the mechanism of which, perhaps, clarity has now arrived (Unger et al. 2010; Fraser et al. 2016). However, there is still no consensus on its biospheric significance (Moyano et al. 2013; Oikawa et al. 2014). The one-time contribution of the additional emission caused by this effect can be very noticeable, especially after prolonged droughts (Karelin et al. 2017), although the overall reduction of soil respiration caused by drought significantly negates this contribution (Lopes de Gerenyu et al. 2018). The winter analogue of such «wetting-drying» cycles can probably be considered sporadic «freezing-thawing» cycles, which also cause a substantial pulse release of CO_2 (Kurganova and Lopes de Gerenyu 2015).

In agro-landscapes, sporadic factors related to agronomic practices (e.g., no-till technology; amount, nature, and form of fertilizers applied; crop rotation in fields, etc.) are also involved. A known pulse component of soil CO_2 emission is the release of carbon dioxide during mechanical tillage (ploughing, harrowing), harvesting, the passage of machinery over the fields, and any sufficientl mechanical load (Markovskaya et al. 2014; Cherkassov et al. 2013; Stupakov 2014; Akbolat et al. 2009; Bojarszczuk et al. 2017; Fiedler et al. 2016).

An additional difficulty in solving the problem is posed by the fact that widely practiced micrometeorological methods of monitoring net CO_2 fluxes are not feasible to instrumentally separate their main components, which has to be done by means of modelling (Suleau et al. 2011). At the same time, the pulse components of C fluxes are usually even more difficult to separate and, hence, to model. Therefore, only instrumental observation methods of soil CO_2 emission on a multiyear basis remain at the disposal of researchers, but such long-term data are still clearly insufficient (Kurganova et al. 2020).

All of the above translates the problem of quantifying the contribution of pulse factors to soil CO_2 emissions into the category of potentially high importance. Our study focuses on the analysis of permanent and sporadic controls of soil carbon dioxide emission in the agronomically well-developed forest-steppe zone of the European territory of Russia, where arable Chernozems are widely distributed.

The goal of the study is to compare estimates of annual soil CO_2 emissions obtained from field observations and by various methods of modelling and statistical analysis, and use them to identify relative contributions of permanent and sporadic carbon dioxide emission drivers in the Chernozem landscape under different land-use variants.

OBJECTS AND METHODS

Field observations

The statistical analysis included field observations during four consecutive growing seasons (2017–2020) in the vicinities of Kursk Biosphere Station of the Institute of Geography of the Russian Academy of Sciences (KBS IG RAS) and Alekhine Central Chernozem Reserve, where the full range of forest-steppe ecosystems is represented compactly. The study area (51.5°N, 36.1°E; ca. 40 km^2), is located in the forest-steppe subzone, in the Medvensky and Kursky districts of the Kursk region (Russia). According to the analysis of the high-resolution satellite image (SCOPE, 14.10.2019), the site is dominated by agro-landscape (arable land and vegetable gardens: 57%); broad-leaved forests and forest strips occupy 17%, perennial fallows, forest-steppe areas, overgrown balks and ravines – 12%, mowed meadows – 10%, roads – 2%, residential areas – 2%.

Soil respiration measurements were carried out with infrared CO_2 analyzers and closed chamber method according to the original technique (Karelin et al. 2014, 2015, 2017, 2020 a,b). Amongst the associated indicators, carbon and nitrogen content in the 0–15 cm soil layer (%), volumetric soil moisture in 0 – 6 cm layer (%), air temperature in vegetation canopy and temperature in soil at 1, 5 and 10 cm depth (°C), total projective plant cover (%), average plant height by tier, and current phenophase were assessed. Measurements were taken annually at 12 permanent observation sites, 1–4 times per month, from April to November. diurnal measurements were performed during daylight hours. As the post hoc analysis showed, there was no significant effect of the measurement time on the emission rate at particular sites. Additionally, winter emission estimates were carried out in January 2019 and January–March 2021 (n=20). The sites represent the most characteristic elements of the local landscape. Each measurement at individual site was carried out in 5–15 site replications.

The total number of intra-season measurements across all sites was 466 (2017: 125; 2018: 116; 2019: 32; 2020: 193), or, including repeats, 4,195. Biotopes in the analysis include mature and overmature forest (>150-year-old oak forest; >60-year-old ash forest; >80-year-old maple-oak forest); ecotone between oak forest and meadow steppe; mature >70-year-old meadow steppe; 2 – 5 years old fallows; permanently used unfertilized vegetable garden with rotating crops; and perennial fertilized arable land (5 plots) with rotating grain or raw crops.

In all cases the soils were Haplic Chernozems (Loamic, Pachic) on forest-steppe plots and agricultural fields, and Luvic Chernozems (Loamic, Pachic) under broad-leaved forest, according to WRB classification (IUSS Working Group 2015).

Statistical analysis and modeling

Soil CO_2 emissions were estimated in several ways:
(a) integration of field observations using trapezoidal method[2]. Winter emission data (December–March) were obtained in January 2019, and January–March 2021.
(b) Using three simulation models:

[1]Short-term (up to several days) but powerful release of nitrogen oxides and CO_2 from dry soil into the atmosphere in response to rewetting. The effect has been known since the early 20th century and was named by H.F. Birch after his detailed field and laboratory experiments in Kenya (Birch 1958).
[2]Trapezoid(al) method – follows the so-called Trapezoidal Rule. Under this integration rule, the area under an experimental or observation curve is evaluated by dividing the total area into little trapezoids rather than rectangles. Used when data are obtained unevenly.

• DNDC (DeNitrification-DeComposition, version 9.5), a process-based model of carbon and nitrogen cycles in agricultural soils (Li et al. 1992). This daily-step model consists of three subunits (thermo-hydrological, nitrogen and carbon), requires a large amount of input data and uses many assumptions on the controls of GHG emissions per soil type. The model is considering climatic variables, soil characteristics, and agricultural technologies.
• RothC (Rothamsted Long Term Field Experiment Carbon Model, version 26.3), a model of organic carbon cycling in the upper layers of non-waterlogged soils (Jenkinson et al. 1987). It uses a monthly time step to calculate total organic carbon, microbial biomass carbon and CO_2 emission from soil and allows to evaluate the effects of soil type, temperature, moisture content and plant cover on the turnover process of organic matter.
• T&P (Temperature and Precipitations, version 2), a climate-dependent regression model estimating heterotrophic CO_2 flux from soil to atmosphere for a wide range of terrestrial ecosystems (Raich et al. 2002). It allows to determine the influence of interannual temperature and precipitation variations on global CO_2 emission at monthly step but it doesn't take into account vegetation.

Note that all three models, originally derived from field observations, simulate carbon dioxide production and transport to the atmosphere, but T&P differs in that. It is only describing the heterotrophic (microbial) component of soil respiration without considering roots.

Different land uses, soil characteristics and meteorological variables were tested for the role of emission drivers. The set of the analyzed permanent and sporadic emission controls is given in Table 1. To assess sensitivity of the models to individual factors, simulation experiments were used, where the known value of factor change was compared with the response value of CO_2 emission from soil. The models were verified by field data on soil CO_2 release.

Simulation using RothC was evaluated for each crop over the entire observation period, as the time step of the model is one month, which significantly reduces the size of the data series for validation. The diurnal step of the DNDC model allowed to carry out its verification sequentially for each year. To assess the adequacy of the models, we used:
• Nash-Sutcliffe Efficiency coefficient (*NS*). The coefficient values are in the range of (-∞;1]; if NS < 0, it indicates the failure of the model. It is effective when NS > 0; the closer the value is to 1, the more accurately the process is reproduced.
• Theil's inequality coefficient (T). The coefficient values lie in the range [0;1], and the closer the coefficient is to zero, the more accurate the simulation. Normally in environmental studies its threshold of significance is T ≤ 0.3.
• One-way ANOVA assesses the equality of mean values of samples: mean estimated and field values are equal if $F_{comp} < F_{crit}$ and $p > 0.05$.

The principles of using the above criteria, as well as the preparation of input information for the models and their adjustment to the conditions of the Chernozem zone of Russia have been described in detail earlier (for DNDC: Sukhoveeva and Karelin 2019; for RothC: Sukhoveeva 2020).

Since the first two models are applicable only to agricultural lands, we calculated the annual emission estimates in case (a) only for arable plots.

Meteorological data were obtained from a Davis Instruments (USA) stationary full-profile wireless weather station owned by KBS IG RAS, as well as from RIHMI WDC data base (Obninsk, Russia) for Kursk weather station (#34009, 51.76° N, 36.16° E, 247 m a.s.l.).

The data processed using MS Excel and SPSS 27 (IBM). Means and their standard errors used elsewhere in the text. The means were compared by one-way ANOVA or Mann-Whitney test at p=0.05. The coefficient of variance was calculated as CV = (standard deviation / mean) · 100%. Nonparametric regression analysis of CO_2 emission drivers performed using PRIMER V. 7 (PRIMER-E Ltd.). In the latter case, all study plots, including forest and steppe, were involved in the analysis. The set of investigated soil CO_2 emission factors is given in the "Results and Discussion" section.

RESULTS AND DISCUSSION

Weather conditions of the observation period

According to Kursk meteorological station (Fig. 1), the average annual air temperature was above the climatic norm (7.1 ± 0.9°): 7.6° in 2017, 7.5° in 2018, 8.7° in 2019 and 8.9° in 2020. Moreover, the last two years were the warmest on record, in line with the global trend (Leskinen et al., 2020). At the same time, the amount of precipitation fluctuated within the norm: from 455 mm in 2020 to 655 mm in 2017, with a norm of 637 ± 103 mm. Based on Selyaninov's hydro-termal coefficients, wetting during active growing seasons was sufficient: 1.00 in 2017, 0.99 in 2018 and 1.03 in 2020, (except 2019: 0.80), with a norm value of 1.1 ± 0.4, which corresponds to the northern boundary of the steppe zone.

Estimates of annual CO_2 soil efflux from arable Chernozems

The results of different methods of estimating annual CO_2 efflux from arable Chernozems are presented in Table 2. The average value of emission from field estimates under different crops for three years was 6742 ± 482 kg C ha^{-1} yr^{-1} (n = 12). This exceeds (p = 0.041) the estimates for agrocenoses on typical and leached Chernozems made in 1961 – 1984 in the same area (5652 ± 642 (n = 14), calculated from Kudeyarov and Kurganova (2005)), which could be attributed to the climate warming. However,

Table 1. Set of permanent and sporadic variables (factors) used in the analysis of their influence on CO_2 emission from arable Chernozems of Kursk region, according to three simulation models

Type of variable	Model Variables	DNDC	RothC	T&P
Permanent	Soil organic carbon storage	+	+	-
	Temperature	-	+	+
	Precipitation		-	+
	Atmospheric concentration of CO_2	+	-	-
Sporadic	Change of crops between years	+	+	-
	Heavy rainfall events	+	-	-
	Agrotechnical practices (ploughing etc.)	+	-	-

«+» in the table denotes the presence of the variable in the model experiments, «-» its absence

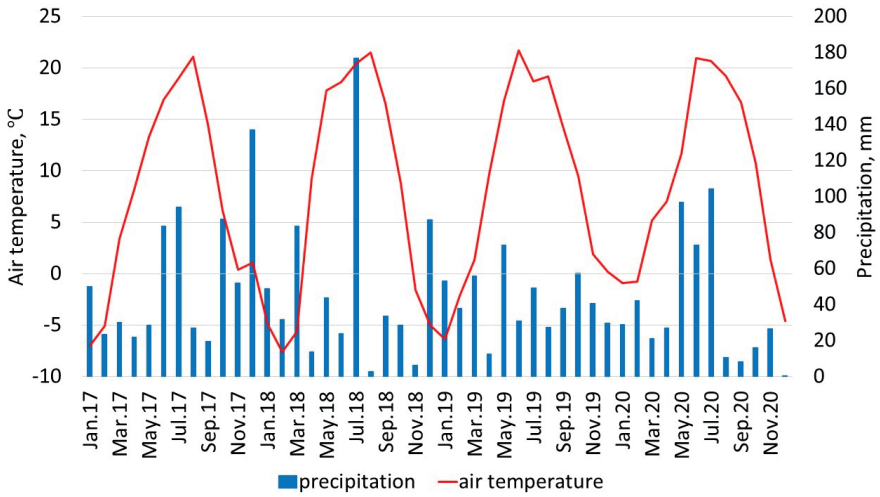

Fig. 1. Meteorological conditions of the period of the study (2017–2020, Kursk region)

it should be noted that the 1961 – 1984 estimates were made by alkaline CO_2 absorption method, whereas now infrared gas analyzers are used for this purpose. In addition, crop and variety sets are somewhat different in the cases compared, which also makes a correct comparison difficult.

The mean estimates obtained from the models do not differ significantly from the field (DNDC: 5929 ± 392 kg C $ha^{-1} yr^{-1}$ (Mann-Whitney, p = 0.27); RothC: 5444 ± 111 (p = 0.08)) and from each other (p = 0.1), although RothC tends to be underestimated. The variation in the obtained estimates of annual emissions is small (CV = 22%) and depends more on crop type (CV = 9.3%) than on year (CV = 3.2%), which is partly due to the short series of observations.

The highest values of soil respiration by mixed estimates for all years and by all methods were obtained for winter wheat (6522 ± 424 kg C $ha^{-1} yr^{-1}$), the lowest for potato (5902 ± 463), but all differences are insignificant (p > 0.05).

The results of the verification of the DNDC and RothC models on field data are shown in Table 3.

The RothC model performed better: it was verified in

Table 2. Estimates of annual soil CO_2 emission (kg C $ha^{-1} yr^{-1}$) from arable Chernozems in Kursk region obtained by different methods

Method	Year / Crops	Winter wheat	Sunflower	Soybean	Barley	Maize	Potato	Bare soil
Trapezoidal on field data	2017	7835	6915	-	6327	-	7044	-
	2018	7847	-	10 725	-	4827	4627	-
	2020	-	5856	4981 6940**	6985	-	-	4196
	Average	7841	6386	7549	6656	4827	5534	4196
DNDC*	2017	5860	6645	-	6695	-	7368	-
	2018	6050	-	3919	-	4063	6114	-
	2020	-	6835	4200	7469	-	-	1956
	Average	5955	6740	4060	7082	4063	6741	1956
RothC	2017	5539	4920	-	5250	-	4905	-
	2018	5999	-	5366	-	5994	5356	-
	2019	-	5433	5448	-	-	5431	--
	2020	-	5411	5375	5772	-	-	4912
	Average	5769	5255	5396	5511	5994	5231	4912
T&P	2017	-	-	-	-	-	-	3870
	2018	-	-	-	-	-	-	3344
	2019	-	-	-	-	-	-	3852
	2020	-	-	-	-	-	-	3429
	Average	-	-	-	-	-	-	3624

* 2019 was excluded from the DNDC simulation due to insufficient data
** for two different fields

Table 3. Verification of models based on field observations of CO_2 emissions from arable Chernozems in Kursk region

Crops		Winter wheat		Sunflower		Soybean		Barley		Potato		Maize
Coefficients of effectiveness and their critical values*	Model	DNDC										
	Year	2017	2018	2017	2020	2018	2020**	2017	2020	2017	2018	2018
Nash-Sutcliffe coefficient (NS > 0)		0.23	0.01	0.26	-1.02	-1.43	-0.20 0.02	0.02	0.38	-0.02	-0.77	0.60
Theil coefficient (T < 0.3)		0.27	0.29	0.26	0.35	0.53	0.36 0.39	0.20	0.23	0.26	0.26	0.16
One-way ANOVA ($F_{comp} < F_{crit}$, p > 0.05)	F_{comp}	0.59	2.07	1.41	0.70	18.34	1.21 3.15	0.98	0.06	1.02	5.12	0.0001
	F_{crit}	4.15	4.17	4.17	4.15	4.17	4.15 4.17	4.15	4.15	4.17	4.17	4.17
	p	0.45	0.16	0.25	0.41	< 0.01	0.28 0.09	0.33	0.81	0.32	0.03	0.99
Model		RothC										
Nash-Sutcliffe coefficient (NS > 0)		0.07		0.19		0.06		-0.03		0.32		0.30
Theil coefficient (T < 0.3)		0.25		0.24		0.29		0.27		0.19		0.20
One-way ANOVA ($F_{comp} < F_{crit}$, p > 0.05)	F_{comp}	1.74		3.28		3.61		1.66		0.57		0.01
	F_{crit}	4.20		4.10		4.11		4.17		4.13		4.97
	p	0.20		0.08		0.06		0.21		0.46		0.92

* The values when the modelling is effective and modelled soil CO_2 emissions is equal to measured one
The cases for which the correspondence between measured and modelled values has not been confirmed are highlighted in grey
** For two different fields as numerator and denominator

at least two of the three criteria in 100% of cases, while DNDC in only 75% of cases. However, the mean values for each of the three criteria for RothC and DNDC did not differ significantly (p > 0.21). Nevertheless, DNDC is slightly better for estimating the mean annual respiration as well as soil respiration of cereal crops. Of the crops considered, the best, in terms of model reproducibility, was shown for maize, while the most unsatisfactory result is shown for soybean.

A comparison of calculations of annual emissions on cropland under crops (DNDC; RothC; interpolation from field data) and under bare soil (T&P; interpolation from field data) further estimates the proportion of microbial soil respiration in arable Chernozems as 66.7%, which is the same as independently estimated (66%; Kudeyarov et al. 2007).

Permanent controls of CO_2 emission from arable Chernozems

When calculating the main C fluxes, the widely used simulation models DNDC and RothC use in their structure mostly permanent-acting factors, which can be spatial (e.g., soil type) or temporal (e.g., air temperature), as well. In order to assess the relative impact of the factors tested (Table 1) on annual CO_2 emissions from soil, we introduced a standard perturbation of the factor value per year (±10%) compared to the baseline value. The perturbation chosen corresponds to the observed average inter-annual variation in temperature and precipitation, and in case of soil organic carbon (SOC) it matches its spatial variability in Chernozems.

The results of estimating the impact of both permanent and sporadic impacts (Tables 4 – 6) are partly determined by specificity of mathematical apparatus of the models: type of functions, the presence of increasing or decreasing coefficients, variables considered, time step, and different sets of equations used. While DNDC has more than 120 equations (Zhang et al. 2002), the T&P model has only one, using two variables and hence unable to estimate the contribution of sporadic controls.

Influence of functional description of the processes on the model outputs is illustrated by an example, in particular, SOC content, which largely determines spatial variance of CO_2 emission (Table 4). Thus, in the DNDC model the dependence of CO_2 emission on SOC stock is parabolic, which is conditioned by introduction of reduction coefficient (μCN) characterizing the carbon to nitrogen ratio in the formula for mineralization of organic matter. This objectively reflects that when SOC stocks increase, nitrogen content becomes limiting for soil respiration and it decreases. Thus, for example, for every 10% increase in SOC stocks, annual soil respiration decreases from 16-18% for potatoes to 33-34% for sunflowers. But for initially low SOC stocks, the respiration rate is also low, and for every 10% decrease in the initial pool, the emission rate drops with the same intensity: from 17–18% in potatoes to 35% in sunflowers. In contrast, in the RothC model, the relationship is direct and linear. With 10% change in SOC stock, annual soil respiration changes by 8.1–9.2%.

Air temperature, soil temperature and moisture are the most important permanent controls governing the formation and emission of CO_2 from the soil surface (Kudeyarov et al. 2007). In our study, only the effects of air temperature and precipitation evaluated, which is related to the original meteorological data (Table 4).

In the models considered, the response of CO_2 emission to changes in temperature and soil moisture represented as simple empirical non-linear functions (Davidson et al. 2006). In RothC,

Table 4. Simulation model experiments with influence of 10% perturbations of permanent variables on annual CO_2 emission from arable Chernozems, %

Variables	Model	Variable	Crop Year	Winter wheat	Sunflo-wer	Soy-bean	Barley	Maize	Potato
Soil Organic Carbon (SOC)	DNDC	Decrease of SOC stocks by 10%	2017	-23.6	-35.2	-	-25.6	-	-18.2
			2018	-30.5	-	-26.4	-	-23.8	-16.9
			2020	-	-35.3	-28.6	-27.4	-	-
		Increase of SOC stocks by 10%	2017	-17.0	-33.6	-	-22.5	-	-17.5
			2018	-28.4	-	-25.5	-	-22.9	-16.4
			2020	-	-33.4	-27.4	-24.5	-	-
	RothC	Increase of SOC stocks by 10%	2017	+8.1	+8.7	-	+8.5	-	+9.1
			2018	+8.2	-	+9.2	-	+8.2	+9.2
			2019	-	+8.8	+9.2	-	-	+9.2
			2020	-	+8.8	+9.1	+8.6	-	-
Meteorological factors		Increase of annual air temperature by 10%	2017	+9.7	+10.2	-	+9.9	-	+10.7
			2018	+10.2	-	+11.1	-	+10.5	+11.2
			2019	-	+10.4	+10.8	-	-	+10.8
			2020	-	+10.3	+10.6	+10.0	-	-
	T&P	Increase of annual air temperature by 10%	2017	+6.8					
			2018	+8.2					
			2019	+7.3					
			2020	+7.9					
		Increase of annual precipitation by 10%	2017	+4.3					
			2018	+4.3					
			2019	+4.8					
			2020	+4.5					

Note. The deviations in %% of the annual CO_2 emission rate from its initial values in the same year taken as 100% are given. The color density of the cells is proportional to the absolute values of the deviations; the sign indicates the direction of the deviation. Positive values are green, negative – brown. Dash means no specific crop in a given year.

these variables are accounted indirectly through the temperature and moisture coefficients. While the former directly contains the variable of interest, air temperature, the latter, in addition to precipitation, includes evapotranspiration and soil moisture capacity. According to calculations based on this model, annual soil respiration changes by 9.7–11.2% for every 10% change in temperature. Note that for conditions of sufficient moistening the moisture coefficient should be excluded from the formula, otherwise it contributes to underestimation of the summer CO_2 emission, which does not correspond to the observed dynamics.

In T&P model, the general equation for both variables is direct, i.e., soil respiration increases with rise of air temperature or precipitation, or declines if the controls are decreasing. The equivalent change in CO_2 emission is 6.8–8.2% for every 10% change in temperature and 4.3–4.5% for every 10% change in precipitation. The greater response of soil respiration to changes in temperature compared to precipitation reflects the predominant influence of the former on the rate of decomposition of soil organic matter (Reichstein et al. 2005).

The stimulating effect of contemporary increase in CO_2 concentration on global photosynthesis has been widely stated (Idso and Idso 2000; Ghannoum et al. 2000; Boretti and Florentine 2019). DNDC model not only taking this into account, but also estimates its impact on other carbon fluxes, including soil respiration. For example, at the current rate of increase in atmospheric CO_2 concentration of 3 ppm per year, according to this model, soil respiration would increase under winter wheat by 1.0%, under sunflowers by 0.5%, under potatoes by 0.4% and under barley by 0.2%.

Sporadic controls of CO_2 emission from arable Chernozems

Because the DNDC has a daily time step and contains large variety of input variables, this allows the assessment of the effects on soil respiration of sporadic factors such as crop and fallow rotation, heavy rainfall events, and agronomic practices separately.

DNDC analysis shows that amongst all basic agro-technical operations (ploughing, cultivation, sowing and fertilizing, pesticide treatment, etc.) it is harvesting that has the greatest impact on soil CO_2 emissions, due to a rapid removal of phytomass and the death of roots, which are responsible for almost one third of soil respiration. The day after harvest, it can decrease (winter wheat by -35 (2018) to 50% (2017); barley by -43% (2017); maize by

-33% (2018); potatoes by -11% (2020)), or increase (sunflowers by +13 (2017) to 96% (2020); potatoes by +34 (2018) to 51% (2017); soybeans by +23 (2018) to 45% (2020); barley by +67% (2020)) soil respiration, as well. However, the contribution of harvesting does not exceed tenths or hundredths of a percent of annual CO_2 emissions. Even if the effects of all agricultural practices summed over the year, it would not exceed 1% of annual carbon dioxide efflux. Crops can be divided into two groups based on their contribution to annual CO_2 soil emission: cereals (winter wheat and barley), where harvesting adds 0.10–0.30% to annual soil respiration, and broad-seeded crops (potato, maize, sunflower, soybean), where harvesting adds only 0.02-0.09% to annual soil respiration.

Among sporadic atmospheric controls, heavy rainfall has the greatest short-term effect on CO_2 emissions (Table 5). On the day of its fallout, compared with the previous day, the flux of CO_2 from the soil increases sharply, and the respiration rate can rise 2.5 times for winter wheat and barley crops, almost 3-fold for soybeans and more than 5-fold for sunflowers. This is due to the coefficient (μw) introduced into DNDC, according to which the rate of mineralization of SOC increases in proportion to the square of the soil moisture content. However, in the model the rate of respiration is not only proportional to the amount of rainfall but also depends on the length of the preceding period without rainfall (this partly accounts for the Birch effect) and the phenological phase. Nevertheless, the contribution of this sporadic factor to annual CO_2 emissions is rather small, amounting to only 0.7–0.8% for cereals (winter wheat, barley) and 1.0–2.0% for crops with wide spacing between rows (sunflower, potato, soybean and maize).

However, crop rotation is found to be the most important sporadic factor affecting annual soil respiration (Table 6). If we take as a reference value for comparison the rate of soil respiration from bare soil in 2020, DNDC under the different crops predicts 3.0-3.8 fold increase of emissions, whereas the surplus predicted by RothC is much smaller and is in the range +0-22%. Thus, the DNDC and RothC results for the five studied crops do not always coincide in terms of magnitude of change.

Table 5. Enhancement of CO_2 emission from arable Chernozems after heavy rainfalls (by DNDC modeling), %

Year	Number of Julian day	Amount of heavy rainfall per day, mm	Winter wheat	Sunflower	Soy-bean	Barley	Maize	Potato
2017	160	34.7	+37.8	+21.1	-	+37.8	-	+53.3
	183	27.9	+25.2	+190.5	-	+29.3	-	+32.6
	352	34.9	+160.1	+40.9	-	+148.5	-	+63.5
	Increase of annual CO_2 emission due to heavy rain events, %		+0.8	+1.0	-	+0.8	-	+1.4
2018	141	31.1	+54.8	-	+136.3	-	+115.4	+42.6
	182	24.1	+18.6	-	+26.6	-	+36.4	+37.6
	188	37.0	+54.5	-	+104.4	-	+115.1	+75.5
	197	23.4	+9.4	-	+15.3	-	+33.9	+22.1
	Increase of annual CO_2 emission due to heavy rain events, %		+0.8	-	+1.6	-	+1.8	+1.1
2020	151	18.3	-	+288.6	+52.2	+37.4	-	-
	181	22.3	-	+53.1	+24.2	+7.8	-	-
	196	57.6	-	+444.5	+388.2	+95.6	-	-
	Increase of annual CO_2 emission due to heavy rain events, %		-	+1.5	+2.0	+0.7	-	-

Note. Soil respiration increase is given in relation to the previous day taken as 100%. The color density of cells is proportional to the absolute values of the deviations; positive sign denotes increase of CO_2 emission. Dash means no specific crop in a given year. The increase of annual emissions due to sum of heavy rainfall events for a given crop in a given year are highlighted in grey.

Table 6. Effect of crop rotation on annual CO_2 emissions from arable Chernozems by two simulation models, %

Year	Model	Winter wheat	Sunflower	Soybean	Barley	Maize	Potato
2017	DNDC	+199.6	+239.7	-	+242.3	-	+276.7
	RothC	+12.8	+0.2	-	+6.9	-	0.0
2018	DNDC	+209.3	-	+100.4	-	+107.7	+212.6
	RothC	+22.1	-	+9.2	-	+22.0	+9.0
2019	RothC	-	+10.6	+10.9	-	-	+10.6
2020	DNDC	-	+249.4	+114.7	+281.9	-	-
	RothC	-	+10.2	+9.4	+17.5	-	-

Note. Soil respiration increase is given in relation to the bare soil respiration rate in 2020, taken as 100%. The color density of cells is proportional to the absolute values of the deviations; positive sign denotes increase of CO_2 emission. Dash means no specific crop in a given year.

In general, we can conclude that annual crop and fallow rotation may be more significant factor for carbon dioxide emissions from arable Chernozems (mean increment: 95.4 ± 21.3 %, n = 25) than the effect of changes in permanent meteorological variables (8.8 ± 0.3 %, n = 36), because the latter change much more slowly. This follows from the fact that the annual increment for the permanent factors (10%) established for computer experiments is close to the observed average variation between consecutive years (for temperature: 6.7%, for precipitation amount: 10.9%).

Assessment of the relative inputs of drivers of CO_2 efflux from Chernozems under different land use

Finally, a non-parametric stepwise multiple regression analysis on similarity matrices (Distance based linear modeling) was performed on available field data on soil CO_2 emissions. The statistical method well applied to the models that contain qualitative and quantitative independent variables, as well, allowing the assessment of their relative contribution. Besides it is well suited for model design with a large number of variables, and is therefore a more powerful tool compared to quantitative or categorical parametric regression analyses (Anderson et al. 2008). The dependent variable was the field values of soil CO_2 emission over the years of observation for all sites (biotopes). All independent variables (18) used in the analysis and their characteristics are given in Table 7.

Among them, in different combinations: 12 permanently acting, and 6 sporadic; 7 spatial and 11 temporal; 6 qualitative and 12 quantitative variables. The sporadic variable, TIMERAIN, reflects the «Birch effect» on CO_2 emission, WIND - the pressure pumping effect.

The results of the analysis are summarized in Table 8.

The optimal model derived from the stepwise analysis of all variables explains 40.6% of CO_2 emission variance, with temporal (hydrothermal) variables accounting for only 35% of the explained variance, and biotope characteristics (spatial) for 65%; qualitative variables for 55.5% and quantitative for 44.5%. Input of the sporadic factors (TIMERAIN, PRECDAY) to the variance explained by this model is rather small (10.3%). Thus, spatial, qualitative

Table 7. Set of factors (independent variables) used for non-parametric regression analysis of CO_2 emissions from Chernozems of Kursk region

ID of the independent variable in the analysis and in the text	Full description of the variable and measuring units	Variable characteristic (a)	Variable characteristic (b)	Variable characteristic (c)
1. SITE	Site number (1-12)	qualitative	permanent	spatial
2. LANDUSE	Type of land use: 1 – plow land, 2 - fallow (self-restoration stages), 3 - climax community, 4 - ecotone	qualitative	permanent	spatial
3. CULTURE	Type of crops: 0 – bare soil, 1 – winter wheat, 2 – maize, 3 – potato, 4 – soybean, 5 – buckwheat, 6 – barley, 7 – sunflower, 8 – beetle, 9 –lupine, 10 – spring wheat, 11 - garlic	qualitative	sporadic	spatial
4. FERTIL	Regular application of fertilizers: 1 – yes. 0 - no	qualitative	sporadic	spatial
5. HOUR	Time of SR measurement (hour of the day, 1-24)	categorial	permanent	temporal
6. MONTH	Number of months in a year (1-12)	categorial	permanent	temporal
7. YEAR	Number of year A.D.	quantitative	permanent	temporal
8. SM	Volumetric soil moisture (%)	quantitative	permanent	temporal
9. TA	Air temperature (°C)	quantitative	permanent	temporal
10. T5	Soil temperature at 5 cm (°C)	quantitative	permanent	temporal
11. T10	Soil temperature at 10 cm (°C)	quantitative	permanent	temporal
12. FITO1	Total live phytomass storage at the moment of SR measurement, t ha^{-1} a.d.m	quantitative	permanent	spatial
13. FITO	Average annual total live phytomass, t ha^{-1} yr^{-1} a.d.m	quantitative	permanent	spatial
14. PROD	Total primary production (t ha^{-1} yr^{-1} a.d.m.)	quantitative	permanent	spatial
15. TIMERAIN	Time to previous rainfall (hours) more than 0.6 mm in 1 h.	quantitative	sporadic	temporal
16. PRECDAY	Sum of precipitation over the previous 10 days before SR measurement (mm)	quantitative	sporadic	temporal
17.RAD	Average solar radiation (w/m^2) per 1 hr of SR measurements	quantitative	sporadic	temporal
18. WIND	Average wind speed per 1 hr over SR measurements (m/s)	quantitative	sporadic	temporal

and constant factors are predominate. Wind speed and soil moisture not found to be significant. The most influential variable in terms of individual contribution is SITE (20.9%), but its disadvantage is that it is too generalized. After excluding the SITE variable from the analysis, the share of variance it explained taken over by yearly rotation of crops (CULTURE) and by land use type (LANDUSE), largely responsible for spatial differences in CO_2 emission between individual biotopes (Table 8). In this case significant sporadic factors (CULTURE, TIMERAIN, PRECDAY) explain 20.5% of the total soil CO_2 emission variance, or 54% of the explained variance. In fact, this statistical analysis reveals that soil CO_2 emission from Chernozem agrolandscape is poorly predictable by weather-related hydrothermal variables (the best among them, T5, explains only 12.2% of variance). It is much more important to know the type of crop, or type of land use. Note that in this case we are using the observation scale «hour-day». In the simulation models described above, a daily and monthly step applied, which tends to increase the influence of weather factors (Karelin et al. 2019).

In this model, hydrothermal controls take 39.3% of the explained variance and biotope characteristics (spatial) take 60.7%. Qualitative variables take 51.3% and quantitative variables - 48.7%. Thus, in both variants of the models spatial factors sharply prevail, which does not allow to apply a single regression model for quantitative forecast.

CONCLUSIONS

Simulation models of different structure and variables sets (DNDC, RothC, T&P) were successfully parameterized and verified using field measurements of CO_2 efflux from arable Haplic Chernozems and Luvic Chernozems in 2017–2020, which corresponds to the period of the most intense contemporary warming. Computer experiments based on DNDC and RothC allow estimating the influence of not only permanent (air temperature, annual precipitation, SOC, atmospheric CO_2 concentration), but also a number of sporadic controls (events of heavy rainfalls, agronomic practices (harvesting), crop rotation) on carbon dioxide emission from soil.

While temperature and precipitation growth increase annual soil CO_2 emissions unambiguously (by 6.8–11.2% for a 10% temperature increment; and by 4.3–4.8% for a 10% precipitation increment), the response of annual soil CO_2 efflux to changes in organic carbon stocks, though more pronounced depends on the mathematical structure of the models: DNDC shows a reduction (-13.8...-36.4% / 10%), while RothC shows an increase (+8.1...+9.2% / 10%). In comparison with this, the influence of the annual increase of CO_2 concentration in the atmosphere on the annual gain of soil emission is very small and amounts to tenths of a percent.

Table 8. Non-parametric regression analysis on similarity matrices applied to data on CO_2 emissions from Chernozems: general model with stepwise inclusion of variables

Independent variables included in the model	Adj. R^2	P	Prop.	Cumul.	res.df	regr.df
T5	0.12	< 0.01	**12.22**	12.22	284	2
SITE	0.29	< 0.01	**20.85**	33.06	268	18
TIMERAIN	0.32	< 0.01	**3.53**	36.59	267	19
FITO1	0.34	0.01	**1.67**	38.26	266	20
TA	0.34	0.10	0.68	38.93	265	21
SM	0.35	0.13	0.55	39.48	264	22
PRECDAY	0.35	0.08	0.68	40.16	263	23
T10	0.35	0.20	0.39	40.55	262	24
After exclusion of the variable SITE:						
T5	0.12	< 0.01	**12.22**	12.22	284	2
CULTURE	0.25	< 0.01	**16.11**	28.33	273	13
TIMERAIN	0.29	< 0.01	**3.61**	31.94	272	14
LANDUSE	0.33	< 0.01	**3.27**	35.21	270	16
T10	0.32	0.11	0.65	35.86	269	17
SM	0.32	0.08	0.66	36.52	268	18
PRECDAY	0.33	0.09	0.67	37.12	267	19
TA	0.33	0.11	0.64	37.83	266	20

Note. Field data for all habitats from 2017–2020 are used. Adj R^2 – partial coefficients of determination of variables, p - significance level of contribution of the variable, Prop. – % of variance explained by the variable, Cumul. – % of the explained variance accumulated by the model, res.df – residual number of degrees of freedom, regr.df – number of degrees of freedom of the regression. Bold font denotes variables significant at p = 0.05. The variables described in table 7.

Among sporadic factors, crop rotation has the most significant effect on CO_2 emissions from arable Chernozems as measured by the potential increase in CO_2 flux between minimum (bare soil) and maximum annual emissions of 22.1% (RothC; winter wheat), 155% (trapezoidal method on field data; soybean), and 281.9% (DNDC; barley). In general, annual crop and fallow rotation is more valuable for CO_2 emissions from soil than the influence of interannual changes of weather and climate, and is much more significant than the other impulse drivers considered (agronomic practices, events of heavy rainfall), whose total contribution does not exceed 1-2% per year.

As shown by statistical analysis for all zonal biotopes, CO_2 emission from forest-steppe Chernozems poorly predicted by commonly used hydrothermal controls (soil temperature and moisture, or air temperature and precipitation amount). In this case, the nature of its long-term use (arable land, fallow, mown meadows, steppe, broad-leaved forest, their ecotones), or the type of crop or fallow used in a given year, if arable, are much more important for predicting the magnitude of carbon dioxide emission from the surface of a given area. However, the use of such indicators does not allow the construction of regression models with quantitative prediction, so the simulation models discussed above are recommended for this purpose. Among them, RothC is the most versatile and suitable for the whole set of crops considered, including bare soil plots; while DNDC is better suited for cereals but underestimates CO_2 emission from fallow areas, and T&R is only suitable for bare soil areas.

Nevertheless, the problem of predicting soil CO_2 efflux and net carbon balance in forested or steppe areas of Chernozem landscapes remains unsolved.

REFERENCES

Akbolat D., Evrendilek F., Coskan A., and Ekinci K. (2009). Quantifying soil respiration in response to short-term tillage practices: a case study in southern Turkey. Acta Agriculturae Scandinavica, Section B – Soil & Plant Science, 59(1), 50-56, DOI: 10.1080/09064710701833202.

Anderson M.J., Gorley R.N., and Clarke K.R. (2008). PERMANOVA+ for PRIMER: guide to software and statistical methods. Plymouth: PRIMER-E Ltd.

Birch H.F. (1958). The effect of soil drying on humus decomposition and nitrogen. Plant & Soil, 10, 9-31.

Bojarszczuk J., KsięŻak J., and Gałązka A. (2017). Soil respiration depending on different agricultural practices before maize sowing. Plant Soil Environment, 63, 435-441, DOI: 10.17221/597/2017-PSE.

Boretti A. and Florentine S. (2019). Atmospheric CO2 concentration and other limiting factors in the growth of C3 and C4 plants. Plants, 8(4), 92, DOI: 10.3390/plants8040092.

Chen S., Zou J., Hu Z., Chen H., and Lu Y. (2014). Global annual soil respiration in relation to climate, soil properties and vegetation characteristics: Summary of available data. Agricultural and Forest Meteorology, 198-199, 335-346, DOI: 10.1016/j.agrformet.2014.08.020.

Cherkassov G.N., Masyutenko N.A., and Masyutenko M.N. (2013). Influence of a crop rotation type, a tillage system and slope exposure on the dynamics of CO2 emission from a typical Chernozem soil. Achievements of Science and Technology of AIC, 6, 34-37 (in Russian with English summary).

Chertov O.G. and Komarov A.S. (2013). Theoretical approaches to modelling the dynamics of soil organic matter. Eurasian Soil Science, 46(8), 845-853, DOI: 10.1134/S1064229313080012.

Davidson E. A., Janssens I. A., and Luo Y. (2006). On the variability of respiration in terrestrial ecosystems: moving beyond Q10. Global Change Biology, 12, 154-164.

Fiedler S.R., Leinweber P., Jurasinski G., Eckhardt K.-U., and Glatzel S. (2016). Tillage-induced short-term soil organic matter turnover and respiration. SOIL, 2, 475-486, DOI: 10.5194/soil-2-475-2016.

Fraser F.C., Corstanje R., Deeks L.K., Harris J.A., Pawlett M., Todman L.C., Whitmore A.P., and Ritz K. (2016). On the origin of carbon dioxide released from rewetted soils. Soil Biology and Biochemistry, 101, 1-5, DOI: 10.1016/j.soilbio.2016.06.032.

Ghannoum O., Caemmerer S.V., Ziska L.H., and Conroy J.P. (2000). The growth response of C4 plants to rising atmospheric CO_2 partial pressure: a reassessment. Plant, Cell and Environment, 23, 931-942.

Idso C.D. and Idso K.E. (2000). Forecasting world food supplies: the impact of rising atmospheric CO_2 concentration. Technology 7 (suppl), 33-56.

IUSS Working Group WRB. (2015). World Reference Base for Soil Resources 2014, update 2015. International soil classification system for naming soils and creating legends for soil maps. World Soil Resources Reports No. 106. FAO, Rome.

Jenkinson D.S., Hart P.B.S., Rayner J.H., and Parry L.C. (1987). Modeling the turnover of organic matter in long-term experiments at Rothamsted. INTECOL Bulletin, 15, 1-8.

Karelin D., Goryachkin S., Zazovskaya E., Shishkov V., Pochikalov A., Dolgikh A., Sirin A., Suvorov G., Badmaev N., Badmaeva N., Tsybenov Y., Kulikov A., Danilov P., Savinov G., Desyatkin A., Desyatkin R., and Kraev G. (2020a). Greenhouse gas emission from the cold soils of Eurasia in natural settings and under human impact: Controls on spatial variability. Geoderma Regional, 22, 1-18, DOI: 10.1016/j.geodrs.2020.e00290.

Karelin D.V., Lyuri D.I., Goryachkin S.V., Lunin V.N., and Kudikov A.V. (2015). Changes in the carbon dioxide emission from soils in the course of postagrogenic succession in the Chernozem forest-steppe. Eurasian Soil Science, 48(11), 1229-1241, DOI: 10.1134/S1064229315110095.

Karelin D.V., Pochikalov A.V., Zamolodchikov D.G., and Gitarskii M.L. (2014). Factors of spatiotemporal variability of CO2 fluxes from soils of southern taiga spruce forests of Valdai. Contemporary Problems of Ecology, 7(7), 743-752, DOI: 10.1134/S1995425514070063.

Karelin D.V., Zamolodchikov D.G., and Isaev A.S. (2017). Unconsidered sporadic sources of carbon dioxide emission from soils in taiga forests. Doklady biological sciences, 475, 165-168, DOI: 10.1134/S0012496617040093.

Karelin D.V., Zamolodchikov D.G., Shilkin A.V., Popov S.Yu., Kumanyaev A.S., Lopes de Gerenyu V.O., Tel'nova N.O., and Gitarskiy M.L. (2020b). The effect of tree mortality on CO_2 fluxes in an old-growth spruce forest. European Journal of Forest Research, 140 (3), 1-19, DOI: 10.1007/s10342-020-01330-3.

Kudeyarov V.N. and Kurganova I.N. (2005). Respiration of Russian soils: database analysis, long-term monitoring, and general estimates. Eurasian Soil Science, 38(9), 983-992.

Kudeyarov V.N., Zavarzin G.A., Blagodatsky S.A., Borisov A.V., Voronin P.Yu., Demkin V.A., Demkina T.S., Yevdokimov I.V., Zamolodchikov D.|G., Karelin D.V., Komarov A.S., Kurganova I.N., Laryonova A.A., Lopes de Gerenyi V.O., Utkin A.I., and Chertov O.G. (2007). Pools and fluxes in terrestrial ecosystems of Russia. Moscow: Nauka. (in Russian).

Kurganova I.N. and Lopes de Gerenyu V.O. (2015). Contribution of abiotic factors to CO_2 emission from soils in the freeze–thaw cycles. Eurasian Soil Science, 48(9), 1009-1015, DOI: 10.1134/S1064229315090082.

Kurganova I.N., Lopes de Gerenyu V.O., Khoroshaev D.A., Myakshina T.N., Sapronov D.V., Zhmurin V.A., and Kudeyarov V.N. (2020). Analysis of the long-term dynamics of soil respiration in forest and meadow cenoses of the Prioksko-Terrasny biosphere reserve in the perspective of current climatic trends. Eurasian Soil Science, 53(10), 1220-1236, DOI: 10.1134/S1064229320100117.

Kuzyakov Y. (2006). Sources of CO_2 efflux from soil and review of partitioning methods. Soil Biology and Biochemistry, 38(3), 425-448, DOI: 10.1016/j.soilbio.2005.08.020.

Kuzyakov Y. and Blagodatskaya E. (2015). Microbial hotspots and hot moments in soil: Concept & review. Soil Biology and Biochemistry, 83, 184-199, DOI: 10.1016/j.soilbio.2015.01.025.

Leon E., Vargas R., Bullock S., Lopez E., Panosso A.R., and La Scala Jr. N. (2014). Hot spots, hot moments, and spatio-temporal controls on soil CO_2 efflux in a water-limited ecosystem. Soil Biology & Biochemistry, 77, 12-21, DOI: 10.1016/j.soilbio.2014.05.029.

Leskinen P., Lindner M., Verkerk P.J., Nabuurs G.J., Van Brusselen J., Kulikova E., Hassegawa M. and Lerink B. (eds.). (2020). Russian forests and climate change. What Science Can Tell Us 11. European Forest Institute, DOI: 10.36333/wsctu11.

Li C., Frolking S., and Frolking T.A. (1992). A model of nitrous oxide evolution from soil driven by rainfall events: 1. Model structure and sensitivity. Journal of geophysical research, 97(D9), 9759-9776.

Lopes de Gerenyu V.O., Kurganova I.N., and Khoroshaev D.A. (2018). The Effect of Contrasting Moistening Regimes on CO_2 Emission from the Gray Forest Soil under a Grass Vegetation and Bare Fallow. Eurasian Soil Science, 51, 1200-1213, DOI: 10.1134/S1064229318100034.

Luo Y. and Zhou X. (2006). Soil respiration and the environment. Burlington: Academic Press.

Markovskaya G.K., Melnikova N.A., and Nechaeva E.H. (2014). The influence of different ways of the main soil cultivation on its biological activity in spring wheat sowing. Vestnik of Saratov state agrouniversity named after N.I. Vavilov, 2, 22-25. (in Russian with English summary).

McGuire A.D., Sitch S., Clein J.S., Dargaville R., Esser G., Foley J., Heimann M., Joos F., Kaplan J., Kicklighter D.W., Meier R.A., Melillo J.M., Moore III B., Prentice I.C., Ramankutty N., Reichenau T., Schloss A., Tian H., Williams L.J., and Wittenberg U. (2001). Carbon balance of the terrestrial biosphere in the twentieth century: analyses of CO_2, climate and land use effects with four process-based ecosystem models. Global Biogeochemistry Cycles, 15, 183-206, DOI: 10.1029/2000GB001298.

Moyano F.E., Manzoni S., and Chenu C. (2013). Responses of soil heterotrophic respiration to moisture availability: An exploration of processes and models. Soil Biology and Biochemistry, 59, 72-85, DOI: 10.1016/j.soilbio.2013.01.002.

Naumov A.V. (2009). Soil respiration: components, ecological functions, geographical regulatiries. Novosibirsk: SO RAS. (In Russian).

Ohashi M., Kume T., Yamane S., and Suzuki M. (2007). Hot spots of soil respiration in an Asian tropical rainforest. Geophysical Research Letters, 34(8), L08705, DOI: 10.1029/2007GL029587.

Oikawa P.Y., Grantz D.A., Chatterjee A., Eberwein J.E., Allsman L.A., and Jenerette G.D. (2014). Unifying soil respiration pulses, inhibition, and temperature hysteresis through dynamics of labile soil carbon and O2. Journal of Geophysical Research: Biogeosciences, 119(4), 521-536, DOI: 10.1002/2013JG002434.

Raich J.W., Potter C.S., and Bhagawati D. (2002). Interannual variability in global soil respiration, 1980-94. Global Change Biology, 8(8), 800-812, DOI: 10.1046/j.1365-2486.2002.00511.x.

Reichstein M., Katterer T., Andren O., Ciais P., Schulze E.-D., Cramer W., Papale D., Valentini R. (2005). Temperature sensitivity of decomposition in relation to soil organic matter pools: critique and outlook. Biogeosciences, 2, 317-321, DOI: 10.5194/bg-2-317-2005.

Roland M., Vicca S., Bahn M., Ladreiter-Knauss T., Schmitt M., and Janssens I.A. (2015). Importance of nondiffusive transport for soil CO2 efflux in a temperate mountain grassland. Journal of Geophysical Research. Biogeosciences, 120(3), 502-512, DOI: 10.1002/2014JG002788.

Sánchez-Cañete E.P., Kowalski A.S., Serrano-Ortiz P., Pérez-Priego O., and Domingo F. (2013). Deep CO_2 soil inhalation / exhalation induced by synoptic pressure changes and atmospheric tides in a carbonated semiarid steppe. Biogeosciences, 10, 6591-6600, DOI: 10.5194/bg-10-6591-2013.

Smagin A.V. and Karelin D.V. (2021). Effect of wind on soil-atmosphere gas exchange. Eurasian Soil Science, 54(3), 372-380, DOI: 10.1134/S1064229321030133.

Stepanov A.L. (2011). Microbial transformation of greenhouse gases in soils. Moscow: GEOS. (In Russian).

Stupakov A.G. (2014). Influence of tillage systems on respiration of soil biota of typical Chernozem. Vestnik of Kursk state agricultural academy, 7, 56-59. (In Russian).

Sukhoveeva O.E. (2020). Assistance for using the RothC model in Russia: the method of preparing input information. Problems of ecological monitoring and ecosystem modelling, 32(3-4), 133-148, DOI: 10.21513/0207-2564-2020-3-133-148 (In Russian with English summary).

Sukhoveeva O.E. and Karelin D.V. (2019). Parametrization of the model DNDC for evaluating components of carbon biogeochemical cycle in the European part of Russia. Vestnik of Saint Petersburg University. Earth Sciences, 64(2), 363-384, DOI: 10.21638/spbu07.2019.211 (in Russian with English summary).

Suleau M., Moureaux C., Dufranne D., Buysse P., Bodson B., Destain J.P., Heinesch B., Debacq A. and Aubinet M. (2011). Respiration of three Belgian crops: Partitioning of total ecosystem respiration in its heterotrophic, above- and below-ground autotrophic components. Agricultural and Forest Meteorology, 151(5), 633-643, DOI: 10.1016/j.agrformet.2011.01.012.

Takle E.S., Massman W.J., Brandle J.R., Schmidt R.A., Zhou X., Litvina I.V., Garcia R., Doyle G., and Rice C.W. (2004). Influence of high-frequency ambient pressure pumping on carbon dioxide efflux from soil. Agricultural and Forest Meteorology, 124, 193-206, DOI: 10.1016/j.agrformet.2004.01.014

The second Roshydromet assessment report on climate change and its consequences in the Russian Federation. (2014). Moscow: Roshydromet.

Tian H., Lu C., Ciais P., Michalak A.M., Canadell J.G., Saikawa E., Huntzinger D.N., Gurney K.R., Sitch S., Zhang B., Yang J., Bousquet P., Bruhwiler L., Chen G., Dlugokencky E., Friedlingstein P., Melillo J., Pan S., Poulter B., Prinn R., Saunois M., Schwalm C.R., and Wofsy S.C. (2016). The terrestrial biosphere as a net source of greenhouse gases to the atmosphere. Nature, 531, 225-228, DOI: 10.1038/nature16946.

Unger S., Máguas C., Pereira J.S., David T.S., and Werner C. (2010). The influence of precipitation pulses on soil respiration – Assessing the «Birch effect» by stable carbon isotopes. Soil Biology and Biochemistry, 42(10), 1800-1810, DOI: 10.1016/j.soilbio.2010.06.019.

Zadorozhniy A.N., Semenov M.V., Khodzhaeva A.K., and Semenov V.M. (2010). Production, consumption, and emission of greenhouse gases in the soil. Agrochemistry, 10, 75-92. (In Russian with English summary).

Zavarzin G.A. and Kudeyarov V.N. (2006). Soil as the key source of carbonic acid and reservoir of organic carbon on the territory of Russia. Herald of the Russian Academy of Sciences, 76(1), 12-26, DOI: 10.1134/S1019331606010035.

Zhang Y., Li C., Zhou X., and Moore B. (2002). A simulation model linking crop growth and soil biogeochemistry for sustainable agriculture. Ecological Modelling, 151(1), 75-108, DOI: 10.1016/S0304-3800(01)00527-0.

Zolotokrylin A.N., Vinogradova V.V., and Cherenkova E.A. (2007). Drought dynamics over European Russia in global warming situation. Problems of ecological monitoring and ecosystem modelling, 21, 160-183. (In Russian with English summary).

RESEARCH PAPER

DYNAMICS OF SEASONAL CHANGES IN INTRODUCED PLANTS IN EASTERN TRANSBAIKALIA

Ekaterina A. Banshchikova
Institute of Natural Resources, Ecology and Cryology SB RAS, 16a, Nedorezova str., Chita, Zabaykalsky krai, 672014, Russian Federation
***Corresponding author:** kait1986@mail.ru
Received: February 8th, 2021 / Accepted: February 15th, 2022 / Published: March 31st, 2022
https://DOI-10.24057/2071-9388-2021-009

ABSTRACT. The article presents a comparative analysis of the seasonal development of introduced plants in the weather conditions of Eastern Transbaikalia for the growing periods from 2014 to 2019. The results presented are taken from 6-year phenological observations conducted in the arboretum of the Institute of Natural Resources, Ecology and Cryology SB RAS. We constructed the phenological spectra of the studied objects by year. We studied the main phenological indicators of vegetation the East Asian forest-steppe and Manchurian-Daurian preboreal species. We analyzed the meteorological data: the mean daily air temperatures and precipitation for the months of the growing season (2014–2019), and the sum of active temperatures and precipitation for this period.

The data on the dynamics of the development of shrubby plant species in conditions of Eastern Transbaikalia for 2014–2019 indicate that plants respond adaptively to changes in weather conditions. Hereditary and physiological characteristics showed that the introduced plants are characterized as cold-resistant and drought-resistant. *Corylus heterophylla* and *Armeniaca sibirica* are most sensitive to temperature extremes in spring, in contrast to Euonymus maackii, which were stable. Low above-zero air temperatures in spring and a large amount of precipitation encourage plants to pass the development stages (phenophases) faster than in dry and warm weather (*Corylus heterophylla, Armeniaca sibirica*). At the same time, low temperatures (frosts) in spring with a wet period at the time of flowering negatively affect the further fruit formation in Corylus heterophylla individuals. Rainy or cloudy days reduce the color intensity of the autumn leaves, and cool, dry, and sunny weather contributes to the autumn color scheme. *Armeniaca sibirica* and *Corylus heterophylla* are variable in terms of the onset of the main phenophases; individuals of the Euonymus maackii species have minimal individual variability. The longest growing seasons on the phenological spectrum were registered in 2014 and 2018–2019 (in *Corylus heterophylla* individuals – 190 days), which contributes to the accumulation of more phytomass. The shortest growing season was registered in 2015 (*Armeniaca sibirica* – 150 days).

KEYWORDS: Eastern Transbaikalia, arboretum, plants, phenological spectrum, weather conditions.

CITATION: Banshchikova E. A. (2022). Dynamics of seasonal changes in introduced plants in Eastern Transbaikalia. Vol.15, № 1. Geography, Environment, Sustainability, p 46-52 https://DOI-10.24057/2071-9388-2021-009

ACKNOWLEDGEMENTS: The research was conducted within the framework of the state assignment of the Institute of Natural Resources, Ecology and Cryology SB RAS.

Conflict of interests: The authors reported no potential conflict of interest.

INTRODUCTION

Researchers around the world study the dependence of plant development on environmental conditions and regional climatic parameters. It is believed that temperature, precipitation, and extreme weather conditions affect phenological patterns by changing flowering and fruiting seasons. Phenological and reproductive shifts of plants due to climate change can have an important impact on population dynamics (Wolfe et al. 2005; Ruml et al. 2011; Nagy et al. 2013; Nikolaeva 2015; Nurul et al. 2016; Reyes-Fox et al. 2014, 2016; Garcia-Cervigon et al. 2018; Yusong et al. 2018; Minin et al. 2018). In recent years, much has been said about climate warming. Some authors believe that "…rather than warming, we should discuss climate mitigation, an upward trend in monthly precipitation, decrease in the mean monthly temperatures in the warm months (from May to September), and increase in the mean monthly temperatures from October to April…" (Minin 2000; Gustokashina and Maksyutova 2006). "…Phenology links the course of seasonal changes in the life of the plant and animal kingdoms to specific meteorological data and inadequate weather conditions…", the authors argue (Merzlenko 2006, Kozlovsky et al. 2014). Model plots for long-term phenological observations make it possible to establish the relationship between shifts in the beginning of the growing season of plants and the temperature regimes in the previous months (Menzel et al. 2006; Golov et al. 2009; Mirjana et al. 2011; Ovchinnikova et al. 2011).

Observations of the dynamics of the seasonal development of shrubby plant species under influence of regional weather conditions of Eastern Transbaikalia were conducted in the arboretum of the Institute of Natural Resources, Ecology, and Cryology of the SB RAS (INREK SB RAS).

The purpose of this work is to analyze the dynamics of seasonal changes in shrub species of introduced plants for

the growing seasons of 2014–2019 in weather conditions of Eastern Transbaikalia.

MATERIALS AND METHODS

Study area

The arboretum where the research was conducted belongs to the Trans-Baikal mountain-forest region and is located in a zone of severe natural and climatic conditions: uneven distribution of precipitation in the annual cycle (annual precipitation is 310–340 mm, of which only 20–40 mm falls in May and June and up to 230 mm falls in August – September); large temperature fluctuations throughout the year and the growing season (the mean annual air temperature is –2.7 °C, the daytime air temperature ranges from –15–20 °C to +10–+15 °C in March – April and from -10–15 °C to +15–+20 °C in September – October; late spring (May – June) and early autumn (August – September) frosts (the frost-free period is 65–75 days) and low relative humidity in spring (15–25% in April – June). The soil of this site is sod mountain-taiga permafrost. Ground water is located at a depth of up to 3 m. Humidification is mainly atmospheric. In general, the soils in the vicinity of the arboretum are characterized by freezing in winter to a great depth (3–3.5 m) and slow thawing in spring and summer (Bobrinev and Pak 2011). The territory of the arboretum is planted on three sides with protective forest strips of scots pine with a blown structure, which creates a special microclimate for the site. Figure 1 shows the site where the research was conducted.

The main phenological parameters were studied in introduced East Asian forest-steppe species: *Armeniaca sibirica* Lam. and *Euonymus maackii* Rupr., and Manchurian-Daurian preboreal species – *Corylus heterophylla* Fisch. ex Trautv. These species are listed as flora objects in the Red Book of the Trans-Baikal Territory (Decree of 2018). The studied objects were brought to the arboretum in the late 1980s from different botanical and geographical areas and planted.

The natural habitat of *Armeniaca sibirica* was noted in Northern, Eastern and Southeastern Mongolia, and in China (in the basin of the Suangri river, in the spurs of the Qinling ridge). In Russia, it grows in the Republic of Buryatia and the Primorsky Territory as well as in the southern and southeastern regions of the Trans-Baikal Territory. *Armeniaca sibirica* grows on the southern macroslopes of ridges at an altitude of 600–900 m above sea level, on mountain chestnut powdery-calcareous soils. It is extremely winter-hardy, drought-resistant, photophilous, undemanding to soil and moisture (Bobrinev et al. 2016; Koropachinsky and Vstovskaya 2012; Red Data Book of the Trans-Baikal Territory 2017).

Euonymus maackii is common on the Korean Peninsula, in Manzhuria andin the south of the Russian Far East. In the Trans-Baikal Territory, it is found in the southeast of the region – in the basin of the Argun riverin the Nerchinsk-Zavodskoy region. *Euonymus maackii* grows on the southern rocky slopes, in light forests, along rocky river banks. It is photophilous, frost-resistant, undemanding to soil, and moderately moisture-loving. It does not tolerate stagnant waterlogging and upper shading, especially in youth (Bobrinev et al. 2016; Koropachinsky and Vstovskaya 2012; Red Data Book of the Trans-Baikal Territory 2017).

Corylus heterophylla is commonin northeastern China, Korea, and Japan. It is also common in the south of the Far East – in Primorye and Amur region. In Siberia, it was recorded only in the Trans-Baikal Territory. *Corylus heterophylla* grows on the south dry mountain slopes, in the open spaces and on the edges of the forest. It is frost-resistant, shade-tolerant, low-demanding for soil moisture, demanding for soil fertility (Bobrinev et al. 2016; Koropachinsky and Vstovskaya 2012; Red Data Book of the Trans-Baikal Territory 2017).

Growth and development of shrubs were studied according to the methods of phenological observations. From the moment of the most obvious phenophase of "bud swelling" (April – May), the beginning of the growing season in plants was considered; the end of the observations was the phase of "end of leaf fall" (September – October) (Methodology of the study of forest ecosystems 2013; Arestova and Arestova 2017). The main meteorological parameters (air temperature, precipitation) were obtained from a portable mini-meteorological station (Davis Vantage Pro_2, USA) located next to the arboretum. Phenological spectra, graphs, and histograms were constructed using Microsoft Excel 7.0.

Fig. 1. Location of the INREK SB RAS arboretum

RESULTS AND DISCUSSION

The sequence and duration of the phenological stages of the seasonal development of each plant are presented in the color graphic form – the phenospectrum (Fig. 2).

When conducting observations in the arboretum for the growing season from 2014 to 2019 (April – October), we analyzed individual phenological variability of the studied objects in dynamics. The sensitivity of plants to the weather conditions of the region varies throughout the seasonal development.

The diagram (Fig. 3) shows an estimate of the weather data of the mean daily air temperature and precipitation for the months of the growing season (2014 – 2019) in the study area.

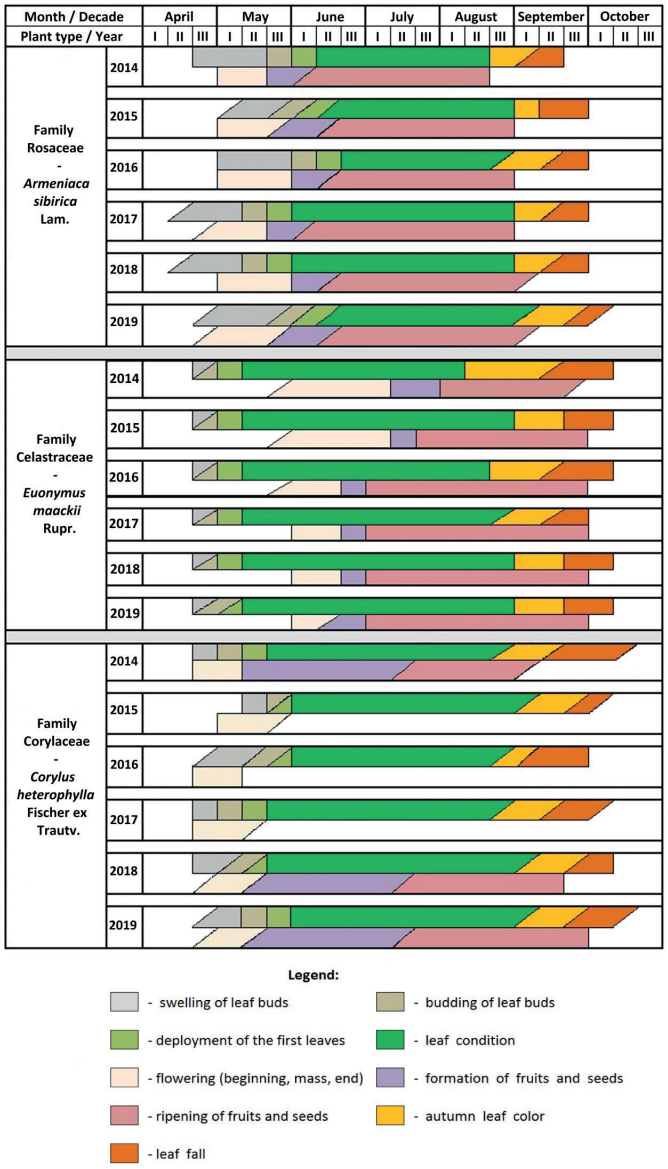

Fig. 2. Phenological spectrum of the growing season of shrubby plant species in the arboretum of INREK SB RAS

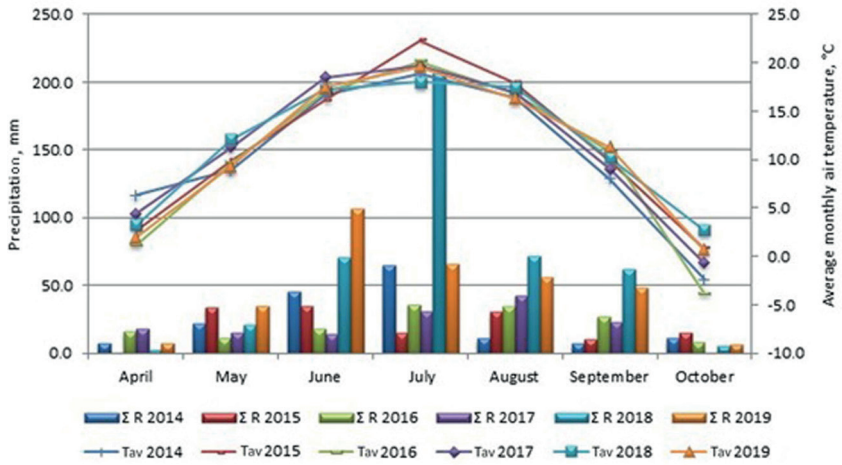

Fig. 3. Weather data by months for the growing season 2014 – 2019: Tav – mean daily temperatures, ° C; Σ R – precipitation, mm

Statistical processing of the main meteorological parameters for the period from 2014 to 2019 showed that the months during the year are characterized by long-term variability. Thus, the highest precipitation variation coefficients recorded within the growing season reached their maximum in mid-summer. The temperature regime showed the greatest variability over the years in April and October and was slightly variable from May to June and from August to September; July was characterized by the greatest instability. It is known that one of the important components of climatic heterogeneity is the high variability of thermal conditions at the beginning and end of the growing season, which determines the different dates of the beginning and end of the growing season and the different time intervals by plants.

Statistical processing of the data of the main meteorological parameters for the six years of the growing season (2014 – 2019) was performed in accordance with generally accepted methods (Table 1).

We analyzed the sum of the mean daily air temperatures above 10 °C for the period from 2014 to 2019. The highest sum of active temperatures (SAT) was recorded in 2015 and amounted to almost 2,182 °C; the lowest was recorded in 2014 (almost 1,933 °C). The maximum precipitation during the period of active temperatures was observed in 2018 (383.3 mm), the minimum was observed in 2017 (98.8 mm) (Fig. 4).

Earlier, the authors (Obyazov and Noskova 2015; Noskova et al. 2019) analyzed the sum of active air temperatures (above 10°C) over the past decades in the entire Trans-Baikal Territory. According to these works, the SAT, on average, varied from 1,500 °C (in the mountainous taiga northern regions) to 2,300 °C (in the steppe south-eastern regions), which confirms our calculations. The authors note that "...days with air temperatures above 10 °C are usually observed from mid-May to the first decade of September, and on average their number is 110, with the maximum values in the south-east of the region (more than 130 days) and the minimum in the north (less than 90 days)…". Our research objects grow in the central part of the Trans-Baikal Territory and manage to complete the full cycle of their development in an average of 110 days.

An increase in air temperature in the spring period boosts vegetation. An increase in temperature (within the normal range) accelerates growth and decreases phenological intervals, while a decrease (within the normal range), on the contrary, slows down development and increases the phenological intervals (Schnelle 1961; Larcher 1978; Shultz 1981). At the same time, the temperature sufficient for vegetation of any species varies from year to year, depending on other conditions, such as, for example, the winter duration and weather or the endogenous dormancy of the plant (Schultz 1981). Let us consider in more detail the dynamics of seasonal changes in introduced plants by phenophases.

The initial phase of the growing season – **"bud swelling"** – changed over the years. For individuals of *Corylus heterophylla*, this phase began somewhat earlier in 2014 (in the 3rd decade of April), compared to 2015–2019. The highest air temperature for that April was 6.3 °C, and the total precipitation in April was 7.6 mm, which exceeds the indicators of 2015 and 2018–2019. The temperature in April of 2017 and 2018 was slightly less – 4.4 and 3.3 °C, respectively, and there was less precipitation. Our

Table 1. Statistical processing of mean monthly air temperatures/precipitation for the growing season 2014 – 2019

Statistical indicator	Years of observation					
	2014	2015	2016	2017	2018	2019
Σ	72.8/170.8	79.7/141.7	71.6/151.2	79.2/144.1	81.1/439.4	76.7/326.2
X	10.4/24.4	11.4/20.2	10.2/21.6	11.3/20.7	11.6/62.8	11.0/46.6
min–max	–2.4–18.8/ 7.5–65.3	0.8–22.3/ 0.6–35.2	–3.9–20.1/ 8.4–36.1	–0.7–19.7/ 0.5–42.8	2.7–18.0/ 3.0–206.8	0.7–19.6/ 6.9–106.7
±σ	3.81/5.84	3.99/5.32	3.78/5.49	3.98/5.38	4.03/9.37	3.92/8.70
V, %	36.6/24.0	35.1/26.3	37.0/25.5	35.2/26.0	34.8/14.9	35.7/17.3

Note. Σ – total value; X – arithmetic mean; min-max – minimum and maximum values; ±σ – standard deviation; V – coefficient of variation, %.

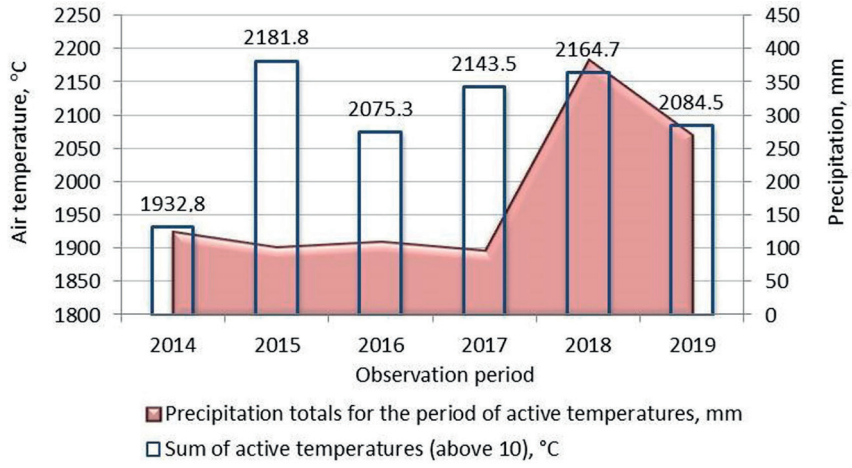

Fig. 4. Meteorological indicators of the growing season from 2014 to 2019: ΣT – sum of active temperatures (above 10), °C; Σ R – sum of precipitation for the period of active temperatures, mm

observations confirm the opinion that warm and dry weather accelerates the development of *Corylus heterophylla*. In 2015–2016 and 2019, these individuals entered the growing season later, at a mean monthly air temperatures of 2.7, 1.2, and 2.0 °C, respectively. For the species *Armeniaca sibirica*, the earliest onset of the growing season was recorded in 2017–2018 (in mid-April), which is one decade earlier than in 2014. In 2019, the growing season began in the third decade of April, as opposed to 2015–2016 (I decade of May). For individuals of *Euonymus maackii*, the onset of this phase remained unchanged from year to year (vegetation begins in the third decade of April and lasts for one decade).

The accompanying phases of **"leaf bud budding"** and **"first leaf budding"** occurred either systematically or in parallel to each other for one week. For example, for individuals of *Corylus heterophylla*, we registered a simultaneous swelling and rapid deployment of the first leaves during the third decade of May 2015, despite the large amount of precipitation and cool weather, compared to other years. In all other years, these two phases occurred one week earlier, successively replacing each other (I–II decade of May). Consequently, cold spring temperatures and humid air accelerate developmental stages of plants. In individuals of *Armeniaca sibirica*, we observed a similar reaction to the weather in 2015–2016 and 2019, including the late opening of leaf buds and their deployment (from late May to mid-June) compared to 2017–2018 (II–III decade of May), with the gradual passage of two phases. The phenospectrum of *Euonymus maackii* samples showed simultaneous swelling of leaf buds, and their flowering was stable from 2014 to 2019 in the third decade of April. However, in 2019, we registered a late consistent opening of the buds (from the 3rd decade of April to the 1st decade of May).

In general, the initial phenological phases of vegetation in the studied species fall on the period from mid-April to the end of May. At this time, there are frequent ground and atmospheric frosts with changes in air temperatures. Based on the data of the graph of meteorological parameters (by month) and the phenospectrum, individuals of *Corylus heterophylla* and *Armeniaca sibirica* were the most sensitive in spring to temperature extremes, in contrast to *Euonymus maackii*, which were stable. The duration of the phenophases was different over the years.

In parallel, the **"onset of flowering"** was recorded in the spring-summer period. It is known that *Armeniaca sibirica* and *Corylus heterophylla* according to the characteristics of phenological development is of the early spring type (generative buds bloom earlier than vegetative ones). The duration of the flowering phase varied: it was within 18–22 days for individuals of *Armeniaca sibirica*; 15–25 days for *Euonymus maackii*; and 10–15 days for *Corylus heterophylla*.

The subsequent phase of **"fruit formation"** follows flowering and occurs in spring or in summer. In individuals of *Armeniaca sibirica*, it was registered in the period from the end of May (2014–2015, 2017, 2019), as well as from the first decade of June (2016, 2018). In individuals of *Corylus heterophylla*, it was registered in the 2nd decade of May (with the exception of 2015–2017, when no fruiting was observed). In individuals of *Euonymus maackii*, it was registered at the end of June (2016–2019) and at the beginning of July (2014–2015). No fruiting in *Corylus heterophylla* can probably be associated with low temperatures (frosts in mid-May) or with a wet period at the time of flowering. It was found that with the highest amount of precipitation and relative air humidity, despite the mean daily air temperature above +10 °C, in individuals of this species, flowering was delayed until a more favorable time. Anemophilic pollen was released from anthers, which cracked under the influence of dry air. In May 2015, when the flowering continued, the highest amount of precipitation was recorded – 34.0 mm. In 2016–2017, the phase came earlier (in April); the amount of precipitation was 16.0 and 17.8 mm, respectively, which exceeded the indicators of this month in other years. In this regard, most likely in these years, the fruits were not formed. However, it is difficult to say unequivocally, since in May 2019, there was also a large amount of precipitation (35.1 mm), with low mean monthly air temperatures (9.3 °C); fruiting in individuals was noted.

This is followed by the **"ripening of fruits and seeds"** phase. In *Armeniaca sibirica*, maturation lasted from 80 to 100 days; in *Corylus heterophylla*, it lasted up to 110 days; and in Euonymus maackii, it lasted 60 to 100 days. However, some fruits in *Euonymus maackii* did not fall over the winter and were recorded on the branches of the plants the following spring. In 2014 and 2015 fruit maturation was faster in all the studied objects; 2017 and 2018 were the years, in which this phase lasted longer.

One of the final stages of the growing season is the **"autumn leaf color"** phase. In 2014, 2016, and 2017, in all species it began earlier (at the end of August), and later leaf coloring (at the beginning of September) was noted in 2015, 2018, and 2019. In general, by the end of September, the full color of the leaves of all the studied plants was recorded over the years, with a mean monthly air temperature in the range of 8.0–11.3 °C (below-zero values were noted only in 2014, in the third decade of September). The influence of short daylight hours and low above-zero temperatures in autumn contributes to the intensity and variety of the color palette of the leaves (from bright red to purple shades). However, early frosts weaken the bright red color of the foliage. Rainy or cloudy days reduce the color intensity of the autumn leaves, and cool, dry, and sunny weather contributes to the autumn color scheme.

The final phase of the growing season is **"leaf litter"**. The East Asian forest-steppe species complete the growing season in late September – early October. The Manchu-Daurian preboreal species turned out to be the most variable over the years. The years of 2014, 2016, and 2017 were characterized by below-zero mean monthly temperatures in October (–2.4 °C; –3.9 °C; –0.7 °C, respectively). It was during these years that the individuals showed early leaf fall and the end of the growing season.

CONCLUSIONS

The dynamics of seasonal changes in introduced plants under conditions of Eastern Transbaikalia indicates that the East Asian forest-steppe and Manchurian-Daurian preboreal species exhibit phenological plasticity in response to sudden changes in air temperatures and insufficient precipitation in the region (*Armeniaca sibirica, Corylus heterophylla*). All objects under study complete a full cycle of phenorhythms – from lignification of shoots and to leaf fall. The observed small deviations in seasonal development (duration of phenophases) over the years are associated with the weather conditions in the region. At the beginning of the growing season, atmospheric frosts with changes in air temperatures are rather common. *Corylus heterophylla* and *Armeniaca sibirica* are most sensitive to temperature extremes in spring, in contrast to Euonymus maackii, which were stable. Warm and dry weather contributes to the early start of

the growing season (*Corylus heterophylla*). Low above-zero air temperatures in spring and a large amount of precipitation encourage plants to pass the development stages faster (phenophases) than in dry and warm weather (*Corylus heterophylla, Armeniaca sibirica*). At the same time, low temperatures (frosts) in spring with a wet period at the time of flowering negatively affect the further fruit formation in *Corylus heterophylla* individuals.

Based on the hereditary and physiological characteristics, it was established that introduced plants are adapted to the conditions of Eastern Transbaikalia and are cold- and drought-resistant. According to the phenological development, the individuals have the following characteristics: early flowering (*Armeniaca sibirica, Corylus heterophylla*) and longer retention of foliage on the branches in the autumn (*Corylus heterophylla*), as well as retention of fruits in winter (*Euonymus maackii, Corylus heterophylla*). The influence of short daylight hours and low above-zero temperatures in autumn contributes to the intensity and variety of the color palette of the leaves (from bright red to purple shades). Rainy or cloudy days reduce the intensity of the color of the autumn leaves, and cool, dry, and sunny weather contributes to the autumn multi-color. Below-zero monthly mean temperatures in October were observed for 2014, 2016–2017 (–2.4 °C; –3.9 °C and –0.7 °C, respectively). It was during these years that the individuals showed early leaf fall and the end of the growing season.

Armeniaca sibirica and *Corylus heterophylla* are variable in terms of the onset of the main phenophases; individuals of the species Euonymus maackii are characterized by minimal individual variability. The longest growing seasons on the phenological spectrum were demonstrated in 2014 and 2018–2019 (in individuals of *Corylus heterophylla*, it was 190 days), which contributes to the accumulation of greater phytomass. The shortest growing season was in 2015 (for *Armeniaca sibirica*, it was 150 days). We assessed the most objectively the resistance of introduced plants under conditions of Eastern Transbaikalia.

REFERENCES

Arestova S.V. and Arestova E.A. (2017). Assessment of adaptation of introduced tree and shrub plants in the conditions of the Saratov Volga region: methodological recommendations. Saratov: Research Institute of the South-East, 28 (in Russian).

Bobrinev V.P. and Pak L.N. (2011). Forest stationary studies in the Trans-Baikal Territory. Chita: Poisk. (in Russian).

Bobrinev V.P., Pak L.N., Banshchikova E.A. (2016) Arboreal flora of Zabaikalsky Krai. Chita: ZabSU. (in Russian).

Garcia-Cervigon A.I., Linares J.C., Garcia-Hidalgo M., Camarero J. J. and Olano J. M. (2018) Growth delay by winter precipitation could hinder Juniperus Sabina persistence under increasing summer drought. Dendrochronologia, 51, 22–31.

Golov V.P., Skvortsov P.M. (2009). Using phenological observations in assessing the ecological situation of their area. Regional ecology problems, 6, 178–183. (in Russian).

Gustokashina N.G. and Maksyutova E.V. (2006). Trends in aridity in the steppe and forest-steppe of the pre-Baikal region. Geography and natural resources, 4, 76–81. (in Russian).

Koropachinsky I.Yu., Vstovskaya T.N. (2012). Woody plants of the Asian part of Russia. Novosibirsk: Academic publisher «Geo». (in Russian).

Kozlovsky B.L., Fedorinova O.I. and Kuropyatnikov M.V. (2014) Regularities of seasonal development of woody plants during introduction in Rostov-on-Don. The scientific journal of the Kuban State Agrarian University, 99(05), 1–12. (in Russian).

Larcher V. (1978) Ecology of plants. Moscow: Mir. (in Russian).

Menzel A., Sparks T. H., Estrella N. et al. (2006). European phenological response to climate change matches the warming pattern. Global Change Biology, 12, 1969–1976.

Merzlenko M.D. (2006). The value of phenological observations for forestry production. Bulletin of the Moscow State University of Forest – Forest Bulletin, 1, 37–40. (in Russian).

Methodology of research of forest ecosystems (2013). Vologda-Molochnoe: IC VGMHA (in Russian).

Minin A.A., Ran´kova E.Ya., Buyvolov Yu.A., Sapel´nikova I.I., Filatova T.D. (2018) Phenological trends in nature of the Central part of the Russian Plain under conditions of modern warming. Earth life, 40, 2, 162–173. (in Russian).

Minin A.A. (2000) Phenological regularities of the state of decades. The reports of the TAA, 271, 282–286. (in Russian).

Mirjana Ruml, Dragan Milatovie, Todor Vulie, Ana Vukovic (2011). Predicting apricot phenology using meteorological data. Int J Biometeorol, 55, 723–732.

Nagy L., Kreyling J., Gellesch E., Beierkuhnlein C. and Jentsch A. (2013). Recurring weather extremes alter the flowering phenology of two common temperate shrubs. Original Paper, 57, 579–588, DOI:10.1007/s00484-012-0585-z.

Noskova E.V., Vakhnina I.L., Rakhmanova N.V. (2019). Amounts of active air temperatures (above 10 °C) in the territory of Trans-Baikal territory. Advances in current natural sciences. 11, 148–153. (in Russian).

Nikolaeva S.A. (2015). Fenological variability of trees and shrubs in Tomsk. Scientific Journal of KubSAU, No. 112(08), 1343–1352. (in Russian).

Nurul L. Winarni, Dewi R. Kurniasari., Diny Hartiningtias, Meyner Nusalawo and Niken Sakuntaladewi (2016). Phenology, climate, and adaptation: how does dipterocarps respond to climate? Indonesian Journal of Forestry Research, 3, 2, 129–141, DOI:10.20886/ijfr.2016.3.2.129–141.

Obyazov V.A., Noskova E.V. (2015). Long-term changes in agroclimatic resources of Transbaikalia. Bulletin of the Transbaikal State University. 8 (123), 20–29 (in Russian).

Ovchinnikova T.M., Fomina V.A., Andreeva E.B., Dolzhkova N.P., Sukhovolskii V.G. (2011). Analysis of changes in the time of seasonal phenomena in woody plants of the reserve Stolby in relation to climatic factors. Conifers of the boreal zone, 28, 1–2, 54–59. (in Russian).

Resolution of the government of the Trans-Baikal territory on approval of the List of flora objects listed in the Red Book of the Trans-Baikal territory (as amended on August 28, 2018) (in Russian).

Ruml M., Milatovie D., Vulie T. and Vukovic A. (2011). Predicting apricot phenology using meteorological data. Int J Biometeorol, 55, 723–732.

Reyes-Fox M., Steltzer H., Trlica M. et al. (2014). Elevated CO_2 further lengthens growing season under warming conditions. Nature 510, 259–262. doi:10.1038/nature13207

Reyes-Fox M., Steltzer H., LeCain D. et al. (2016). Five years of phenology observations from a mixed-grass prairie exposed to warming and elevated CO2. Sci Data 3, 160088. DOI:10.1038/sdata.2016.88

Schnelle F. (1961). Plant phenology. Leningrad: Gidrometeoizdat. (in Russian).

Shultz G.E. (1981). General phenology. Leningrad: Nauka. (in Russian).

Wolfe D.W., Schwartz M.D. and Lakso A.N. (2005). Climate change and shifts in spring phenology of three horticultural woody perennials in northeastern USA. Original article, 49(5), 303–309, DOI:10.1007/s00484-004-0248-9.

Yusong Cao, Yi'an Xiao, Sisi Zhang and Wenhai Hu (2018). Simulated warming enhances biological invasion of Solidago canadensis and Bidens frondosa by increasing reproductive investment and altering flowering phenology pattern. Scientific reports, 8(1), 1–8, DOI:10.1038/s41598-018-34218-9.

RESEARCH PAPER

NATURAL DIFFERENCES IN THE LEGAL DIMENSION: INSTITUTIONALISATION OF THE NORTHERN AND MOUNTAIN REGIONS OF RUSSIA

Yuri N. Golubchikov[1], Alexey N. Gunya[2*], Matthias Schmidt[3]

[1]Faculty of Geography, Lomonosov Moscow State University, Leninskie Gory, 119991, Moscow, Russia

[2]Institute of Geography, Russian Academy of Sciences, Staromonetny pereulok 29, 119017, Moscow, Russia

[3]Institute of Geography, Augsburg University, 86159, Augsburg, Germany

***Corresponding author:** a.n.gunya@igras.ru

Received: July 29th, 2021 / Accepted: February 15th, 2022 / Published: March 31st, 2022

https://DOI-10.24057/2071-9388-2021-084

ABSTRACT. Natural differences in the regional development of Russia are presented in many legislative acts dedicated to the Russian Far North. In contrast, the unique nature and complexity of mountainous and high-mountain territories are protected only by a few regional acts. The reason for this lies in the complexity and multicomponent criteria required for assigning these territories the status of protected areas and in the fact that their boundaries do not correspond with administrative boundaries. The main materials underlying the article are legal documents (regulations, laws, etc.) concerning the institutionalization of the northern and mountainous territories. A comparative analysis of regional policy in relation to mountainous and northern territories takes into account similar criteria, such as vegetation types and patterns, forest borders or crop frontiers. Almost two-thirds of the territory of Russia refers to the North and more than half of the territory is occupied by mountains. The first attempts to institutionalize the North were undertaken in the 1930s, while the programmes for the development of mountainous territories gained legal support only at the end of 20th century and only in some regions. The most important difference between the institutionalization of the North and the mountains is the fact that the state initiated the creation of special legal conditions for the North. In the case of the mountains, the initiator was the public, initially at the regional level. Currently, three constituent entities of the Russian Federation adopted laws on mountain areas, but so far there are no all-Russian laws. The main lobbyists are the North Caucasian regions, while the Siberian regions (with the exception of the Altai Republic) are rather passive in discussing mountain issues. The elaborated legislation for the North seems to be closely related to the potential and realised income from natural resource extraction. For this reason, corresponding legislation for the mountain regions is not expected particularly soon, due to the lack of legal resources. Efforts aimed to provide legal support for mechanisms that compensate the socio-economic discrepancies between mountainous areas and more developed "flat places" should take into account the experience of institutionalizing the Northern territories of the Russian Federation.

KEYWORDS: Russia, northern regions, Arctic, mountain territories, regional development, institutionalisation

CITATION: Golubchikov Y. N., Gunya A. N., Schmidt M. (2022). Natural Differences in the Legal Dimension: Institutionalisation of the Northern and Mountain Regions of Russia. Vol.15, № 1. Geography, Environment, Sustainability, p 53-60
https://DOI-10.24057/2071-9388-2021-084

ACKNOWLEDGEMENTS: Part of the work was executed within the framework of the State task FMGE-2019-0007 "Assessment of physiographic, hydrological, and biotic environmental changes and their impacts on the foundation of sustainable resource management" (AAAA-A19-119021990093-8).

Conflict of interests: The authors reported no potential conflict of interest.

INTRODUCTION

Russia has huge regional differences in terms of natural conditions and living environments. This impacts state policy and Russians' way of life, resulting in a special geographical outlook. According to Laruelle (2012), there are three important geographic meta-narratives about Russia that characterise its territorial-spatial position: Eurasianism, Cosmism, and Arcticism. In line with these meta-narratives, Russia occupies an intermediary position in the Eurasian space and unites European and Eastern civilisational components. The northern region of the country is considered a promising geopolitical axis.

Russia's huge natural differences are mirrored in instruments of governance such as strategic planning and regional development. The Federal Law on strategic planning (2014)[1] originally outlined many spatial development priorities that were later reflected in the

[1]*Federal Law "On Strategic Planning in the Russian Federation". 2014. Available at http://www.consultant.ru/document/cons_doc_LAW_164841/. [Accessed 29 July 2021].*

spatial development strategy (2019)[2]. In particular, the document on the foundations of state policy for regional development (2017)[3] calls for a reduction in regional disparities in terms of the socio-economic situation and quality of life. It is barely possible to take into account the diversity of living conditions and developments within existing administrative zones. Therefore, the Spatial Development Strategy, in addition to administrative units, designates new territories and regions, such as urban agglomerations, border regions, special strategic areas, etc. By taking into account the spatial characteristics and natural contrasts of Russia, the state's regional policy pays most attention to differences caused by the country's location in the extreme natural and climatic conditions of the North. Much less attention is paid to the particularities of Russia's mountain areas. Meanwhile, according to the latest data, mountains occupy more than 50% of the country's territory and are characterised by no less difficult conditions for living and regional development. Recognition of the importance of mountain specifics in state policy is a noticeable global trend, with which Russia has recently begun to join. An important event in this regard is the adoption by the CIS Interparliamentary Assembly of the Model Law on the protection and development of mountain territories[4] at the end of 2020. The adoption of specific laws and establishment of corresponding institutions for mountain regions can be based on legal support experiences of not only other countries, but also on the Russia's own experience on the development of the North.

The purpose of this article is to analyse the relationship between the natural and socio-political factors that have influenced the institutionalisation of the northern and mountainous regions of Russia. We will focus on the analysis of two types of institutions: a) underlying the official recognition and the legalization of geographical differences, which is primarily expressed in the definition of the boundaries of the north and mountains, b) regulating social relations arising from special (northern or mountainous) conditions.

MATERIALS AND METHODS

This work is based on legal documents (regulations, laws, etc.) on the institutionalisation of the northern and mountainous territories. There are two types of such documents: 1) advisory decisions (declarations, conventions, charters, etc.) and 2) documents of mandatory execution (laws, regulations) (Galinovskaya 2020). In the regions themselves, in the course of field research, we revealed the connections between decisions made and their implementation, the involvement of various actors in the institutionalisation, in particular, and the role of the state and the local community.

We summarised the current efforts on the institutionalisation of mountainous areas and the Russian Arctic. Thus, the Russian experience of institutionalising the Arctic reveals that in this process involves aspects such as leading actors (for example, the state), coverage, national status, development priorities, correlation with other grids, regionalisation, etc. (Katorin 2016). The institutionalisation of mountainous regions, as a rule, is accompanied by the formalisation of traditional practices and customary law (adats), which to one degree or another are enshrined in documents, although some of the traditional rules remain unformalised but still play an important role in regulating mountain management at local levels (Gunya 2013).

Theoretical context

This work uses an institutional approach to analyse the specifics of modern territorial processes, in particular legalisation on new spatial boundaries and regions that do not coincide with administrative boundaries. Institutionalisation is initially understood as a process involving the development of new institutions, i.e. rules governing political life, the use of resources, environmental protection, etc. In the context of our work, the emerging new institutions did not replace but supplemented existing ones. Lindner (1998) singled out two complementary directions for the emergence of new institutions: the organisation of new conditions and rules from above (for example, imposed by central authorities through the introduction of new laws), and the formalisation of existing, including traditional, institutions that are not officially recognised. Institutionalisation, if it is based on socio-cultural and political roots, is called "regionalisation" (c.f., Paasi 2010, Agnew 2013). Natural factors can also play an important role in regionalisation. The designation of a new region according to natural criteria is often referred to as "framing" (De Vreese 2012; Debarbieux et al. 2014). Therefore, the framing of drainage basins (for example, identification of the Danube region), mountainous countries (the region of the Alpine Convention), etc. can be indicative in this sense. The experience of institutionalising a region (be it socio-political regionalisation or framing based on natural-ecological unity) is a complex process of interaction at the social, spatial, and temporal large-scale levels (Dörrenbächer 1998).

The Russian North and the mountainous territories of Russia are macro-regions covering an area of several million square kilometres. They do not coincide with administrative boundaries, but they are nevertheless often used in socio-political documents and serve as the subject of legal relations. As will be shown below new laws developed for them create a special institutional environment that contributes to the development of these macro-regions. In this context, by "institutionalisation" herein we mean the process involved in the legalisation of the North and the mountainous territories of Russia as special macro-regions with their inherent and special legal preferences that differ from other Russian regions. Considering the huge amount of sources devoted to the institutionalisation of the Arctic and, to a lesser extent, mountain regions, the task of the study is limited to the geographical aspects of institutionalisation and their comparative analysis. The aim is to analyse the ratio of natural and socio-political factors that have influenced: 1) the allocation of the northern and mountainous regions of Russia into special territorial units and 2) the delimitation of their areas (substantiation of their boundaries). Achieving the stated goal will also make a certain contribution to the development of interdisciplinary areas in geography, social anthropology, and political ecology.

[2]The Spatial Development Strategy of the Russian Federation until 2025.2019. Available at https://www.economy.gov.ru/material/file/a3d075aa813dc01f981d9e7fcb97265f/130219_207-p.pdf. [Accessed 11 December 2021].
[3]Fundamentals of State Policy for Regional Development of the Russian Federation for the period up to 2025" (2017). Available at http://www.consultant.ru/document/cons_doc_LAW_210967/. [Accessed 29 July 2021]
[4]Model Law "On the Protection and Development of Mountain Territories". 27 November 2020. Available at https://iacis.ru/baza_dokumentov/modelnie_zakonodatelnie_akti_i_rekomendatcii_mpa_sng/modelnie_kodeksi_i_zakoni/10. [Accessed 29 July 2021].

RESULTS

The North and mountains as the study objects

In Soviet-Russian geography, the term "Northern studies" (or Severovedenie in Russian) has long existed as a scientific direction for the comprehensive study of problems relating to the northern regions (c.f., Zaydfudim, Golubchikov 2003; Agranat 2007). The population of the vast sub-Arctic and Arctic areas (zones typified as tundra, forest-tundra, and northern woodlands) account for less than 0.1% of the world's population, i.e. approximately 5 million people. There are no permanent settlements north of 78º N or south of 54º S (Golubchikov 1996). The largest cluster of the world's circumpolar population is concentrated in Russia. Among the Arctic countries, the Russian North is distinguished by the highest ethnic diversity, with eleven ethnic groups, and the total indigenous population amounting to approximately 200,000 people, of which the Nenets account for the largest share with 34,000 people; the smallest group is the Enets (209 people) (Golubchikov 2015).

Much less attention in Russia has been paid to the comprehensive study of mountains as a separate subject (sectoral studies, such as the study of mountain glaciers, have of course been conducted for a long time). Global trends in the study of mountains (Debarbieux and Price, 2012; Adler et al 2020), which have also penetrated into Russian geography, have gradually begun to receive more and more attention (c.f., Kotlyakov and Badenkov 1999; Kotlyakov et al 2014). Furthermore, geographical surveys of the mountains of Eurasia have recently appeared (Schmidt and Stadelbauer 2017; Schmidt 2017).

Mountains and northern territories exhibit many similarities and are dealt with by specific scientific approaches and sub-disciplines, such as periglacial geography (Golubchikov 1996). In our understanding, periglacial environments encompass cold, treeless, non-glacial spaces mainly in tundra and forest-tundra, or their high-altitude analogues. The snow line and cold forest boundaries – some of the planet's most complex frontiers – constrain periglacial environments, the geography of which covers both high-altitude and high-latitude areas (Golubchikov 1992, 1996).

Significantly different from many other areas, periglacial environments are particularly difficult to live in, and so they are the harshest environments, in which the human still constantly lives. Moreover, these mainly "peripheral" regions are usually economically underdeveloped.

Geographical aspects of the institutionalisation of the North

The allocation of the northern territories into a special macro-region of Russia is due to their resource significance and the urgent need for their development. This macro-region began being institutionalised a relatively long time ago and now it is well studied (c.f., Lukin 2013). Therefore, it makes sense to dwell on some of the geographical features of its institutionalisation.

The "Far North" concept was mentioned for the first time in the regulation on benefits for persons working in the Far North of the RSFSR (1932)[5]. Later, a list of localities equated to the Far North regions was determined (1945). To date, the list of regions in the Far North and equivalent areas covers 25 constituent entities of the Russian Federation, covering an area of more than 11 million km^2 (two-thirds of the territory of Russia) with a population of more than 10 million people.

The current growth in the geopolitical "weight" of the North has led to the allocation of the Arctic Zone, covering the territory of the Murmansk region, as well as the Nenets, Chukotka, and Yamalo-Nenets autonomous areas and the municipal formation of the Vorkuta urban district (Komi Republic)[6]. In 2021, the list of territories belonging to the Arctic zone changed and now it includes nine regions, including four entire constituent entities of the Russian Federation (Chukotka Autonomous Area, Yamalo-Nenets Autonomous Area, Nenets Autonomous Area, and Murmansk Region) and 45 municipalities of five subjects of the Russian Federation (the republics of Karelia, Komi, Sakha (Yakutia), Arkhangelsk region, Krasnoyarsk Territory[7]) (Fig. 1).

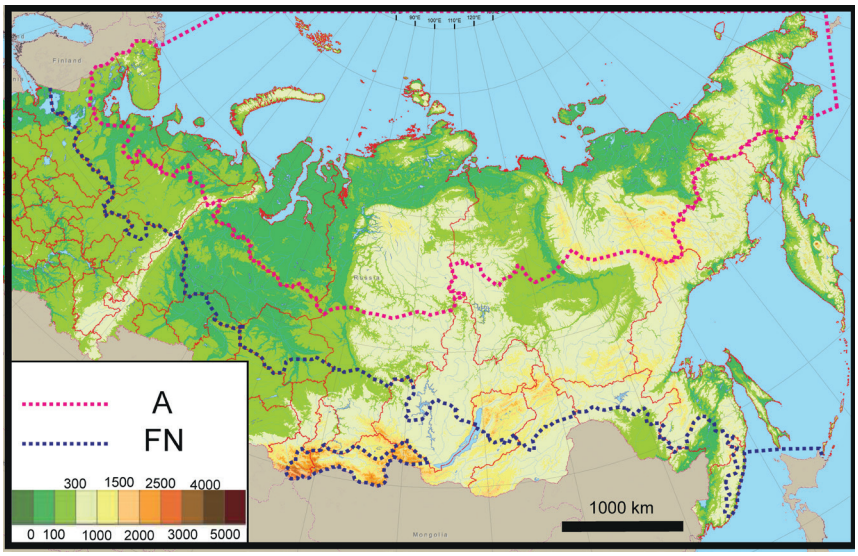

Fig. 1. The southern borders of the Arctic Zone (A) and the „Far North" (FN).

[5]*Resolution of the All-Russian Central Executive Committee, SNK RSFSR dated 05/10/1932. "On Approval of the Regulations on Benefits for Persons Working in the Far North of the RSFSR". Available at http://www.consultant.ru. [Accessed 29 July 2021]*
[6]*Decree of the President of the Russian Federation of May 2, 2014 No. 296 "On the land territories of the Arctic Zone of the Russian Federation".*
[7]*Decree of the Government of the Russian Federation of October 30, 2021 No. 1877 "On Amendments to the State Program of the Russian Federation" Social and Economic Development of the Arctic Zone of the Russian Federation"*

The goals of special policy in the Arctic Zone are related among other things to the need to preserve the natural environment and to ensure general live standards. Currently, institutionalisation is closely related to international processes and trends in the Arctic Zone, in particular to initiatives and projects within the Arctic Council (an intergovernmental forum of the Arctic countries) framework, created in 1996, which contributes to sustainable development and environmental protection of the Arctic regions. An increase in energy prices at the beginning of the new millennium and a clearly manifested trend toward climate warming fueled interest in the Arctic, which in turn led to the adoption by the polar countries of strategic documents for the development of their own zones. It is these factors, according to Katorin (2016), that became a key prerequisite for the formation of the modern state policy of the Russian Federation in the Arctic, thus highlighting the Arctic Zone of the Russian Federation (AZRF) as an object of state policy regulation.

One highly relevant feature of the "North", "Far North", and "Arctic" lies in their boundaries. Agranat (2007, p. 8) noted that "The lack of firm ideas about the borders has a detrimental effect on policies and practices 'for the North' and 'in the North'." As such he correlated the borders of the North with the areas where the reliable cultivation of grain crops ceased (Concept ... 1992). Other well-known criteria for referring to northern territories are climatic discomfort, inaccessibility, and remoteness from transport hubs (including seaports). However, the allocation of the Far North was also motivated by political issues, due to the inclusion of new localities in the development project with the aim of attracting new people to the region by offering them "northern" benefits (higher wages, early retirement, higher pensions, etc.).

Modern Russian official documents, instead of the concept of the North, use the concept of the Russian Arctic (AZRF), distinguished by a combination of many features. The Arctic zone is very heterogeneous; geographically it is an island or a quasi-mainland (Pilyasov 2020). From physical and geographical points of view, the delimitation of the AZRF's southern borders raises questions: in the western (relatively highly populated) areas, it runs in the northern taiga zone; in the east, this border shifts to the north. As a result of this shift large areas of tundra do not fall into the Arctic Zone. Savchenko and Treivish (2017) note that in Russia, due to the climate and spatial location, the more east it is, the more north it is. These territories are subject to a general pattern involving the displacement of natural zones and subzones to the equator on the eastern margins of the continent, which are exposed to cold ocean currents (in contrast to the western margins washed by warm currents). However, the official southern border of the AZRF, on the contrary, moves to the north in the east, and to the south in the west. For example, the northern regions of the Arkhangelsk Region (excluding the Nenets District) and the Republic of Karelia included therein are located outside the tundra zone or permafrost. They are found in the northern and even middle taiga. Magadan region or Koryak autonomous area, on the contrary, are not included in the AZRF, even though their main areas are occupied by subarctic chars, cedar thickets, and coastal tundra. Furthermore, even the "Pole of cold" for the northern hemisphere, which is home to the forest-tundra of the Abyisky ulus on the middle Indigirka, the Oleneksky ulus with a population density of 1 person per 100 km^2 and the Koryaksky district of the Kamchatka region, are not included in the AZRF.

Obviously, substantiation of the Arctic Zone's southern border requires further scientific research that could define the criteria and adapt them to modern challenges, such as melting permafrost, population outflow, and unfavorable conditions – the most specific factors relevant to the northern regions.

Geographical aspects involved in the institutionalisation of mountain areas

Why have the mountain specifics of Russia not become a meta-narrative contributing to the development of mountain policy and the adoption of relevant laws and programmes? For Russia, the mountainous component of the nation's development has long remained in the shadow of the "northern" trend. A number of mountainous regions of Russia located in the south (Altai, Tuva, and Buryat republics, etc.) were included in the list of territories equated to the regions of the Far North (see Fig. 1). Thus, in the absence of their own mountain laws, the regulation and economic and social support in some mountainous areas has relied on legal mechanisms developed for the Far North.

For a long time, the "invisibility" of mountains in the policies of the Russian Federation was associated with the fact that their significance was underestimated; in fact, an accurate calculation of the mountainous area did not exist (Samoilova 1999). The mountains were considered atypical of Russia and mountainous regions were considered too sparsely populated to have any political significance. Insufficient information about the mountains and their specificities did not contribute to the emergence of public opinion and the development of a mountain "lobby", which could have encouraged higher political engagement.

The current attention to mountain issues is largely determined by the influence of knowledge transfer from other mountainous countries, and by the social problems of the mountain population, which have worsened in recent decades and led to a number of conflicts, primarily in the North Caucasus. Some publications have thus stated that Russia needs to develop and adopt a special mountain policy (Gornye Issledovaniya 2014).

Globally, the importance of mountains was first recognised in an ecological context. At the 1992 UN conference, the mountain theme was highlighted among other key themes in Agenda 21, and the International Year of Mountains was held ten years later – in 2002.

The Mountain Chapter 13 of Agenda 21, adopted at the UN summit in 1992, can be considered as the most important documents of "soft" law. Paragraph 42 of the Plan of Implementation of the World Summit on Sustainable Development published ten years later in 2002 was also devoted to mountains. In 2012, at the UN Conference Rio + 20, the problem of mountain regions was also included in the 2030 and 2050 agendas.

In some countries, the importance of mountain specificity was recognised even earlier. In the early 1950s was initiated an agreement to protect the Alps, which later resulted in the Alpine Convention. At the UN World Mountain Summit in Bishkek (in the International Year of Mountains 2002), five Central Asian countries (Kazakhstan, Kyrgyzstan, Uzbekistan, Tajikistan, and Turkmenistan) adopted the Central Asian Mountain Charter. The Charter deals with the issues, use, and management of mountainous areas. On the initiative of the Congress of Local and Regional Authorities of Europe (an advisory body to the Council of Europe), the Charter of the European Mountain Regions was drafted. It defines the basic principles of the

European mountain policy (Report 2003). It is addressed to all member states of the Council of Europe and, in a sense, is an extension of the principles of the European Union's mountain policy and the Regional Alpine Convention. The Charter consists of six parts and 31 articles. The first part defines a mountainous region in terms of localities where elevation, relief, and climate create special conditions that affect daily human activities" (Treves et al. 2004).

The authorities of countries such as Switzerland, France, Bulgaria, Georgia, Kyrgyzstan, Tajikistan, etc, pay special attention to mountain legislation. Mountain areas there have a special status, and the legislation aims at enhancing living conditions of the mountain population. At the same time, the fundamental concept, on which the institutionalisation of mountain differences is based, is the definition of mountain territory. In France, for instance, a mountainous zone is defined as a territory of communes, at least 80% of which is located at an altitude of more than 600 m above sea level, or in which the difference in altitude between the lower and upper boundaries of cultivated land is at least 400 m. The European Agricultural Fund for Rural Development has identified mountain areas that may be eligible for payments in case of significant restrictions on the use of the land and a significant increase in the cost of its cultivation. This is caused by one or a combination of two factors: mountain climate and mountainous relief. At the same time, areas north of 62nd parallel, and some adjacent areas, should be considered as "mountainous". According to literature (c.f., Castelein et al. 2006; Mountain 2004; White Book 2000), the criteria for classifying an area as mountainous differ from country to country. In Germany and Austria, for example, any territory higher than 700 m above sea level is deemed mountainous. In Austria, the areas even higher than 500 m above sea level are deemed mountainous if the slopes occupy more than 20% of the area. In Poland, mountain areas are deemed those above 350 m and even lower if slopes with a steepness of more than 12 degrees occupy at least 50% of agricultural land in the municipality. About two-thirds of Switzerland's area is designated as "mountainous" under the 1974 Federal Mountain Investment Act (Castelein et al. 2006). In 2001, the Committee on Agriculture of the European Parliament adopted a more general view of mountainous areas within the EU. Administratively separate regions with more than 50% of the agricultural area used are located at least at an altitude of more than 600 meters above sea level (if necessary, with a higher limit of up to 1000 m above sea level, depending on the number of frost-free days) and with a shorter growing season as well as in regions where the average slope exceeds 20% (Report 2003).

In Russia, as in the case with the definition of the North's border, the level, from which the area is deemed mountainous, is not clearly defined. As a result, at the regional level, there are several definitions of mountainous territory. For example, in the Law of the Republic of Dagestan (2010)[8], mountainous areas include zones 1,000 m above sea level and those with rugged relief and relative elevations 500 m above sea level or more within a radius of 25 km. According to the Law of the Republic of North Ossetia-Alania (2019)[9], a mountainous territory is understood as an area with rugged relief and an absolute relief height above 800 m.

Our research in the regions of the Russian Federation, which included the use of GIS, showed that purely formal criteria, such as absolute height above sea level, are insufficient to classify a municipality as a mountainous territory. Thus, classification of mountainous territories in the Russian Federation should be based on elevation marks. Presumably, if the mountains begin at a height of more than 1,000 m, then the mountainous territories occupy about 8% of the land mass of the Russian Federation. If mountains 300 m above sea level are counted, then the mountains occupy 40% of the total area of Russia.

According to GIS analysis, the mountainous territories of the North Caucasus Federal District (NCFD)300 m above sea level occupy almost half of the entire territory of the district; around a quarter of the area lies 1,000 m above sea level (Table 1).

The maximum height of settlements differs by almost 1,000 m. For instance, the village of Dombai in the Western Caucasus is located at an altitude of 1,600 m above sea level and the village of Kurush in the east is located at an altitude of 2,650 m above sea level. In the Urals, in mountains of Siberia and the Far East, the overwhelming majority of settlements are located below 1,000 m. A few settlements in the mountains of Southern Siberia, for example, in Altai are located at a height of 1,500 m. This means that territories above the indicated marks are not inhabited. However, the local population in these places uses the high mountains for cattle grazing and breeding or for tourism.

Assessments of population living in particular mountainous areas show large differences in the number of people registered and actually residing. In Dagestan, most mountain inhabitants registered in mountain settlements live seasonally on the plain (in kutans).

Studies of the entire variety of mountainous areas have shown that in order to develop criteria for classifying municipalities as mountainous areas, it is first necessary to identify mountain zones characterised by a complex mix of natural and socio-economic conditions for life and nature management. The location of rural settlements in a particular mountain zone, as well as the location of the bulk of land, which form the core of these settlements (regardless of the location of the settlement itself) are the main criteria for classifying municipalities as mountainous.

Table 1. The share of mountains in the North Caucasus Federal District (according to GIS analysis)

Sea level, at which the area is deemed mountainous	Share of mountain area
more than 300 m	47.7%
more than 500 m	40.3%
more than 800 m	33.0%
more than 1000 m	26.7%

[8]*Law of the Republic of Dagestan "On the mountainous territories of the Republic of Dagestan" 16.12.2010 N 72. Collected Legislation of the Republic of Dagestan, 31.12.2010, N 24, Art. 1205.*
[9]*Law of the Republic of North Ossetia-Alania dated February 12, 2019 No. 9-RL. Available at https://docs.cntd.ru/document/802042100. [Accessed 29 July 2021].*

The list of mountain municipalities should be determined by the authorities of the constituent entities of the Russian Federation, based on the historically established settlement system and on a detailed analysis of local characteristics with the involvement of scientists, experts, and representatives of local municipalities.

DISCUSSION

The main similarities in the development of institutional mechanisms in mountains and in the North are the complex and multi-component criteria used to delineate mountains or the northern territories, aligned with non-coincidence in administrative boundaries (Table 2). There are also significant differences in the institutionalisation of the mountains and the North (Table 3).

The most important difference between the institutionalisation of the North and the mountains is that in the case of the North, it was the state that initiated the creation of special legal conditions. In the case of the mountains, the initiator was the public, initially at the regional level (North Ossetia-Alania, Dagestan, etc.) and then via federal discussion and the eventual adoption of special laws. The years 2014–2016 became an important milestone in the formation of state mountain policy, facilitated by the activities of the Head of the Republic of Dagestan, R.G. Abdulatipov. A number of conferences and forums were held. In particular, in 2014, at the Gray Caspian forum, the Gunib Declaration "Mountainous regions of the North Caucasus: development through the integration of the culture of economy and ecology" was adopted. Next, 2016 was declared the Year of the Dagestan Mountains. The Government of Dagestan appealed the Russian president to support the Charter for Sustainable Development of the Mountainous Areas of Russia, as well as the Federal Law "On the Socio-Economic Development of Mountainous Regions of Russia". However, the Presidential Administration deemed both factors non-viable and did not promulgate special measures to support mountainous areas at the federal level. As a result, mountain institutionalisation is not included in the list of the tasks priority for the state; instead, it is associated with costs that are unlikely to pay off in the short term (in contrast to the North, which provides income).

Nevertheless, there are important signs that the state is starting to pay more attention to the mountains. In the Strategy for Spatial Development of the Russian Federation (2019)[10], there is no direct mention of mountainous territories or mountainous regions receiving special status. However, clause 60 of the Plan for the Spatial Development Strategy of the Russian Federation (2019)[11] provides for the development of criteria for classifying municipalities of the Russian Federation as mountainous areas, as well as for adopting a set of measures for the sustainable development of the Russian regions in mountain areas. This decision necessitates scientific substantiation of the criteria for "mountainousness", which requires detailed research in different regions of Russia.

The institutions of the North and the mountains differ in legal, economic, political, and other aspects. Geographically, institutional differences can be correlated with the main functions of institutions according to Paasi (1986): 1) fixing boundaries; 2) regulating social relations arising from special conditions (northern or mountainous); 3) ensuring the emergence of northern or mountain symbols; 4) supporting the development of a northern or mountain identity. These types of institutions may be indicative of some kind of institutional evolution. Thus, the development of a special regional identity may indicate deeper results of the development processes (Zamyatina, Pilyasov 2018).

While formal institutions that secure boundaries and provide benefits for the North were established long ago, institutions that secure symbols and maintain identity are at the stage of formation or are absent at all. At the socio-cultural level, in particular in terms of identity and values, mountains have undoubtedly greater potential. In contrast to the mostly utilitarian goals of the institutionalisation of the North, mountainous regions are able to reveal the deep

Table 2. Comparison of "North" and "mountain" factors

Characteristics	Territories of the North and those included	Mountains
Number of regions in the Russian Federation	25	43
Share (%) of the country's area	65	53
Assignment criteria	Geographic latitude, climate severity determined by the degree of discomfort of living, northern limit of grain growing, presence of permafrost, transport accessibility, working capacity and labour productivity, duration of the heating period, etc.	Altitude, terrain ruggedness, small outlines, shortage of arable land, increased risk of natural disasters, accessibility, increased construction costs, fuel consumption, etc.
The beginning of institutionalisation – taking into account factors in legal regulation	1932 (Acts on benefits for persons working in the Far North of the RSFSR)	1998 (Acts on mountainous territories in the Republic of North Ossetia-Alania)
Major challenges	Melting of permafrost and shelf ice, population outflow	Melting of mountain glaciers, hazards
Scientific institutions in the Russian Federation, dealing with complex issues in the development of northern and mountain areas	Arctic and Antarctic Research Institute, Arctic institutes and universities in some regions (Yakutsk, Murmansk, etc.), laboratory of geoecology of the North at Moscow State University, etc.	Laboratory of Mountain Geosystems at the Institute of Geography of the Russian Academy of Sciences (in the 1990s), Institute of Ecology of Mountain Territories in Nalchik, etc.

[10]*The Spatial Development Strategy of the Russian Federation until 2025.2019. Available at https://www.economy.gov.ru/material/file/a3d075aa813dc01f981d9e7fcb97265f/130219_207-p.pdf. [Accessed 11 December 2021].*
[11]*Implementation Plan for the Spatial Development Strategy of the Russian Federation for the period up to 2025 (2019). Order of the Government of the Russian Federation of December 27, 2019 No. 3227-r.*

Table 3. The institutional differences between the North and mountainous regions

Institutions	North	Mountainous regions
1) Fixed boundaries	The laws define the border of the Arctic zone, the North.	Regional laws define the boundaries of mountainous territories (North Ossetia, Dagestan, Ingushetia).
2) Regulation of social relations arising from special conditions	The laws regulate the use of natural resources and providing benefits.	Regulations exist only at the regional level (support of mountain residents through development programmes in certain regions).
3) Ensuring the emergence of northern or mountain symbols	at the stage of formation (for example, the establishment of cultural and administrative centers with own symbols)	no institutions
4) Supporting the development of a northern or mountain identity	no institutions	no institutions

spiritual and cultural potential of the mountain population. The priority task in the development of the Arctic Zone is to ensure national security and to develop the resource base, while the main objective for the mountains is sustainable development, in which the cultural component plays an important role. The boundaries of the North are defined 'from above', but for the mountain territories, this principle is inapplicable, that is why their borders should be determined at the municipal level, which in turn would give the local population a chance to be involved in the decision-making process.

In relation to cross-border and international cooperation, the North remains a relatively closed territory. Many mountainous regions are also closed, due to border regimes. However, mountainous transboundary rivers, ecological, migrational and ethnical problems make it necessary to include the transboundary issue in lawmaking.. In particular, the Model Law of the CIS countries (Article 8. Transboundary cooperation in the development and protection of mountain areas) provides for establishing national and (or) interstate councils for the development and protection of mountain areas. The prevailing economic focus is another important distinctive feature of laws on the North; thus, the criteria for granting state benefits and guarantees are determined primarily by economic payback. After a series of environmental disasters in the Arctic Zone, for which large business enterprises were responsible, the monitoring system has undergone significant changes. However, the principles of interaction between government, business, and society are still based on economic interests and income. This situation is almost impossible in the mountains, since there is not enough (potential) income to cover costs. A striking example in this regard is the constant conflict of interests around the tourist complexes of the North Caucasus, initiated and financed by the state (Gunya 2017).

CONCLUSION

The comparison of different territories as subjects of legal regulation is dealt by interdisciplinary areas of research, primarily geography, social anthropology, political ecology, and law. This study focused on the Russian North and the mountain territories of Russia, which, due to their natural characteristics, differ significantly from regions in the temperate zone or lowland territories in their potential of natural resources and environmental management. An institutional approach based on the analysis of mechanisms (institutions) that fix the boundaries of regions, regulate the use of natural resources and life standards, and lay the foundations for future development can serve as a methodological approach for such an interdisciplinary analysis. The available material allows tracing the logic and history of the institutionalization of Russia's North. The borders of the North and the Arctic have changed several times. Legislation on these regions has been developing for almost a hundred years. The main initiator promoting the institutionalization of the North was the state interested in exploiting the rich resources and protecting its geopolitical interests. The institutionalization of Russia's mountainous regions is just beginning. The mountains, in comparison with the northern territories, have significantly smaller reserves of natural resources; they require large expenditures for the development and regulation of emerging social conflicts. The initiators of the institutionalization are scientific and public organizations that disseminate legal practices in the development of mountains. Institutionalization is initiated by scientific and public organizations that disseminate legal practices in the development of mountains and is supported by politicians. It is necessary to adopt laws on mountain areas in three North Caucasian constituent entities of the Russian Federation, as well as a model law on the protection and development of mountain areas in the CIS countries. It is obvious - that the "mountain" factor has begun to influence the processes of institutionalization to foster the development of mountainous territories in Russia albeit with a certain amount of delay. The comparison of the institutionalization of the North and of mountainous territories shows that it is important to define borders (both external and internal differentiating the region). The definition of the mountainous territory and its boundaries is still discussed. In regions where mountain laws have been adopted, these boundaries are drawn in different ways. It seems that the selection of the border of the mountainous territories of Russia according to uniform criteria is hardly possible due to large natural and socio-economic differences. The development of institutions that regulate social relations and benefits for the resident population reveals more similarities in the institutionalization of the North and mountainous territories. Other aspects of institutionalization associated with the development of northern or mountain symbols and identity remain understudied. The range of tasks for a deeper study of the processes of institutionalization of regions should include interdisciplinary aspects that reveal the peculiarities of the constellation of key actors (first of all, the state, local population, and business) competing for access to key natural resources, as well as claiming the right to participate in institutionalization itself.

REFERENCES

Adler C., Balsiger J., Grêt-Regamey A., Heinimann A., Huggel C., Weingartner R., Alcántara-Ayala I., Gebrekirstos A., Grau R., Jimenez Zamora E. (2020). Making connections for our changing mountains: Future directions for the mountain research initiative, Mountain Research and Development, 40 (1), 1–6, DOI: 10.1659/MRD-JOURNAL-D-20-00054.1.

Agnew J. A. (2013). Arguing with Regions, Regional Studies, 47(1), 6–17.

Agranat G.A. (2007). "Russian North" in life and in books (abstract and analytical review, Geography at school, No. 4, 7–13 (in Russian).

Castelein A., Dinh T.T.V, Mekouar A., Villeneuve A. (2006). Mountains and the law: emerging trends, Rome, Food and Agriculture Organization of the United Nations.

De Vreese C. H. (2012). New Avenues for Framing Research, American Behavioral Scientist, No. 56(3), 365–375.

Debarbieux B., Price MF. (2012). Mountain regions: A global common good? Mountain Research and Development, 32(1), 7–11.

Debarbieux B. (2012). How regional is regional environmental governance? Global Environmental Politics, No. 12(3), 119–126.

Dörrenbächer P. (1998). Baie James: Institutionalisierung einer indigenen Region, Erdkunde, 52(4), 301–313.

Galinovskaya E.A. (2020). Problems of state and legal support for sustainable development of mountainous regions of Russia, Issues of state and municipal administration, 1, 166–196 (in Russian with English summary).

Golubchikov Yu.N. (1992). Modern periglacial nature in connection with the problems of its development, Bulletin of Moscow University, series 5 Geography, 3, 3–9 (in Russian with English summary).

Golubchikov Yu.N. (1996). Geography of mountainous and polar countries. Moscow. Moscow State University (in Russian).

Golubchikov Yu.N. (2015). Modern periglacial natural environment and its humanitarian and geographical features, Earth's Cryosphere, Volume 19, 3, 3–9 (in Russian with English summary).

Gunya A. (2013). Institutional restructuring of geographic space: the impact of land privatization on the mountainous landscapes of the North Caucasus, Palmarium Academic Publishing, Saarbrücken (in Russian with English summary).

Gunya A. (2017). Land Reforms in Post-Socialist Mountain Regions and their Impact on Land Use Management: a Case Study from the Caucasus, Journal of Alpine Research | Revue de géographie alpine [En ligne], 105–1 | 2017, mis en ligne le 07 mars 2017, consulté le 06 avril 2017, DOI: 10.4000/rga.3563.

Katorin I.V. (2016). Features of the institutionalization of the Arctic zone of Russia, Territory development problems, No. 5 (85), 191–200 (in Russian with English summary).

Kotlyakov VM, Badenkov Yu.P. (1999). Foreword, Mountains of the World. Global priority, Moscow, Noosphere, vii – ix. (in Russian with English summary).

Kotlyakov V.M., Badenkov Yu.P., Chistyakov K.V. (eds.). (2014). Mountain research. Mountain regions of northern Eurasia. Development in the context of global changes, Issues of geography, Ed. 137, Russian Geographical Society, Moscow, Publishing house Kodeks (in Russian with English summary).

Laruelle M. (2012). Larger, Higher, Farther North … Geographical Metanarratives of the Nation in Russia, Eurasian Geography and Economics, 53, No. 5, 557–574, DOI: 10.2747/1539-7216.53.5.557.

Lindner P. (1998). Zur geographischen Relevanz einer institution-orientierten Analyse von Industrialisierungsprozessen, Geographische Zeitschrift, 86, Heft 4, 1998, 210–224.

Lukin Yu.F. (2013). The Russian Arctic in a Changing World, North (Arctic) Federal university of Lomonosov, Arkhangelsk, CPC NArFU (in Russian with English summary).

Mountain Areas in Europe: Analysis of mountain areas in EU member states, acceding and other European countries. (2004). Final report for the European Commission. Nordic centre for spatial development. Available at https://ec.europa.eu/regional_policy/sources/docgener/studies/pdf/montagne/mount1.pdf. [Accessed 28 July 2021].

Paasi A. (1986). The institutionalization of regions: a theoretical framework for understanding the emergence of regions and the constitution of regional identity, Fennia, 164, 105–146.

Paasi A. (2010). Regions are social constructs, but who or what `constructs' them? Agency in question, Environment and Planning, 42, 2296–2301.

Pilyasov A.N. (2020). Arctic entrepreneurship development factors. Geography, Environment, Sustainability, 13(1), 46–56, DOI: 10.24057/2071-9388-2019-91

Report of the Committee of the Regions on 'Community action for mountain areas'. (2003). Official Journal of the European Union. P 128/05.

Samoilova G.S. (1999). Morphometric analysis of mountainous territories of Russia, Izvestiya RAS, geographical series, No. 2, 110–113 (in Russian with English summary).

Savchenko A.B., Treivish A.I. (2017). Historical and geographical features of the development of the northern and arctic territories of Russia in the 17th–19th centuries, Izvestiya RAS, geographical series, 3, 90–102 (in Russian with English summary).

Schmidt M. (2017). Human Geography of Post-Socialist Mountain Regions, Journal of Alpine Research | Revue de géographie alpine. 2017, 105–1 15 mars 2017, DOI: 10.4000/rga.3573.

Schmidt M., Stadelbauer J. (2017). Humangeographische Forschungen zu (post)sowjetischen Hochgebirgen, Mitteilungen der Österreichischen Geographischen Gesellschaft, 159. Jg. (Jahresband), Wien, 55–81.

TTreves T., Pineschi L.. and Fodella A. (eds.). (2004). Sustainable Development of Mountain Areas – Legal Perspectives beyond Rio and Johannesburg, University of Milan, Milano.

White Book 2000 on Mountain Forests in Europe. European Observatory of Mountain Forests. (2000). European Union DG Agriculture and EOMF, Saint Jean d'Arvey.

Zamyatina N.Yu., Pilyasov A.N. (2018). Russian Arctic: Towards a New Understanding of Development Processes. Moscow, URSS. (in Russian).

Zaydfudim P.Kh., Golubchikov S.N. (2003). Introduction to Russian Northern Studies. Moscow, ART (in Russian).

RESEARCH PAPER

PHYLOGENETIC PHYTOGEOGRAPHY OF SELECTED GROUPS OF SEAGRASSES (MONOCOTYLENDONEAE - ALISMATALES) BASED ON ANALYSING OF GENES 5.8S RRNA AND RUBISCO LARGE SUBUNIT.

Anton A. Iurmanov[1*]
[1]Main Botanical Garden named after N. V. Tsitsin RAS, st. Botanicheskaya, 4, Moscow, 127276, Russia
***Corresponding author:** yurmanov–anton.ya.ru@yandex.ru
Received: September 25th, 2021 / Accepted: February 15th, 2022 / Published: March 31st, 2022
https://DOI-10.24057/2071-9388-2021-111

ABSTRACT. Seagrasses are representatives of the families Cymodoceaceae, Posidoniaceae, Zosteraceae, Hydrocharitaceae (Monocotylendoneae - Alismatales), adapted to growing in seawaters and all their important life circle events are taking place under the water including pollination and distribution of diasporas. Seagrasses are widespread in the littoral areas of the World Ocean, except for Antarctica, and play an important ecosystem role. Due to the insufficiently studied history of dispersal and formation of modern seagrasses habitats, we carried out a phylogenetic analysis of representatives of the families Cymodoceaceae (*Amphibolis, Halodule, Syringodium, Cymodocea,* and *Thalassodendron*), Posidoniaceae (*Posidonia*), Zosteraceae (*Zostera*, and *Phyllospadix*), and Hydrocharitaceae (*Enhalus, Halophila*, and *Thalassia*). The cladograms constructed based on molecular data analysis of the 5.8S ribosomal RNA and ribulose–1,5–bisphosphate carboxylase/oxygenase large subunit genes are used as the basis for reconstructing the history of dispersal of the studied taxa. It is found that the main stages of dispersal of selected groups of seagrasses took place in the Late Cretaceous period. The main track of historical distribution is largely predetermined by the modern ranges of almost all genera of seagrasses, stretches from the southwestern waters of eastern Gondwana to the northwestern waters of the Eurasian part of Laurasia. The main route of movement of diasporas and seagrasses populations was the Tethys water area, which was modified in the Late Mesozoic and early Cenozoic. It was revealed that the main method of dispersal of seagrasses was long-distance dispersal, which is confirmed by both molecular genetic data and very fast (on a geological time scale) processes of penetration into new water areas, and analysis of the features of dissemination of modern representatives. An alternative vicar scenario was proposed only for the reconstruction of the formation of the *Posidonia* range.

KEYWORDS: seagrasses, higher Alismatales, phylogenetic phytogeography, dispersal history, cladistic analysis, molecular data

CITATION: Iurmanov A. A. (2022). Phylogenetic phytogeography of selected groups of seagrasses (Monocotylendoneae - Alismatales) based on analysing of genes 5.8S rRNA and RuBisCo large subunit. Vol.15, № 1. Geography, Environment, Sustainability, p 61-69 https://DOI-10.24057/2071-9388-2021-111

ACKNOWLEDGEMENTS: The reported study was funded by RFBR, project number 19-34-90164. Anton A. Iurmanov carried out the work in the framework of the state assignment of the Main Botanical Garden named after N. V. Tsitsin RAS, project number 18-118021490111-5 based on the USI Fund greenhouse.

Conflict of interests: The authors reported no potential conflict of interest.

INTRODUCTION

Seagrasses are an ecological group of marine monocotyledonous angiosperms (Monocotylendoneae - Alismatales) adapted for growing in seawater. This ecological group includes representatives of the families Cymodoceaceae (*Amphibolis, Halodule, Syringodium, Cymodocea, Thalassodendron*), Posidoniaceae (*Posidonia*), Zosteraceae (*Zostera, Phyllospadix*), and Hydrocharitaceae *(Enhalus, Halophila, Thalassia*) and the plants grow, become pollinated, and produce fruits underwater (Hogarth 2015; Iurmanov et al. 2021). Seagrasses grow in estuaries, bays, lagoons, banks, and shoals in most parts of the Northern and Southern Hemispheres, except for the coastal areas of Antarctica (Hemminga and Duarte 2000). The distribution of seagrasses depends on the ability to spread and occupy new areas of the littoral and sublittoral zones. The highest diversity of seagrasses is observed in Southeast Asia and in different directions out of this area the number of species decreases along the trajectory of the main ocean currents (Green and Short 2003). Seagrasses populations are productive ecosystems that create three-dimensional shelter structures and generally form the habitat for dozens of companion species (Nagelkerken and van der Velde 2004), including breeding and growth sites, the final link in the food chain in such ecosystems often become marine mammals (Irlandi and Peterson 1991). They are important carbon sinks, accounting for about 10% of the total carbon sequestration in the atmosphere. Seagrasses communities sequester about 27.4 million tons of CO_2

annually (Macreadie et al. 2013). All this gives reason to consider them as habitat formers, similar in importance to the meadows of monocotyledonous plants on land (Coleman and Williamc 2002). Since a decrease in the cover of seagrasses in the sublittoral leads to a decrease in biodiversity and a change in the entire structure of coastal marine biocoenosis, they require attention not only as biological species but also as biotopes (Hemminga and Duarte 2000).

The available information on seagrasses fossils is not very extensive, but it is sufficient to establish in general terms the main stages of their evolution. Reliable fossils records are present for two extinct genera, *Thalassocharis* and *Archeozostera*, from the Upper Cretaceous of Western Europe (Voigt 1981) and Japan, respectively (Larkum and den Hartog 1989), and the modern genus *Posidonia* is represented by fossil species *Posidonia cretacea* Hosius von der Marck found in the sediments of the Upper Cretaceous, belonging to the Late Santonian - Campanian stages (84.9 - 70.6 Ma ago), in Ahrenfeld (Germany) (Hosius and Von der Marck 1880). Presumably, the first angiosperms returned to the marine environment during the Cretaceous, about 100 to 70 million years ago (Les et al. 1997). However, early Cretaceous seagrasses are almost unknown. The initial invasion of the ancestral sea by seagrasses occurred later, presumably in the Tertiary along the shores of the Tethys in parallel with the evolution of mangrove forests (Hogarth 2015). After that, the change in the areas of distribution of seagrasses was a consequence of tectonic movements, the emergence of barriers (landmasses), fragmenting the Tethys into partially isolated water areas. These barriers explain, for example, the phenomenon of habitation of morphologically closely related pairs of species from the genera *Thalassia, Halodule*, and *Syringodium* in the Pacific Ocean and the Caribbean, as well as *Zostera* and *Phyllospadix* on opposite coasts of the Pacific, separated, respectively, by the Isthmus of Panama and the vast water area of the central part of the Pacific. Throughout history, seagrasses have probably never been represented by a large number of species. Some of the fossil species are now extinct, but it is unlikely that the total number of species ever exceeded 50-60. Supposedly this can be explained by the reproductive limitations of life in the marine environment and the tendency for the spread of seagrasses by vegetative reproduction (the phenomenon of "vegetative mobility"), and not with the help of seed reproduction.

At the end of the Eocene, about 40 million years ago, most modern seagrasses genera evolved, including *Thalassia, Thalassodendron, Cymodocea*, and *Halodule*, while *Enhalus* and *Phyllospadix* appeared more recently (Larkum and den Hartog 1989). The origin of the seagrasses remains unclear as far as the fossil data are insufficient, and the modern molecular data support the concept that the life form of seagrasses arose during the evolution of monocots of the order Alismatales s. l. more than once and independently. The genera of Hydrocharitaceae (*Enhalus, Halophila*, and *Thalassia*) are most likely descended from freshwater ancestors that acquired salt tolerance and spread downstream into the sea; whereas the representatives of other families of seagrasses (Posidoniaceae, Cymodoceaceae, Zosteraceae) descended from freshwater or marine ancestors independently from each other and developed largely in parallel (Les et al. 1997). To model the history of dispersal of seagrasses the relationship between the genera of seagrasses was revealed based on molecular genetic data and taking into account paleobotanical data. The resolving of the evolutionary relationships of various species of key genera and families of seagrasses will make it possible to reconstruct the processes of their dispersal and to gain an idea of the hypothetical origin of modern marine biosystems.

MATERIALS AND METHODS

For the reconstruction of the dispersal history of the seagrasses, it was analyzed almost half (35 out of a total of 70 species) of the representatives, distributed in different parts of the range. As outgroup was selected *Hydrocharis morsus-ranae L*. (Hydrocharitaceae) and *Scheuchzeria palustris* F. Muell. (Scheuchzeriaceae) sister to seagrasses (APG IV 2016). Molecular genetic data was not enough to create a single cladogram of these species, so it was necessary to separate molecular cladograms for two groups of species. For molecular genetic analysis of genes was selected the data are shown in GenBank: 5.8S ribosomal RNA gene, and ribulose-1,5-bisphosphate carboxylase/oxygenase (RuBisCo) large subunit gene (Table 1.). Because of the formation of two groups of analyzed species, we created several phylogenetic scenarios (for greater representativeness of the results obtained) for most families. These two concepts of evolutionary relationships served as the basis for the reconstruction of a unified dispersal history model.

Table 1. Selected species for the study, sequenced for the 5.8S ribosomal RNA gene and ribulose–1,5–bisphosphate carboxylase/oxygenase large subunit gene

Gene	5.8S ribosomal RNA gene	ribulose–1,5–bisphosphate carboxylase/oxygenase large subunit gene
Species	*Hydrocharis morsus–ranae L., Scheuchzeria palustris F. Muell., Posidonia australis Hook. f., P. oceanica (L.) Delile, Zostera asiatica Miki, Z. capricorni Asch., Z. japonica Asch. & Graebn., Z. marina L., Z. mucronata Hartog, Z. noltii Hornem., Z. novazelandica Setch., Phyllospadix torreyi S. Watson, Cymodocea nodosa* (Ucria) *Asch., C. serrulata* (R. Br.) *Asch. & Magnus, Halodule pinifolia* (Miki) *Hartog, H. uninervis* (Forssk.) *Boiss., H. wrightii Asch., Thalassia hemprichii* (Ehrenb.) *Asch., Th. testudinum Banks ex K. D. König, Enhalus acoroides* (L. f.) *Royle, Halophila australis Doty & B. C. Stone, H. beccarii Asch., H. decipiens Ostenf., H. engelmannii Asch., H. hawaiiana Doty & B. C.Stone, H. major* (Zoll.) *Miq., H. ovalis* (R.Br.) *Hook. f., H. tricostata M. Greenway*	*Hydrocharis morsus–ranae L., Scheuchzeria palustris F. Muell., Posidonia australis Hook. f., P. oceanica (L.) Delile, Zostera angustifolia* (Hornem.) *Reichenb., Z. asiatica Miki, Z. capensis Setch., Z. capricorni Asch., Z. japonica Asch. & Graebn., Z. marina L., Z. mucronata Hartog, Z. noltii Hornem., Phyllospadix scouleri Hook., Ph. torreyi S. Watson, Ph. japonicus Makino, Amphibolis antarctica* (Labill.) *Asch., A. griffithii* (J. M. Black) *Hartog, Cymodocea serrulata* (R. Br.) *Asch. & Magnus, Halodule pinifolia* (Miki) *Hartog, H. uninervis* (Forssk.) *Boiss., H. wrightii Asch., Syringodium filiforme Kütz., S. isoetifolium* (Asch.) *Dandy, Thalassodendron pachyrhizum Hartog, Thalassia hemprichii* (Ehrenb.) *Asch., Th. testudinum Banks ex K. D. König , Enhalus acoroides* (L. f.) *Royle, Halophila decipiens Ostenf., H. engelmannii Asch., H. ovalis* (R.Br.) *Hook. f.*

Using DNA sequences data from GenBank, phylogenetic molecular genetic cladograms were constructed for genera of families of seagrasses and outer groups. After that, the encoded gene portions are copied into one file, which has loaded into the WinClada program to build a phylogenetic cladogram (Hall 2011). Selected portions of the DNA sequence are quite large, their length is in selected species from 477 to 670 (5.8S ribosomal RNA gene) and from 619 to 970 (RuBisCo large subunit) nucleotides.

The alignment for non-homologous portions was performed in Jalview Version: 2.9.0b2 (Waterhouse et al. 2009) using the Clustal W algorithm with standard parameters. The end portions that were not present in all sequences were excised. As a result, an alignment was obtained with a length of 670 (5.8S ribosomal RNA gene) and 970 (RuBisCo large subunit) nucleotides. The resulting alignment was also saved in FASTA format and processed in WinClada ver. 1.00.08 using the NONA ver. 2. Using bootstrap analysis, phylogenetic trees were constructed for 26 and 27 species seagrasses with outer groups.

RESULTS

As a result of our research, cladograms were obtained (Fig. 1, A, and B, respectively). The resulting cladograms are generally similar with high at most nodes bootstrap index, but there are differences in the topology of cladogram A, which reflects the relationship of 26 species of seagrasses (analysis of the RuBisCo large subunit gene) and cladogram B, reflecting the relationship of 27 species of seagrasses (analysis of the 5.8S ribosomal RNA gene).

Basal in both of these cladograms is the outgroup species - *Hydrocharis morus-ranae*. This is followed by a division into two large clades. The first consists of the seagrasses Hydrocharitaceae family species. The basal taxon in clades A and B is *Enhalus acoroides*. The sister species *Thalassia hemprichii* and *Thalassia testudinum* are closest to it. Also in this segment of the cladogram is the *Halophila* group of species. The second clade consists of the families Cymodoceaceae, Posidoniaceae, and Zosteraceae. A similar feature is the proximity of the Halodule and Posidonia clades. In the group of species of the Zosteraceae family, the clade begins with the species of the genus Phyllospadix, and the terminal taxa are the group of species of the genus Zostera.

Also, in the topology of cladograms, there are differences. The first distinguishing feature of the two phylogenetic trees is the topology of the genus *Halophila*. In contrast to cladogram A, in cladogram B, *Halophila decipiens* and H. *ovalis* have a sister, not a daughter position.

The position of one of the species of the outgroup, the *Sheuchzeria palustris* group, which in cladogram B goes immediately after the group of the genus *Halophila*, also differs. On cladogram A, before *Sheuchzeria palustris*, there are groups in sister relationships with a high bootstrap index (minimum 99); they form the species *Cymodocea nodosa* and C. *serrulata*, followed by closely related groups *Posidonia australis* and P. *oceanica*, as well as the clade of the genus *Halodule*, which includes all 3 studied species - H. *pinifolia*, H. *uninervis*, H. *wrightii*. While H. *pinifolia* and H. *wrightii* occupy a daughter position to H. *uninervis* in cladogram B.

In cladogram A, the representative of the outgroup, *Sheuchzeria palustris*, is followed by *Phyllospadix torreyi*. It, in turn, is followed by the terminal genus *Zostera* on the cladogram, in which the basal *Zostera marina* is sister to all other studied species. The next bifurcation is represented by sister Z. *noltii* and closely related species of the genus (Z. *asiatica* and Z. *japonica*), as well as three species – Z. *capricorni*, Z. *mucronata*, Z. *novazelandica*. In cladogram B, a similar clade begins with *Phyllospadix japonicus*, inhabiting the northwest of the Pacific followed by a sister group of species from *Ph. torreyi* and *Ph. scouleri*, distributed in the northeast of the Pacific. The terminal taxon in the cladogram, as in the previous case, is *Zostera*; however, the relationships between the species of the genus are markedly different. The *Zostera* species form two sister clades, the first of which includes Z. *asiatica* and the sister species Z. *angustifolia*

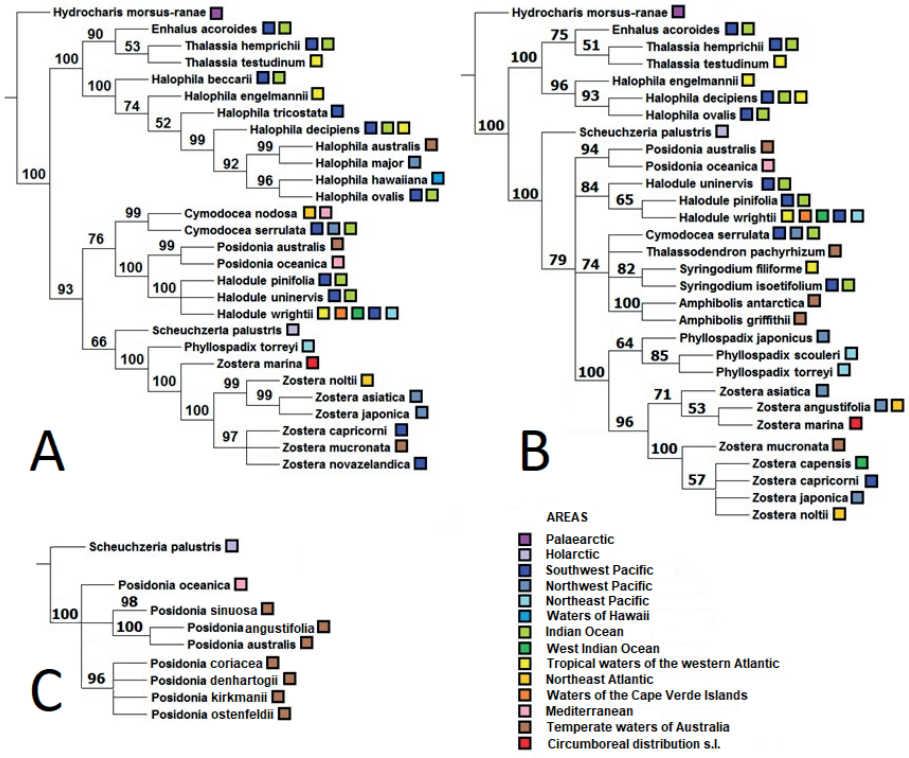

Fig. 1. Original phylogenetic trees of selected representatives of seagrasses, indicating their range, numbers - bootstrap index: A - 26 species (analysis of the RuBisCo large subunit gene), B - 27 species of sea grasses (analysis of the 5.8S ribosomal RNA gene), C - 8 species of the Posidoniaceae family (5.8S ribosomal RNA assay)

and Z. *marina*; in the second clade, the basal species is Z. *mucronata*, sister to which is a polytomy of four species: Z. *capensis*, Z. *capricorni*, Z. *japonica*, Z. *noltii*. This position of the freshwater representative of the outgroup *Sheuchzeria palustris* in both cladograms of the Zosteraceae family indicates the origin of the family independent of other seagrasses.

DISCUSSION

To begin with, it is necessary to turn to the individual stages of the geological history of the Earth and the change in the position of the continents during the collapse of Gondwana, that is, the opening of new water areas, littoral bridges for the settlement of seagrasses. The penetration of seagrasses through the littoral zones into new water areas is associated with the disintegration of Eastern Gondwana, which included Australia, Antarctica, Madagascar, and India, as well as the course of such geological processes as the end of the Messinian crisis (5 million years ago) and the separation of Japan from Eurasia (15 -20 million years ago) (Barnes 2003; Garcia-Castellanos et al. 2009).

The complete separation of the southern part of Gondwana took place 120-100 million years ago, leaving the Subantarctic Islands as the only connecting link between Antarctica and South America (Gabdullin 2005), the littoral of which could have become through the dispersal of seagrasses from the water area of Australia. Dissemination of seagrasses occurs both vegetatively and by seeds, but, unfortunately, has not yet been any studies that determine the time that the fruit can be held in the water and does not rot, as well as how long may be part of the plants by the roots and leaves is a substrate (that is, to vegetate in the water column, drawn by currents, until the moment when they can be fixed in the substrate). That is, the distance that seagrasses can travel in one "act of resettlement" is not known. In this regard, an interesting example is *Halophila hawaiiana*, an endemic to the Hawaiian Islands, which, according to our data, penetrated its present range from the southwestern Pacific. The flora of the Hawaiian Islands - both terrestrial and coastal - was formed due to the influx of new species and their further evolution in isolation for a long time (70 million years ago - the formation of the first islands, and the age of the oldest of the current surface, Midway - 28.3 million years ago (Clague & Dalrymple 1987). The remoteness and isolation of the Hawaiian Islands predetermined that the first marine monocots were able to make a long way to them without intermediate "stops". The proposed seagrasses dispersal model is based on phylogenetic trees (Fig. 1) and paleobotanical data (Fig. 2).

Seagrasses Hydrocharitaceae family

In addition to small families formed only by taxa of seagrasses, there is the freshwater family Hydrocharitaceae, in which there are three genera of marine (Cook 1998). The genus *Enhalus* (family *Hydrocharitaceae*) includes a single species, *Enhalus acoroides* (L. f.) Royle is a perennial herb (Cook 1998). *Enhalus* lives in the tropical coastal waters of the Indian and western Pacific oceans. The genus *Halophila* (family *Hydrocharitaceae*) includes 19 species of perennial or annual rhizome herbaceous plants (Cook 1998). Dissemination of seeds is hydrochory (pericarp rots underwater) or endozoochory (juicy fruits are eaten by aquatic animals). The genus *Halophila* is widespread in tropical waters, but its range also covers subtropical and temperate waters, primarily the Indian and Pacific Oceans. Also, representatives of the genus grow on the coasts of the Mediterranean and Caribbean Seas, the Gulf of Mexico. The genus *Thalassia* (family *Hydrocharitaceae*) includes 2 species: *Thalassia hemprichii* (Ehrenb.) Asch. and *Thalassia testudinum* Banks ex K. D. König is a perennial rhizome herbaceous plant (Cook 1998). Dissemination is hydrochloric (conical seeds with a massive basal part have a displaced center of gravity). Two species belonging to the genus Thalassia have a non-overlapping range. *Thalassia hemprichii* (Ehrenb.ex Solms) Asch. grows in the littorals of the tropical zone of the Indian Ocean and the western part of the Pacific, and *Thalassia testudinum* Banks & Sol. ex K. D. Koenig lives in the littoral areas of the Caribbean Sea.

Unfortunately, now, fossil marine representatives of this family, represented mainly by freshwater forms, have not been found. Our data suggest that the family settled in the Southwest Pacific/Indian Ocean, where most species of the genus still live (Fig. 3). In particular, the basal Enhalus acoroides and the closely related genus *Thalassia*, possibly widespread earlier. Later, the formation of land barriers divided the common range into two

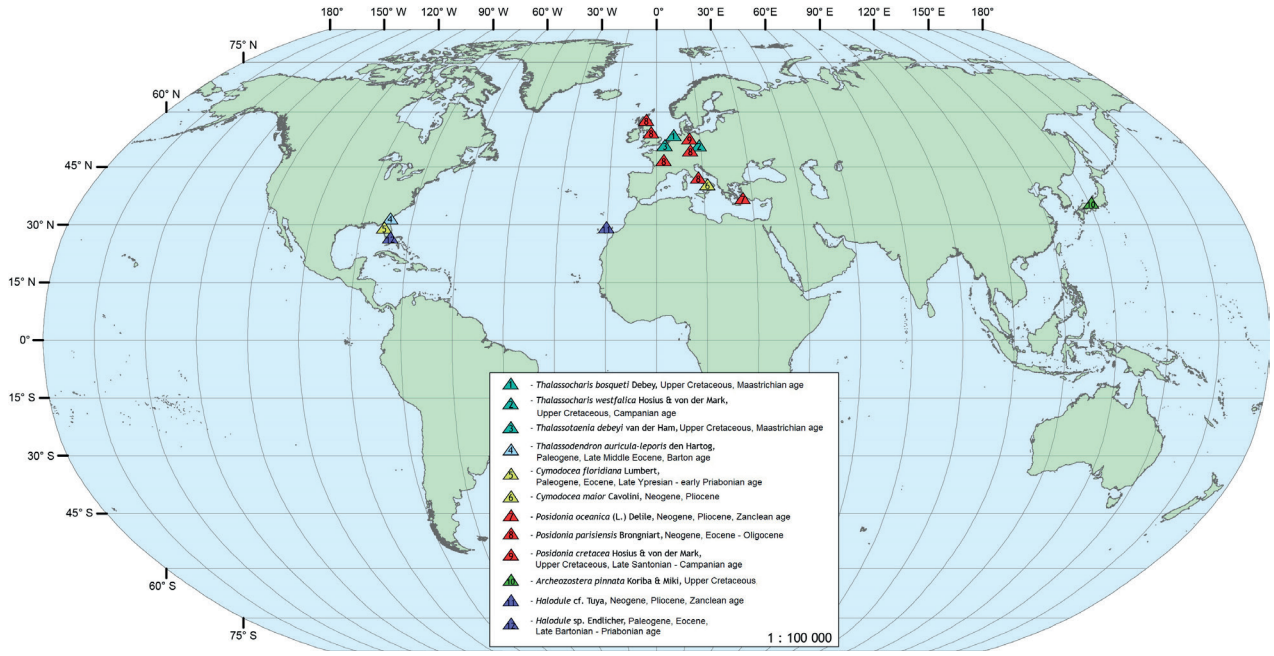

Fig. 2. Localities of discovery of fossils seagrasses

species growing in the warm waters of the Southwest Pacific, Indian Oceans (*Thalassia hemprichii*), and in the Caribbean Sea with adjacent waters (*Thalassia testudinum*). As for the numerous and widespread genus *Halophila*, representatives of the genus inhabited the tropical waters of the Atlantic twice independently (*Halophila engelmannii* and *Halophila decipiens*), two other tracks of the *Halophila* dispersal reached the center/northwest of the Pacific Ocean (*Halophila* major) and temperate waters of Australia (*Halophila australis*). The sister position of *Halophila hawaiiana*, which reached the water area of the Hawaiian Islands, in relation to *Halophila ovalis*, testifies to the fact that this species, whose range is noticeably isolated from other taxa of the genus, settled from the southwestern Pacific (Iurmanov 2018).

Family Cymodoceaceae

The Cymodoceaceae family includes 5 genera (17 species): *Amphibolis* (2 species), *Cymodocea* (4 species), *Halodule* (6 species), *Syringodium* (2 species), *Thalassodendron* (3 species) (APG IV) of perennial herbaceous plants (Kuo and McComb 1998a). Hydrochory dissemination (*Amphibolis* fruits with 4 hard blades covered with thin thorns can spread epizoochory, juicy bracteole of *Thalassodendron* fruits can be eaten by fish), for *Cymodocea nodosa* (Ucria) Asch. autobasichoric is characteristic.

The genus *Amphibolis* is distributed along the western and southern coasts of Australia and Tasmania. The genus *Cymodocea* is widespread in the littorals of the tropical and subtropical seas of the Old World. The genus *Halodule* is widespread on tropical and subtropical coasts. It is found, in fact, on most continents, except for Europe and Antarctica. Representatives of the genus Syringodium are found on the coasts of the Indian and Pacific Oceans, the Caribbean, and the Gulf of Mexico. The genus *Thalassodendron* grows in the western part of the Indian Ocean and the western part of the Pacific Ocean - *Thalassodendron ciliatum* (Forssk.) Hartog littoral of the tropical seas of the Indian and western Pacific oceans, *Thalassodendron pachyrhizum* Hartog littoral of the temperate coast of Western Australia, Thalassodendron leptoarteaule Mariade , sp. nov. littoral of the coast of Mozambique and KwaZulu-Natal.

The evolution of this family is relatively well documented by fossil remains (Fig. 2). For example, there are reliably dated and well-preserved fossils of the genus *Halodule* on the western and eastern sides of the Atlantic. Fossils of the genus *Halodule* have long been represented only by finds of *Halodule sp.* from the Paleogene, Eocene, Late Bartonian - Priabonian stages (40.4 - 37.2 Ma ago) in Florida (USA) (Taylor 2008). However, in 2017, fossils of this genus were discovered in the Canary Islands. The presence of fossil remains of *Halodule sp.*, on the island of Gran Canaria (Canary Islands), was explained by warm currents during the Neogene, Pliocene, Zanklian stage (5.332 - 3.6 million years ago). The identification was confirmed by the presence of fossilized plagiotrophic rhizomes and fruits in the sedimentary deposits of the Early Pliocene. This fossil material from seagrasses is the first on the West African coast (Tuya et al. 2017). *Thalassocharis bosqueti* Debey was discovered in Limburg (Netherlands) and dates from the Upper Cretaceous, more precisely, its Maastrichtian stage (70.6 - 66.043 million years ago) (Voigt 1981). Also *Thalassocharis westfalica* Hosius von der Marck, dated to the Campanian Stage (83.6 - 72.1 Ma ago), was discovered in Westphalia (Germany) (Hosius and Von der Marck 1880). *Thalassodendron auriculaleporis* den Hartog occurs in sediments of the Paleogene, Late Middle Eocene, Bartonian Stage (40.4 - 37.2 Ma ago) in Florida (USA) (Lumbert et al. 1984). The appearance of the first reliable fossil representatives of this genus in America, where it is now widespread, corresponds to the concept of den Hartog (1970), according to which the range of this genus is relict. It is also worth noting *Thalassotaenia debeyi* van der Ham from the Maastrichtian Stage, the Upper Cretaceous System (70.6 - 66.043 Ma ago), found in Belgium (van der Ham et al. 2007). Various fossils and possibly existing species represent the genus *Cymodocea*. These are, for example, *Cymodocea floridana Lumbert*, which occurs in sediments of the Paleogene, Late Middle Eocene, Bartonian Stage (48.6 - 37.2 Ma ago) in Florida (USA) (Lumbert et al. 1984), and *Cymodocea maior* Cavolini, belonging to the Neogene, Pliocene (5.332 - 2.558 Ma ago), discovered in Copanello (Italy) (Ruggieri 1952).

The dominant in the processes of dispersal of the genera Cymodoceaceae was probably the same track as

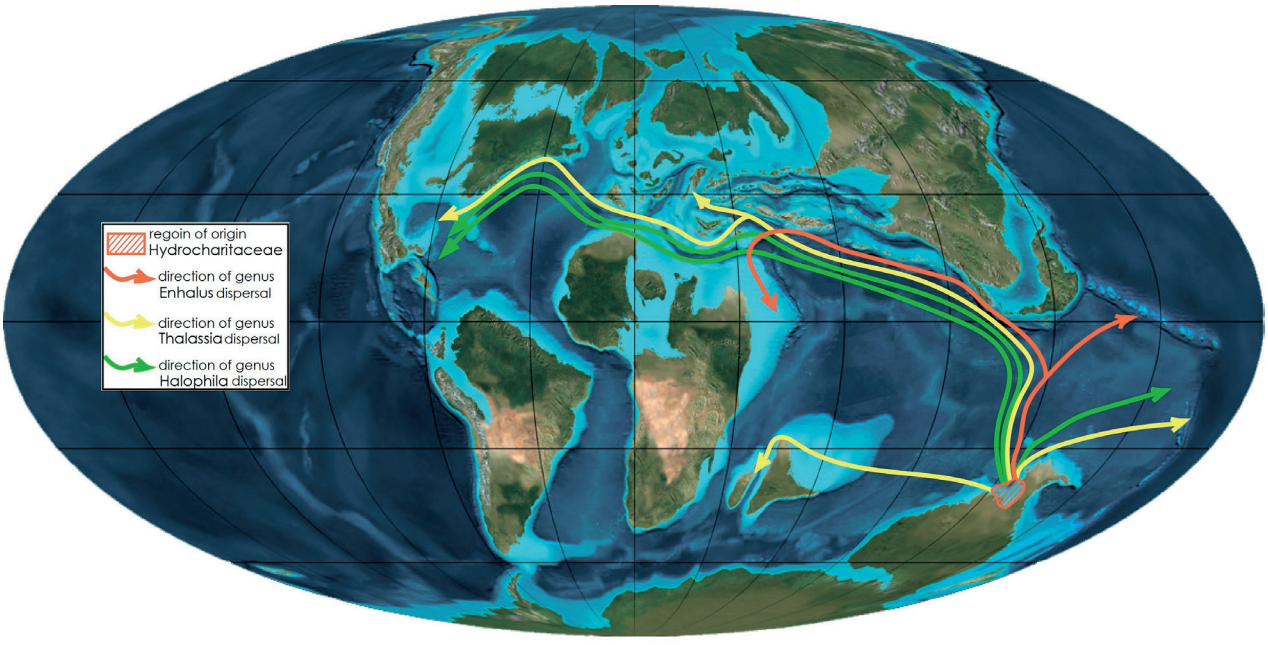

Fig. 3. Formation of the range of marine representatives of the Hydrocharitaceae family. Hereinafter: The position of the land corresponds to the Upper Cretaceous period (90 million years ago). Basemap - Paleogeographic map by Ron Blakey, Colorado Plateau Geosystems (2011)

in the marine taxa Hydrocharitaceae (Fig. 4). Halodule from the waters of the southwestern Pacific, where the genus probably arose (which is confirmed by the distribution of the basal species here - *Halodule uninervis*), spread to the Indian and South Pacific Ocean (*Halodule uninervis* and *Halodule pinifolia*), reaching even the western coast of Central America (*Halodule wrightii)*. Another track was the settlement of *Halodule* in the tropical waters of the Atlantic across the waters of western Africa, where the *Halodule wrightii* range now remains. The dispersal of other Cymodoceaceae taxa proceeded according to a different scenario. The genus *Syringodium (Syringodium filiforme)*, which appeared in this water area, settled from the tropical waters of the western Atlantic, from which, upon reaching the western coast of Africa (*Syringodium isoetifolium*). The genus *Cymodocea (Cymodocea serrulata)* probably originated, and then - and the genera *Thalassodendron (Thalassodendron pachyrhizum)* and *Amphiobolis (Amphiobolis antarctica* and *Amphiobolis griffithii)*, which reached the southern coast of Australia during further dispersal (Iurmanov et al. 2020a).

Family Posidoniaceae

The Posidoniaceae family includes 1 genus (9 species) - *Posidonia* (APG IV) of perennial herbaceous rhizome plants (Kuo and McComb 1998b). Dissemination is hydrochory, fish and seabirds eat juicy fruits. The genus Posidonia has a disjunctive range - the Mediterranean Sea and the Atlantic coast of the Iberian Peninsula (*Posidonia oceanica* (L.) Delile), as well as the southern coast of Australia and Tasmania.

According to den Hartog (1970), two *Posidonia* fossils are known (Fig. 2): *Posidonia cretacea* Hosius and Von der Marck (Hosius and Von der Marck 1880), and *Posidonia parisiensis* (Brongt.) Freitel (= *Caulinites parisiensis Brongt. Posidonia perforata* Saporta & Marion) from the Eocene of the Paris Basin, Germany, Italy, Great Britain, also found in the Oligocene deposits of Great Britain (48.6 - 23.03 million years ago) (Stockmans 1932). These species have thick rhizomes with short internodes and flattened pointed leaves. Among other things, in the sediments of the Neogene, Pliocene, Zanklian stage (5.332 - 3.6 million years ago), on the territory of the island of Rhodes (Greece), a recent species, *Posidonia oceanica*, was found (Moissette et al. 2007).

To analyze the hypothetical history of the settlement of the Posidoniaceae family and to better understand the relationships within the family, it is necessary to refer to a separately constructed cladogram (Iurmanov, 2017) (Fig. 1C). The basal species in this cladogram is *Posidonia oceanica*, probably the oldest taxon of the genus (and family). Fossils of *Posidonia* are found only in Europe. The described cladogram considers two equally probable scenarios: the first, within the framework of the long-distance dispersal concept, and the second, based on the vicar paradigm. (Fig. 5). The first scenario assumes that the genus *Posidonia* originated in the water area that corresponds to the modern Mediterranean Sea, no later than the Cretaceous period. Probably, at the end of the Cretaceous through the water area of the increasing Tethys Ocean, the species of the genus migrated to the Southern Ocean, where they settled in the water areas adjacent to Australia. The content of the second scenario is that at the end of the Cretaceous period, the hypothetical "progenitor species" *Posidonia* inhabited almost the entire Tethys basin. *P. oceanica* is probably closest to this basal species since the relatively stable conditions of the Mediterranean basin contributed to the conservation of the traits of the "progenitor species," whose descendants are so widely represented as fossil remains in Europe. Taxa of the genus, distributed in the southeastern regions of Tethys (den Hartog 1970), evolved at a faster rate, transforming during the Tertiary period into riverine species of temperate waters in Australia and Tasmania (Iurmanov, 2017).

Family Zosteraceae

The Zosteraceae family includes 2 genera (22 species) of perennial herbaceous plants (Kuo and McComb 1998c): *Phyllospadix* (6 species) and *Zostera* (16 species) (APG IV). Dissemination is hydrochloric. The genus *Zostera* is generally widespread along the coast of most of the Northern Hemisphere, as well as Australia, New Zealand, Southeast Asia, and southern Africa. One species of the genus is *Zostera noltii* Hornem. – also grows in the waters of the enclosed Caspian Sea. *Phyllospadix* is native to the temperate North Pacific.

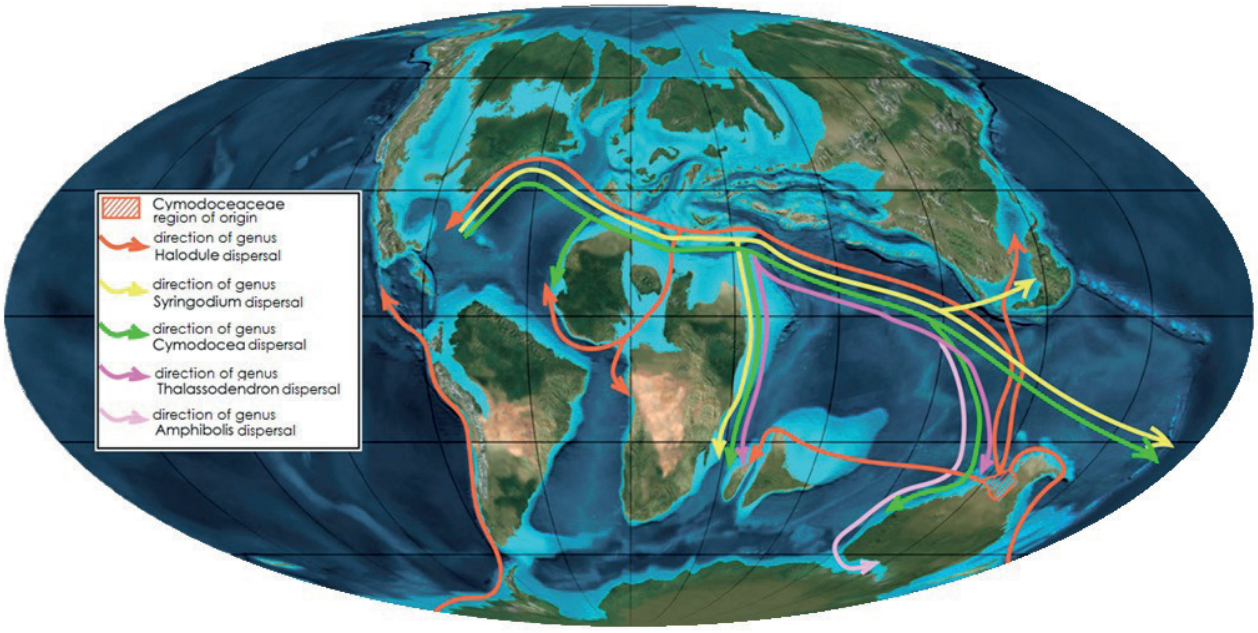

Fig. 4. Formation of the range of the Cymodoceaceae family

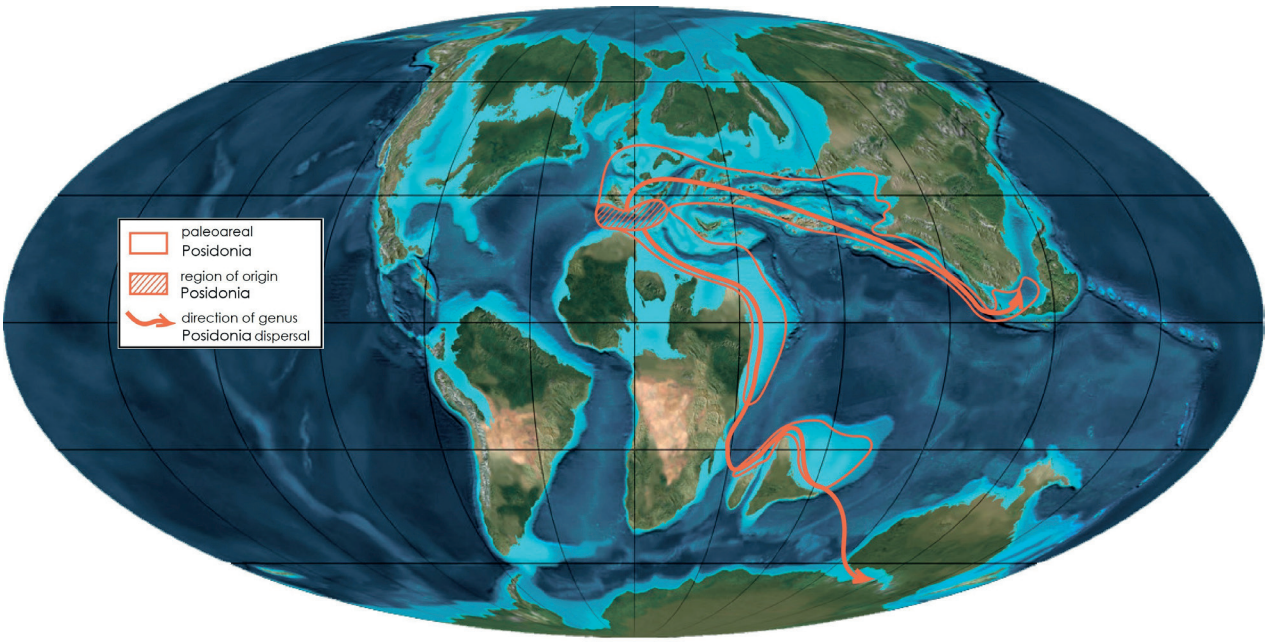

Fig. 5. Formation of the range of the Posidoniaceae family

The reconstruction of the history of distribution and settlement of this family is based on the results of original phylogenetic research and paleobotanical data (Fig. 6). Well-preserved fossils of Archeozostera Koriba & Miki (= *Archaeozostera*) (1931, 1958), have been described from the Upper Cretaceous (99.7 - 66.043 Ma ago) from several ranges of Japan, in particular Izumi, and were considered as protozosteroid - ancestral forms of modern Zosteraceae (den Hartog 1970; Larkum and den Hartog 1989). However, a re-examination of these fossils led to the conclusion that *Archeozostera* was not a marine monocot (Kuo and McComb 1989). They were inland freshwater so, we assume, that *Archeozostera pinnata* was a freshwater, this ancestor of modern Zosteraceae, which are quite resistant to desalination. Therefore, we can assume that the dispersal of representatives of this family began precisely from this range (Fig. 3).

The basal species in the cladogram (Fig. 1 B) is the species *Phyllospadix japonicus* inhabiting the waters of China, Korea, and Japan, while the *Phyllospadix* species from the west coast of North America are sister species to the first taxon. Presumably, the genus *Phyllospadix* settled on the North American coast of the North Pacific - from west to east; some species of the genus *Zostera* likely followed the same path, which also appeared, most likely, in the water area corresponding to the present Far Eastern seas. The genus *Zostera* could have two, not mutually exclusive, tracks in the future dispersal. The first is along the northern coasts of Eurasia. This fact is confirmed by the fact that the modern *Zostera* marina in this region overwinters under ice and endures desalination (water area of the White Sea), that is, *Zostera* may have been resettled along the "northern route" along the confluence of large rivers and further drift of diasporas to the west, which allowed representatives sort to reach the northeastern Atlantic and further - the northwestern part of its water area. At the same time, the sister species of *Zostera marina, Zostera angustiflora*, and *Zostera asiatica*, spread from west to east along the littorals of Beringia. Another dispersal track for Zostera passed through the southwest Pacific and the Indian Ocean, reaching Australia (*Zostera mucronata*), New Zealand and New Guinea (*Zostera capricorni*), and the east coast of Africa (*Zostera capensis*). Possible competition with other species of primordially tropical seagrasses (and, hypothetically, with abundant macrophyte algae in temperate waters of the Southern Hemisphere) could significantly complicate the dispersal of the genus *Zostera* in the waters of the southern Indian and Pacific oceans (Iurmanov et al. 2020b).

Phylogenetic phytogeography of selected groups of seagrasses

Thus, despite the presumably different regions of origin of the selected families of seagrasses, we can distinguish common tracks of their dispersal. The most important of them originate in the subtropical waters of Australia, follow through southern Asia to the east coast of Africa and the waters of Madagascar. The seagrasses colonization of the eastern coast of North America proceeded from the waters of eastern Asia through the waters of northern Europe, and from the basin, widely understood as Tethys, through the western coasts of Africa. But the settlement of the western coast of the Americas, most likely, was carried out from the waters of Eastern Eurasia through the waters of Beringia, as well as from the waters of eastern Australia along with the littoral islands of the Antarctic - up to the western coast of South America. Representatives of the genus Zostera performed the last track (Iurmanov and Romanov 2020).

CONCLUSIONS

1. The analysis of fossil remains of seagrasses concludes that the main families of this ecological group arose at the turn of the Early/Late Cretaceous and rather quickly settled in the World oceans, by the end of the Mesozoic having settled in tropical and subtropical littorals, as well as penetrated temperate waters in certain water areas.

2. The family Zosteraceae probably arose in the waters corresponding to the present northern part of the Pacific, and settled from there along the northern and southern coasts of the Eurasian landmasses, penetrating the waters of the Southern Hemisphere at least twice.

3. The region of origin of the only genus of the family Posidoniaceae was the water area of the Tethys, or only its extreme western part (corresponding to the modern Mediterranean basin). According to the most probable dispersal scenario, the ancient Posidonia species settled in the Southern Hemisphere, "moving" along the littoral zones of the western part of the Indian Ocean.

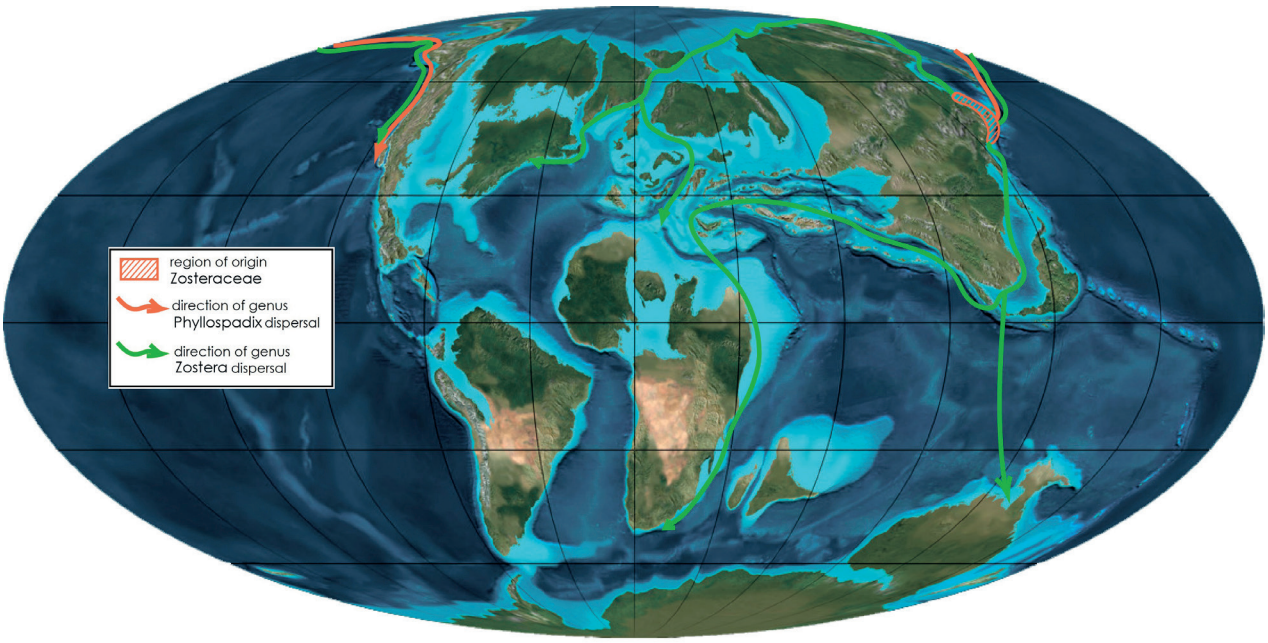

Fig. 6. Formation of the range of the Zosteraceae family

4. In the waters of the tropical part of East Gondwana (Australia + Antarctica), the Cymodoceaceae family arose. This most polymorphic (5 genera) group of seagrasses spread across the World Ocean through various tracks, the most important of which passed along the southern coast of the Eurasian continental masses (through the Tethys' residual basin) and then reached the water area of the modern Atlantic. The genera Cymodocea and Syringodium formed in these waters used the same track to populate the waters of the Indian Ocean and the southwestern Pacific, but "moving" along it, however, in the opposite direction.

5. Analogously, marine representatives of the Hydrocharitaceae family - the genera *Enhalus, Halophila*, and *Thalassia* - settled into the Atlantic from the waters of the tropical part of Eastern Gondwana. Just like in the representatives of Cymodoceaceae, seagrasses from the number of Hydrocharitaceae also spread along other, secondary tracks, penetrating the waters of the Pacific and the southwestern Indian Ocean.

6. The main method of dispersal of the studied groups of seagrasses was long-distance dispersal, which is confirmed not only by molecular genetic data and very fast (on the scale of geological time) penetration into new water areas but also by the analysis of the features of dissemination of modern representatives. Only for the reconstruction of the formation of the range of the genus *Posidonia* was an alternative vicar scenario proposed.

REFERENCES

APG IV. Angiosperm Phylogeny Group IV. (2016). An update of the Angiosperm Phylogeny Group classification for the orders and families of flowering plants: APG IV. Botanical Journal of the Linnean Society, 181, 1–20.

Ascherson P. (1871). Die geographische Verbreitung der Seegr¨aser. Petermann's Geographische Mittheilungen, 17, 241–248.

Ascherson P. (1875). Die geographische Verbreitung der Seegr¨aser. In: Anleitung zu wissenschaftlichen Beobachtungen auf Reisen, mit besondere R¨ucksicht auf die Bed¨urfnisse der kaiserlichen Marine. Berlin: Robert Oppenheim Verlag, 359–373.

Ascherson P. (1906). Die geographische Verbreitung der Seegr¨aser. In: Anleitung zu wissenschaftlichen Beobachtungen auf Reisen. 3rd Ed, Band 2. Hannover: Dr. Max Janecke Verlagsbuchhandlung, 389– 413.

Barnes G. (2003). Origins of the Japanese Islands: The New «Big Picture». Nichibunken Japan Review, 15, 3–50.

Bobrov A., Roslov M., Romanov M. (2020). Phylogenetic biogeography of Hamamelidaceae s. l. based on molecular data. Bulletin of St. Petersburg University. Earth Sciences, 65(2), 224–244. (In Russian with English summary).

Borum J., Duartes C., Krause Jensen D. and Greve T. (2004). European seagrasses: an introduction to monitoring and management. London: EU Project Monitoring and Managing of European Seagrasses (M&MS).

Cambridge M. and Kuo J. (1979). Two new species of seagrass from Australia, Posidonia sinuosa and Posidonia angustifolia (Posidoniaceae). Aquatic Botany, 6, 307–328.

Clague D. and Dalrymple G. (1987). The Hawaiian-Emperor Volcanic Chain. Geologic Evolution. Volcanism in Hawaii, 1, 5–54.

Coleman F. and Williams S. (2002). Overexploiting marine ecosystem engineers: potential consequences for biodiversity. Trends in Ecology and Evolution, 17(1), 40–44.

Cook C. (1998). Hydrocharitaceae. In: The Families and Genera of Vascular Plants. Vol 4. Monocots. Alismatanae and Commelinanae (expect Gramineae). Berlin: Springer, 234–248.

den Hartog C. (1970). The sea-grasses of the World. Rotterdam: A. A. Balkema.

Gabdullin R. (2005). Historical Geology. Book. 1. Moscow: Publishing house of Moscow State University. (In Russian) Garcia-Castellanos D., Estrada F., Jiménez-Munt I., Gorini C., Fernàndez M., Vergés J. and De Vicente R. (2009). Catastrophic flood of the Mediterranean after the Messinian salinity crisis. Nature, 462, 778—781.

Green E. and Short F. (2003). World Atlas of Seagrasses. Berkeley: University of California Press.

Hall B. (2011). Phylogenetic Trees Made Easy: A How To Manual. 4th Ed. Sunderland: Sinauer Ass.

Hemminga M. and Duarte C. (2000). Seagrass Ecology. Cambridge: Cambridge University Press.

Hogarth P. (2015). The Biology of Mangroves and Seagrasses. 3rd Ed. Oxford: Oxford University Press.

Hosius A. and Von der Marck W. (1880). Die Flora der Westfälische Kreideformation. Palaeontographica, 26, 125–236.

Irlandi E. and Peterson C. (1991). Modification of animal habitat by large plants: mechanisms by which seagrasses influence clam growth. Oecologia, 87, 307–318.

Iurmanov A. (2017). Phylogenetic biogeography of the Posidoniaceae family: molecular genetic analysis. In: Proceedings of the VI International Scientific and Practical Conference "Marine Research and Education (MARESEDU-2017)". Tver: LLC PoliPRESS», 507–510. (In Russian).

Iurmanov A. (2018). Phylogenetic biogeography of Halophila Thouars (Hydrocharitaceae) In: Proceedings of IV (XII) International Botanical Conference of Young Scientists in Saint-Petersburg. Saint-Petersburg: Komarov Botanical Institute of the Russian Academy of Sciences. 256.

Iurmanov A., Romanov M. and Bobrov A. (2020a). Phylogenetic phytogeography of the family Cymodoceaceae. Problems of Botany of South Siberia and Mongolia, 19(2), 94-97. (In Russian with English summary).

Iurmanov A., Romanov M. and Bobrov A. (2020b). Phylogenetic phytogeography of the family Zosteraceae. // Problems of Botany of South Siberia and Mongolia, 19(2), 98-9101. (In Russian with English summary).

Iurmanov A., Romanov M. (2020). Phylogenetic phytogeography of selected groups of seagrasses (Monocotylendoneae - Alismatales). In: Materials of the International Youth Scientific Forum Lomonosov-2020 (Electronic resource). Moscow: MAKS Press, 1–3.

Iurmanov A., Romanov M. and Bobrov A. (2021). Fruit morphology and histology of Zostera asiatica Miki and Phyllospadix iwatensis Makino (Zosteraceae) in connection with comparative carpology of higher Alismatales. Botany Letters, 168(4), 570-576.

Koriba K. and Miki S. (1931). On Archeozostera from the Izumi Sandstone. Chikyu (The Globe), 15, 165–201. (In Japanese).

Koriba K. and Miki S. (1958). Archeozostera, a new genus from Upper Cretaceous in Japan. The Palaeobotanist, 7, 107-111.

Kuo J. and den Hartog C. (2000). Seagrasses: A profile of an ecological group. Biologia Marina Mediterranea, 7(2), 3–17.

Kuo J. and McComb A. (1989). Seagrass taxonomy, structure and development. In: Biology of seagrasses: A treatise on the biology of seagrasses with special reference to the Australian region. Amsterdam: Elsevier, 6–73.

Kuo J. and McComb A. (1998a). Cymodoceaceae. In: The Families and Genera of Vascular Plants. Vol 4. Monocots. Alismatanae and Commelinanae (expect Gramineae). Berlin: Springer, 133–140.

Kuo J. and McComb A. (1998b). Posidoniaceae. In: The Families and Genera of Vascular Plants. Vol 4. Monocots. Alismatanae and Commelinanae (expect Gramineae). Berlin: Springer, 404–407.

Kuo J. and McComb A. (1998c). Zosteraceae. In: The Families and Genera of Vascular Plants. Vol 4. Monocots. Alismatanae and Commelinanae (expect Gramineae). Berlin: Springer, 496–502.

Larkum A. and den Hartog C. (1989). Evolution and biogeography of seagrasses. In: Biology of Seagrasses. A Treatise on the Biology of Seagrasses with Special Reference to the Australian Region. Amsterdam: Elsevier, 112–156.

Larkum A., McComb A. and Shephard S. (1989). Biology of Seagrasses. Elsevier: Amsterdam. Larkum A., Orth J. and Duarte M. (2006). Seagrasses: biology, ecology and conservation. Berlin: Springer.

Les D., Cleland M.and Waycott M. (1997). Phylogenetic studies in Alismatidae, II: Evolution of marine angiosperms (Seagrasses) and hydrophily. Systematic Botany, 22, 443–463.

Lumbert S., den Hartog C., Phillips R., and Olsen F. (1984). The occurrence of fossil seagrasses in the Avon Park Formation (Late middle Eocene), Levy County, Florida (U.S.A.). Aquatic Biology, 20,121-129.

Macreadie P., Baird M.; Trevathan-Tackett S., Larkum A. and Ralph P. (2013). Quantifying and modelling the carbon sequestration capacity of seagrass meadows. Marine Pollution Bulletin, 83(2), 430–439.

Moissette P., Koskeridou E., Cornée J., Guillocheau F. and Lécuyer C. (2007). Spectacular preservation of seagrasses and seagrass-associated communities from the Pliocene of Rhodes, Greece. Palaios, 22, 200–211.

Nagelkerken I. and van der Velde G. (2004). Relative importance of interlinked mangroves and seagrass beds as feeding habitats for juvenile reef fish on a Caribbean island. Marine Ecology Progress Series, 274, 153–159.

Ostenfeld C. (1915). On the geographical distribution of the seagrasses. A preliminary communication. Proceedings of the Royal Society of Victoria, 27, 179–191.

Paling E., van Keulen M., Wheeler K., Phillips J. and Dyhrberg R. (2001). Mechanical seagrass transplantation in Western Australia. Ecological Engineering, 16, 331–339.

Petrov K. (2008). Ocean biogeography.2nd ed. Moscow: Academic Project; Alma Mater. (In Russian). Ruggieri G. (1952). Segnalazione di frutti fossili di Cymodocea maior (Cavol.) Grande. Webbia, 8(1), 141–146.

Setchell W. (1920). Geographical distribution of the marine Spermatophytes. Bull Torrey Botanical Club, 47, 563–579.

Short F., Carruthers T., Dennison W. C. and Waycott M. (2007). Global seagrass distribution and diversity: a bioregional model. Journal of Experimental Marine Biology and Ecology, 350, 3–20.

Short F. and Coles R. (2001). Global Seagrass Research Methods. Elsevier: Amsterdam.

Stockmans F. (1932). Posidonia perforate Saporta et Marion des mares de Gelinden (Paleocene). Bulletin de l'Institut Royal des Sciences Naturelles de Belgique, 8(27), 1–9.

Taylor T., Taylor E. and Krings M. (2008). Paleobotany: The Biology and Evolution of Fossil Plants. 2nd Ed. Burlington: Academic Press (an imprint of Elsevier).

Tiner R., Bergquist H., Halavik T. and MacLachlan A. (2003). Eelgrass Survey for Eastern Long Island Sound, Connecticut and New York. Hadley: National Wetlands Inventory report.Tuya F., Betancort J., Haroun R., Espino F., Lomoschitz A. and Meco J. (2017). Seagrass paleo-biogeography: Fossil records reveal the presence of Halodule cf. in the Canary Islands (eastern Atlantic). Aquatic Botany, 143, 1–7.

van der Ham R., van Konijnenburg-van Cittert J. and Inderherberge L. (2007). Seagrass foliage from the Maastrichtian type area (Maastrichtian, Danian, NE Belgium, SE Netherlands). Review of Palaeobotany and Palynology, 144(3-4), 301-321.

Voigt E. (1981). Upper Cretaceous bryozoan-seagrass association in the Maastrichtian of the Netherlands. In: Recent and Fossil Bryozoa. Fredensborg: Olsen & Olsen, 281–298.

Waterhouse A., Allen S. and Bowie A. (2009). Upwelling flow dynamics in long canyons at low Rossby Number. Journal of Geophysical Research, 114, 1–18.

RESEARCH PAPER

MONITORING OF FRAGILE ECOSYSTEMS WITH SPECTRAL INDICES USING SENTINEL-2A MSI DATA IN SHAHDAGH NATIONAL PARK

Emil A. Jabrayilov
Institute of Geography, Azerbaijan National Academy of Sciences, 115 H.Javid ave, Baku, AZ1143, Azerbaijan
***Corresponding author:** emil.jabrayilov@gmail.com
Received: January 20th, 2021 / Accepted: February 15th, 2022 / Published: March 31st, 2022
https://DOI-10.24057/2071-9388-2021-006

ABSTRACT. Studying ecosystems using remote sensing technologies is very relevant since it checks the accuracy of the results of modern research. This study aims to monitor environmental changes in ecosystems of the Shahdagh National Park and its surrounding areas in Azerbaijan using Sentinel 2A MSI data. The study aimed to examine and monitor changes in vegetation, water resources, and drought conditions of the study area in recent years. For analyzing and observing these ecosystems Normalized Difference Vegetation Index (NDVI), Normalized Difference Water Index (NDWI), and Normalized Difference Drought Index (NDDI) were calculated using multi-band methods. Obtained indices were compared and changes were investigated analyzing satellite-derived methods. For proper monitoring and assessment of relevant ecosystems, there had been determined 3,825 fishnet points for the study area. This made it possible to compare and coordinate the results of the indices more accurately. After linking fishnet points to raster indices, classification had been made for measuring ecosystems indicators. Vegetation assessments revealed a partial expansion of sparse vegetation or bare rocks, river valleys, as well as nival, subnival, and partial subalpine meadows from 15.1% to 18.1%. Another growth indicator is a significant increase of dense forest ecosystems from 2.3% to 9.2%. According to the results decreases are observed in sparse forests, arable lands, pastures, and shrubs, which are more sensitive to anthropogenic factors. Monitoring of the indices shows that low-humidity areas increase as droughts intensify, especially in plain areas. Finally, the study revealed that the introduction of a specially protected regime within the national park makes ecosystems more sustainable.

KEYWORDS: environmental monitoring, NDVI, NDWI, NDDI, Shahdagh National Park, ecosystem

CITATION: Jabrayilov E. A. (2022). Monitoring of Fragile Ecosystems with Spectral Indices Using Sentinel-2A MSI Data in Shahdagh National Park. Vol.15, № 1. Geography, Environment, Sustainability, p 70-77 https://DOI-10.24057/2071-9388-2021-006

ACKNOWLEDGEMENTS: The author would like to acknowledge to European Union's Copernicus Earth Observation Programme for accessing and using Sentinel 2 data and express his sincere gratitude to anonymous reviewers for the necessary recommendations and valuable suggestions.

Conflict of interests: The authors reported no potential conflict of interest.

INTRODUCTION

The recent acceleration of economic and social development has led to the wider use of the concept of sustainable development. The term, first mentioned in the Brundtland Report (1987), is defined as "… the needs of the present without compromising the ability of future generations to meet their own needs". The subsequent Rio Declaration (UNCED 1992) on sustainable development states that the only way to achieve long-term economic progress is to link it to environmental protection. At the 2005 World Summit of the United Nations, the concept was explained in more detail with three key directions: economic development, social development, and environmental protection.

Today, environmental protection has become a very important part of the sustainable development approach, as well as our daily activities as a common commitment. In terms of ensuring sustainable development the identification of fragile ecosystems is an essential part of the management of nature conservation. Although some researchers attribute this approach to natural factors, others explain it by the human's impact on nature (Nilsson 1995). The increasing impact of human activities on ecosystems in recent years has provided a basis for assessing such areas.

Recent studies show that remote sensing (RS) technologies provide data support for environmental assessments, which has become an important evaluation tool along with Geographic Information Systems (GIS) (Hou et al., 2016; Zhao et al., 2018; Belgiu & Csillik 2018; Phinzi & Ngetar 2019). These methods are widely used to monitor environmental issues. For example, Vihervaara et al. (2017) analyzed how national biodiversity monitoring could be developed by using RS. Griffiths et al. (2014) used Landsat data with five-year intervals to investigate changes in forest types, forest disturbances, and forest recovery. Rawat & Kumar (2015) tried to illustrate dynamics of land use/cover by using multi-temporal satellite imagery. Chu & Guo (2014) attempted to provide RS data tools for preventing and monitoring forest fires and understanding how the environment responds to them. Zhao & Lu (2018) analyzed data and methods of landslide processes using remote sensing techniques used

in many different studies. Shahabi et al. (2020) identified flood-prone areas using Sentinel sensors in their studies and propose flood sensitivity mapping techniques.

In this research, the datasets used in the analysis are Sentinel 2A MSI (Toming et al. 2016; Sakowska et al. 2016; Sonobe et al. 2018; Othman et al. 2014) for evaluating remote sensing indices. Recent studies in this area are showing positive results in the research of environment and ecosystem issues (Filipponi et al. 2018; Giuliani et al. 2019; Wang et al. 2019).

This study aims to monitor environmental changes and to determine the fragile ecosystems using spectral indices calculated from Sentinel 2A MSI data. For this purpose, Normalized Difference Vegetation Index (NDVI), Normalized Difference Water Index (NDWI), and Normalized Difference Drought Index (NDDI) were determined for the study area, using Green, Red, and NIR bands with 10 m resolution from relevant multispectral images. The multi-band method is based on reflective variations of the bands and extracts index-based values for analysis of appropriate natural resources (Qiao C. et al. 2012). In recent years these indices have been used very widely in ecosystem monitoring (Li Y. et al. 2017; Ali et al. 2019; Higginbottom 2020; Semeraro et al. 2020).

The main objectives of the study are to apply and examine the NDVI, NDWI, and NDDI in addition to providing a basis for monitoring changes in vegetation, water resources, and drought conditions of the Shahdagh National Park and its surroundings over the past three years using Sentinel 2A multispectral satellite imagery. This procedure ensures that the environment is examined in a combined and transparent manner, considering the needs for the progress of the area; informs stakeholders about the impacts of the area on the environmental planning activities or processes. Assessing the indices can help identify areas of strategic significance for nature conservation, including environmental networks.

Ecological conditions are mainly associated with an effective assessment of ecosystems (Yang and Chen 2015). Consequently, the evaluation of ecosystems is very significant for achieving sustainable development in the regional case and environmental security for the national park and surroundings. Within modern technologies, satellite-based assessments and comparisons of ecosystems can save time and money as well. More importantly, there has been no regional studies of the ecosystems of Shahdagh National Park using remote sensing technologies. Therefore, conducting research in the study area is not only an attempt to study the ecosystems of the South Caucasus in general, but also the basis for future research.

MATERIALS AND METHODS

Study Area

The study was conducted in the Shahdagh National Park, the largest national park in the South Caucasus. The National Park covers the middle and high mountains of the Greater Caucasus within Azerbaijan. The current area of the National Park is 130,508.1 hectares. The National Park covers the mountainous parts of six administrative districts of Azerbaijan: Oghuz, Gabala, Ismayilli, Shamakhi, Guba, and Gusar (Jabrayilov 2021).

The territory of the National Park includes the mountain landscapes unique in the region, begins approximately at an altitude of 1000 m above sea level and continues to the highest peaks (Bazarduzu mt, 4466 m; Shahdagh mt, 4243 m; Tufandagh mt, 4191 m, etc.) of the country. Hypsometric indicators and location of the study area is shown in Figure 1. The elevation difference above sea level is based on a Digital Elevation Model (JAXA/METI 2007). The main types of landscapes in the national park and surrounding areas are forest, forest-steppe, and shrub landscapes of low and medium mountains, subalpine and alpine meadows, subnival and nival landscapes of high mountains. The study area is divided into four climate types according to climatic characteristics: 1. Cold climate type with dry winters on the north-eastern slopes of the Main Caucasus Range at an altitude of 1,400–2,700 m above sea level. 2. Mild-warm climate with equal distribution of precipitation among all seasons on the southern and north-eastern slopes of the Greater Caucasus. 3. Cold climate with abundant rainfall in all seasons in the southern zone of the Main Caucasus Range, high mountain-forest, and alpine zone. 4. Mountain tundra climate in high mountain areas with an absolute height of more than 2,700 m.

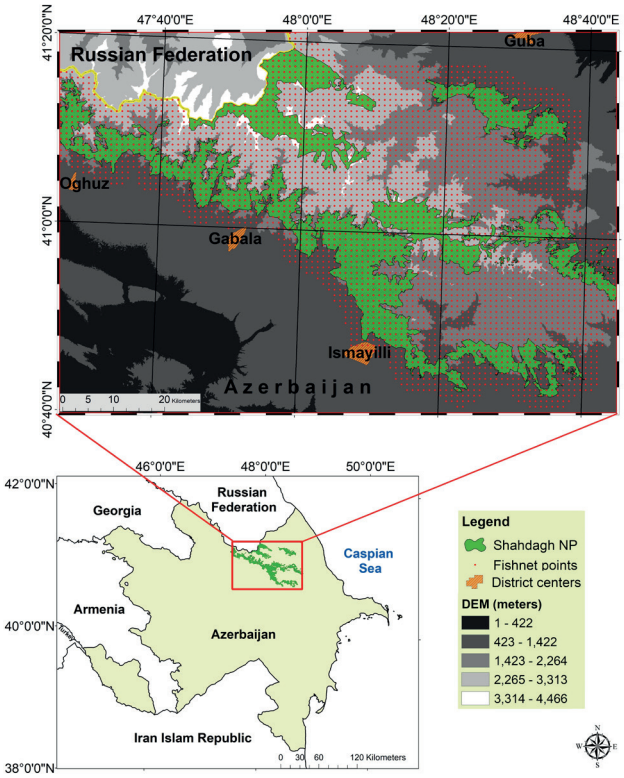

Fig. 1. Shahdagh National Park and fishnet of study area

Data and methodology

Sentinel 2A satellite imagery provided by the European Space Agency (ESA) was used in the study. The data were downloaded from USGS Global Visualization Viewer. The acquisition date of the images is July 28, 2017 and June 2, 2020. It was impossible to select the same months for the study. This is because the satellite images for the 6th, 8th, and 9th months of 2017 were not selected due to high cloudiness. Images for the 7th and 8th months of 2020 were also not considered appropriate due to high cloud cover (sometimes up to 70%). Thus, the images were selected because of the minimum value of the cloud cover. The cloud cover of the images is 0.203% and 0.278%, respectively. From the multispectral data for the study, the 3rd, 4th, and 8th bands were processed with a spatial resolution of 10 m for each using Coordinate System WGS 1984, UTM Zone 39N (Table 1). ArcGIS 10.8 and ERDAS İmagine softwarewere used for data analysis, processing, and mapping.

It is known that by using multispectral images, it is possible to increase the brightness value of the target objects and reduce the brightness of other objects by calculating the difference between the reflection values of multiple bands (Jiang et al. 2021). To observe and assess fragile ecosystems there were calculated Normalized Difference Vegetation Index (NDVI) (Carlson and Ripley 1997; Pettorelli et al. 2005; Yuan et al. 2019), Normalized Difference Water Index (NDWI) (McFeeters 1996, Zhang et al. 2008; Yang 2017), and Normalized Difference Drought Index (NDDI) (Dobri et al. 2021; Gu et al. 2007; Lange et al. 2017) (Fig. 2). According to the existing methodology (Renza 2010), the NDVI and NDWI values were converted to eight bits (0–255) so that the values obtained from the NDDI calculation varied between -1 and +1. To compare the values obtained from indices, a fishnet was set up for the study area. The number of points for fishnet is 3,825. The distance between the points is 1,000 m (figure 1).

RESULTS AND DISCUSSION

Using Sentinel 2 imagery in the study has made the determination of potential fragile ecosystems more effective for real time. The integration of Geographic Information Systems (GIS) and remote sensing technologies have considerably facilitated the observation of such areas. These assessments can be used as a basis of land use standards at more detailed planning levels or on environmental optimization. These satellite images allowed for attempts to identify changes in ecosystems in the Shahdag National Park and surrounding areas in recent years. The fishnet assigned to the area is linked to compare the calculated values of the corresponding indices. The indices obtained on the basis of satellite data for 2017 and 2020 were divided into categories and the number of points belonging to each category was determined. Because the area is mountainous, our analysis was conducted for the summer months.

Figure 3 shows colored NDVI values calculated from Sentinel 2 images for 2017 and 2020. For the fishnet area, NDVI values range from 0.84 to -0.14 for 2017 and from 0.85 to -0.16 for 2020. Average values were almost the same for both years – 0.50 and 0.51 respectively. The standard deviation for 2017 was 0.24; for 2020 it was 0.26. The NDVI values were categorized to compare the number of overlapping fishnet points for each year (Table 2). As can be seen from the table the number of points increased up to 0.2 index values for the relevant years. Landscapes with sparse vegetation or bare rocky river valleys are more compatible for such areas. High mountainous areas are very typical for these points. Thus, this indicator shows a slight expansion of the nival, subnival, and partially subalpine meadow zones according to the satellite images. The number of values between 0.2 and 0.8 decreased. Such areas may include sparse or medium-density forests, arable lands, pastures, and shrubs as well. In particular, given that these landscapes are more sensitive to anthropogenic factors, the reduction leads to increased fragility of these

Table 1. Sentinel 2A satellite data bands used in the study

Spectral bands	Central wavelength, µm	Wavelength, µm (min - max)	Bandwidth	Resolution, m
Band 3 – Green	0.560	0.5425–0.5775	0.045	10
Band 4 – Red	0.665	0.646 – 0.685	0.039	10
Band 8 – NIR	0.842	0.7845–0.8995	0.141	10

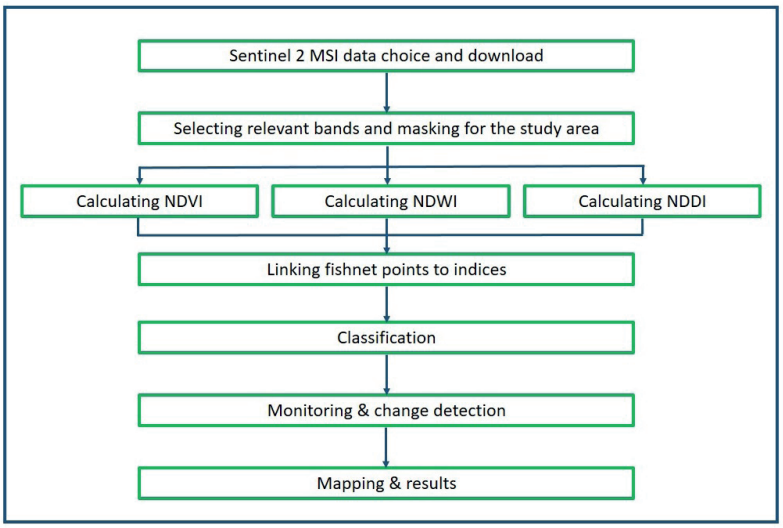

Fig. 2. Flowchart of the study

natural resources in these zones. It should be noted that such areas are most common in the surrounding areas of the national park. These sensitive landscapes are transformed due to the intensification of human activity in recent years in the settlements located in the surroundings of the national park and the consequent increase of anthropogenic impacts. In the alpine meadow zone, this transformation is due to unsystematic grazing (Ismayilov and Jabrayilov 2019). Grazing pressure, especially in the summer months, leads to degradation and deterioration of vegetation and soil cover. These landscapes should be considered more fragile ecosystems.

And finally, there was a significant increase in the number of points above the index value of 0.8 (from 86 to 350). These points are suitable for densely forested areas. Dense forest landscapes are more pronounced within the territory of the national park.

Water is one of the most valuable and important natural resources of the region. For this purpose, spectral signature feature analysis for the study area was performed. Another calculated index is NDWI, which is shown in Figure 4. This multi-band method uses the reflective varieties of each band and extracts relevant resources for the analysis. The values of these indices are adjusted to the fishnet points. The maximum index value for 2017 is 0.30; for 2020 it is 0.17. Minimum values are -0.72 and -0.74 respectively. The average value of the points is -0.45 for both years. The standard deviation is 0.19 for 2017 and 0.20 for 2020.

As can be seen from the NDWI maps, zero or positive humidity index values are characteristic of water areas (lakes, rivers) and high-altitude areas. Since waters or humid areas are assessed with the NDWI index, points are assigned up to a value of -0.2 (low-humid areas) to the same group when assigning categories. The number of these points was 3,191 in 2017 and 3,290 in 2020 (Table 3). As can be seen, there has been an increase in these areas. The increase in land acquired from NDWI at low index values can be seen as an example of the water shortage problem in the country in recent years. Thus, the reduction of precipitation in the country over the past few years, including in mountainous areas, is today's reality. Due to this, the volume of water in mountain rivers and lakes is decreasing. As a result, declining freshwater resources and water required for irrigation in the foothills, including plains, are factors that increase environmental stress (Mammadov et al. 2020). Given that ecosystems are interconnected in a chain, disruption of one natural process increases fragility and sensitivity in others.

There was a slight increase in the number of points receiving values between -0.2 and 0 for the fishnet area (from 484 to 590 points). These points are more characteristic of high mountainous areas and zones close to riverbeds.

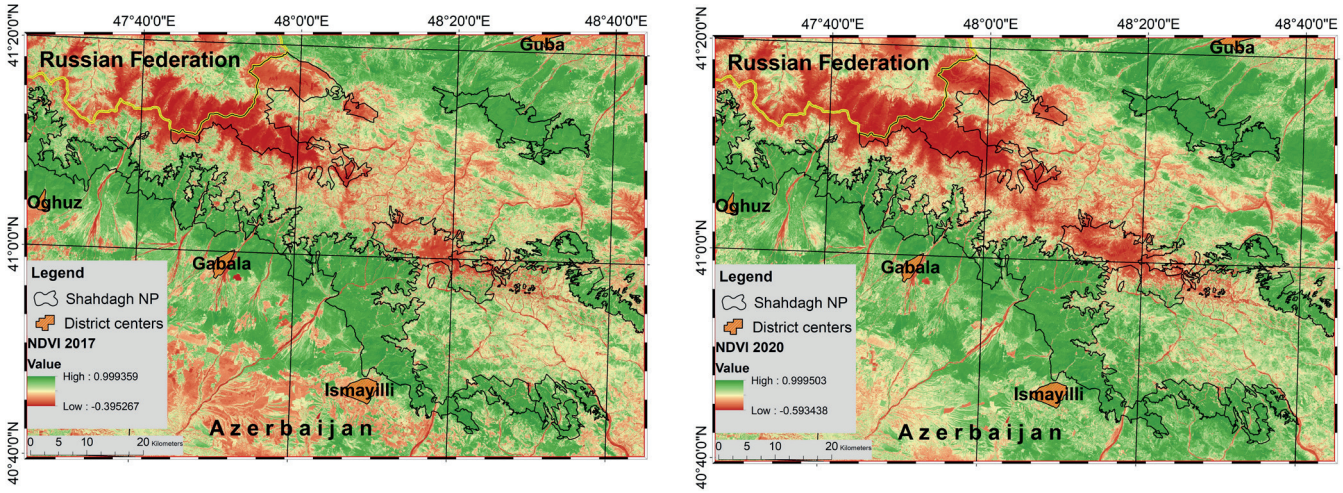

Fig. 3. NDVI maps obtained from Sentinel 2 images (2017 and 2020)

Table 2. The number of fishnet points matching the NDVI values

Ranges	Number of points by year	
	2017	2020
0 >	41	95
0 – 0.1	301	332
0.1 – 0.2	235	266
0.2 – 0.3	298	245
0.3 – 0.4	381	316
0.4 – 0.5	450	404
0.5 – 0.6	460	431
0.6 – 0.7	453	407
0.7 – 0.8	1120	979
0.8 <	86	350

But naturally, the area was recorded very few positive points. It should be noted that positive values are observed mainly in open water areas (Xu 2006). There is a slight decrease in the latter indicators (from 46 to 43). This shows that there is a slight change in the mountain lakes and riverbeds.

The next index calculated for the area during the study is NDDI (Figure 5). NDDI combines NDVI and NDWI data, which means using Green, Red, and NIR bands of the satellite images. The main purpose of calculating this index was to identify arid areas, which are one of the important factors to get information about fragile or more sensitive ecosystems. According to calculations, maximum and minimum values for these indices are 0.74 and -0.20 in 2017 and 0.75 and -0.13 in 2020, respectively, for fishnet points. The average value is the same (0.46) for each year.

However, some deviations were recorded in the obtained drought indices. Thus, the forest areas, which are mostly covered by Shahdagh National Park, received high values according to the NDDI. This gives a reason to say that errors occur when calculating the drought index for mountainous and forest areas due to the reflectance of the cover. For this reason, only the number of points below the average value of NDDI was calculated to avoid errors. According to the calculation, the number of points for 2017 was 1,646, while in 2020 it was 1,638 of them. Thus, it was determined that the areas with almost no drought indices decreased only slightly in these years.

In the study, there has also been calculated the range in which all three index values were most commonly obtained from fishnet. According to the designed boxplot (Fig. 6), most of the points for NDVI values vary approximately between 0.33 and 0.73 for 2017 and 0.31 and 0.75 for 2020. The boxplot shows that the range between the lower and upper quartiles in the NDVI slightly increased. In particular, a slight increase in the upper limit can be considered a positive development. Thus, despite the small difference between the studied years, the growth rate of green mass is observed for the study area. This positive result may be due to the strict observance of the security regime in the national park. Another indicator for the boxplot is NDWI values. Given that the study area is essentially mountainous, most of the values of NDWI get points below zero. It is due to the fact that only water areas can get above-zero values as discussed above. According to the boxplot, most NDWI points change from -0.34 to -0.6 for 2017 and from -0.32 to -0.62 for 2020. Finally, from this boxplot, most values of the NDDI index vary between 0.34 and 0.62 for 2017 and 0.31 and 0.63 for 2020. The extension of the lower NDDI limit should also be noted here as a positive nuance. The results of the NDDI were commented on above.

To illustrate the relationship between all indices, correlations have been identified and shown in Figure 7. The relationships allow determining and visualizing a correlation between pair of indices. The dots in a scatter plot report all the values. Scatter plots also show if there are any unexpected breaks in the data and if there are any exceptional cases. From these connections, the strong positive correlations between NDVI and NDDI for the same years imply the influence of anthropogenic impact on the ecosystem. Since human activities have greatly influenced the water regimes, the effects of droughts on NDVI need to be further studied. NDVI values between 2017 and 2020 and NDWI values between 2017 and 2020 are weakly positively correlated. The close values of correlations of NDVI indicate that variables are of similar significance in determining vegetation growth change. The relationship of other mixed indices is mainly weakly or strongly negative. It is clear that the correlation between NDWI and NDDI is strongly negative. It is because one of them is the index of water and the other is the index of droughts.

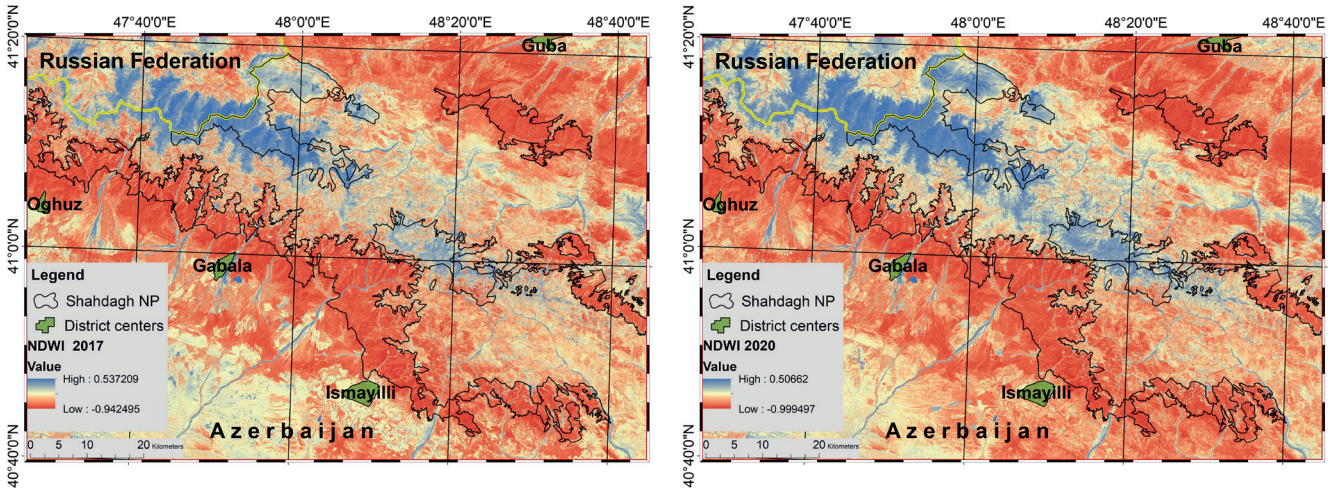

Fig. 4. NDWI maps obtained from Sentinel 2 images (for 2017 and 2020)

Table 3. The number of fishnet points matching the NDWI values

Category of values	Number of points by year	
	2017	2020
>-0.2	3,191	3,290
-0.2–-0.1	275	306
-0.1–0	209	284
0–0.1	37	40
0.1–0.2	9	3

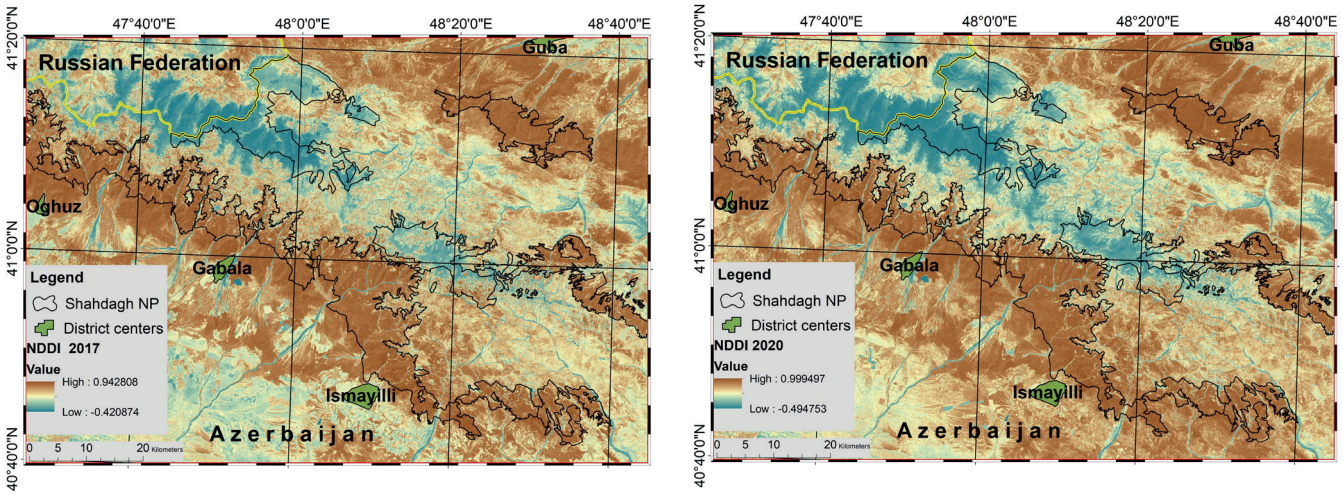

Fig. 5. NDDI values for 2017 and 2020

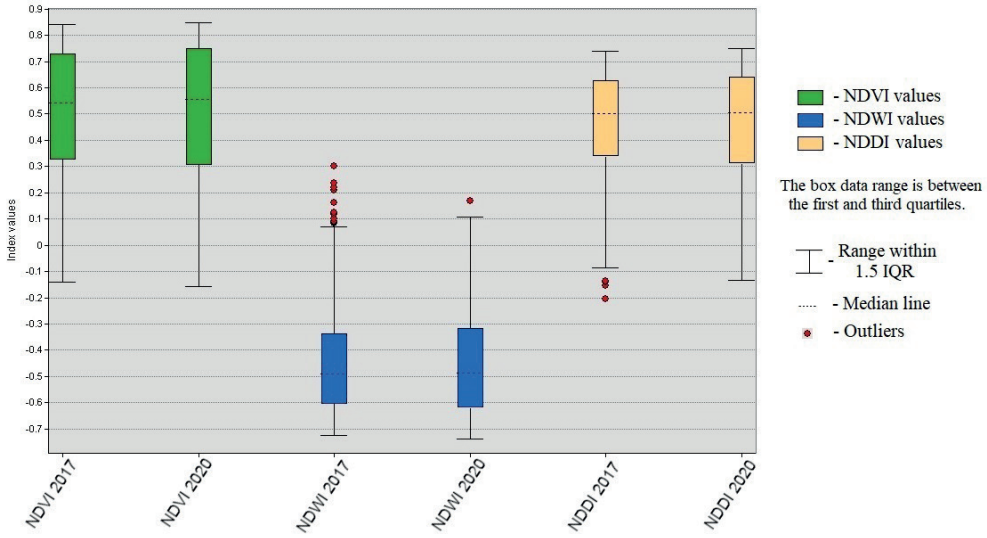

Fig. 6. Boxplot for NDVI, NDWI, and NDDI values

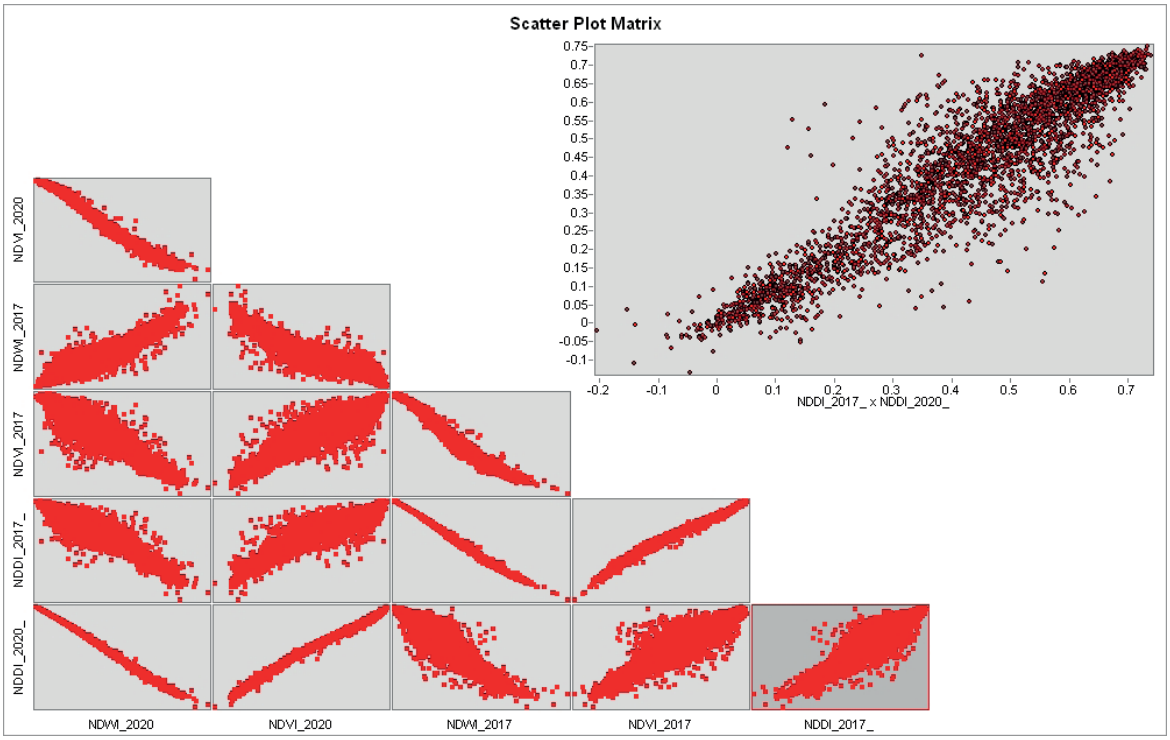

Fig. 7. Bivariate relationships of NDVI, NDWI, and NDDI indices

CONCLUSIONS

The study determined the environmental changes and monitored the recent remote sensing data for acquiring the relevant results. The environment has been properly monitored for defining fragile ecosystems and the methodology used for the study showed itself perfectly for obtaining for accurate results. The use of satellite-based indices allows for a clearer view of the relevant ecosystem indicators. It is reasonable to monitor the real-time state of the components of the environment, especially during the implementation of management and environmental impact assessment plans and programs, socio-economic activities, and strategies aimed at the development of local areas.

The use of formulas of the NDVI, NDWI, and NDDI gave relevant results for ecosystem quality assessment by Sentinel 2A multispectral image data. The results of the observation of degradation processes in low-lying areas and plains are concerning. Such areas are especially common for the national park. Thus, the results of anthropogenic impacts are visible in the surrounding areas of the national park, especially around the settlements and in the mountain meadows. This leads to the transformations and fragility of natural ecosystems in these areas. However, within the national park, the application of a special protection regime accelerates the process of natural recovery. The increase in dense forest ecosystems within the national park from 2.2% to 9.2% of the total can be considered a positive development. This is due to the serious and effective organization of the security regime in the national park. The increase in low-humidity areas or negative water index values from 83% to 86% is estimated to be the result of a decrease in precipitation observed in recent years.

As ecosystems are interconnected, the disruption of one natural component can lead to the degradation of others in a chain. Thus, the use of remote sensing methods allows detecting the changes in the environment in the study area, and initially assessing the risks associated with various impacts, considering future generations.

REFERENCES

Ali M.I., Dirawan G.D., Hasim A.H., & Abidin M.R. (2019). Detection of Changes in Surface Water Bodies Urban Area with NDWI and MNDWI Methods. International Journal on Advanced Science Engineering Informatioan Technology, 9(3), 946–951. DOI: 10.18517/ijaseit.9.3.8692.

Belgiu M., & Csillik O. (2018). Sentinel-2 cropland mapping using pixel-based and object-based time-weighted dynamic time warping analysis. Remote sensing of environment, 204, 509–523. DOI: 10.1016/j.rse.2017.10.005.

Brundtland G.H. (1987). Report of the world commission on environment and development: our common future (1987). World Commission on Environment and Development, UN, Oxford; New York.

Carlson T.N., Ripley D.A. (1997) On the relation between NDVI, fractional vegetation cover, and leaf area index. Remote Sensing of Environment. 62(3), 241–252. DOI: 10.1016/S0034-4257(97)00104-1.

Chu T., & Guo X. (2014). Remote sensing techniques in monitoring post-fire effects and patterns of forest recovery in boreal forest regions: A review. Remote Sensing, 6(1), 470–520. DOI: 10.3390/rs6010470.

Dataset: © JAXA/METI ALOS PALSAR L1.0 (2007). Accessed through NASA's Alaska Satellite Facility Distributed Active Archive Center (accessed June 25, 2021), DOI:10.5067/J4JVCFDDPEW1.

Dobri R.V., Sfîcă L., Amihăesei V.A., Apostol L., & Ţîmpu S. (2021). Drought Extent and Severity on Arable Lands in Romania Derived from Normalized Difference Drought Index (2001–2020). Remote Sensing, 13(8), 1478. DOI:10.3390/rs13081478.

Filipponi F. (2018). BAIS2: Burned area index for Sentinel-2. Proceedings, 2(7), 364; DOI:10.3390/ecrs-2-05177.

Giuliani C., Veisz A.C., Piccinno M., & Recanatesi F. (2019). Estimating vulnerability of water body using Sentinel-2 images and environmental modelling: the study case of Bracciano Lake (Italy). European Journal of Remote Sensing, 52(s4), 64–73. DOI:10.1080/22797254.2019.1689796.

Griffiths P., Kuemmerle T., Baumann M., Radeloff V.C., Abrudan I.V., Lieskovsky J., ... & Hostert P. (2014). Forest disturbances, forest recovery, and changes in forest types across the Carpathian ecoregion from 1985 to 2010 based on Landsat image composites. Remote Sensing of Environment, 151, 72–88. DOI:10.1016/j.rse.2013.04.022.

Gu Y., Brown J.F., Verdin J.P., Wardlow B.D. (2006) A five-year analysis of MODIS NDVI and NDWI for grassland drought assessment over the central Great Plains of the United States. Geophysical Research Letters 34(L06407):6, DOI: 10.1029/2006GL029127.

Higginbottom T.P., & Symeonakis E. (2020). Identifying Ecosystem Function Shifts in Africa Using Breakpoint Analysis of Long-Term NDVI and RUE Data. Remote Sensing, 12(11), 1894. DOI:10.3390/rs12111894.

Hou, K., Li, X., Wang, J., et al., (2016). Evaluating ecological vulnerability using the GIS and Analytic Hierarchy Process (AHP) method in Yan'an, China. Polish J. Environ. Stud. 25 (2), 599–605.

Ismayilov M., Jabrayilov E. (2019) Protected Areas in Azerbaijan: Landscape-Ecological Diversity and Sustainability. Ankara Üniversitesi Çevrebilimleri Dergisi. 7(2): 31–42. [Google Scholar].

Jabrayilov E.A. (2021) Ecological Network Model in Shahdagh National Park. Proceedings of Voronezh State University. Series: Geography. Geoecology, 2, pp. 61–69, DOI: 10.17308/geo.2021.2/3449.

Jiang W., Ni Y., Pang Z., Li X., Ju H., He G., ... & Qin X. (2021). An Effective Water Body Extraction Method with New Water Index for Sentinel-2 Imagery. Water, 13(12), 1647. DOI:10.3390/w13121647.

Lange M., Dechant B., Rebmann C., Vohland M., Cuntz M., & Doktor D. (2017). Validating MODIS and sentinel-2 NDVI products at a temperate deciduous forest site using two independent ground-based sensors. Sensors, 17(8), 1855. DOI:10.3390/s17081855.

Li Y., Cao Z., Long H., Liu Y., & Li W. (2017). Dynamic analysis of ecological environment combined with land cover and NDVI changes and implications for sustainable urban–rural development: the case of Mu Us Sandy Land, China. Journal of Cleaner Production, 142, 697–715, DOI:10.1016/j.jclepro.2016.09.011.

Mammadov R.M., Hasanov M.S., Ismayilov M.C. (2020) Freshwater ecosystems of Azerbaijan: problems and expectations. Geography and Natural Resources, 2 (12), p. 16–22.

McFeeters S.K. (1996) The use of the Normalized Difference Water Index (NDWI) in the delineation of open water features. Int. J. Remote Sens, 17, 1425–1432. DOI:10.1080/01431169608948714.

Nilsson C., Nilsson G., (1995) The Fragility of Ecosystems: A Review. Journal of Applied Ecology 32(4):677–692, DOI: 10.2307/2404808.

Othman A.A., Al-Saady Y.I., Al-Khafaji A.K., & Gloaguen R. (2014). Environmental change detection in the central part of Iraq using remote sensing data and GIS. Arabian Journal of Geosciences, 7(3), 1017–1028, DOI:10.1007/s12517-013-0870-0.

Pettorelli N., Vik J.O., Mysterud A., Gaillard J.M., Tucker C.J., Stenseth N.C., (2005) Using the satellite-derived NDVI to assess ecological responses to environmental change, Trends in Ecology & Evolution, 20 (9), pages 503–510, DOI: 10.1016/j.tree.2005.05.011.

Phinzi K., & Ngetar N.S. (2019). The assessment of water-borne erosion at catchment level using GIS-based RUSLE and remote sensing: A review. International Soil and Water Conservation Research, 7(1), 27–46, DOI:10.1016/j.iswcr.2018.12.002.

Qiao C., Luo J., Sheng Y., Shen Z., Zhu Z., & Ming D. (2012). An adaptive water extraction method from remote sensing image based on NDWI. Journal of the Indian Society of Remote Sensing, 40(3), 421–433, DOI:10.1007/s12524-011-0162-7.

Rawat J.S., & Kumar M. (2015). Monitoring land use/cover change using remote sensing and GIS techniques: A case study of Hawalbagh block, district Almora, Uttarakhand, India. The Egyptian Journal of Remote Sensing and Space Science, 18(1), 77–84, DOI:10.1016/j.ejrs.2015.02.002.

Renza D., Martinez E., Arquero A., & Sanchez J. (2010). Drought estimation maps by means of multidate Landsat fused images. Proceedings of the 30th EARSeL Symposium. 775–782. [Google Scholar].

Sakowska K., Juszczak R., & Gianelle D. (2016). Remote sensing of grassland biophysical parameters in the context of the Sentinel-2 satellite mission. Journal of Sensors. DOI:10.1155/2016/4612809.

Semeraro T., Luvisi A., Lillo, A.O., Aretano R., Buccolieri R., & Marwan N. (2020). Recurrence Analysis of Vegetation Indices for Highlighting the Ecosystem Response to Drought Events: An Application to the Amazon Forest. Remote Sensing, 12(6), 907. DOI: 10.3390/rs12060907.

Shahabi H., Shirzadi A., Ghaderi K., Omidvar E., Al-Ansari N., Clague J.J., ... & Ahmad A. (2020). Flood detection and susceptibility mapping using Sentinel-1 remote sensing data and a machine learning approach: Hybrid intelligence of bagging ensemble based on k-nearest neighbor classifier. Remote Sensing, 12(2), 266, DOI:10.3390/rs12020266.

Sonobe R., Yamaya Y., Tani H., Wang X., Kobayashi N., & Mochizuki K. I. (2018). Crop classification from Sentinel-2-derived vegetation indices using ensemble learning. Journal of Applied Remote Sensing, 12(2), 026019, DOI: 10.1117/1.JRS.12.026019.

The Rio Declaration on Environment and Development (1992) United Nations Conference on the Environment and Development – UNCED, Rio de Janeiro.

Toming K., Kutser T., Laas A., Sepp M., Paavel B., & Nõges T. (2016). First experiences in mapping lake water quality parameters with Sentinel-2 MSI imagery. Remote Sensing, 8(8), 640, DOI: 10.3390/rs8080640.

Vihervaara P., Auvinen A. P., Mononen L., Törmä M., Ahlroth P., Anttila S., ... & Virkkala R. (2017). How essential biodiversity variables and remote sensing can help national biodiversity monitoring. Global Ecology and Conservation, 10, 43–59, DOI: 10.1016/j.gecco.2017.01.007.

Wang J., Ding J., Yu D., Ma X., Zhang Z., Ge X., ... & Guo Y. (2019). Capability of Sentinel-2 MSI data for monitoring and mapping of soil salinity in dry and wet seasons in the Ebinur Lake region, Xinjiang, China. Geoderma, 353, 172–187, DOI: 10.1016/j.geoderma.2019.06.040.

Xu H. (2006). Modification of normalised difference water index (NDWI) to enhance open water features in remotely sensed imagery. International journal of remote sensing, 27(14), 3025–3033, DOI: 10.1080/01431160600589179.

Yang G., Chen Z., (2015) RS-based fuzzy multiattribute assessment of eco-environmental vulnerability in the source area of the Lishui River of northwest Hunan Province, China. Natl. Hazards 78, 1145–1161, DOI: 10.1007/s11069-015-1762-2.

Yang X., Zhao S., Qin X., Zhao N., & Liang L. (2017). Mapping of urban surface water bodies from Sentinel-2 MSI imagery at 10 m resolution via NDWI-based image sharpening. Remote Sensing, 9(6), 596, DOI: 10.3390/rs9060596.

Yuan L., Chen X., Wang X., Xiong Z., & Song C. (2019). Spatial associations between NDVI and environmental factors in the Heihe River Basin. Journal of Geographical Sciences, 29(9), 1548–1564, DOI: 10.1007/s11442-019-1676-0.

Zhang W.J., Lu Q.F., Gao Z.Q., Peng J. (2008) Response of remotely sensed Normalized Difference Water Deviation Index to the 2006 Drought of eastern Sichuan Basin. Science in China Series D-Earth Sciences, 51(5) 748–758, DOI: 10.1007/s11430-008-0037-0.

Zhao C., & Lu Z. (2018). Remote sensing of landslides—A review. Remote Sensing, 10(2), 279, DOI: 10.3390/rs10020279.

Zhao J., Ji, G., Tian Y., Chen Y., & Wang Z. (2018). Environmental vulnerability assessment for mainland China based on entropy method. Ecological Indicators, 91, 410–422., DOI:10.1016/j.ecolind.2018.04.016

RESEARCH PAPER

WADI AGRICULTURE FUTURE INSIGHT: SOIL, TOPOGRAPHICAL, AGRICULTURAL, AND HUMAN PERSPECTIVES IN RAHMA BEDOUIN VILLAGE, HANEGEV HIGHLANDS, ISRAEL

Amir Mor-Mussery[1,2*], Salem El-Freijat[3]

[1]The Department of Soil and Water Sciences, Faculty of Agriculture, Hebrew University of Jerusalem, Hertzel 10, Rehovot, P.O.B 76100001, Israel

[2]Atid Bamidbar, Nahal Zin 2, Yeroham, P.O.B 8055401, Israel

[3]Bedouin farmer, Rahma village, P.O.B 8055401, Israel

***Corresponding author:** amir.mussery@gmail.com

Received: September 17th, 2021 / Accepted: February 15th, 2022 / Published: March 31st, 2022

https://DOI-10.24057/2071-9388-2021-106

ABSTRACT. The Arab peninsula suffers from intense wadi erosion, which is been expressed by a dense net of wadis that are correlated by overland flows to their surrounded landforms (e.g. loess slopes and rocky grounds). Therefore, the study hypothesized that the wadi reclamation will affect all these correlated landforms. The following objectives were defined: determining the influence of check damming, savanna tree plantation, and grazing on the wadi 'Aboveground net primary production' (ANPP) and determining the influence of wadi ANPP on neighboured area state. Two sites were studied: Project Wadi Atir (PWA) and Rahma. PWA site is located adjacent to Hura Bedouin municipality. The soil is loessial with a dense wadis net. In 2011 the area was leased to the PWA association for its agricultural utilization and conservation. The second site is located on Yeroham hills, Hanegev highland. The area is settled by Bedouin for the El-Azzazma tribe (Rahma village). Half of the area is covered by a 1-2m loess layer, while the other is exposed limestone. Two measurements were carried out to determine the ANPP, manual measurement of the herbaceous biomass weight and SAVI imaging. The finding for both methods indicates a yearly annual increase of 100-150% of ANPP. In addition, a tight correlation was found between the ANPP of the reclaimed wadi and an increase ANPP of 200-450% in the 4m neighboured areal slot. The study of Rahma reveals a positive ANPP feedback loop between the wadi shape, check dams location, and the grazing regime. The study principles may suit wadies all over the Arab peninsula.

KEYWORDS: Wadi agriculture, Rahma Bedouin village, Wadi reclamation and influence on surrounding, Wadies landform

CITATION: Mor-Mussery A., El-Freijat S. (2022). Wadi Agriculture Future Insight: Soil, Topographical, Agricultural, and Human Perspectives in Rahma Bedouin Village, Hanegev Highlands, Israel. Vol.15, № 1. Geography, Environment, Sustainability, p 78-86 https://DOI-10.24057/2071-9388-2021-106

ACKNOWLEDGEMENTS: The Foundation for Conservation of Open Lands®, Israeli Land Authority 2019-2020 and Yeroham municipality. The authors wish to thank Ms. Debbie Goldman Golan and Ms. Hadas Nisan for their encouragement and assistance in Yeroham study, Dr. Stefan Leu. On his highly appreciable assistance in Wadi Attir study and Dr. Gad Ridbo, Field Laboratory Services, Hadera on the implementation of the soil analyses.

Conflict of interests: The authors reported no potential conflict of interest.

INTRODUCTION

The wadies landform represents a highly incised area with a dense net of wadis. Wadi can define as the last phase of the gully erosion evolution, rill, gully (in initial and then after stabilized state), and last one, wadi, (Gong et al. 2011). In the Arab peninsula the wadies area, the wadis, and their connected landform, sized > 2 million km2 and laid mostly over loamy deposits or limestone (Abdel-Fattah et al. 2017), Fig. 1. The wadies areas are settled by indigenous residents mostly from previously nomadic tribes, termed: 'Bedouin' dealing mostly with traditional agricultural practices as grazing (mostly small ruminant and camels) and rainfed crops breeding. The wadies area is characterized by the existence of highly eroded landforms embedded between the wadis as incised loessial plains, salty plains, and rocky grounds, all of them are tightly connected to the existing wadis (Mor-Mussery and Laronne 2020). The integration of the unique three-dimensional shape of the wadi, arid climate (short-termed but intensified rainfall events), reduced vegetation coverage, and thin soil layer leading to flash floods. The floods are resulting in massive sediments removal, an enhanced incision, and rocky karst desertification. As an actively incised landform the size of the wadies area is been rapidly enlarged due to worldwide process, but mostly due to implementation of improper land management and agriculture cultivations in its' neighboured area, resulting, at the end to a reduced agriculture utilization. Recent studies indicate the ability of soil to act as a buffer to

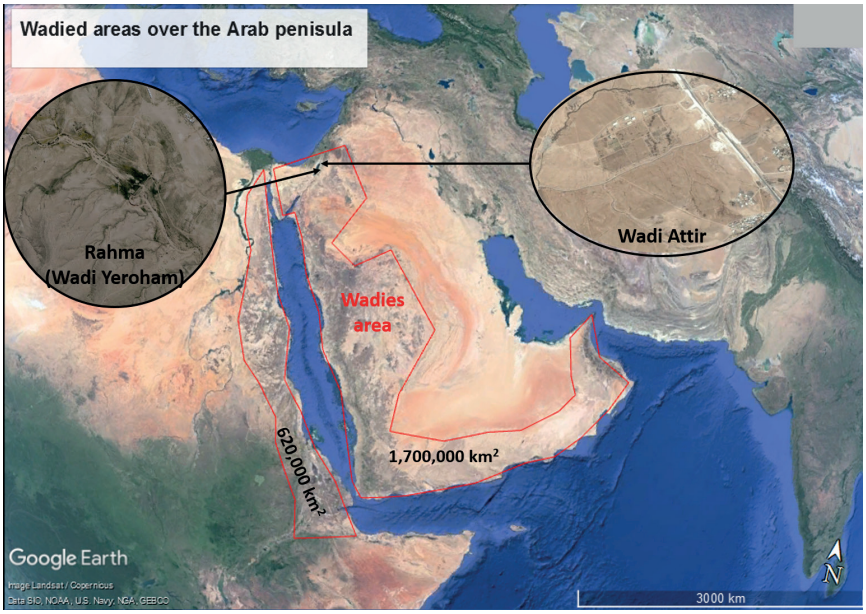

Fig. 1. Wadies areas over the Arab peninsula and the location of the sites of study (GoogleEarth 2020®)

extreme climatic events by the implementation of conservative and rehabilitative practices (e.g. Bai et al. 2019). Therefore, the study hypothesized that adequate agriculture practices implemented in the wadies, such as wadi check damming, implementing of no-tillage and control grazing regimes, and tree plantation may lead to the wadi reclamation and the whole wadies area, and the following objectives were defined: (i) determining the influence of check damming, savanna tree plantation, and management on the wadi reclamation, (ii) determining the influence of wadi reclamation on the neighboured area, and (iii) designing and analyzing in situ cultivation scheme for wadies area reclamation.

MATERIALS AND METHODS

Sites of study

Two study areas were located, Project Wadi Atir- PWA (2011-2019) and Rahma (2020-present).

Project Wadi Atir- PWA

PWA site is located south of the town of Hura on the west bank of Wadi Atir, southern from the Yattir-Eshtemoa confluence and northern to Beer Sheva Valley. The topography is hilly with gentle slopes. The area is underlined by late Cretaceous limestones and composed mainly of loess deposits and rocky ground. The loess was from a quaternary Aeolian source and contained terrestrial clastic sediment, which was formed from wind-blown dust and mainly contained fine particles of silt and clay with about 40% sand (Amit et al. 2006). The area is intensively cultivated by neighboring farmers for cereals breeding and livestock grazing, which resulted in the high incision and dense wadies net crossing it (Mor-Mussery and Laronne, 2020). In 2011, the land was leased to the Project Wadi Atir association for rehabilitation and the establishment of a sustainable arid farming scheme. In 2001 remodeling of the topography was carried by damming previous wadies with check dams, perpendicular to the water flow direction

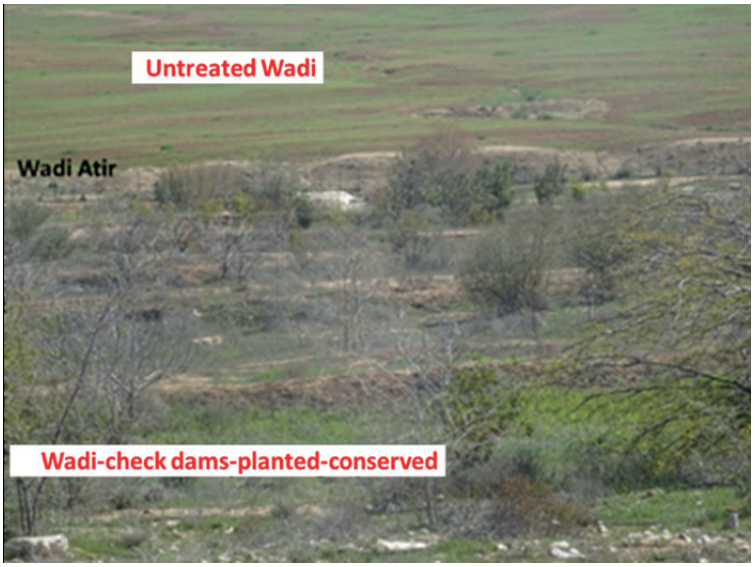

Fig. 2. Wadi Atir site. The check dammed region inside the fenced farm and untreated one, outside the west bank of Yattir stream (2017)

*The savanna trees were from species that are suited for arid regions, as follows. *Acacia raddiana, A. victoriae, Albizia lebbeck, Eucalyptus camaldulensis, Ficus sycomorus, Morus sp., Pistacia lentiscus, Retama raetam, Spartium sp., Ziziphus spina-christi, Ceratonia silique, Punica granatum,* and *Prosopis juliflora*. The trees, which were taken from several nurseries, were 3-4 years old. The trees were planted in a density of 1600 trees ha^{-1} in the 2015 summer.

without interference to the wadi topographic outlines. The site is used to study the influence of check damming, savanna tree plantation*, and different grazing regimes on wadies area fertility changes and rehabilitation (Leu et al., 2020), Fig. 2.

Rahma site of study

Rahma site is located on the eastern bank of Yeroham ephemeral stream adjacent to the estuary to Yeroham valley, Israel. The area is actively incised characterized by a dense coverage of wadies, in initial and stabilized state and wadis confluent Yeroham stream from its' west and south sides resulting by a wide range of intensively eroded landforms, such as loess slopes, rocky grounds, and salty loess plains (the erosion rate was determined by comparison of orthophotos between 2012 and 2020). The area is settled by Bedouin residents belonging to the El Azzazma tribe, specifically to El-Frejat and Zanoon Hamulas (Big family). The area is long-term agriculturally cultivated for rain-fed wheat breeding, and small ruminants and camels grazing by the village indigenous Bedouin farmers that affected the existing landforms. The following landforms and hot plots were selected in Rahma site (Fig. 3).

Data and Methodology

Significance was determined for all measurements by JMP® ver. 15 α=0.1

Aboveground net primary production (ANPP)

The most observable and affecting factor on the rehabilitation state is the change in vegetation patterns, as expressed mostly by the 'Aboveground net primary production (ANPP). Natural changes, such as differences in rainfall or anthropogenic causes such as cultivation changes or afforestation have a crucial influence on soil health and the rehabilitation state of a given area (Helman et al. 2014). To assess the influence of check dams' construction, plantation of savanna trees inside the 'wadi terraces' (the embedded area between two adjacent check dams), and grazing regime, in Wadi Attir site, two ANPP measurements were carried out. A manual one of herbaceous biomass weight and 'Soil adjusted vegetation index (SAVI) imaging from Landsat 8*. The measurements were carried out on three representative wadies, one without wadi terraces, one with check dams and grazing, and one with check dams without grazing. Two analyses were carried out, one aimed to determine the ANPP changes in the wadies over time, and one analyzed the influence of the existing vegetation of the wadi on its' neighbored area. The calculated values were compared to the reference plot outside the wadies area (Leu et al. 2020).

The manual measurement was carried out when the biomass reached its' maximal size and began to dry (February-March) by randomly annuals harvesting using an iron frame of 20X 30cm six samples for each treatment. The herbaceous biomass was harvested, dried in an oven, 650C for 48hours, and weighted (Sava, 1994).

The manual ANPP measurements were carried out using six randomly selected replicates.

* The SAVI is calculated as follows: (1+L)(NIR-Red)/(NIR+Red+L)while the 'NIR' is the intensity of the emitted Near InfraRed wavelength, 'Red'- is the intensity of the emitted 'Red' one, and 'L' is canopy background adjustment parameter, here L=0.5 (reflects arid regions). The SAVI was calculated from Landsat 8 satellite, pixel size equals 30 X30m. Here for each analyzed wadi, the maximal calculated SAVI of the summer (July-September) was reduced from the spring one (February-May) hypothesizing the calculated value represents the net herbaceous biomass production (Helamn and Mor-Mussery, 2020). The number of replicates ranged between 6 to 15 replicates, based on landform size and Landsat imaging pixel.

Soil properties

Hanegev highlands suffer from extreme drought between 2017 and 2020, which prevents analysis of ANPP, therefore, we focused on soil fertility. The following soil properties were studied: Soil organic matter (SOM), Electrical conductivity (EC), Total Nitrogen, Relative humidity (RH). From each location four, randomly selected samples were taken and analyzed in Hadera Ministry of Agriculture Lab Services. The measurement procedures are summarized in Table 1.

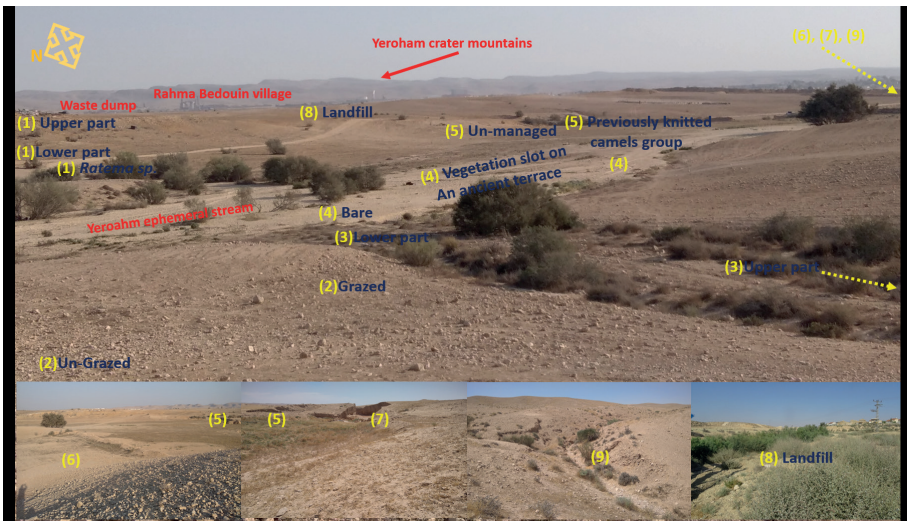

Fig. 3. Rahma site of study, landforms, and hot plots for the study

(1)- Loessial young wadi with a comparison of its upper and lower parts and in an area settled with *Ratema* sp. plots (2)-Rocky slope grazed and un-grazed plots (3)- Mature wadi on limestone, (4) Ephemeral stream bare and on a soil covering an ancient Byzantine terrace plot (5)- Managed aquifer recharge (MAR) cultivated area, which harvests the flood-water from the wadis, built by local Bedouin farmer, unmanaged and with previously knitted camel group plots, (6)- wadis' floodplain, (7) Yeroham ephemeral stream estuary, (8)- Wadi that was used as landfill for construction waste resulted in a salty loess plain with invasive plant species, (9) young wadi on limestone

Table 1. Soil properties measurement procedure

Soil property	Procedure
SOM (Soil organic matter)	Soil samples were washed with 1% HCl and left in an oven at 105ºC for 24 hours. The dry soil was weighed and transferred to a furnace (650ºC) for 8 hours and then weighed again. The difference corresponds to organic matter concentration (Ben-Dor and Banin, 1989), which calculates organic carbon by multiplying by 0.58 (Carter and Gregorich, 2007) (n=4).
EC	Thirty grams of soil mixed with double-distilled water (1:1) were shaken for 15 minutes at 25°C and then filtered (Whatman No.1) until a clear liquid solution was obtained. Conductivity and pH were tested in this solution.
NH_{4+}, NO_{2-} (for N_{Total})	Content was determined by extraction with 1M KCl followed by colorimetric analyses with Nessler reagent for the soil NH_{4+} Diazotizing reagent for the NO_2. The reading of each of the samples was taken in a spectrometer with a wavelength of 420 nm for and NH_{4+} and 543 nm for the NO_{2-} (APHA, 2017)
Relative humidity (RH)	was determined by comparing the weight of the soil samples and the permanent wilting point based on soil physical properties according to soil texture, before and after drying overnight at 105ºC for 48 hours (Campbell, 2008)
Soil particles size (sand content)	Filtering the soil samples using 1000µm net to take out the organic matter and stones. Using 56 µm for separating the sand particles. Adding water solution with Na_2CO_3 to separate the silt and clay. Drying the phase and weighting (Kroetsch and Wang, 2008).

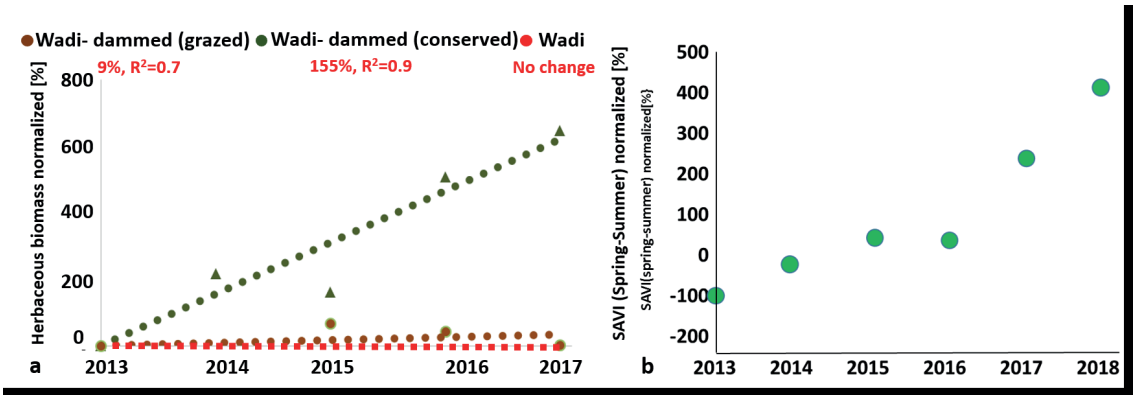

Fig. 4. The ANPP changes over the wadis in Wadi Atir between 2012 and 2018 normalized with reference plot a- Herbaceous biomass [Kg m^{-2}], b- Landsat SAVI for the Wadi. Check dams (conserved)

RESULTS

The ANPP changes over time in the different wadies at PWA sites

In both methodologies for ANPP determination, the manual one and the SAVI-based one, the combination of check dams' construction and conservation from grazing leads to a steep yearly increase of the ANPP in the wadi. Nevertheless, the calculated increase from the SAVI data is lighter than the manual one, possibly to the SAVI calculation limitation (Helman et al. 2020). An important character of the utilization of check dams can be observed from the SAVI data (Fig. 4a), during the 3 years after construction, the yearly ANPP change was lighter than the following years, possibly due to the use of heavy machinery to build check dams. In addition, a light ANPP increase of 9% was additionally observed in the grazed wadi, which possibly can be explained by reduced grazing intensity (Fig. 4b).

The influence of wadi reclamation on surrounding area productivity

The correlation between the wadi ANPP of a conserved wadi terrace with constructed check dams and the ANPP of an adjacent area can be observed by comparison of the herbaceous biomass weights in a representative wadi terrace, its' adjacent aerial slots, and embedding area. Such

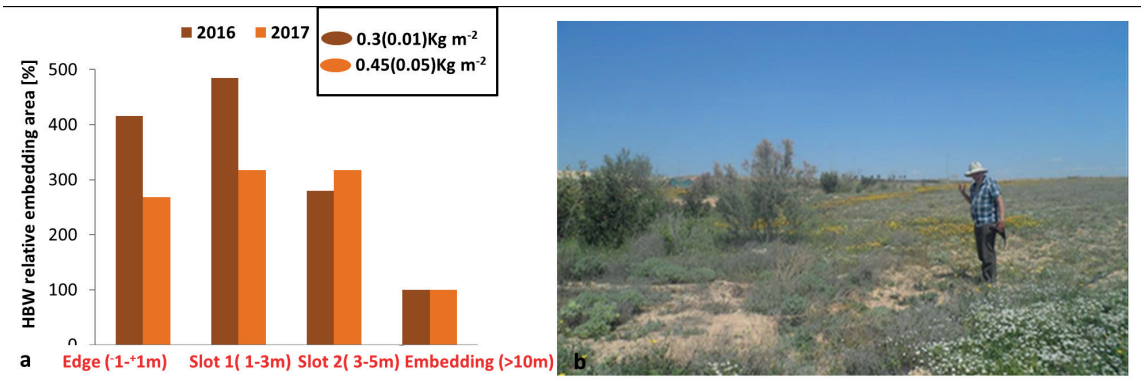

Fig. 5. The influence of representative wadi terrace on the herbaceous biomass of neighboured area.

a- Empirical data from February 2016 and 2017, b- Visual view (Each aerial slot width 2m, 'edge'- wadi terrace edge, 'Embedding- the embedding area, in the upper rectangle- the herbaceous biomass in the wadi terrace, in brackets- the ±SE)

correlation was not found before 2016, possibly to lack of influence the in first years after the check damming (Biomass weight- Fig. 5A and local color- Fig. 5b).

The influence of the different wadies area landforms on soil properties

To determine the influence of the different wadies landforms on the soil properties, a crucial step for suiting the breeding crop and the adequate cultivation, three soil samples were randomly taken from each wadies landform covering the profile from surface until 20cm depth based on Figure 3 scheme and wide range of measurements were carried out on each sample including potassium, phosphorus, ammonium, EC, organic matter, granular content, and relative humidity. The main findings are summarized in Table 2. The grazed rocky slopes are characterized by higher organic matter and nitrogen content compared to the un-grazed ones. In addition, higher moisture and fine particle content were observed (possibly due to the animals trampling, Mor-Mussery et al. 2020b), (Table 2, 'a'). The plot was settled by a knitted camel group characterized by higher soil fertility and fine particles content ('b'). The Bedouin-managed aquifer recharge (MAR) demonstrates higher organic matter content compared to undammed wadis flooded plain ('c'). Younger wadi in loess plain has higher sand content and less organic content than adult one located in an area with exposed limestone and loess deposits (rocky slope), ('d'). Similar soil properties were found in the area over the ancient Byzantine agriculture terrace slot in Yerohan ephemeral wadi, except a little higher moisture content in the agriculture terrace slot and Nitrogen ('e'). The *Ratema sp*. in the loess wadi increased the organic matter, moisture, and fine particles contents reflecting high ecosystem engineering activity ('f').

Results summary

a. The afforestation and ecological management of the wadis raised their and their surrounding area productivity.

b. The wadies area is characterized by versatile landforms that are correlated by overland flows.

c. The landform versatility is accompanied by different soil chemical content.

d. Successful reclamation of wadis has to take into consideration the local soil, geographic outlines, flora, fauna, and previous agriculture utilizations (from ancient eras and Bedouin ones).

e. Grazing is taking an important role in the wadi ecosystem's functioning.

DISCUSSION

The high rehabilitative efficiency of wadi with adequate constructed, savanna tree planted and grazing managed check dams over wadi in an arid area is well demonstrated in PWA findings. Nevertheless, implementation of the determining principles for wadi reclamation in the wadies area of Rahma is highly challenging, due to its' active cultivated manner, the existence of ancient agriculture ruins (e.g. stone dams, wells, and agriculture terraces) that have to be conserved, and ecological 'hot spots' (Mor-

Table 2. The influence of different wadies landforms, ancient agriculture ruins, and Bedouin practices on soil properties

	EC	RH[%]	Ntotal[mg kg^{-1}]	SOM[%]	Sand[%]
(a) Influence of grazing on a rocky slope					
Grazed rocky slope	0.75(0.1)	30(1.0)	85.3(30.0)	1.5(0.2)	53(10)
No-grazed rocky slope	1.4(1.0)	37(3.05)	44.9(7.0)	0.2(0.2)	61(3.0)
(b) Influence of knitting camel group for a month					
Untreated	0.55(0.06)	39(1.45)	42.8(16.3)	3.05(0.45)	61.7(5.0)
Knitting plot	1.44(0.04)	29(2.5)	65.75(6.45)	16.9(14.2)	54.7(2.0)
(c)Managed aquifer recharge area vs. Wadis flooded plain					
Managed aquifer recharge	0.55(0.06)	39(1.45)	42.8(16.3)	3.05(0.45)	61.7(5.0)
Wadis flooded plain	N/S	N/S	N/S	0.7(0.6)	48.7(6.0)
(d) Loess wadi (young) vs. Loess/lime stone wadi (adult)					
Loess wadi (young)	0.3(0.16)	27.6(0.5)	19.6(12.5)	2.1(0.24)	85.7(9.0)
Loess/lime stone wadi (adult)	1.1(0.12)	39(1.1)	59.6(5.9)	2.7(0.35)	72.0(3.7)
(e) Vegetation slots over ancient agriculture terraces vs. Untreated area(Yeroham stream)					
Untreated area	0.25(0.02)	26.7(0.85)	40 (*)	0.3 (*)	86.7 (*)
Vegetation slots	0.6(0.04)	29.0(0.9)	51.5(9.25)	0.9 (0.5)	88.7 (2.0)
(f) Influence of Ratema sp. on the soil properties of the loess wadi					
Loess wadi (young)	0.3(0.16)	27.6(0.5)	19.6(12.5)	2.1(0.24)	85.7(9.0)
Loess wadi(young)-Ratema sp.	0.44(0)	29.6(0)	12.1(0)	2.3(0)	78.7(0)
EC- Electrical conductivity (salinity), RH- Relative humidity, N- Nitrogen, SOM- Soil organic matter four samples per each plot, '*'- one sample mix of 3 plots, In brackets- ±SE					

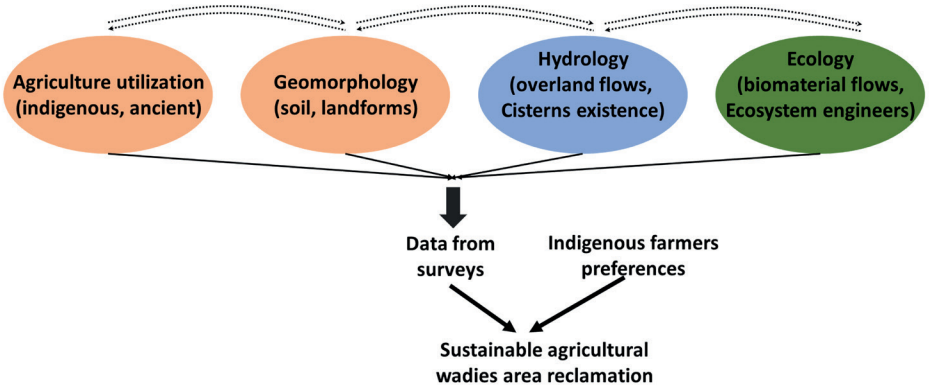

Fig. 6. Scheme for a successive wadis area reclamation

Mussery et al. 2020a). The steps for a successive agricultural reclamation of the wadies area are summarized in Fig. 6.

The first phase is surveyed by experts aimed to suit the reclamation design to the wadis area. Four surveys are suggested, including ecology, hydrology, geomorphology, and agriculture utilization, each of them has to be treated with relation to the other ones. Here, each unit will be described with samples from this and other studies.

(i) Ecology survey.

The first study action is an examination of the biomaterial flows over the wadies and their connected landforms. The close view reveals that the wadis with the expanded vegetation up-slopes are characterized by grazing on the slopes, while in the other without the grazing the vegetation expansion up-slopes missed. This finding enables us to illustrate the whole mechanism that correlates the wadi shape, wadi terraces, grazing on slopes, and vegetation expansion up slopes, as follows. The formed ecological feedback loop in the wadi terraces as empirically approved in the PWA site is been intensified by floods enriched with animal excrement and nutrients (Mor-Mussery et al. 2020b) (Fig. 7).

The intensification of the ecological feedback loops in the wadi terraces caused in turn to vegetation expansion (and land rehabilitation) up-slopes. As many wadies areas, the Rahma area was intensively cultivated at ancient times by its' indigenous residents, nevertheless, due to temporal landform changes, lack of documentation by its' farmers, and lack of maintenance or abandonee of these plots, the principles of reimplementation of these cultivations or land management practices are missing and the only way to determine the principles is indirectly by a detailed analysis of the ecological pattern of these plots (Jackson 2011).

Except for the determination of the biomaterial flows over the wadi, analysis has to be carried out to determine the local ecosystem engineers. Data from this survey may be used for increasing the crop yield, as plantation the *Rathem sp*. that form fertile soil patches and host pollinators for crops even in the drought season (Fig. 8a). An additional unique landform characterized by sandy soil in wadies area is Nabakcha. Until recently the Nabakha was concerned as a seasonal landform caused by an accumulation of sand from wind storms over the shrub root system (Li et al. 2020). Nevertheless, recent studies claim it can be used for agriculture utilization after its' stabilization with organic matter (Fig. 8b).

(ii) Hydrology survey

The hydrology survey aimed first and foremost to design a sustainable agriculture utilization with minimal additive irrigation (Hrachowitz et al. 2011). In addition, water pools and cisterns have also high landscape and tourism importance (Akash 2012). The study was carried out in drought years, therefore cisterns were not located, and nevertheless, oral data from local Bedouin locate several cisterns in the site of study at rainy years.

(iii) Geomorphology survey

The geomorphology and soil affect the ecology of the area and, as a result, agriculture utilization. In the wadies area, the geomorphology also play important role in the

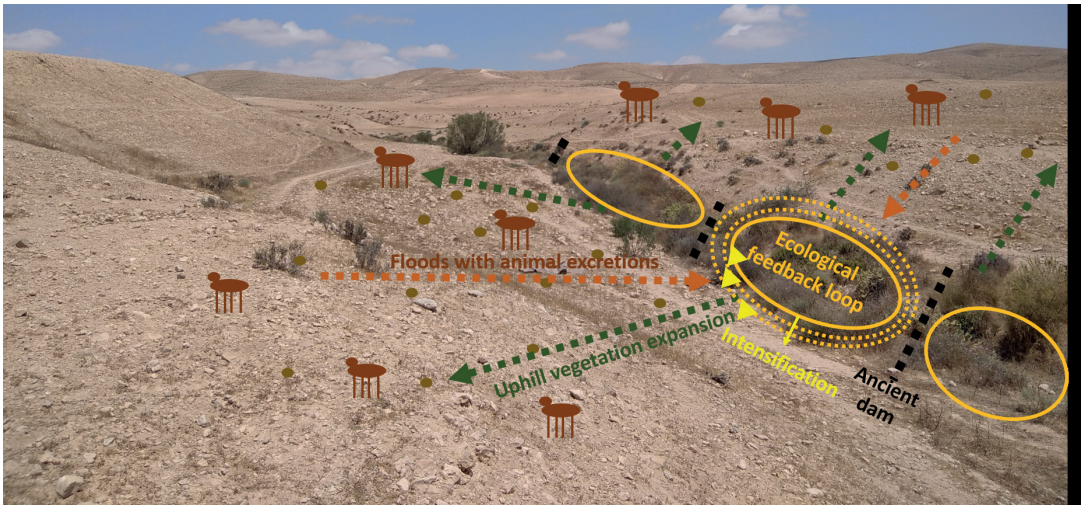

Fig. 7. The high ecosystem functioning in the wadi caused from the channel, banks patterns, and the dam's existence. This functioning may be intensified by an adequate grazing regime in the wadies area leading to up slopes vegetation expansion and rehabilitation of the whole area. Rahma, 7/2020

landscape visibility for tourism (Elassal 2020). Therefore, here we studied plots with different soil characters as loessial, sandial, and regolith ones with a wide range of natural and remodeled landforms (e,g. Fig. 8e, 8f)

(iv) Agriculture utilization survey

Adequate cultivations and land management practices may accelerate the whole wadies area rehabilitation by increasing the soil water holding capacity (Mahe et al. 2005), CO2 sequestration into organic matter (Bai et al. 2019), and soil thickness by an enhanced bedrock weathering (Pawlik et al. 2016). Therefore, we studied first and foremost plots that caused from current Bedouin cultivations and land management practices as ones used to temporarily locate and transport knitted camel groups on the soil (Fig. 7g). Using natural arid regions suited trees for breeding orchard trees and groves with a reduced supplementary irrigation need (Norfolk et al. 2013; Shen et al. 2017) (Fig. 8h).

In addition, analysis of ancient archaeological ruins is crucial, because ancient dams over wadi may form a highly productive environment due to the high stone coverage (Bruins et al. 2019). The high vegetative slot along Yeroham stream with high moisture and sediments contents (Fig. 3, Table 2) may indicate the potential of planting fruit trees suited to wet regions (Hüneburg et al., 2020). In addition, reclamation of such ancient agriculture terraces may increase their current influence on soil fertility until reaching sustainable agriculture utilization of the land (Fig. 8c& 8d).

Finally, after collecting the data from the surveys, it is crucial to build a sustainable cultivation design with

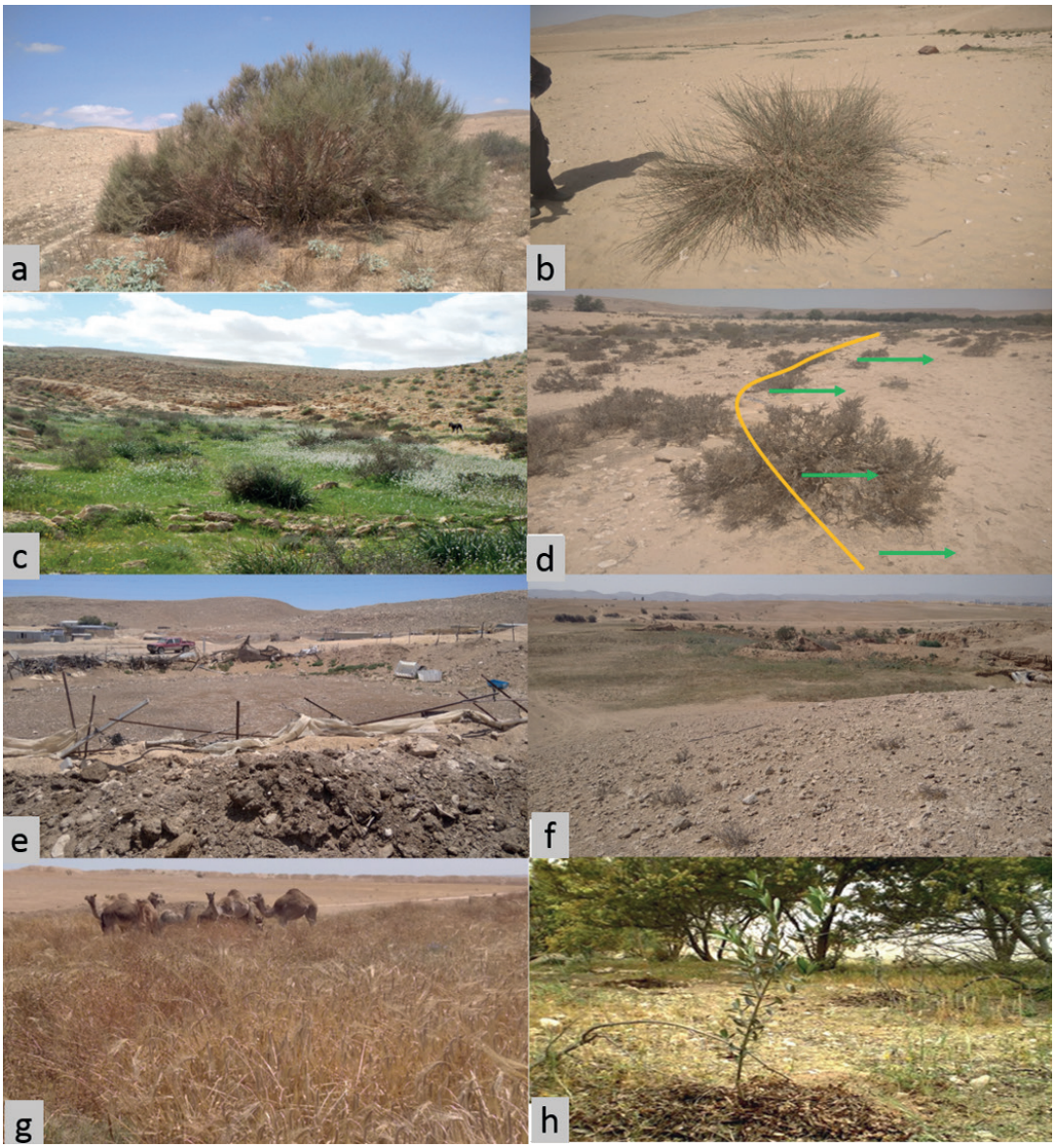

Fig. 8. Ecological, ancient agriculture facilities utilization, wadies areas landforms, and indigenous Bedouin agriculture knowledge hot plots with potential for commercial and sustainable agricultural utilization in wadies arid areas

Ecological: (a) Nebakha settled by Anabasis articulate may be used as a fertile island for crop breeding in sandy wadies area. (b) The Ratema sp. may serve as successful ecosystem engineers to cultivated areas by forming fertile patches and places for bee grazing and other fruit tree pollinators. Ancient agriculture facilities utilization: (c) Reclaimed Byzantine wadi dams may be used for agriculture (Shualim wadi, Photo by S. Leu, 2019), (d) Ancient Byzantine agriculture terrace with current influence on their neighbored area soil fertility, for managed aquifer recharge (MAR) crop breeding. Wadies area landforms (e) Gully terraces, which represent the area between adjacent check dams along the wadi, may be used for agriculture using the flood-water for irrigation, the loess check dams are stabilized by manure layers (f) A Bedouin managed aquifer recharge (MAR) area on wadies flooded plain for cereals breeding, Indigenous Bedouin agriculture knowledge (g) Acacia victoriae that sheltered grove trees, Yattir farm 2016. (h) Temporary locating and transporting of a knitted camel group over the cultivated area, which serves as 'manure management action' (Norris et al. 2020) aimed to increase the soil fertility of the cultivated area.

the indigenous farmers based on suitability to the wadis areas, profitability, and their preferences as previously demonstrated on grazing (Mor-Mussery et al., 2019).

CONCLUSIONS

Wadies area is a highly sensitive landform. From one side, they are intensively incised, which requires intermediate intervention to halt the incision, but from the other side, such an intervention must not damage the picturesqueness of habitat due to the unique geographic outlines, ecological flows, existent of ancient remains, and the indigenous farmers, which increases its' tourism value. Therefore, only sustainable agriculture reclamation of these areas will conserve their uniqueness and supply work to their inhabitants.

REFERENCES

Abdel-Fattah M., Saber M., Kantoush S.A., Khalil M.F., Sumi T., Sefelnasr A.M. (2017). A hydrological and geomorphometric approach to understanding the generation of wadi flash floods. Water 9(7), 553, DOI: 10.3390/w9070553.

Abu Rabia K., Solowey E., Leu S. (2008). Environmental and economic potential of Bedouin dryland agriculture: A case study in the Northern Negev, Israel Man Environ Qual Int J 19(3), 353-366, DOI: 10.1108/14777830810866464.

Akasheh, T. S. (2012). The Environmental and Cultural Heritage Impact of Tourism Development in Petra–Jordan. In Tourism and archaeological heritage management at Petra (pp. 131-144). Springer, New York, NY, DOI: 10.1007/978-1-4614-1481-0_6.

Amit R., Enzel Y., Sharon D. (2006). Permanent Quaternary hyperaridity in the Negev, Israel, resulting from regional tectonics blocking Mediterranean frontal systems. Geology 34(6), 509-512, DOI: 10.1130/G22354.1.

American Public Health Association (APHA) (2017). Standard Methods for the water and wastewater, American Water Works Association, Water Control Federation. Examination of Water and Wastewater, 21st Eds. Washington, DC. ISBN: 9780875532875.

Bai X., Huang Y., Ren W., Coyne M., Jacinthe P.A., Tao B., ..., Matocha C. (2019). Responses of soil carbon sequestration to climate-smart agriculture practices: A meta-analysis. Global Change Bio 25(8), 2591-2606, DOI: 10.1111/gcb.14658.

Ben-Dor E., Banin A. (1989). Determination of organic matter content in arid-zone soils using a simple «loss-on-ignition» method. Comm. Soil Sci. Plant Anal. 20, 1675-1696, DOI: 10.1080/00103628909368175.

Bruins H.J., Bithan-Guedj H., Svoray T. (2019). GIS-based hydrological modeling to assess runoff yields in ancient-agricultural terraced wadi fields (central Negev desert). J Arid Environ 166, 91-107, DOI: 10.1016/j.jaridenv.2019.02.010.

Campbell G. (2008). Modeling available soil moisture. Decagon devices® Support Appl. 1-4. SN: 800-755-2751 Online: http://publications.decagon.com/Application%20Notes

Cao C., Abulajiang Y., Zhang Y., Feng S., Wang T., Ren Q., Li H. (2016). Assessment of the effects of phytogenic nebkhas on soil nutrient accumulation and soil microbiological property improvement in semi-arid sandy land. Eco Engin 91, 582-589, DOI: 10.1016/j.ecoleng.2016.03.042.

Elassal M. (2020). Geomorphological Heritage Attractions Proposed for Geotourism in Asir Mountains, Saudi Arabia. Geoheritage, 12(4), 1-18, DOI: 10.1007/s12371-020-00505-z.

Gong J.G., Jia Y.W., Zhou Z.H., Wang Y., Wang W.L., Peng H. (2011). An experimental study on dynamic processes of ephemeral gully erosion in loess landscapes. Geomorphology 125(1), 203-213, DOI: 10.1016/j.geomorph.2010.09.016.

Hrachowitz M., Bohte R., Mul M.L., Bogaard T.A., Savenije H.H.G., & Uhlenbrook S. (2011). On the value of combined event runoff and tracer analysis to improve understanding of catchment functioning in a data-scarce semi-arid area. Hydrology and Earth System Sciences, 15(6), 2007-2024, DOI: 10.5194/hess-15-2007-2011.

Helman D., Mor-Mussery A., Lensky I.M., Leu S. (2014). Detecting changes in biomass productivity in different land management regimes in drylands using satellite-derived vegetation index. Soil Use Mana 30(1), 32-39, DOI: 10.1111/sum.12099.

Helman D., Mor-Mussery A. (2020). Using Landsat satellites to assess the impact of check dams built across erosive gullies on vegetation rehabilitation. Sci. Total Envi 730, 138873, DOI: 10.1016/j.scitotenv.2020.138873.

Hüneburg L., Hoelzmann P., Knitter D., Teichert B., Richter C., Lüthgens C., ... & Luciani M. (2019). Living at the wadi–integrating geomorphology and archaeology at the oasis of Qurayyah (NW Arabia). Journal of Maps, 15(2), 215-226, DOI: 10.1007/s12371-020-00505-z.

Jackson W. (2011). Consulting the genius of the place: An ecological approach to a new agriculture. Counterpoint Press. ISBN: 978-1-58243-513-8.

Kroetsch D., Wang C. (2008). Particle size distribution. Soil sampling and methods of analysis, 2, 713-725. ISBN: 13: 978-0-8493-3586-0.

Leu S., Ben-Eli M., Mor-Mussery A. (2021). Normalized biological productivity and soil fertility gains indicate rapid ecosystem restoration and soil carbon sequestration in heavily degraded loess plains by grazing control in the Northern Negev, Israel. Land Deg Dev: 32: 2580-2594, DOI: 10.1002 /ldr.3923.

Li J., Wang Y., Yao Q. (2020). Nebkhas origination in arid and semi-arid regions: An overview. Acta Ecologica Sinica, DOI: 10.1016/j.chnaes.2020.10.006.

Mahe G., Paturel J.E., Servat E., Conway D., Dezetter A. (2005). The impact of land use change on soil water holding capacity and river flow modelling in the Nakambe River, Burkina-Faso. J Hydrol 300(1-4), 33-43, DOI: 10.1016/j.jhydrol.2004.04.028.

Mor-Mussery A., Shuker S., Zaady E. (2019). New approach for sustainable and profitable grazing systems in arid open lands – a case study in the northern Negev. Geog Environ Sustain 12(2), 106-127, DOI: 10.24057/2071-9388-2019-15.

Mor-Mussery A., Helman D., Agmon Y., Ben Shabat I., El-Frejat S., Goldman Golan D. (2020a). The indigenous Bedouin farmers as land rehabilitators - setup of an action research program in the Negev. Land Deg Dev (Online, 06/06/2020), DOI: 10.1002/ldr.3637.

Mor-Mussery A., Laronne B.J. (2020). The effects of gully' erosion on the ecology of arid loess agro-ecosystems. Wadi Atir area, the northern Negev a case study. Catena. 194, 104712, DOI: 10.1016/j.catena.2020.104712.

Mor Mussery A., Abu-Glaion H., Shuker S., Zaady E. (2020b). The influence of small ruminants trampling on soil fertility in the semi-arid region of the south-western Negev. Arid Land Res Manag 2020, 1-9, DOI: 10.1080/15324982.2020.1827083.

Norfolk O, Eichhorn M.P., Gilbert F. (2013). Traditional agricultural gardens conserve wild plants and functional richness in arid South Sinai. Basic App Ecol 14(8), 659-669, DOI: 10.1016/j.baae.2013.10.004.

Norris A.B., Smith W.B. (2020). Farming characteristics and manure management of small ruminant and cervid livestock. Animal Manure: Production, Characteristics, Envi. Concerns Manag 67: 129-144, DOI: 10.2134/asaspecpub67.c7.

Pawlik Ł., Phillips J.D., Šamonil P. (2016). Roots, rock, and regolith: Biomechanical and biochemical weathering by trees and its impact on hillslopes—A critical literature review. Earth Sci Rev 159: 142-159, DOI: 10.1016/j.earscirev.2016.06.002.

Sava R. (1994). Guide to sampling air, water, soil, and vegetation for chemical analysis. FAO press

Şen Z., Al-Harithy S., As-Sefry S., Almazroui M. (2017). Aridity and risk calculations in Saudi Arabian wadis: Wadi Fatimah case. Earth Sys Environ 1, 26, DOI: 10.1007/s41748-017-0030-x.

Shen Q., Gao G., Fu B., Lü Y. (2015). Sap flow and water use sources of shelter-belt trees in an arid inland river basin of Northwest China. Ecohydrology, 8(8), 1446-1458, DOI: 10.1002/eco.1593.

RESEARCH PAPER

SPATIAL FEATURES OF COVID-2019 DIFFUSION IN RUSSIAN REGIONS: THE VIEW OF THE TRANSPORT GEOGRAPHER

Sergey A. Tarkhov
Institute of Geography, Russian Academy of Sciences, Staromonetnyi per. 29, Moscow 119017, Russia
***Corresponding author:** tram.tarkhov@gmail.com
Received: September 19th, 2021 / Accepted: February 15th, 2022 / Published: March 31st, 2022
https://DOI-10.24057/2071-9388-2021-107

ABSTRACT. The purpose of the article was to analyze the spatial spread of COVID-2019 in the regions of Russia in comparison with European countries in 2020–21 from a transport-geographical point of view. The article reveals interregional differences in the number of cases and the incidence (sickness) rate as of August 1, 2021 for individual regions of Russia. The coronavirus entered two Russian regions directly from Wuhan (China) and eight regions from Northern Italy. The first virus carriers arrived by air transport, which was the main means of spreading the epidemic. Spatial diffusion of COVID-2019 in Russia was extremely uneven with epicenters in the large cities. In the early stages the coronavirus spread in an exclusively hierarchical way through the established extensive air communication system. The later stages of its spread were characterized by mixed diffusion with the dominance of the hierarchical form. COVID-2019 has six gradations of the incidence (sickness) rate expressed in the number of cases per 1 million inhabitants: very high (more than 140), high (90–140), moderate (70–90), medium (45–70), low (20–45), very low (6–20). For the Russian regions the most typical were low (51 regions) and medium (20 regions) incidence rates – 60% and 23.5% (84% in total), respectively. The incidence rate, according to official data from Rospotrebnadzor (Russian Agency of Consumer Supervision), is 38% lower than in European countries. The average number of Russian cases in the first seven months of 2021 was 1.8 times more than for the entire 2020.

KEYWORDS: COVID-2019, hierarchical diffusion, Russia, incidence rate

CITATION: Tarkhov S. A. (2022). Spatial Features of Covid-2019 Diffusion in Russian Regions: the View of the Transport Geographer. Vol.15, № 1. Geography, Environment, Sustainability, p 87-101 https://DOI-10.24057/2071-9388-2021-107

ACKNOWLEDGEMENTS: The study was conducted in pursuance of the state order within the theme AAAA-A19-119022190170-1 (FMGE-2019-0008) "Problems and prospects of Russia's territorial development in the context of its unevenness and global instability."

Conflict of interests: The authors reported no potential conflict of interest.

INTRODUCTION

The COVID-2019 pandemic has completely changed the world and our understanding of its sustainability, having a strong impact on society and the economy, including the spatial allocation of the tertiary sector of the economy (especially tourism and transport). Its impact turned out to be far-reaching in terms of geography. Therefore, it is relevant to study social and the economic effects of the pandemic. It is important for geographers to understand the spatial differentiation of this impact, which largely depends on the spatial distribution of COVID-2019. The geographical features of the impact of the COVID-2019 pandemic on the structures of the economy and society in the most general terms are analyzed in a series of short articles in a special section of the Russian journal "Vestnik ARGO" (Bulletin of the Association of Russian Human Geographers) No. 9 for 2020 (Druzhinin 2020; Gerasimenko and Gerasimenko 2020; Kagansky 2020; Kolosov 2020; Kuznetsova 2020; Rodoman 2020; Shuper 2020; Zyryanov 2020, and others).

The publication (Zemtsov and Baburin 2020a) indicates that the spread of the epidemic in the regions of Russia obeys the patterns of diffusion of innovations and depends on the structure and interaction within regional communities. The first to become infected are innovators (tourists from the foci of the disease) and early adopters (social leaders) who spread the disease throughout the community. At the first stage of diffusion, more than 80% of all infected were concentrated in Moscow, the Moscow region, and the largest urban agglomerations. At an exponential stage, the number and proportion of cases outside Moscow grew steadily. The number of confirmed cases of the disease is higher in wealthy large urban regions, where the share of the more socially active part of the population is higher, its density and intensity of interaction are higher. In regions near large agglomerations, the number of cases is also significant due to the rapid spread of the disease from Moscow to neighboring regions. These authors rightly point out that in conditions of administrative pressure, imperfect statistics of the disease, many cases of illness and death associated with the epidemic will not be included in the coronavirus statistics.

The work (Kaganskiy 2020) shows that global crises such as the COVID-2019 pandemic lead to spatial inversions – loosely connected and backward regions and areas of

the world have advantages in their preservation, while the most developed and globally connected areas (regions, countries) turn out to be the most vulnerable and suffer the most from the consequences of such crises.

A number of other Russian publications that appeared a little later analyzed the diffusion of the pandemic, the factors of its spread, and considered the impact of the pandemic on the Russian economy in the regional context (Zemtsov and Baburin 2020b; Zubarevich and Safronov 2020; Pelyasov et al. 2021).

The article (Makhrova and Nefedova 2021) examines the possibilities of transition from seasonal countryside mobility to real suburbanization and deurbanization in areas of varying degrees of remoteness from Moscow under the new conditions of quarantine restrictions.

Panin et al. (2021) presented a cartographic analysis of the spatial patterns of the spread of the COVID-19 pandemic in Russia. They state that the three initial centers of its diffusion were the Moscow region, the oil and gas producing regions in the Western Siberia and the North Caucasus. The main factors of the rapid spread of COVID-19, from the point of view of the authors, were not only transport and logistics parameters, but also a high proportion of the creative class in the Moscow region, rotational flows and overcrowding of shift camps in the Yamal-Nenets autonomous area, increased contact and a weak healthcare system in regions of the North Caucasus.

The problems of the geographical study of the epidemics are also highlighted in the Russian monographs on medical geography. Thus, a monograph (Malkhazova 2001) is devoted to the methods of medical-geographical mapping, and a book (Semenova and Chistobaev 2015) considers the general problems of medical geography. An article by Pogorelov (2020) with an extensive bibliography (39 sources) presents a general overview of the current state of medical geography in Russia. Among foreign monographs on medical geography, especially famous are (Haggett 2000; Cliff et al. 2004; Lawson 2006; Souris 2019).

The article (Chen et al. 2021) is devoted to the study of the spatial diffusion of the COVID-19 disease, which spread from Wuhan (China) to cities in Hubei province by the gravity model. The simulation results showed that the total number of confirmed cases of the disease depended on the size of provincial cities and the distance from them to Wuhan (the epicenter of the pandemic). Its spread was hierarchical, while the immediate neighborhood of cities with each other did not matter much.

An increasing number of European articles analyze the geographical factors in the spread of COVID-19. The special issue of the Dutch magazine Tijdschrift voor economische en socale geografie (Journal of Economic and Social Geography) # 3 for 2020 contained a series of articles on the topic "Geography of the COVID-19 Pandemic, 2020" (Geography of the COVID-19 Pandemic 2020).

In the publication (Sigler et al. 2021), the authors, using regression analysis, come to the following conclusions: the spread of COVID-19 in countries with a large number of reported cases (per 1 million residents) could be predicted by the values of human development and the total population ; the larger the households, the older the population and the more intense globalization, which involves closer interaction between people, the better the spread of COVID-19 can be predicted in countries with a low incidence rate (cases per million inhabitants). Population density and other characteristics such as total population, proportion of elderly people, and household size are reliable indicators in the early weeks of the epidemic, but have little impact on the spread of COVID-19 over time. In contrast, the impact of interpersonal globalization and out-of-shop trade has increased over time, indicating that higher human mobility may best explain the persistent spread of the disease.

In (Kuebart and Stabler 2020), a spatial diffusion model is used to study the spread of COVID-19 within Germany. Some recent geographical publications are devoted to the spread of coronavirus in Italy (Ascani et al. 2020), Sweden (Florida and Mellander 2020), Iran (Ramírez-Aldana et al. 2020); new e-book (Shaw and Sui 2021) is devoted to the COVID-19 mapping.

The analysis of the literature showed that many economic-geographical aspects of the spread of the coronavirus infection have already been considered or studied to one degree or another. However, the spatial features of this process from a transport-geographic point of view are still poorly studied. The purpose of the article is to analyze the spatial characteristics of the spread of the COVID-19 pandemic over the territory of Russian regions from this point of view.

MATERIALS AND METHODS

In the economic-geographical analysis of the spread of coronavirus infection, the main parameters are the number of cases (registered cases) and the incidence (morbidity) rate (the number of cases per 1 million inhabitants). The latter indicator is more effective because it reflects relative incidence rates, rather than absolute values (which, sometimes, can be misleading in their size or distract from an appropriate comparison); in addition, it clearly shows the level of falsification of the initial statistics of the registered cases due to different diagnoses and underestimation of the incidence .

In addition, there are two more important indicators that describe the spatial diffusion of the disease – the geographical lag of its spread and the number of areas (countries, regions, loci) involved in this process. The first means the number of days of registration of the first cases of the disease in *all geographic areas* (countries, regions, localities) from the first to the last day, that is, the number of days from the record of the first case in the first area to its fixation in the last area of the analyzed territory. The second indicator reflects the cumulative increase in the number of geographical areas covered by the epidemic (pandemic). It increases slowly and then very quickly (exponentially) decreases along an S-shaped curve (see theoretical works on the diffusion of innovations by Torsten Hägerstrand and his followers; Hägerstrand 1967), covering at the end all the areas (countries, regions, loci).

To achieve the above goal, we used statistical data on the number of COVID-19 cases and the incidence rate taken from the sites https://stopcoronavirus.rf (https://стопкоронавирус.рф; Coronavirus COVID-2019: official information for the regions of Russia), https://github.com/CSSEGISandData / COVID-19 (COVID-2019 statistics by countries of the world by John Hopkins University).

These statistics were collected for three dates (August 2, 2020; January 16, 2021; and August 1, 2021), and then systematized by individual regions of Russia (regions (oblast'), territories (kray), republics, and autonomous regions; the latter were then aggregated by 11 macro-regions). This made it possible to conduct comparative geographical analysis and to identify the spatial characteristics of the spread of COVID-19, the differences in the number of cases and the incidence (sickness) rate in Russian individual regions.

The interregional differences in the number of cases and the incidence rates were analyzed as of August 1, 2021. The data for August 2, 2020 and January 16, 2021 were collected for understanding the course of the disease diffusion, but were not analyzed in detail (with a number of exceptions), since during the first seven months of 2021 the number of cases in the regions of Russia turned out to be almost two times higher than in the entire 2020.

RESULTS

Spatial distribution of the coronavirus in Russia: transport-geographical analysis

Table 1 presents the geographical origin of the first cases of the disease. It shows that on the first day (January 31), the carriers of the disease were Chinese citizens who came to Russia. These were isolated cases and the patients were quickly discharged. A month later, from February 27 to March 12, the main source of infection for Russia was Italy , from where arrived 32 infected people by air (including one Italian student who returned to classes at the St. Petersburg Medical University, and the rest were Russian travelers who had been vacationing in the ski resorts of the northern Italy and other regions). On March 13, the first sick Russian tourists arrived from France and Austria; on March 14–15 arrived infected tourists from Spain and Switzerland.

The last right column of the Table 1 proves that the main mode of transmission of the infection to Russia from abroad in the first phase of the epidemic was air transport.

Geographic patterns of the spread of COVID-2019 in Russia

To understand the spatial nature of the spread of the disease, we compiled Table 2, which chronologically ordered the first detection cases in each Russian region in the context of macro-regions (it is divided into two parts: the first, 2A, indicates the regions of European Russia; the second, 2B, indicates the regions of – Asian Russia). It shows that the spatial diffusion of COVID-2019 across the territory of Russia was extremely uneven, not only throughout the country, but even within the socio-economic macro-regions.

Since the old grid of Soviet economic regions has become somewhat obsolete due to the great changes in economic and settlement structure that have taken place over the past 30 years, we have proposed its modified version of large-scale territories for our study, which we call socio-economic macro-regions. They include entire units (regions) of the first administrative-territorial level[1]. In the course of empirical calculations and taking into account the proximity and transport connectivity of individual regions, we compiled the following grid of socio-economic macro-regions of Russia in contrast to traditional economic regions:

1) the European Center of Russia (the Big Center includes the former Central (excluding the Kostroma region) and Central Black Earth (Chernozyom) economic regions, as well as including the Penza and Nizhny Novgorod regions, Mordovia);

2) Kaliningrad (due to its exclave location and great remoteness from the rest of Russia, it is singled out as a special region, since it has strong territorial isolation, insignificant size, weak economic ties even with the North-West macro-region);

3) North-West (Pskov, Novgorod, Leningrad regions, but

Table 1. Geographical features of the spread of the SARS-CoV-2 coronavirus in Russian regions in the first days of the 2020 epidemic

Regions are ranged in the chronological order the first cases were registered

Date of record of the first case	Where it was brought from	Areas affected by the epidemic; number of people	Mode of transport, by which the infected people arrived
31.01.2020	China	Tyumen (1 Chinese citizen)	air transport
31.01.2020	China	Chita (Trans-Baikal Territory, 1 Chinese citizen)	air transport
27.02.2020	Northern Italy, ski resort	Moscow (1 Russian citizen)	air transport
2.03.2020	Italy	Moscow Region (1 Russian citizen)	air transport
5.03.2020	Italy	St. Petersburg (Italian student studying in St. Petersburg, arrived February 29, 2020)	air transport
6.03.2020	Italy	5 persons in Moscow + 1 person in Nizhny Novgorod (all Russian citizens)	air transport
8.03.2020	Italy	1 person in Kaliningrad, 1 person in Belgorod, 1 person in the Moscow region	air transport
12.03.2020	Italy	4 persons in Moscow, 1 person in Kaliningrad, 1 person in the Krasnodar Territory	air transport
13.03.2020	Italy	3 persons in Lipetsk, arrived in Moscow	air transport
13.03.2020	Italy, France, Austria	11 Russian citizens: 5 persons in Moscow, 1 person in the – Moscow region, 3 persons in the – St. Petersburg, 1 person in the – Leningrad region	air transport
14.03.2020	Italy, France	14 Russians: 9 persons in Moscow, 1 person in the – Moscow region, 1 person in – St. Petersburg, 2 persons in the – Kemerovo region, 1 person in the – Kaliningrad region	air transport
15.03.2020	Italy, France, Spain, Switzerland	4 Russians: 3 persons– in the Moscow region, 1 person – in the Tyumen region	air transport

Source: 304 references links to media reports and Rospotrebnadzor newsletters in https://en.wikipedia.org/wiki/Template:COVID-19_pandemic_data/Russia_medical_cases

[1]In legal language they are called subjects of the federation, that is, these are regions, territories, republics, autonomous districts and regions. Economic geographers often use not the legal term «subject of the federation» (or simply «subject», which, from the point of view of the literary language, does not quite adequately convey the meaning of the concept), but a more neutral (although also not very successful) term «region», which we will see below and used in the text.

without the Kaliningrad region);

4) European North (Karelia, Murmansk, Arkhangelsk, Vologda, Kostroma, Kirov regions, Komi Republic, and Nenets autonomous area);

5) Volga macro-region (Chuvash and Mari El Republics, the Republic of Tatarstan; Ulyanovsk, Samara, and Saratov regions);

6) European South (former North Caucasian economic region, as well as Volgograd and Astrakhan regions, Kalmyk Republic, Crimea including the city of Sevastopol);

7) Urals (the same);

8) Western Siberia (the same);

9) Eastern Siberia (Krasnoyarsk Territory, Khakas and Buryat Republics, as well as Republic of Tuva, Irkutsk region, and Trans-Baikal Territory);

10) North-East (Sakha-Yakut Republic, Magadan region, Chukotka autonomous area, Kamchatka Territory);

11) South of the Far East (Amur and Sakhalin regions, Primorsky and Khabarovsk Territories, Jewish autonomous region).

In European Russia (see Table 2A), the first foci of the disease were Moscow city, Moscow region, St. Petersburg, Nizhny Novgorod, Lipetsk and Kaliningrad regions. It outstripped Asian Russia in terms of the number of infected regions, in which the very first cases of COVID-2019 import from China were recorded. The largest macro-regions (the European Center and the European South) naturally comprised the largest number of European Russian regions – 20 and 15, respectively.

Although isolated cases of coronavirus on January 31 in Asian Russia were the first in the country (registered in Chinese citizens who arrived to Chita and Tyumen), the first wave of the *mass epidemic* came a little later than in the regions of European Russia – on March 14–19 (see Table 2B). Most recently the coronavirus was registered in the Asian regions of Russia: the Republic of Tuva (April 10), the Chukotka autonomous area (April 15) and the Altai Republic (April 17). In the European part the coronavirus was registered most recently in the Nenets autonomous area (April 15).

Table 2A. Geographic distribution of the first reported cases of COVID-2019 by regions of European Russia in February-April 2020 in the context of macro-regions

Regions are ranged in the chronological order the first cases were registered

Date of record of the first case	European Center	North-West and Kaliningrad	European North	Volga macro-region	European South	Urals
27.02.2020	Moscow					
2.03.2020	Moscow region					
5.03.2020		St. Petersburg				
6.03.2020	Nizhniy Novgorod region					
7.03.2020	Lipetsk region					
8.03.2020	Belgorod region	Kaliningrad region				
12.03.2020					Krasnodar Territory	
13.03.2020		Leningrad region				Perm Territory
16.03.2020			Komi republic, Kirov region	Samara region		
17.03.2020	Kaluga, Tambov, Tver', Yaroslavl, and Penza regions		Arkhangelsk region	Republic of Tatarstan		Sverdlovsk region
19.03.2020	Ivanovo, Ryazan, Tula, and Voronezh regions		Murmansk region	Chuvash Republic, Saratov region		Orenburg region
20.03.2020				Ulyanovsk region		
21.03.2020					Crimea, Kabardino-Balkar Republic, Stavropol Territory	Chelyabinsk and Kurgan regions
22.03.2020	Bryansk region	Novgorod region				Udmurt Republic
24.03.2020	Orel region				Volgograd region, Chechenia	Republic of Bashkortostan
25.03.2020		Pskov region			Rostov region	
27.03.2020	Republic of Mordovia				Sevastopol, Republic of Dagestan	

28.03.2020	Smolensk region		Kostroma region		Republic of Adygea	
30.03.2020	Vladimir region		Vologda region	Republic of Mari El	Kalmyk Republic	
31.03.2020					Astrakhan region	
1.04.2020	Kursk region				Republic of North Ossetia	
3.04.2020					Ingushetia	
6.04.2020			Republic of Karelia			
7.04.2020					Karachay-Cherkess Republic	
15.04.2020			Nenets autonomous area			

Source: References 1-304 in https://en.wikipedia.org/wiki/Template:COVID-19_pandemic_data/Russia_medical_cases

Table 2B. Geographic distribution of the first registered cases of COVID-2019 in the regions of Asian Russia in January-April 2020 in the context of macro-regions

Regions are ranged in the chronological order the first cases were registered

Date of fixation of the first case	West Siberia	East Siberia	North-East	South of the Far East
31.01.2020	Tyumen region	Zabaikalsky (Trans-Baikal) Territory		
14.03.2020	Kemerovo region			
17.03.2020		Krasnoyarsk Territory, Khakass Republic		
18.03.2020	Novosibirsk and Tomsk regions			
19.03.2020	Khanty-Mansi autonomous area		Sakha-Yakut Republic	Khabarovsk Territory
24.03.2020				Primorsky Territory
26.03.2020		Buryat Republic		
28.03.2020				Sakhalin region
29.03.2020	Omsk region	Irkutsk region		Amur region
30.03.2020	Altai Territory			
31.03.2020			Magadan region	
2.04.2020	Yamalo-Nenets autonomous area			
3.04.2020				Jewish autonomous region
5.04.2020			Kamchatka Territory	
10.04.2020		Republic of Tuva		
15.04.2020			Chukotka autonomous area	
17.04.2020	Altai republic			

Source: References 1-304 in https://en.wikipedia.org/wiki/Template:COVID-19_pandemic_data/Russia_medical_cases

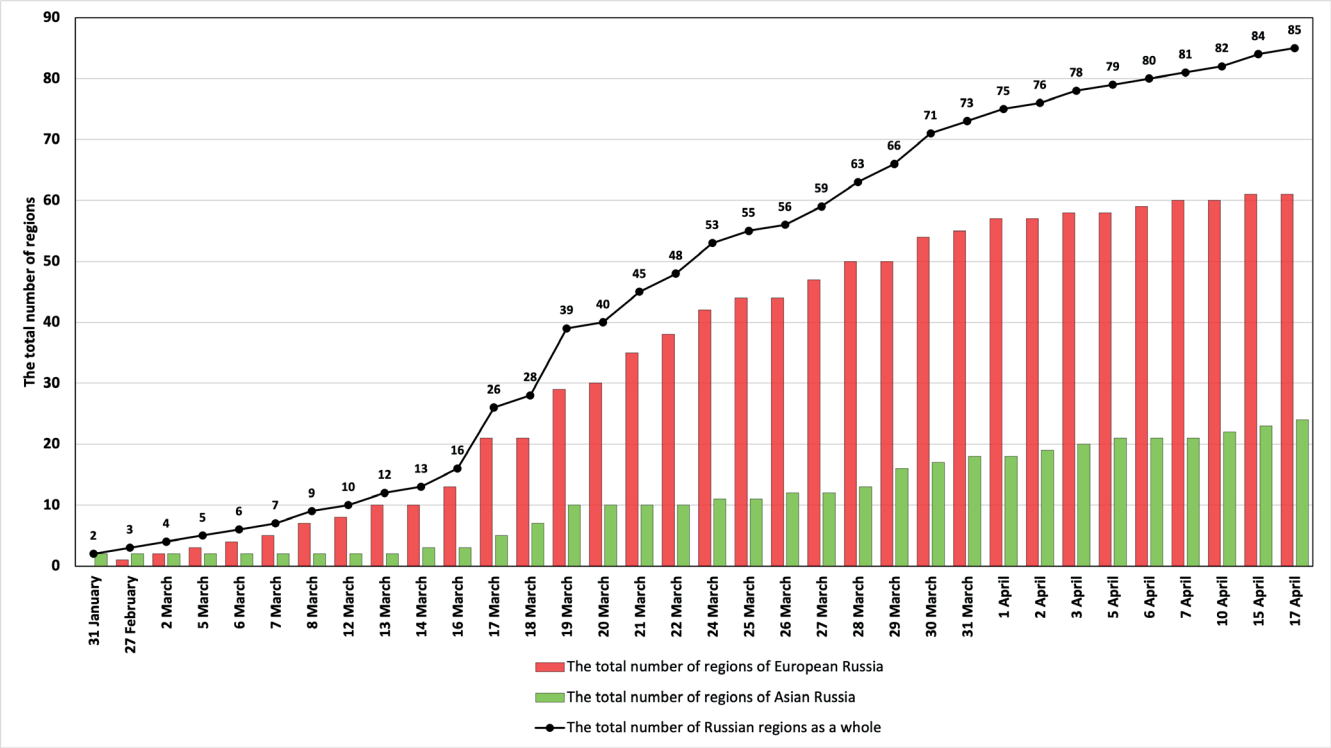

Fig. 1. Cumulative increase in the number of Russian regions with the first coronavirus cases in March-April 2020 in chronological order

Further, the epidemic began to expand rapidly in all geographic directions. The first and second peaks were concentrated in European Russia, the subsequent waves covered all the country.

By March 10, 2020, cases were registered in nine regions of the country (including in seven European and two in Asian regions); by March 20 – cases were registered in 40 regions (including in 30 European and 10 Asian regions), by March 25 – cases were registered in 55 regions (including in 44 European and 11 Asian regions), by March 30 – cases were registered in 71 regions (including in 54 European and 17 Asian regions), by April 5 cases were registered in – 79 regions (including in 58 European and 21 Asian regions), by April 17 – cases were registered in 85 regions (including in 61 European and 24 Asian regions). Due to its transport-geographical remoteness and complete or partial overland isolation, the last regions where the disease came to were Tuva and Altai republics as well as Nenets and Chukotka autonomous areas. This happened on April 10–17, 2020.

Thus, the geographical lag of the epidemic throughout Russia was 51 days (February 27 – April 17) apart from the first two cases on January 31.

The first regions involved in the epidemic were the European Center (February 27 – March 6), North-West (March 5), and Kaliningrad (March 8); a little later the coronavirus came to other regions of European Russia (March 12–17) and then to Asian Russia (from March 14–17) and some of the most remote regions of European Russia (first half of April) with unfavorable transport-geographical position (the Republics of Karelia and Karachay-Cherkessia and Nenets autonomous area).

The diffusion lag of the epidemic differed greatly from macro-region to macro-region – the rapid spread of infection was typical for the Urals (10 days), the Volga region (15 days), and the South of the Far East (15 days); in the North-West, East Siberia, European South and North-East it spread slower (20–27 days); protracted spread was registered in the European North (31 days) and the most protracted spread was registered in the West of Siberia (34 days) and the European Center of Russia (35 days). In European Russia, the duration of this lag was 49 days, in Asian Russia it lasted 34 days; the country's average was 51 days.

Thus, the coronavirus was the last to arrive in remote, mostly socio-economically backward regions with a deep-peripheral transport-geographic location.

Territorial differentiation by the number of cases. The first five regions in terms of the number of cases in August 2021 included Moscow city, St. Petersburg, Moscow, Nizhny Novgorod and Rostov regions. On August 2, 2020, 28.7% of the total number in Russia was registered in Moscow city; on January 16, 2021 this value was 25.0%; on August 1, 2021 this value was 24.0 %. As of August 2021, the shares of other regions in the total number of cases in the country was the following: St. Petersburg – 8.4%, Moscow region – 6.2%, Nizhny Novgorod region – 2.2%, Sverdlovsk region – 1.7%, Rostov region – 1.8%. In August 2021 the first five regions of Russia (combined) in terms of the number of coronavirus infected accounted for 42.6% of all cases.

The first 10 regions of the country (by their absolute number) accounted for 50.0% of cases in August 2021 i.e., half of all cases. In August 2021, the number of cases by regions decreased in the following order: Moscow city, St. Petersburg, Moscow, Nizhny Novgorod, Rostov, Sverdlovsk and Voronezh regions, Krasnoyarsk Territory, Irkutsk and Samara regions. As can be seen from this list, it mainly includes densely populated regions.

In August 2021, the first ten regions accounted for 49.99%, the second ten regions accounted for 11.00%, the third ten regions accounted for 9.23%, the fourth ten regions accounted for 8.27%, and in total, the first 40 regions accounted for 78.49% of cases (more than three quarters). The remaining 45 regions accounted for 22.5%. The last five regions with the minimum number of cases in August 2021 included the Chechen Republic (16.1 thousand people), Magadan region (9.5 thousand), Jewish autonomous region (5.8 thousand), Nenets (1.6 thousand) and Chukotka (1.2 thousand people) autonomous areas.

Thus, a high concentration of the number of cases was registered in the main urbanized areas of the country (50% in the first ten regions and 78% in the first forty regions), and the ratio of cases to the population in them is approximately 2:1.

Table 3. The number of cases and the incidence rate of COVID-2019 by regions of Russia from August 2, 2020 to August 1, 2021

Regions are sorted by incidence in descending order as of August 1, 2021

Region (oblast'), territory (krai), republic, autonomous area, federal city	The number of cases of infection (cumulative) as			Number of cases per 1 million people (incidence (sickness) rate)		Increase in the number of cases from January 16, 2021 to August 1, 2021,
	2.08.2020	16.01.2021	1.08.2021	16.01.2021	1.08.2021	
Russia	845,443	3,544,623	6,288,677	24,250	42,854	1.77
First 5 regions	383,333	1,499,885	2,677,290	45,157	80,606	1.78
First 10 regions	451,758	1,657,883	3,143,800	37,990	72,039	1.90
Moscow city	242,713	887,636	1,508,610	70,014	118,859	1.70
St. Petersburg	31,785	294,161	530,637	54,633	98,394	1.80
Republic of Kalmykia	2,659	16,245	24,932	60,170	91,988	1.53
Republic of Karelia	2,357	31,983	55,988	52,511	91,092	1.75
Altai republic	1,606	14,660	19,489	66,349	88,530	1.33
Murmansk region	10,507	39,989	62,122	54,565	83,778	1.55
Yamalo-Nenets autonomous area	11,235	34,290	43,757	62,686	80,434	1.28
Pskov region	3,797	26,941	43,758	43,436	69,896	1.62
Magadan region	1,357	7,489	9,525	53,865	67,939	1.27
Arkhangelsk region	8,842	47,446	74,156	43,823	67,891	1.56
Republic of Komi	5,396	33,969	55,454	41,752	67,613	1.63
Republic of Tuva	6,159	15,109	21,501	45,734	65,674	1.42
Novgorod	3,791	21,462	36,635	36,228	61,450	1.71
Khakass Republic	2,876	19,160	30,470	36,013	57,040	1.59
Sakhalin region	2,685	17,953	27,536	36,969	56,374	1.53
Orel region	5,707	24,165	40,254	33,345	54,866	1.67
Kamchatka territory	3,401	11,286	16,834	36,212	53,879	1.49
Ulyanovsk region	9,307	40,351	65,894	33,120	53,586	1.63
Trans-Baikal territory	4,106	30,970	56,590	29,398	53,404	1.83
Buryat Republic	4,159	28,162	52,572	28,578	53,313	1.87
Moscow region	63,755	176,026	386,895	22,835	50,327	2.20
Khabarovsk territory	7,759	40,096	65,773	30,816	50,006	1.69
Karachay-Cherkess republic	4,465	16,457	22,445	35,364	48,199	1.36
Vologda region	2,461	28,376	54,981	24,652	47,368	1.94
Sevastopol	352	8,224	20,960	16,126	46,699	2.55
Sakha-Yakut Republic	5,899	28,557	44,721	29,081	46,099	1.57
Bryansk region	7,430	26,264	54,362	22,207	45,584	2.07
Voronezh region	11,330	52,453	104,503	22,750	44,974	1.99
Smolensk region	5,705	19,611	41,666	21,290	44,575	2.12

Nizhny Novgorod region	24,097	77,255	141,093	24,320	44,039	1.83
Astrakhan region	4,657	21,770	43,676	21,818	43,417	2.01
Penza region	6,594	29,314	56,438	22,708	43,253	1.93
Kostroma region	2,261	16,180	27,318	25,747	43,130	1.69
Tver' region	4,655	25,910	53,898	20,801	42,764	2.08
Kaliningrad region	2,917	21,080	43,265	20,695	42,741	2.05
Kursk region	6,270	23,587	46,641	21,511	42,283	1.98
Ivanovo region	6,479	24,156	41,508	24,473	41,625	1.72
Kaluga region	7,260	23,638	41,287	23,615	41,284	1.75
Kirov region	4,888	29,329	50,426	23,460	39,940	1.72
Yaroslavl' region	6,112	25,320	49,935	20,396	39,846	1.97
Khanty-Mansi autonomous area	16,671	44,580	65,543	26,415	39,152	1.47
Tambov region	6,047	20,203	37,778	20,316	37,517	1.87
Jewish autonomous region	538	3,969	5,774	25,361	36,456	1.45
Nenets autonomous area	275	837	1,590	18,856	36,046	1.90
Irkutsk region	13,711	44,745	85,831	18,840	35,900	1.92
Republic of Adygea	2,803	12,211	16,351	26,364	35,281	1.34
Amur region	2,801	17,852	27,843	22,833	35,214	1.56
Lipetsk region	4,578	18,648	39,971	16,529	35,078	2.14
Republic of Ingushetia	3,729	13,247	17,692	25,694	34,917	1.34
Tomsk region	4,261	26,617	37,301	24,868	34,568	1.40
Tula region	8,379	26,104	47,546	18,014	32,432	1.82
Omsk region	6,990	34,110	61,623	17,918	31,986	1.81
Vladimir region	5,635	21,192	43,435	15,790	31,972	2.05
Krasnoyarsk territory	13,422	51,631	91,462	18,079	31,892	1.77
Ryazan region	6,352	20,221	35,292	18,412	31,825	1.75
Republic of Crimea	1,241	29,198	60,204	15,355	31,487	2.06
Kurgan region	2,303	13,708	25,899	16,746	31,319	1.89
Kabardino-Balkar Republic	6,008	17,398	27,092	20,016	31,206	1.56
Tyumen region	6,019	25,903	46,842	16,783	30,463	1.81
Saratov region	9,597	39,449	73,330	16,471	30,279	1.86
Republic of Mordovia	4,553	14,847	23,934	19,060	30,264	1.61
Leningrad region	5,955	27,356	56,327	14,453	30,019	2.06
Orenburg region	7,131	31,523	56,617	16,225	28,942	1.80
Primorsky territory	7,019	33,014	54,821	17,581	28,925	1.66
Belgorod region	6,042	24,769	44,732	16,071	28,905	1.81
Volgograd region	9,328	39,607	71,565	16,006	28,721	1.81

Perm Territory	6,018	35,404	73,526	13,726	28,287	2.08
Republic of North Ossetia	4,568	13,343	18,821	19,251	27,000	1.41
Altay Territory	9,326	36,150	62,365	15,742	26,916	1.73
Republic of Udmurtia	2,398	22,877	40,057	15,319	26,687	1.75
Rostov region	13,205	57,921	110,055	13,852	26,233	1.90
Sverdlovsk region	20,983	64,807	107,941	15,106	25,039	1.67
Samara region	6,930	36,011	76,773	11,417	24,150	2.13
Chuvash Republic	6,811	17,955	29,364	14,865	24,112	1.64
Republic of Mari El	3,800	9,980	16,142	14,778	23,770	1.62
Stavropol territory	8,449	38,949	64,912	13,946	23,158	1.67
Chukotka autonomous area	154	580	1,173	11,711	23,124	2.02
Chelyabinsk region	11,416	39,447	73,846	11,458	21,300	1.87
Novosibirsk region	9,548	30,181	52,919	10,834	18,911	1.75
Kemerovo region	3,702	27,704	46,069	10,520	17,334	1.66
Republic of Dagestan	9,350	25,996	41,917	8,297	13,472	1.61
Republic of Bashkortostan	6,815	21,735	48,509	5,415	12,014	2.23
Chechen Republic	2,082	10,110	16,092	6,749	10,897	1.59
Krasnodar territory	8,472	30,769	59,314	5,413	10,447	1.93
Republic of Tatarstan	5,664	14,735	23,982	3,784	6,145	1.63

Compiled by the author based on materials from sites:
https: //stopkoronavirus.rf – Coronavirus COVID-19: Official information. Some demographers argue that the data provided on this website underestimates the number of actual cases, since those infected are diagnosed with other diseases than coronavirus.

Table 3 shows that the number of cases of COVID-2019 and the incidence rate (number of cases per 1 million inhabitants) increased sharply during 2021 compared to 2020. In general, the number of cases in Russia during January-July 2021 turned out to be 1.8 times more than for the entire 2020, despite the fact that 2021 is not over yet. At the same time, in a significant number of regions it grew more than the national average (there are 38 of them, including more than 2 times in Sevastopol (2.6 times), Republic of Bashkortostan (2.2), Moscow region (2.2), Lipetsk, Smolensk, Samara regions, Perm territory, Bryansk region, Republic of Crimea, Leningrad and Vladimir regions, Chukotka autonomous area), and in most others (there are 41 of them), on the contrary, it is less than the national average, and in some of them it is very small (Magadan region and Yamalo-Nenets autonomous area) – less than 1.3 times. This growth is due to the continuation of the pandemic, which covers more and more cohorts of the population.

Territorial differentiation of the number of cases by socio-economic macro-regions. If we consider the distribution of the number of cases in August 2021 by large socio-economic macro-regions, then within each of them there are spatial disparities (see Fig. 2).

Thus, in the macro-region European Center, the number of cases reached 2.840 thousand, i.e. 45% of all in the country. The share of the Moscow area (Moscow city + Moscow region) was 66.7% of all cases in this macro-region.

The *Kaliningrad* region was distinguished by a rapid increase in the number of cases – in January 2021 (22 thousand) it ranked 57th among the regions of Russia, but by August 2021 it had moved up to 50th place (43 thousand people).

In the *North-West* macro-region, the number of cases was 667 thousand, i.e. almost 11% of the total number in the country. The share of St. Petersburg was 79.5% of all cases in this macro-region (in August 2021 there were 531 thousand infected).

In the macro-region *European North*, the number of cases was 382 thousand, i.e. 6% of the total number in the country. The region was characterized by an even spread (due to shallow polycentricity), and the Arkhangelsk and Murmansk regions (74 and 62 thousand infected, respectively) accounted for 35.7% of all cases in this macro-region.

In the *Volga macro-region*, the number of cases was 285 thousand, i.e. 4.5% of the total number in the country. The region was characterized by an even spread due to polycentricity with the highest indicators in the centers. These include the Samara (77 thousand infected), Saratov (73 thousand), and Ulyanovsk (66 thousand) regions; these three regions together accounted for 75.7% of all cases in this macro-region.

In the macro-region *European South*, the number of cases on August 1, 2021 was 616 thousand, i.e. 10% of the total number in the country. Here, the highest incidence

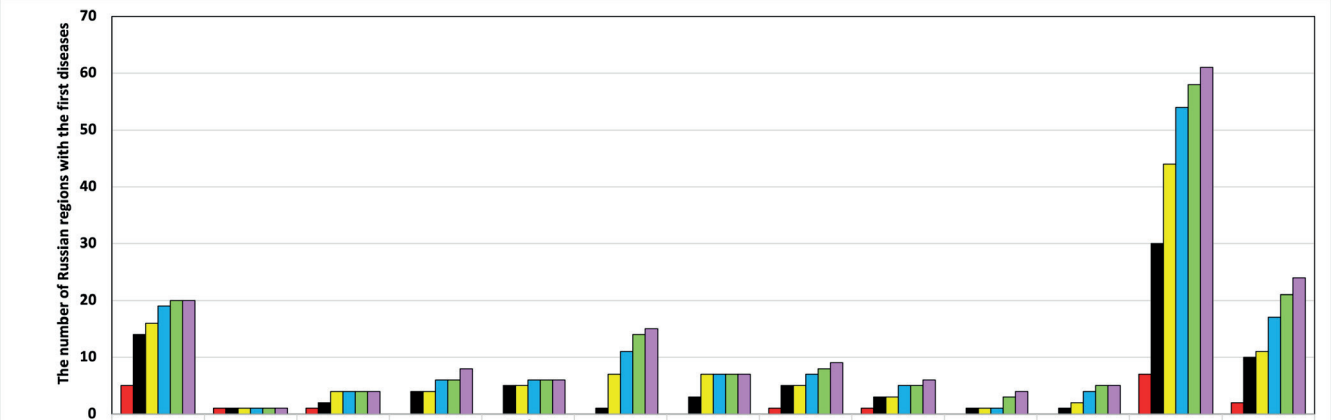

	European Center	Kaliningrad	North-West	European North	Volga macro-region	European South	Urals	West Siberia	East Siberia	North-East	South of the Far East	European Russia	Asian Russia
10 March	5	1	1					1	1			7	2
20 March	14	1	2	4	5	1	3	5	3	1	1	30	10
25 March	16	1	4	4	5	7	7	5	3	1	2	44	11
30 March	19	1	4	6	6	11	7	7	5	1	4	54	17
5 April	20	1	4	6	6	14	7	8	5	3	5	58	21
17 April	20	1	4	8	6	15	7	9	6	4	5	61	24

Fig. 2. Cumulative increase in the number of regions with the first cases by macro-regions of Russia in March-April 2020

rate was registered in the Rostov region (110 thousand people). But this macro-region is polycentric, and there are secondary foci of concentration of the disease – the Volgograd region (72 thousand infected), Stavropol territory (65 thousand people) and Crimea (60 thousand people). These four foci accounted for 49.8% of all cases in this macro-region, i.e. the concentration is high, but not as high as in the European Center and North-West.

In the *Urals* macro-region, the number of cases was 426 thousand, i.e. 7% of the total number in the country. This region is traditionally characterized by tri-centricity, although Yekaterinburg and Sverdlovsk region in general (108 thousand cases) still dominates, but two other centers are also important – the Chelyabinsk region (74 thousand infected) and the Perm territory (74 thousand). These three regions accounted for 60% of all cases in this macro-region.

In the *Western Siberia* macro-region, the number of cases was 436 thousand, i.e. 7% of the total number in the country. Although nominally the center of the macro-region is Novosibirsk (its zone of influence includes the Tomsk and Kemerovo regions and Altai territory), it does not dominate so much in comparison, for example, with Tyumen and Omsk regions. The main foci of morbidity here are the Khanty-Mansi autonomous area (66 thousand cases), the Altai territory (62 thousand cases), and the Omsk region (62 thousand cases); altogether they accounted for 43% of all cases in this macro-region.

In the *East Siberia* macro-region, the number of cases was 338 thousand, i.e. 5% of the total number in the country. It is polycentric, and there is no single major center. The main foci of morbidity are the Krasnoyarsk territory (91 thousand cases) and the Irkutsk region (86 thousand cases); they accounted for 52% of all cases in this macro-region.

In the *North-East* macro-region, the number of cases was 72 thousand, i.e. 1% of their total number in the country. It is characterized by a system with a very weak and very diffuse polycentricity. The main focus of morbidity here is the Sakha-Yakut Republic (45 thousand cases; average level), i.e. it accounts for 62% of all cases in this macro-region.

In the macro-region *South of the Far East*, the number of cases was 182 thousand, i.e. 3% of the total number in the country. It is characterized by bi-centricity. The main foci of morbidity here are the Khabarovsk (66 thousand infected) and Primorsky (55 thousand) territories; they accounted for 66% of all cases in the macro-region.

In macro-regions with a pronounced strong monocentricity (European Center, North-West, Kaliningrad), the share of the main central area of the region is high; in macro-regions with strong polycentricity (European South, Volga region, Urals, and Western Siberia), the shares of large numerous centers are moderate; in macro-regions with fractional polycentricity (Eastern Siberia and the South of the Far East), the number of cases is concentrated in two main foci; in macro-regions with a very weak, diffuse polycentricity (European North and North-East), the shares of the main foci of morbidity are insignificant.

Territorial differentiation by the incidence (morbidity) rate

The average incidence rate (number of cases per 1 million inhabitants) in Russia in August 2020 was 6 thousand; in January 2021 – it was 24 thousand; in August 2021 – it was 43 thousand people per 1 million inhabitants. That is, due to the expansion of the pandemic, it increased by 7.4 times (the number of cases also increased by 7.4 times). For comparison, in European countries, on August 1, 2021, it averaged 69 thousand per 1 million inhabitants. This means that in Russia the incidence rate, according to official data from Rospotrebnadzor, is 38% lower than in European countries.

A high incidence rate (number of cases per 1 million inhabitants; see Table 4) in August 2021 was in Moscow and St. Petersburg, regions of the European North (republics of Karelia and Komi, Murmansk and Arkhangelsk regions), North-West (especially the Pskov region), the north of Western Siberia (Yamalo-Nenets autonomous area), the North-East and some republics of the south of Siberia (that is, where the share of the urban population is greater, and it is concentrated in several urban settlements; or the share of ethnic rural population), in the Republic of Kalmykia (92 thousand). A moderate incidence rate (thousand cases per 1 million inhabitants in August 2021) was characteristic of the most economically backward Republic of Altai (89 thousand); –a medium incidence rate was registered in the Republic of Tuva (66 thousand) and the Magadan region (68 thousand).

A low incidence rate in August 2021 was observed in the south of the Far East, East Siberia, Kaliningrad region, West of Siberia, the Urals, the European South (where the share of the rural population is relatively high, but there are exceptions, for example, the republics of Karachay-Cherkessia, Adygea, and Ingushetia), and in the Volga macro-region.

The minimum incidence per 1 million inhabitants on August 1, 2021 (a very low incidence rate) was registered in the republics of Dagestan (13 thousand people), Bashkortostan (12), Chechen Republic (11), Krasnodar territory (10), and the Republic of Tatarstan (6 thousand). Such extremely low values, for example, in the Krasnodar territory, republics of Bashkortostan and Tatarstan, where the share of the rural population is relatively high, suggest that the initial data are somewhat unreliable, since there are many large cities. The same doubts arise about the Kemerovo, Chelyabinsk and a number of other regions with very low incidence rates. Therefore the incidence rate here, apparently, is underestimated when compared with the values in the neighboring regions. For example, in the Republic of Ingushetia there are 35 thousand cases per 1 million inhabitants, and in the neighboring Chechen Republic was registered 11 thousand cases; in Adygea was registered 35 thousand cases, but in the surrounding Krasnodar territory – 10 thousand cases; in the Ulyanovsk region – was registered 54 thousand cases, but in neighboring Tatarstan – 6 thousand cases.

When compared with European countries, the overall incidence rate in Russian regions is much lower (see Fig. 5 and 6): in 51 out of 85 regions incidence rate is low (20–45 cases per 1 million inhabitants) and in 20 regions incidence rate is medium (45–70 cases).

Territorial differentiation of the incidence rate by socio-economic macro-regions (see Figures 3 and 4). In the macro-region *European Center*, Moscow city was registered a high incidence rate (119 thousand people per 1 million inhabitants); –four regions were registered a low medium incidence rate (20–45 thousand), and low rate – 15 regions (most).

The *Kaliningrad* region is characterized by medium incidence rate (43 thousand cases per 1 million inhabitants).

In the *North-West* macro-region, only St. Petersburg (98 thousand cases) had a high incidence rate, the medium rate was registered in Pskov (70 thousand cases) and Novgorod (62 thousand cases) regions and the lowest rate was registered in the Leningrad region (30 thousand cases). This macro-region stands out among the rest with an increased incidence rate.

The same is true for the *European North* macro-region. Only the Republic of Karelia was registered a high incidence rate (91 thousand cases per 1 million inhabitants); moderate incidence rate was registered only in the Murmansk region (84 thousand cases); the medium incidence rate was registered in the Arkhangelsk region (68 thousand cases), the Komi Republic (68 thousand cases) and the Vologda region (47 thousand cases); the low incidence rate was registered in the remaining three regions.

In the *Volga macro-region*, the medium incidence rate was only in the Ulyanovsk region (54 thousand cases per 1 million inhabitants). Most of its regions (four) had low and very low incidence rates. Minimal rate among all Russian regions was registered in the Republic of– Tatarstan (6 thousand cases).

In the *European South* macro-region, only one region – the Republic of Kalmykia – was registered a high incidence rate (92 thousand cases per 1 million inhabitants). There were no regions with a moderate level at all. The medium level was noted in two regions; low level was noted – in eight regions; very low level was noted – in the Republic of Dagestan (14 thousand cases) and in the Chechen Republic (11 thousand cases) as well as in the Krasnodar territory (10 thousand cases).

In the *Urals*, there were no regions with high, moderate, and medium incidence rates. Six regions had a low level (20–45 thousand) and only the Republic of Bashkortostan had a very low level (12 thousand cases per 1 million inhabitants).

In the macro-region of *West Siberia*, a moderate incidence rate was in the Altai Republic (89 thousand people per 1 million inhabitants) and the Yamalo-Nenets autonomous area (80 thousand). There were no regions with a medium level. Five regions had a low incidence rate; two regions had a very low incidence rate.

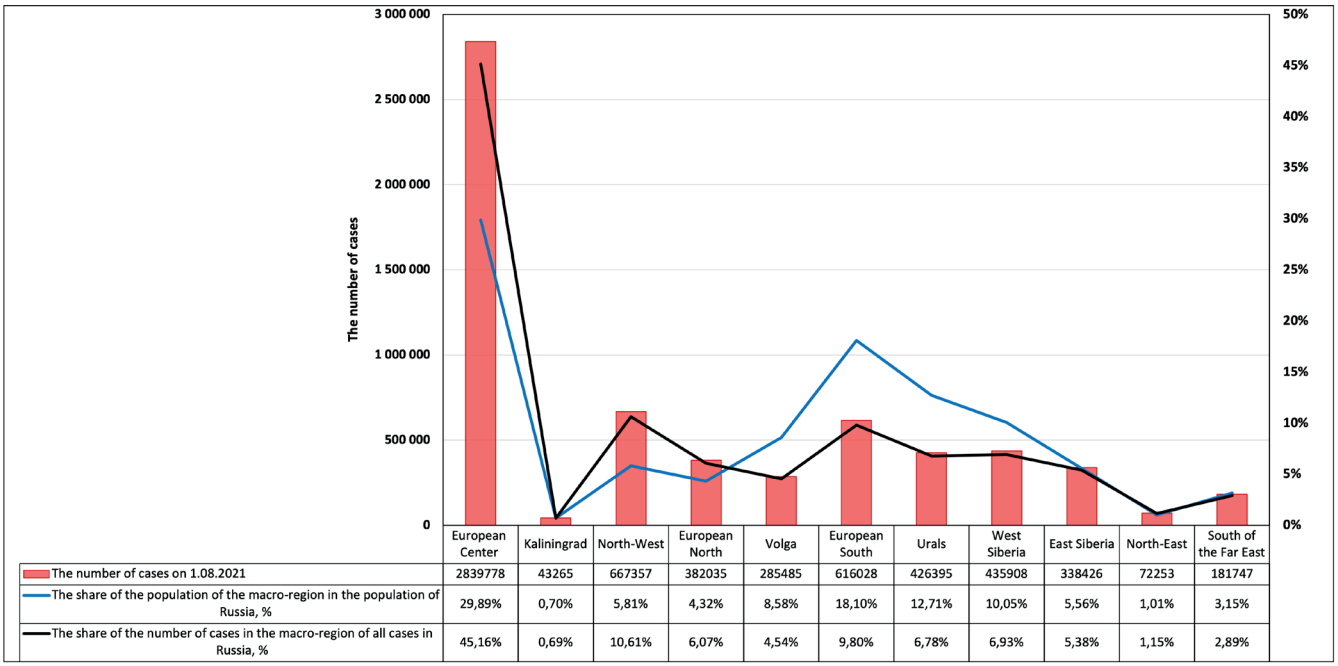

	European Center	Kaliningrad	North-West	European North	Volga	European South	Urals	West Siberia	East Siberia	North-East	South of the Far East
The number of cases on 1.08.2021	2839778	43265	667357	382035	285485	616028	426395	435908	338426	72253	181747
The share of the population of the macro-region in the population of Russia, %	29,89%	0,70%	5,81%	4,32%	8,58%	18,10%	12,71%	10,05%	5,56%	1,01%	3,15%
The share of the number of cases in the macro-region of all cases in Russia, %	45,16%	0,69%	10,61%	6,07%	4,54%	9,80%	6,78%	6,93%	5,38%	1,15%	2,89%

Fig. 3. Distribution of the number of SARS-CoV-2 coronavirus cases and its shares by Russian macro-regions (%) as of August 1, 2021

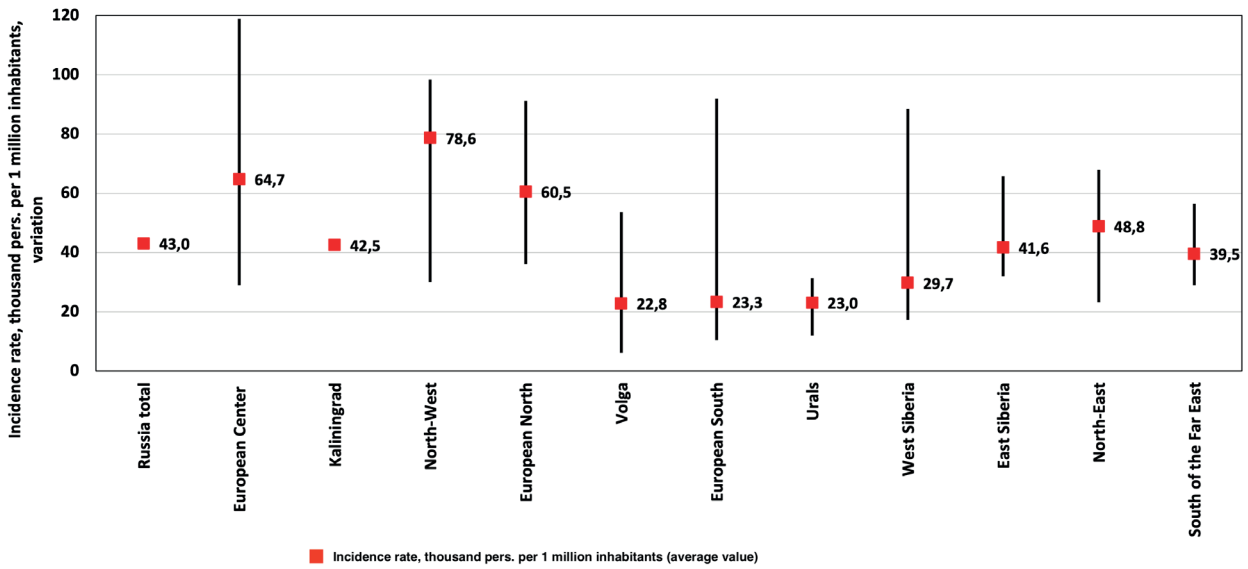

Fig. 4. Distribution of the morbidity rate of SARS-CoV-2 coronavirus by socio-economic macro-regions of Russia as of August 1, 2021

Tuva (66 thousand) and Khakass (57 thousand cases) republics, Trans-Baikal territory (53 thousand) and Buryat Republic (53 thousand cases) had a medium incidence rate (45–70 thousand cases per 1 million inhabitants) in the *East Siberia* macro-region; low incidence rate was registered in the Irkutsk region (36 thousand cases) and the Krasnoyarsk territory (32 thousand cases).

The *North-East* macro-region included three regions with a medium incidence rate and one (Chukotka autonomous area) with a low (23 thousand cases) incidence rate.

In the *South of the Far East*, the medium incidence rate was typical for the Sakhalin region (56 thousand) and Khabarovsk territory (50 thousand); in the other regions the incidence rate was low.

In the south of Siberia and the Far East, a low incidence rate is characteristic of the Krasnoyarsk and Primorsky territories, which are leading here in the absolute number of cases. This is due to the large population in these regions compared to other regions of these macro-regions.

Thus, there are very large geographical differences between Russian regions, both in the number of cases and in the incidence rate. They are characterized by a high concentration of cases in the largest urbanized areas.

DISCUSSION

With the application of theory of spatial diffusion (see Hägerstrand 1967; Smirnyagin and Tarkhov 2013), geographers in the 2000s studied the spatial distribution of influenza and epizootic epidemics (Haggett 2000; Cliff et al. 2004; Lawson 2006; Souris 2019).

With the spread of diseases, the features of three special forms (contact, hierarchical, mixed) are as follows. Contact (wave) diffusion of infection is characterized by an outbreak in one region (area) and then spread to neighboring regions and districts, so that the disease has the highest intensity at the place of origin and spreads with less intensity to neighboring territories. On the contrary, hierarchical spread is characterized by the onset of the disease in a certain place and its transfer to more distant areas and points associated with the initial place of its origin by hierarchical connections. The process of diffusion of the disease can also be mixed, when its wave and hierarchical spread are observed simultaneously.

If in the pre-aviation era epidemics spread linearly and hierarchically through land and water transport, then in the modern era, when air transport dominates, they spread hierarchically pointwise through airports.

From the point of view of the theory of spatial diffusion of innovations, the ***coronavirus spread at the first stages*** in an exclusively ***hierarchical way through*** the existing extensive ***air communication system*** – the largest and big cities, large urban agglomerations, to which direct flights from Italian air hubs were made, were the first to suffer. Of these, the coronavirus at later stages began to penetrate with the passengers through land transport to medium and small cities located in the zone of influence of the largest and large cities; last but not least, it penetrated into the countryside. At the ***later stages*** of its spread, it was characterized by a ***mixed form of diffusion*** dominated by a hierarchical form.

Carriers of coronavirus in the late stages of diffusion moved not so much by air as by land transport, except for remote and inaccessible regions, which were reached exclusively by air. The first cases were registered in people who arrived by air transport, which became the main means of spreading COVID-2019.

As a result of such a hierarchical spread of the epidemic, the regions affected first of all were the most economically advanced cities with the largest airports, then the virus spread to the regions with middle level of economic development, and to a lesser extent – the virus spread to the peripheral regions with a more disadvantageous transport-geographical position and the dominance of air transport against the background of weak development of the other modes of transport.

Empirically, our study[2] established the following gradations of the incidence rate (number of cases in thousand per 1 million inhabitants) as of August 1, 2021: very high values are considered from 140 to 200, high values are considered – from 90 to 140, moderate values are considered – from 70 to 90, medium values are considered – from 45 to 70, low values are considered – from 20 to 45, very low values are considered – less than 20. Comparison of the distribution of the number of Russian regions and European countries by the incidence rate is shown in Figures 5 and 6.

[2] including European countries

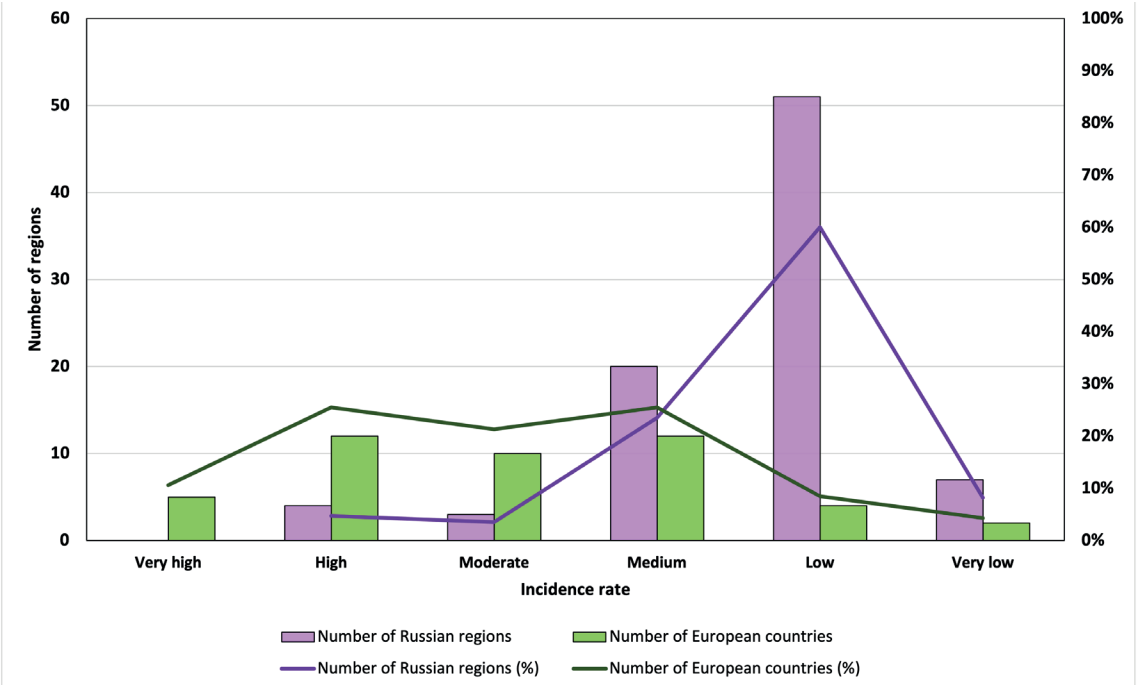

Fig. 5. Distribution of the number of Russian regions and European countries (and its shares in %) by the incidence rate of COVID-2019 as of August 1, 2021

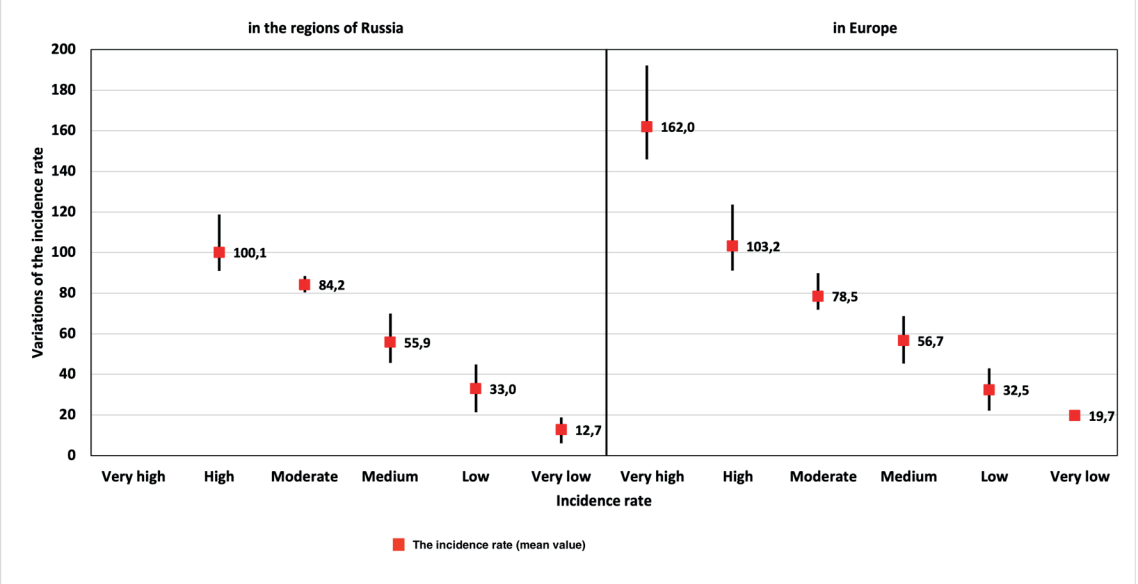

Fig. 6. The variation of the mean incidence rate in the regions of Russia and European countries as of August 1, 2021

The analysis of these Figures showed that most Russian regions have a low (60%) and medium (24%) incidence rate (71 regions out of 85; 74% overall), while in European countries the incidence rate is generally higher and more dispersed – in 26% of countries it is high; in 21% of countries it is moderate; in 26% of countries it is medium (73% overall). This distribution of shares across European countries and Russian regions (skewed distribution towards higher values in European countries and towards lower values in Russian regions) indicates both obvious geographical differences and partial unreliability of the initial data on the number of registered cases.

Attention is drawn to the average values of the incidence rate in Russian regions in comparison with European countries (6.1 thousand cases and 19.7 thousand cases per 1 million inhabitants). Therefore, such a comparison of the incidence rate makes it possible to judge the quality of the primary registration statistics, to determine the geographically obvious discrepancies in real terms. Given this circumstance, the initial statistics on the absolute number of diseases should be used very carefully, since for a number of regions and countries it may be underestimated.

CONCLUSIONS

The COVID-2019 pandemic spread in space extremely unevenly, covering first the most economically developed regions, and later semi-peripheral and peripheral regions. The spatial diffusion model of innovations is most suitable for explaining the spread of this disease. For this pandemic, the disease spread mostly hierarchically, that is, from the main focus (center), it penetrated into the centers of the 2nd and then the 3rd level, from where it already spread within the zones of their influence.

Air transport became the main source of the spread of the disease. Cities and agglomerations, where airports with a large share of international air passengers were located, that is, the largest cities, were the first to suffer.

The first infected arrived to Russia by air from China and Italy. In March, the virus was brought to Russia mainly by tourists returning from cities and ski centers in Northern

Italy. Further, from Moscow and St. Petersburg, where they originally arrived, they moved by air and by train to their places of residence, spreading the disease, first of all, to all the largest cities of the country. At the same time, the disease was transmitted by ground transport passengers in the zones of influence of these major cities. Those ill at the later stages of diffusion moved not so much by air as by land transport, but to remote and inaccessible regions they travelled exclusively by air. Thus, at the first stage of the infection spread, the main role was played by air traffic and flights from Moscow and St. Petersburg to the largest regional centers of the country; in the later ones, it was combined (air, rail and road transport).

The spread of coronavirus infection in Russian regions had a small peak during the first six days (early March), when the pandemic covered nine regions. The second, largest peak occurred on March 16–19, when 26 more regions were covered, and the third peak occurred on March 21–25, when another 17 regions were added to the list. Later, the number of new regions involved in the pandemic did not increase so quickly: on March 30 there were 71 regions, on April 5 there were 79 regions. The S-curve reached its saturation by April 17, when the first cases were registered in all 85 regions. Thus, the geographical lag of the spread of the epidemic in the Russian regions was 51 days (February 27 – April 17).

The coronavirus came to remote, mostly socio-economically more backward regions with a deep peripheral transport-geographical location the latest, and first of all to the regions with a favorable transport-geographical location and a high level of socio-economic development (especially in the largest urban areas and agglomeration). The main urbanized areas account for the most of the cases.

Most Russian regions have low and medium incidence rates – 60% and 23.5%, respectively – with some exceptions with a very low level. A very high incidence rate was not registered in any Russian region.

In the regions with a pronounced monocentricity, the share of the main central area is high; in regions with strong polycentricity, the share of large numerous centers is moderate; in regions with fractional polycentricity, the number of cases is concentrated in two main foci; in regions with very weak, diffuse polycentricity, the shares of the main foci of the disease are insignificant.

REFERENCES

Ascani A., Faggian A., Montresor S. (2020). The geography of COVID-19 and the structure of local economies: The case of Italy. Journal of Regional Science, December. DOI: 10.1111/jors.12510 Available at: https://www.ncbi.nlm.nih.gov/pmc/articles/PMC7753650/ [Accessed 18.09.2021]

Chen Y., Yajing Li Y., Feng S., Man X., Long Y. (2021). Gravitational scaling analysis on spatial diffusion of COVID-19 in Hubei Province, China. PLoS ONE, 16(6), e0252889, DOI: 10.1371/journal.pone.0252889

Cliff A., Haggett P., Smallman-Raynor M. (2004). World Atlas of Epidemic Diseases. Hodder Education Publishers.

Druzhinin A.G. (2020). Social-geographical metamorphosis in the mirror of a pandemic COVID-19. Vestnik ARGO, 9, 129–131. (in Russian with English summary)

Florida R. and Mellander C. (2020). The Geography of COVID-19 in Sweden. Working Paper Series in Economics and Institutions of Innovation, Royal Institute of Technology, CESIS (Centre of Excellence for Science and Innovation Studies), 487. Available at: https://swopec.hhs.se/cesisp/abs/cesisp0487.htm [Accessed 18.09.2021]

Geography of the COVID-19 Pandemic (2020). Tijdschrift voor economische en sociale geografie, 111(3), 201–583.

Gerasimenko T.I. and Gerasimenko A.S. (2020) Some geographical aspects of the coronavirus pandemic. Vestnik ARGO, 9,124–126. (in Russian with English summary)

Hägerstrand T. (1967). Innovation Diffusion as a Spatial Process. Chicago and London: University of Chicago Press.

Haggett P. (2000). The Geographical Structure of Epidemics. Oxford: Oxford University Press.

Kaganskiy V.L. (2020). Coronavirus pandemic. Anthroposphere testing. Vestnik ARGO, 9, 138–140. (in Russian with English summary)

Kolosov V.A. (2020). A New Field of Research in Social Geography: Taking the Time Without Haste. Vestnik ARGO, 9, 140–142. (in Russian with English summary)

Kuebart A. and Stabler M. (2020). Infectious Diseases as Socio-Spatial Processes: The COVID-19 Outbreak in Germany. Tijdschrift voor economische en sociale geografie, 111(3), 482–496, DOI: 10.1111/tesg.12429

Kuznetsova O.V. (2020). Economic relations between the center and regions in the context of the coronavirus. Vestnik ARGO, 9, 144–147. (in Russian with English summary)

Lawson A.B. (2006). Statistical Methods in Spatial Epidemiology. 2nd ed. New York: Wiley.

Makhrova A.G. and Nefedova T.G. (2021). Can the Covid-19 pandemic stimulate suburbanization in Central Russia? Vestnik Moskovskogo universiteta. Seria 5. Geografiya, 4, 104–115. (in Russian with English summary)

Malkhazova S.M. (2001). Medical geographic analysis of territory: mapping, evaluations, predictions. Moscow: Nauchnyi mir. (in Russian with English summary)

Panin A.N., Ryl'skiy I.A., Tikunov V.S. (2021). Spatial patterns of the spread of the COVID-19 pandemic in Russia and the world: cartographic analysis. Vestnik Moskovskogo universiteta. Seria 5. Geografiya, 1, 62–77. (in Russian with English summary)

Pelyasov A.N., Zamyatina N.Yu., Kotov E.A. (2021). The spread of the Covid-19 pandemic in the regions of Russia in 2020: models and reality. Ekonomika regiona, 17, 4, 1080–1096. (in Russian with English summary)

Pogorelov A.R. (2020). Recent problems of human-geographical discourse in medical geography. Vestnik ARGO, 9, 113–123. (in Russian with English summary)

Ramírez-Aldana R., Gomez-Verjan J. C., Yaxmehen Bello-Chavolla O. (2020). Spatial analysis of COVID-19 spread in Iran: Insights into geographical and structural transmission determinants at a province level. PLOS Neglected Tropical Diseases, 14(11): e0008875. DOI: 10.1371/journal.pntd.0008875. Available at: https://pubmed.ncbi.nlm.nih.gov/33206644/ [Accessed 18.09.2021]

Rodoman B.B. (2020). Territorial estates and coronavirus. Vestnik ARGO, 9, 150–152. (in Russian with English summary)

Semenova Z.A. and Chistobayev A.I. (2015). Medical geography and public health: evolution of knowledge. St.-Petersburg: Evropeyskiy Dom. (in Russian with English summary)

Shaw S.-L. and Sui D. (2021). Mapping COVID-19 in Space and Time: Understanding the Spatial and Temporal Dynamics of a Global Pandemic. eBook: https://link.springer.com/book/10.1007%2F978-3-030-72808-3

Shuper V.A. (2020). The idea of progress after the coronavirus pandemic. Vestnik ARGO, 9, 155–157. (in Russian with English summary)

Sigler T., Mahmuda S., Kimpton A., Loginova J., Wohland P., Charles-Edwards E., Corcoran J. (2021). The socio-spatial determinants of COVID-19 diffusion: the impact of globalisation, settlement characteristics and population. Globalization and Health, 17, Article number 56. Available at: https://globalizationandhealth.biomedcentral.com/articles/10.1186/s12992-021-00707-2 [Accessed 8 Sept. 2021].

Smirnyagin L.V. and Tarkhov S.A. (2013). Innovation Diffusion In Social-economic geography: Terms and concepts. Reference dictionary. Smolensk: Oykumena, 94–95. (in Russian with English summary)

Souris M. (2019). Epidemiology and Geography: Principles, Methods, and Tools of Spatial Analysis. New York: Wiley. DOI:10.1002/9781119528203

Zemtsov S.P. and Baburin V.L. (2020a). COVID-19: spatial dynamics and factors of distribution in the regions of Russia. Izvestiya Rossiyskoy Akademii Nauk, Seriya Geograficheskaya, 84 (4), 485–505. (in Russian with English summary)

Zemtsov S.P. and Baburin V.L. (2020b). Coronavirus in Russia: scale and consequences. Vestnik ARGO, 9,133–135. (in Russian with English summary)

Zubarevich N.V. and Safronov S.G. (2020). Russian regions in the acute phase of the coronavirus crisis: differences from the previous economic crises of the 2000s. Regional'nye issledovaniya, 2, 4–17. (in Russian with English summary)

Zyryanov A.I. (2020). Geographical features of the spread of coronavirus. Vestnik ARGO, 9, 135–137. (in Russian with English summary)

RESEARCH PAPER

THE PALAEOENVIRONMENT OF THE CENTRAL RUSSIAN PLAIN DURING THE END OF THE VALDAI GLACIATION BASED ON SMALL MAMMAL DATA FROM THE LATE PALAEOLITHIC SITE BYKI 7 (SEIM R. BASIN)

Anastasia K. Markova [1*], Andrey Yu. Puzachenko[1]

[1]Institute of Geography, Russian Academy of Science, Moscow, 119017, Russian Federation

***Corresponding author:** amarkova@list.ru

Received: November 7th, 2021 / Accepted: February 15th, 2022 / Published: March 31st, 2022

https://DOI-10.24057/2071-9388-2021-124

ABSTRACT. The analysis of the Late Pleistocene small mammals' faunas from the three cultural layers of the Late Palaeolithic site Byki 7 (the Seim River basin) consist of a combination of steppe and tundra species. Steppe species definitely prevail and include Ochotona pusilla, Marmota bobac, Spermophilus sp., Spalax microphthalmus, Ellobius talpinus, Lagurus lagurus and Lasiopodomys (Stenocranius) gregalis. Tundra species (collared lemming and Siberian lemming) are only represented by a small amount of remains. The lack of forest dwellers in the Byki 7 small mammal assemblage indicates of the absence of a continuous forest zone on the Central Russian Plain during the end of the Valdai glaciation. The Eurasian geographical distribution of the Rodentia and Lagomorpha species represented in the Byki–7 assemblages, have been reconstructed for the period of deposition of the site. Radiocarbon dates indicate that the multilayer Late Palaeolithic Byki 7 site correlates with the second part of the Valdai Glaciation Maximum cooling (LGM) (22–17 ka BP). Based on the small mammal data the former palaeoenvironmental conditions of the non-analogue periglacial tundra-steppe are reconstructed.

KEYWORDS: Late Palaeolithic; small mammals; species composition; palaeoenvironment reconstruction; Seim River basin; periglacial tundra-steppe

CITATION: Markova A. K., Puzachenko A. Yu. (2021). The Palaeoenvironment Of the Central Russian Plain During the End Of the Valdai Glaciation Based on Small Mammal Data From the Late Palaeolithic Site Byki 7 (Seim R. Basin). Vol.15, № 1. Geography, Environment, Sustainability, p 102-111 https://DOI-10.24057/2071-9388-2021-124

ACKNOWLEDGEMENTS: We express our gratitude to N.B. Akhmetgaleeva, the archaeologist, who investigated the Palaeolithic site for many years, for the opportunity to study the small mammalian assemblages of the Byki 7 site. We highly appreciated the useful comments of the reviewers of an earlier draft of this paper. We are very grateful to Prof. Thijs van Kolfschoten (Leiden University, the Netherlands) for his important advices and great help with edition and correction of English text. The paper was written within the framework of the theme of the Institute of Geography, Russian Academy of Sciences no. 0148-2019-0007 (AAAA-A19-119021990093-8) «Assessment of Physical-Geographical, Hydrological and Biotic Environmental Changes and their Consequences for Establishing the Basis of Sustainable Nature management».

Conflict of interests: The authors reported no potential conflict of interest.

INTRODUCTION

The complex investigation of the archaeological sites, including the Late Palaeolithic ones, are relevant both for the discovering of the features of archaeological tools and cultures, as well as for reconstructing the environments during the human occupation based on palaeontological materials. There are many Late Palaeolithic sites discovered on the Russian Plain. The studies of these sites include archaeological researches, the studies of their geological and geomorphologic position of the site, and also paleontological investigations of remains of large and small mammals, mollusks and plants. These complex researches permit to reconstruct the past environments surrounding ancient humans. Such comprehensive studies have been carried out on the Late Palaeolithic site Byki 7.

The Byki 7 site has been discovered in 2000 by archaeologist N.B. Akhmetgaleeva. The site is a part of the "Byki Sites complex" that includes the following sites: Byki 1, Byki 2, Byki 3, Peny (Byki 4), Byki 5, Byki 6, and Byki 8 (Fig. 1). The sites of this complex have been studied by a several archaeologists and geographers (Grigorieva and Fillipov 1978; Chubur 2001; Akhmetgaleeva et al. 2010; Akhmetgaleeva 2015; Akhmetgaleeva and Burova 2021).

A specific Upper Palaeolithic culture with triangular microlites (crystalloids) has been detected in the 4 upper cultural layers of Byki 7. The lowermost II cultural layer includes the gravettoid industry. Archaeological data show that humans seasonally inhabited the Byki 7 site, as well as other sites of the Byki complex. Unique zoomorphic artefacts produced from mammoth and other animals' bones have been found at the site (Akhmetgaleeva 2015). Archaeological studies at the site are, for many years, conducted under the leadership of N.B. Akhmetgaleeva (Akhmetgaleeva 2015; Akhmetgaleeva and Burova, 2021). The geological deposits have been studied by Yu.N.

Gribchenko and E.V. Voskresenskaya (Akhmetgaleeva et al., 2020), and by A.V. Panin and colleagues in 2019-2020 yrs. Large mammals' remains were studied by N.D. Burova (Akhmetgaleeva and Burova 2021). Small mammal remains have been handed over for identification in 2019 by the archaeologist N.B. Akhmetgaleeva to A.K. Markova.

MATERIALS AND METHODS

General description of the site Byki 7

Byki 7 site is located on the south-western slope of the Central Russian Upland (51°38′N, 35°30′E, Fig. 1a), on the high dune formed on an ancient terrace, which is not younger than the Middle Pleistocene, on the River Seim left bank (the Desna R. basin), Kursk Region. The significant distance from the site to the riverbed indicates that the water resources were not the main factor to Palaeolithic people in choosing a place to this site (Akhmetgaleeva 2015, A.V. Panin per. comm.) (Fig.1b). The site location is within the boundaries of the modern forest-steppe zone with the temperate continental climate. The mean annual temperature in the region ranges between +5.9C (in the north) and +7.1C (in the southwest). The annual precipitation is 627 mm. The main vegetation type is a meadow and forbs steppes with the patches of oaks.

The archaeological finds excavated at most of the Byki sites belong to the so-called "Bykovian" archaeological culture. A large number non-calibrated radiocarbon dates fall within 25,000-14,300 BP and most of calibrated dates of the Byki 7 site fall within the 22000-17000 cal BP interval (Akhmetgaleeva 2015) (Table 1). It is important to note that the Byki 2, Byki 3, Byki 6, and Byki 8 assemblage consist of surface finds.

There are more than 60 mammal species in the Kursk region nowadays. The modern faunal assemblage includes simultaneously forest (elk, roe deer, wild boar, red squirrel, Eurasian beaver, yellow-necked mouse, forest dormouse, bank vole, etc.) and meadow and steppe species (steppe polecat, brown hare, great jerboa, bobac-marmot, greater mole-rat, European hamster, grey hamster, steppe lemming, etc.).

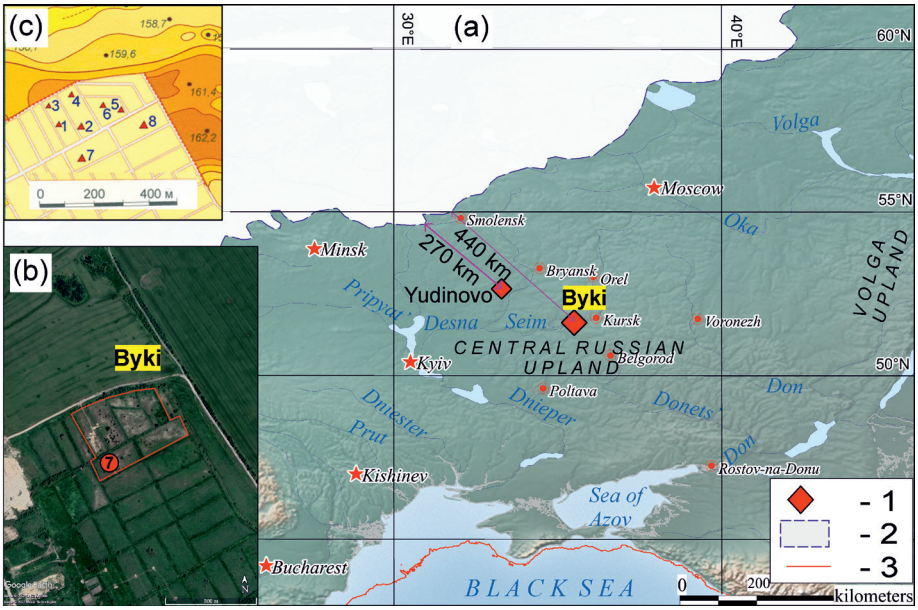

Fig. 1. a – The geographical position of the Upper Palaeolithic Byki sites. Legend to Fig.1a: 1 – Upper Palaeolithic sites Byki 7 and Yudinovo, 2 – the Scandinavian Ice Sheet during the last glaciation (after Svendsen et al. 2004), 3 – isobate 125 m indicated the coast line. The minimum distances between the Byki and Yudinovo (52°40′N, 33°17′E) sites and the edge of Scandinavian Ice Sheet shown on the map (after J. Ehlers and P. Gibbard (2008)), b – Byki sites complex and the location of Byki 7 site; c – the plan of the Byki sites complex with the position of the Byki 1 – 8 sites (after N.B. Akhmetgaleeva and N.D. Burova (2021))

Table 1. Radiocarbon Dates of Byki 7 site. Dates calibrated with OxCal 4.4.0 software and the calibrated curve IntCal20 was used (after (Akhmetgaleeva and Burova 2021)

Layer	Lab code	Material	Conventional ^{14}C date, BP	Calibrated date, ca BP
Layer Ia	GIN–13082	fragments of bones of mammals and birds	14,300 ± 370	17,430 ± 500
	GIN–11755	broken bones of reindeer and horse	16,000 ± 130	19,300 ± 160
	IGAN–7582	fragments of bones of hare, fox, reindeer, horse and birds	17,250 ± 45	20,820 ± 80
	LE–7794	hare and fox bones	17,320 ± 640	21,050 ± 800
	IGAN–7581	fragments of bones of hare, fox, reindeer, horse and birds	17,350 ± 45	20,920 ± 60
	IGAN–7583	- // -	17,440 ± 40	21,020 ± 90
Layer Ib	GIN–13083	fragments of bones of mammals and birds	14,600 ± 250	17,800 ± 320
	GIN–11754	- // -	16,600 ±140	20,050 ± 200
	LE–11703	horse scapula	17600 ± 300	21,360 ± 400

Layer I	IGAN–7585	?	13,250 ± 35	15,910 ± 70
	GIN–13084	broken bones of reindeer and horse	15,600 ± 400	18,960 ± 450
	IGAN–7584	?	16,570 ± 45	20,020 ± 80
	IGAN–7590	broken bones of reindeer and horse	16,800 ± 40	20,320 ± 70
Layer II	IGAN-7576	?	18,190 ± 45	22,150 ± 70

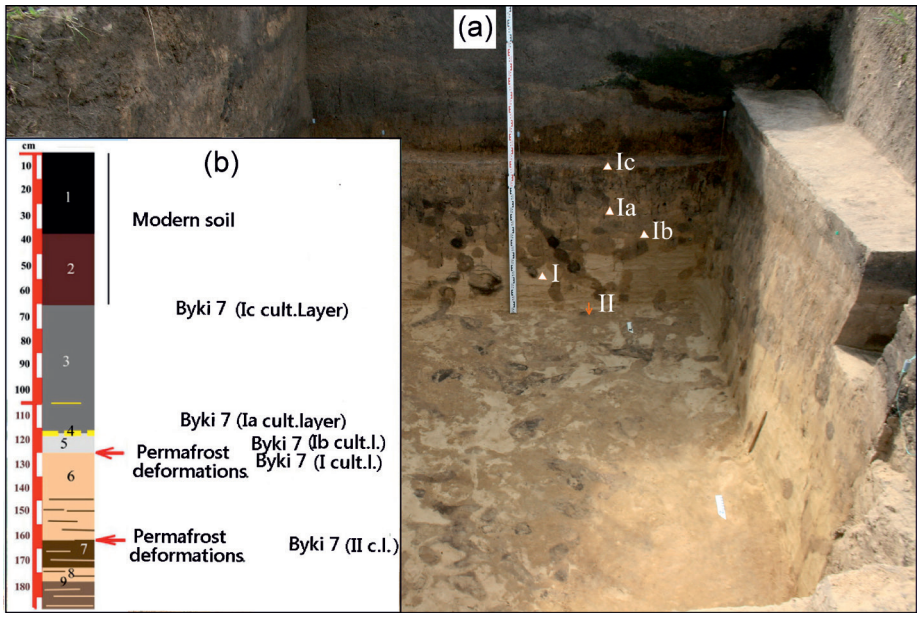

Fig. 2. The photo of the east, south and west walls of the Byki 7 site excavation (a) and the diagram with the position of the cultural layers of the Byki sites on a generalized stratigraphic column (modified after Akhmetgaleeva and Burova (2021). The photo of the excavation was provided by N.B. Akhmetgaleeva

Geology

Byki 7 is a multilayer site that includes the following cultural layers: Ic, Ia, Ib, I, II. (Fig. 2).

The following geological horizons are detected at the sequence exposed at the site Byki 7 (from the top downwards) (Fig. 2) (Akhmetgaleeva and Burova 2021):

1–recent (modern) soil A horizon (thickness – 0.5-0.60 m)

2–recent (modern) soil B horizon (thickness – 0-0.40 m)

3–grey-brown loessic sandy clay (thickness – 0.50-0.80 m).

Cultural layer Ia forms the lower part of this horizon)

4– greenish sand lenses (thickness - 0 – 0.06 m)

5– brown clay loam (thickness - 0.10-0.25 m), with two generation of cryogenic wedges. Cultural layer Ib is from this horizon

6– yellow sand with clay loam strata in the lower part (thickness - 0.05-0.55 m). Cultural layer I is from the top of this horizon, and cultural layer II, from the base

7–brown laminated clay loam (thickness - 0.1-0.5 m)

8–laminated sands (thickness - 0.2 m).

Cryogenic deformations are located between the horizons 5 and 6, as well as between the horizons 6 and 7.

Time interval

The time interval for the "Bykovian" archaeological culture existence in Byki 7 site is estimated as ~22.2–17.0 ka BP. The single date only falls outside the upper limit of this interval (IGAN–7585, Table 1). The interval corresponds to the "cold" Greenland Stadial 2.1 (2.1c – 2.1b) (Rasmussen et al. 2014) and the end of R1 and the beginning of R2 retreat phases of the Scandinavian Ice Sheet (Boulton et al., 2001). During the retreat phase R2, it was a large net and retreat in the southern sector of the Ice Sheet whilst the eastern sector was probably stationary or advancing to the maximum extent (Boulton et al., 2001; Demidov et al., 2006). According to conceptions of different authors Last Glacial Maximum (LGM) duration covered the wide time interval: 26.5–20 (19) ka BP (Clark et al., 2009), 25–23 ka BP (Velichko et al. 2011), 25–20 ka BP (Patton et al. 2017), 22–20 ka BP (Boulton et al. 2001), 22–18 ka BP (Ehlers and Gibbard 2008), 20–15 ka BP (Svendsen et al. 2004), 18–16 ka BP (Demidov et al., 2006). The time of the coldest interval of the Last Glaciation differs depending on the accepted data proxy. According to Greenland oxygen isotope (δ18O) series, the maximum cooling may be corresponded to the stadial GS-3 (27.54–23.34 ka b2k) (Rasmussen et al., 2014). If the marine benthic δ18O series is used as the data proxy (Lisiecki and Raymo 2005), the most cooling period is defined between 22 and 17 ka BP or even between 20 and 18 ka BP. P.U. Clarke et al. (2009) suggested that the duration of the maximum extent of most global ice sheets correlated with the global sea-level lowstand. Thus, the maximum cooling possibly began after the maximum expansion of ice sheets. S.O. Rasmussen et al. (2014) did not define the Last Glacial Maximum and the Late Glacial at all within the INTIMATE stratigraphical scheme, in contrast with such intervals as the Bølling-Allerød and the Younger Dryas chronozones. The different authors' opinions make us use the concepts of the LGM with caution, as well as the Late Glacial Transition, in applied palaeozoological studies. In this study we correlate the time of "Bykovian" archaeological culture existence within the second part of the Late Glacial Maximum before the "Lateglacial" sensu stricto. The last one is defined in different ways: 16–10 ka BP (Nakagawa et al. 2021), 15–12 ka BP (Nenasheva 2013), 15–11.5 ka (Doughty et al. 2012), 14.7–11.7 ka BP (Asch et al. 2013; Šeirienė et al. 2021). Thus, since the dates of Byki 7 temporal interval falls within the 22-17 ka BP, we put this interval within the Late Glacial Maximum (LGM).

Fossil material

About 1800 small mammals (Lagomorpha and Rodentia) remains were found in the three cultural layers (Ia, Ib and I). The fossil material was studied with SMC 4, ASKANIA binocular microscope and with reference material stored at the Institute of Geography Russian Academy of Sciences. Approximately 600 teeth of Lagomorpha and Rodentia were identified up to the species level. The bone material is heavily mineralised and difficult to clean. A significant number of mandibles and maxilla's with well-preserved molars indicate that the material have not been transported over a large distance.

RESULTS

Large mammals

The large mammal remains from the site Byki 7 site were investigated by N.B. Burova (Akhmetgaleeva and Burova 2021) who indicated that ancient men mainly hunted for: broad-fingered horse *Equus ferus* Boddaert, 1985, reindeer *Rangifer tarandus* (Linnaeus 1758), arctic fox *Vulpes (Alopex) lagopus* (Linnaeus 1758), and Don hare *Lepus tanaiticus Gureev*, 1964. Remains of mammoth *Mammuthus primigenius* (Blumenbach 1799), woolly rhinoceros *Coelodonta antiquitatis* (Blumenbach, 1799), and bison *Bison priscus* Bojanus, 1827 are extremely rare. The fossil assemblages includes, in addition, a small nubber of remains of wolf *Canis lupus* Linnaeus, 1758, brown bear *Ursus arctos* Linnaeus, 1758, wolverine *Gulo gulo* (Linnaeus 1758), and polecat *Mustela (Putorius) eversmanni* (Pallas 1779).

Small mammals

The cultural layers Ia,Ib, and I yielded small mammal remains: there are so far no small mammal remains found in the layers Ic and II are so far lacking. The majority of the small mammal finds are from the cultural layers Ia and Ib; only very few Lagomorpha and Rodentia remains derived from the cultural layer I (Table 2).

The analysis of the BYKI 7 small mammal fauna resulted in the following data: remains of 11 rodent and lagomorphs species have been found in the upper cultural layer Ia and 8 species in cultural layer Ib, respectively (Table 2). Remains of only two species were detected in the cultural layer I: steppe pika Ochotona pusilla (Pallas, 1769) (5) and collared lemming Dicrostonyx torquatus (Pallas, 1778) (Table 2).

Byki 7 fauna includes the subarctic collared lemming *Dicrostonyx torquatus* and the Siberian lemming (*Lemmus sibiricus* (Kerr, 1792)), as well as many steppe species, and one subaquatic species (*Microtus oeconomus* Pallas, 1773). A composition that is characteristic for the majority of late Palaeolithic faunas in Eastern Europe which includes often also Subarctic species. Remains of forest species which prefer a forested biotope, the common inhabitants of the modern forest-steppe zone, are not represented in the Byki 7 fauna (Table 2).

The collared lemming is a typical inhabitant of the modern dry, and well drained, tundra a biotope that occurs from the White Sea in the West to Chukotka in the East of Eurasia. During the Last Glacial Maximum (LGM, MIS2, 28.6–22.5 ka BP), the range of this species was larger, including the British Isles in the west and it expanded southward in Eastern Europe to 48° N, and in Western Europe up to 45° N (Fig. 3a). During the Lateglacial, the range of collared lemming decreased; its remains were found in the Desna R. Basin and in the south of the Urals. During the Bølling–Allerød interstadial (14.7–12.9 ka BP) the range of the collared lemming began to degrade: the species only occurred in the isolated areas in Western Europe (a.o. in the south of the British Isles), in the upper basin of the River Don, as well as in the Urals (Smirnov 1996; Markova et al. 2019; Ponomarev and Puzachenko 2015). At the end of Pleistocene, collared lemming did not longer inhabit Eastern Europe, except for the Urals. In Western Europe, isolated findings are known from the Rheine Basin and from the British Isles (Markova et al. 1995; 2019).

Table 2. Species composition of small mammals from cultural layers 1a and 1b of the Byki 7 site

Species	Cultural layer Ia		Cultural layer Ib	
	N	%	N	%
Lagomorpha – lagomorphs				
Ochotona pusilla Pallas, 1762 – steppe pika	75	35,55	120	41,20
Rodentia – rodents				
Marmota bobac Müller, 1776 - bobac-marmot	1	0,47		
Spermophilus sp. – ground squirrel	12	5,68	1	0,34
Spalax microphthalmus Gueldenstaedt, 1770 – Russian mole rat	8	3,79	2	0,68
Ellobius talpinus Pallas, 1770 - Northern mole-vole	3	1,42		
Cricetus cricetus (Linnaeus, 1758) – East European hamster	8	3,79		
Lemmus sibiricus (Kerr, 1792) – Siberian lemming	13	6,16	15	5,10
Dicrostonyx torquatus Pallas, 1778 – collared lemming	14	6,64	15	5,10
Lagurus lagurus (Pallas, 1773) – steppe lemming	4	1,90		
Microtus (Alexandromys) oeconomus Pallas, 1776 – root vole	3	1,42	6	2,04
Lasiopodomys (Stenocranius) gregalis (Pallas, 1779) – narrow-skulled vole	70	33,18	130	44,18

The presence of only a few collared lemming remains in the Byki 7 small mammal assemblage (Table 2), indicates a significant geographical distance between this site and the borders of Valdai ice sheet (~ 440 km). It should be noted, that the collared lemming is a dominant in the assemblage from the Late Palaeolithic Yudinovo site (Sudost River basin) with a comparable age (Markova 1995). The explanation is the fact that the Yudinovo site is located closer to the border of Valdai ice sheet (only ~270 km) (Fig. 1). That points out unfavourable, too arid conditions for this species as evidenced by some climate reconstructions (Ludwig et al. 2016; Višnjević et al. 2020).

During the second half of the Late Pleistocene, the range of Siberian lemming expanded south- and westward (Fig. 3b). The Siberian lemming is represented in the fauna of Byki 7 site, though the number of remains is very low (Table 2). During the LGM the lemming inhabited Upper Dnieper River basin at ~ 50º N, and in the Urals at ~ 54º N. During the Lateglacial, the Siberian lemming inhabited the Upper Dnieper River. basin and the Mid-Urals (Markova et al. 2019). Nowadays, the species inhabits the Eurasian tundra and forest-tundra, and prefers moist bushy, sedge, cotton sedge and moss tundra (Gromov and Erbaeva, 1995).

The steppe pika and narrow-skulled vole *Lasiopodomys (S.) gregalis* (Pallas, 1779), are dominant in the assemblage from all the Byki 7 cultural layers. The steppe pika is a typical representative of open landscapes (steppes, forest-steppes and semi-deserts). Nowadays, it inhabits the rocky slopes of ravines and gullies covered with bushes and open areas with Chernozem or sandy clay soils along the forest edge. The species occurs in the area that stretches from Middle Volga R. Basin (Samara Region) to the foothills of the Altai Mountain range. During the second part of the. During LGM time steppe pika expanded its range far to the west and even reached the British Isles. The species was an indicator of periglacial landscapes that covered significant European areas (Markova et al. 2019) (Fig. 3c). The species was an indicator of periglacial landscapes that covered significant European areas (Markova et al. 2019). During the Lateglacial, the range of steppe pika decreased slightly, and its westernmost occurrence was in the northern foothills of the Alps, at 5º E (Markova et al. 2019). In Central Europe, this species was widespread between 50–60ºN. In Eastern Europe the steppe pika inhabited the Dniester, Dnieper, Desna and Don River' basins, and the Crimea (Fig. 3c), as well as the Urals (Markova 2011; Markova et al. 2019).

The narrow-headed vole *Lasiopodomys (S.) gregalis* was one of the dominant species in the Byki 7 small mammal fauna. Nowadays, the species inhabits variety open landscapes. The northern subspecies *L. (S.) gregalis major* Ognev, 1923, is an inhabitant of the tundra biotope. It is endemic to this natural zone, where it forms quite large colonies (Sheftel et al. 2020). During the Pleistocene, the narrow-skulled vole was a representative of the mammoth fauna that was widely distributed during the glacial epochs, when periglacial steppe and tundra-steppe prevailed (Markova et al. 1995; 2019; Markova and Puzachenko 2007). Low temperatures were in no way a hurdle for this animal. The species was widely distributed during the interglaciations in steppe and forest-steppe zones, as well as during glaciations in periglacial steppes and tundra-steppes (Markova et al. 1995; 2019; Markova and Puzachenko 2007). The remains of narrow-headed vole are present at almost all Late Palaeolithic sites and Late Pleistocene localities of Eastern Europe (from the Black Sea coast to the Subarctic Region) (Agadjanian, 2009, Rekovets, 1973; Markova et al. 2019; Baryshnikov and Markova 2002). The range of this species covered huge territories: during LGM it reached the British Isles in the west (Fig. 3d). In the Lateglacial the range of the narrow-skulled vole was also quite broad and differed insignificantly from its area during the LGM. The expansion of its range was connected with the wide prevalence of open periglacial landscapes and the degradation of the continuous forest zone in Europe during the period of the Last Glaciation.

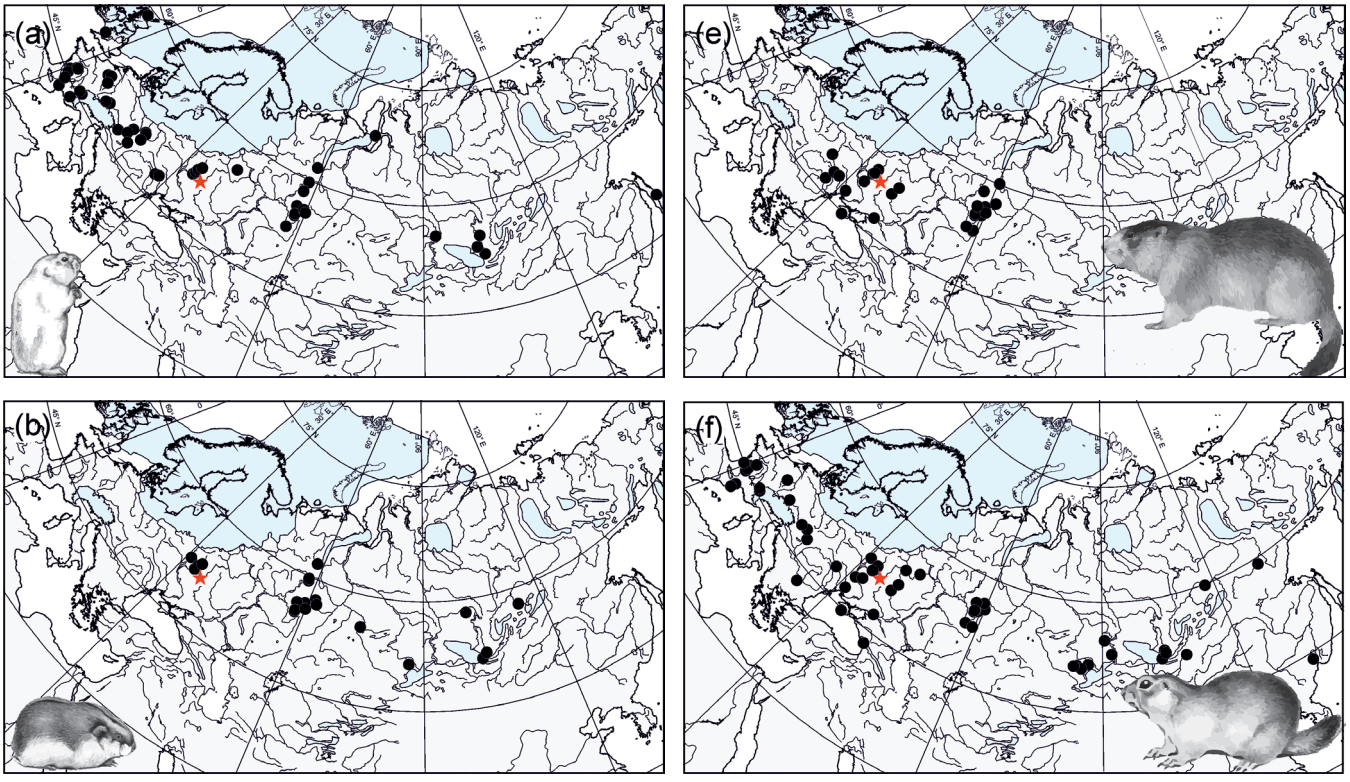

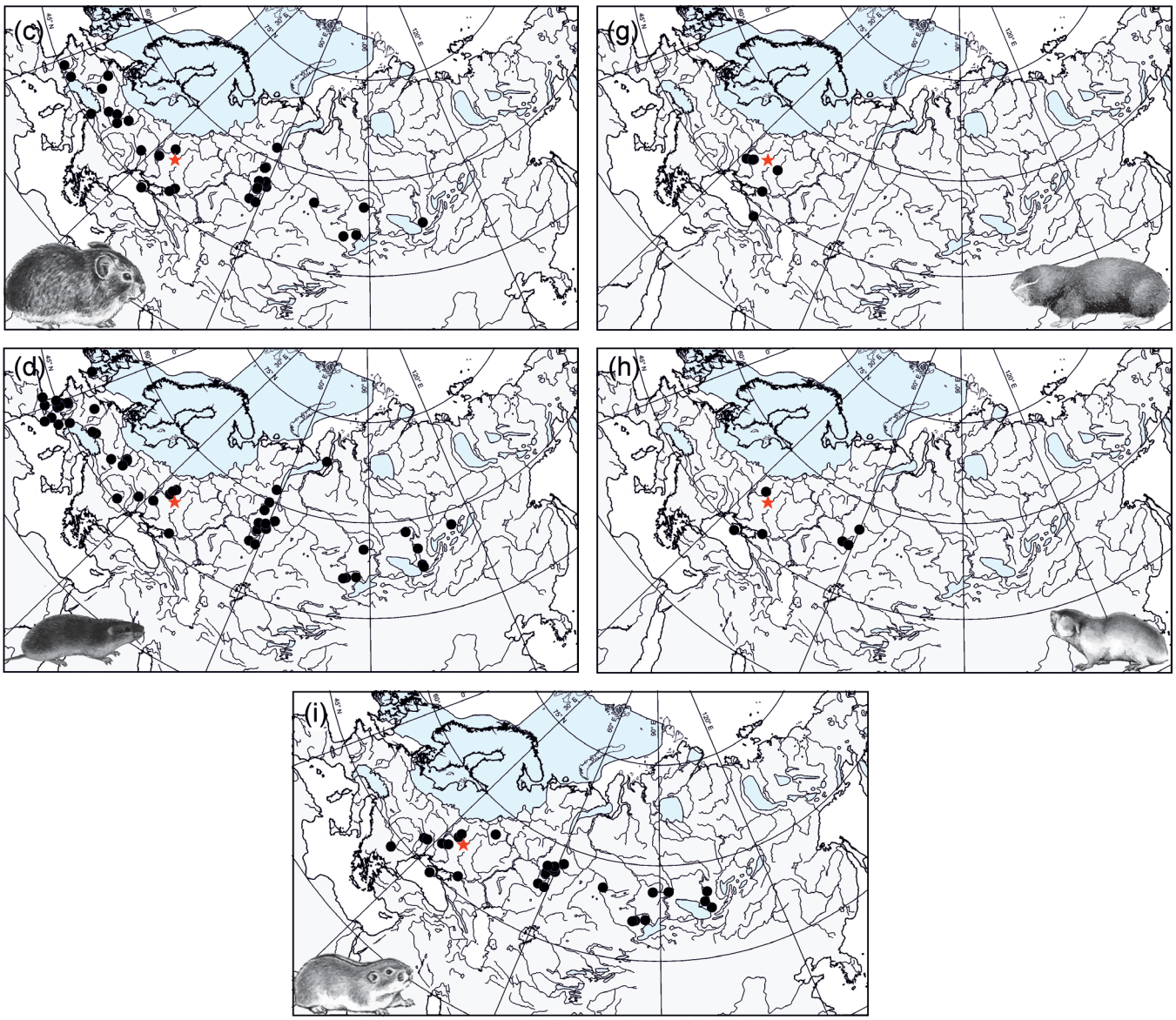

Fig. 3. a – The European localities of *Dicrostonyx torquatus* (a), *Lemmus sibiricus* (b), *Ochotona pusilla* (c), *Lasiopodomys S gregalis*, (d), *Marmota bobac* (e), *Spermophilus sp.* (f), *Spalax microphthalmus* (g), *Ellobius talpinus* (h), and *Lagurus lagurus* (i) during the occupation of the Byki 7 site (the maps were prepared by the authors of this article). The red asterisk indicates the location of the Byki 7 site. The blue contours indicate the borders of the Scandinavian Ice Sheet and mountain glaciations during the Valdai Glaciation Maximum (LGM) (Svendsen et al. 2004; Velichko 2009)

Other small mammals which are the typical inhabitants of the open landscapes have few numbers of remains (Table 2). In cultural layer Ia, one mandible of the bobac-marmot *Marmota bobac* Müller 1776 was found. This species inhabits the modern steppe and forest-steppe zones of Northern Eurasia. Its historic range spanned from Hungary to the Irtysh River basin. Its preferred habitats are cereal-forb steppes. The bobac-marmot is an intensive digger; the tunnels (krotovinas) they make, during the winter time, are up to 7 meters deep and their dwellings are 2-3 meters below the surface (Gromov and Erbaeva 1995). The presence of the bobac-marmot in the Byki 7 fossil assemblage indicates the absence of permafrost during human occupation of the site. Bobac remains are known from Late Pleistocene faunal assemblages from localities in the south of the Russian Plain, the Crimea, the Mid- and Southern Urals, and in Kazakhstan (Markova 1995, 2011; Markova et al. 1995) (Fig. 2e).

Remains of ground squirrels (*Spermophilus* sp.) are rare in the layers Ia and Ib (Table 2). Ground squirrels inhabit forest-steppe, steppe, and semi-desert zones. During the Late Pleistocene the geographical range of the ground squirrels expanded west- and southward due to the wide dispersal of various types of open landscapes - periglacial tundra-steppe and steppe (Markova et al. 2019) (Fig. 2f).

Greater mole-rat *Spalax microphthalmus* Gueldenstaedt, 1770 is also a characteristic representative of the forest-steppe and steppe faunas. Nowadays, it inhabits an area that stretches from the Caucasus foothills in the south up to the border of the forest zone in the north of the Russian Plain. The mole rat is a fossorial species lives underground except young growth period. Its nests may be located at a depth of 3–4 meters below the surface (Topachevsky 1969). Their presence in the fossil record of the Byki 7 cultural confirms the absence of continuous permafrost during time of deposition. Fossil, Late Pleistocene, remains are known from many localities and sites of Eastern Europe (Fig. 2g), but the amount of the remains was always insignificant (Markova et al. 2019).

The Northern mole-vole *Ellobius talpinus* Pallas, 1770 is a typical representative of faunas that inhabit steppes and semi-deserts. It prefers to dwell in habitats with unconsolidated soils. The species inhabits the steppe zone of Eastern Europe, the Trans-Urals, Kazakhstan, and the Central Asian foothills. Northern mole-vole is fossorial animal and its burrows reach to a depth of 0.5 meters

(Gromov and Erbaeva 1995). The Late Pleistocene fossil record demonstrates that the mole-vole occurred during the Pleistocene in Eastern Europe (including the Crimea) and the Fore-Caucasus (Markova 2011; Markova et al. 2019) (Fig. 2h). The Late Palaeolithic Byki 7 fossil, found at ~ 51^0 N is an exception in the Eastern European record. A few *E. talpinus* remnants are known from the site Yudinovo, another Late Palaeolithic site on the Central Russian Plain (Markova 1995).

Only 4 specimens of the steppe lemming, *Lagurus lagurus* (Pallas, 1773) were found in cultural layer Ia (Table 2). This animal is a typical inhabitant of open landscapes (forest-steppes to semi-deserts). Nowadays, the steppe lemming prefers to live in a herb-bunch grass steppe, a feather-fescue steppe, and a sagebrush steppe. Burrows of this species reach to a depth of 50-60 cm (Gromov and Erbaeva 1995). The phylogeny of the steppe lemmings during the last 1.5 Ma is rather well-know due to the studies of the fossil record from several Early– Late Pleistocene localities (Markova 1974, 1982, 2006, 2011, 2017; Rekovets 1994; Topachevsky 1965; Terzea 1995; Janossy 1986). It should be mentioned, that the Pleistocene steppe lemmings' remains are found in interglacial, as well as in the glacial faunas. During glacial periods (including the Valdai Glaciation), the range of the species expanded to the north as well as to the west, while during the interglacial periods, the northern border of its distribution area shifted south- and eastward (Fig. 2i). The latter was caused by the formation of a continuous forest zone during the warmer interglacials. The steppe lemming is represented by a great number of remains at most Late Palaeolithic sites located in the area of the Russian Plain and the Crimea (Markova et al. 1995, 2019). However, at the Byki 7 site steppe lemming remains were only found in one layer and in low numbers.

DISCISSION

The analysis of small mammals from the Site Byki 7 allows a palaeoenvironmental reconstruction. The fauna belongs to the so called "mixed" or "non-analogue" faunas that were widely distributed during the Valdai (= Vistulian) Glaciation, and during previous Pleistocene glacial periods (Dnieper, Oka, Don glaciations) (Agadjanian 2009; Baryshnikov and Markova 2002, 2009; Vereshchagin 1979; Rekovets 1994; Markova and Puzachenko 2007; Markova et al. 2019). The species composition of the "non-analogue" faunas consists of species that occur nowadays in different natural zones, steppe and tundra in particular. Species that usually inhabit forests are absent, or occur in very small quantities. Middle and Late Palaeolithic sites as well as non-archaeological sites dates to the second part of Late Pleistocene located on the Russian Plain yield this kind of "non-analogue" faunas (Markova et al. 1995, 2019; Markova and Puzachenko 2007). These faunas reflect the broad prevalence of open landscapes – periglacial tundra-steppes, periglacial tundra-forest-steppes and periglacial steppes. Zones with continuous forest did not exist during that glacial epoch. The dispersal of steppe animals to the far north indicates the absence of a continuous forest zone at that time (Grichuk 1989). The forest species survived in refugees in mountainous areas where a variety of environments occur and in the river valleys. The presence of the high number of large herbivores, extinct by the end of the Pleistocene – beginning of the Holocene, also characterise these "non-analogue" assemblages. The huge geographical range of many tundra species during the second part of the Late Pleistocene, indicates cold climatic conditions and the wide distribution of periglacial types of vegetation in Northern and Central Europe. Steppe animals also extended their ranges and migrated to the open landscapes in north as well as to those in the west. The open landscapes were favourable for such assemblages.

It is important to keep in mind, that small mammal species that prefer to live in a forested environment are lacking. Nowadays, southern forest steppes prevail the region and not only steppe, but also forest species are well represented (Table 3), but the last group was totally absent during the LGM. The number of remains of subarctic species (collared and Siberian lemmings) in the Byki 7 assemblage is low in comparison to other Late Palaeolithic sites on the Russian Plain. At the Yudinovo site, with radiocarbon dates close to those of the Byki 7 site, subarctic species were predominated (Markova 1995). At the Byki 7 site their number is only ~11–12 % of all small mammalian remains (Table 3). An explanation could be the significant distance between the site and the border of the Valdai ice sheet (Fig. 1). As mentioned above, the dominant small mammal species at Byki 7 are typical representatives of open landscapes, steppe pika and narrow-skulled vole. These species are well adapted to the low temperatures that characterize the second half of the Late Pleistocene. However, the determining factor of their occurrence was the presence of open landscapes with periglacial tundra-steppe, forest-steppes and steppes.

Table 2. Lagomorphs and rodents from the cultural layers of the Byki 7 site (Kursk Region)

Small mammals from Byki 7 site				Present time	Proposed ecology in the Late Pleistocene
Species	Cult. layer Ia	Cult. Layer Ib	Cult. Layer I		
Lagomorpha – lagomorphes					
Lepus europaeus – European hare				+	Steppe, forest-steppe
Lepus tanaiticus – Don hare (N.D. Burova' definition)	+				Steppe, tundra-steppe
Ochotona pusilla – steppe pika	+	+	+		Steppe
Rodentia – грызуны					
Sciurus vulgaris – Eurasian red squirrel				+	Forest
Marmota bobac – bobac-marmot	+			+	Steppe
Spermophilus suslicus – spotted ground squirrel				+	Steppe
Spermophilus sp. – ground squirrel	+	+			Steppe, periglacial steppe

Castor fiber – Eurasian beaver				+	Aquatic biotopes
Sicista severtzovi – Severtsov birch mouse				+	Steppe
S. subtilis – southern birch mouse				+	Steppe
S. strandi – Strandi birch mouse				+	Steppe
Allactaga major – great jerboa				+	Steppe, periglacial steppe
Cricetus cricetus – European hamster	+			+	Steppe, periglacial steppe
Spalax microphthalmus – greater mole rat	+			+	Steppe, forest-steppe, periglacial steppe
Ellobius talpinus – Northern mole-vole	+				Open landscapes of different types
Mus musculus – house mouse				+	Steppe
Micromys minutus – dwarf mouse				+	Steppe, glades
Sylvaemus uralensis – small forest mouse				+	Forest
S. flavicollis- yellow-necked mouse				+	Forest
Apodemus agrarius –striped field mouse				+	Floodplain meadows, meadows
Dryomys nitedula – forest dormouse				+	Forest
Arvicola amphibius – water vole				+	Hydrogenous biotopes
Clethrionomys glareolus – bank vole				+	Forest
Lagurus lagurus – steppe lemming	+			+	Steppe, periglacial steppe
Dicrostonyx torquatus – coloured lemming	+	+	+		Dry tundra
Lemmus sibiricus – Siberian lemming	+	+			Wet tundra
Microtus arvalis – common vole				+	Meadows
M. rossiaemeridionalis – East European vole				+	Meadows
M. (Alexandromys) oeconomus – root vole				+	Hydrogenous biotopes, Meadows
Lasiopodomys (Stenocranius) gregalis – narrow-headed vole	+	+			Open landscapes of different types including periglacial tundra-steppe and periglacial steppe

CONCLUSIONS

The fossil mammal data from the site Byki 7 indicate the occurrence of periglacial steppes in the central part of the East European Plain. The fact that the site is located relatively far from the borderline of the Valdai ice sheet (~440 km) impacted the fauna composition. Typical tundra species are present in small quantities in the Byki 7 assemblage whereas the steppe species dominate and forest species are absent.

Our data indicate that during the LGM a periglacial mesic and dry tundra-steppe with wormwood-haze steppe vegetation, sparse pine-birch forests with alder (Alnus), fir (Picea), pine (Pinus) and Asteraceae, Cichoriaceae, Sphagnum, Polypodiaceae, etc prevailed in the centre of East European Plain. The rich mammal assemblage included: woolly mammoth, woolly rhinoceros, primitive bison, reindeer, broad-fingered horse, saiga, cave lion, brown bear, fox, arctic fox, steppe lemming, bobac-marmot, ground squirrel, mole rat, Northern mole vole, collared and Siberian lemmings (Dicrostonyx and Lemmus), steppe and yellow lemmings, narrow-headed vole, etc.

Based on result of this study, a moderate climate is proposed during ancient men settled the site Byki 7.

REFERENCES

Agadjanian A.K. (2009). Pliocene-Pleistocene small mammals of the Russian Plain, Proc. Paleontol. Inst. 40, Nauka Press, Moscow (in Russian).

Akhmetgaleeva N., Panin A., Kurenkova E., Zazovskaya E. & Burova N. (2020). Problems of radiocarbon dating of sites of the Upper Paleolithic Byki on the center of the Russian Plain. In: Radiocarbon in archaeology and paleoecology: past, present and future time. Materials of the intern. conf., S-Petersburg, 15-16, DOI: 10.31600/978-5-91867-213-6-15-16

Akhmetgaleeva N.B. & Burova N.D. (2021). The originality of the Byki sites among known LGM industries on the Russian Plain. Quaternary International, 581-582, 296-314, DOI: 10.1016/j.quaint.2020.08.035

Akhmetgaleeva N.B. (2015). Stone Age of Seim R. basin: Late Palaeolithic site Byki 7. Mechta Press, Kursk (in Russian).

Akhmetgaleeva N.B., Burova N.D., Voskresenskaya E.V. & Gribchenko Yu. N. (2010). Complex study of Late Palaeolithic sites in Seim basin. Archeological discoveries 1965-2007. Archeological Inst. RAS, Moscow (In Russian).

Asch N. Van, Heiri O., Bohncke S.J.P. & Hoek W.Z. (2013). Climatic and environmental changes during the Weichselian Lateglacial Interstadial in the Weerterbos region, the Netherlands. Boreas 42, 123–139, DOI: 10.1111/j.1502-3885.2012.00281.x

Baryshnikov G.F., & Markova A.K. (2002) Animal world. Theriocomplexes of the Late Valdai In.: Landscape and inner seas dynamics of Northern Eurasia during last 130-th. years. Atlas-Monograph. Chapter 7. GEOS Press, Moscow, 123-137 (in Russian).

Baryshnikov G.F., & Markova A.K. (2009). Main theriocomplexes during the cold epoch of the Late Pleistocene. In.: Paleoclimates and paleolandscapes of extratropical part of Northern Hemisphere. Atlas-Monograph. GEOS Press, Moscow, 79-87 (in Russian).

Boulton G.S., Dongelmans P., Punkari M. & Broadgate M. (2001). Palaeoglaciology of an ice sheet through a glacial cycle: The European ice sheet through the Weichselian. Quaternary Science Reviews, 20(4), 591–625, DOI: 10.1016/S0277-3791(00)00160-8

Ludwig P., Schaffernicht E.J., Shao Y. & Pinto J.G. (2016). Regional atmospheric circulation over Europe during the last Glacial maximum and its links to precipitation. Journal of Geophysical Research, 121(5), 2130–2145, DOI: 10.1002/2015JD024444

Chubur A.A. (2001). New Paleolithic microregion and its place in the Late Palaeolithic of the Russian Plain. Briansk, Briansk-Segodnia Press. (in Russian).

Clark P.U., Dyke A.S., Shakun J.D., Carlson A.E., Clark J., Wohlfarth B., Mitrovica J.X., Hostetler S.W. & McCabe A.M. (2009). The Last Glacial Maximum. Science 325(5941), 710–714, DOI: 10.1126/science.1172873

Demidov I., Houmark-Nielsen M., Kjær K. & Larsen E., 2006. The last Scandinavian Ice Sheet in northwestern Russia: Ice flow patterns and decay dynamics. Boreas 35(3), 425–443, DOI: 10.1080/03009480600781883

Doughty A.M., Anderson B.M., Mackintosh A.N., Kaplan M.R., Vandergoes M.J., Barrell D.J.A., Denton G.H., Schaefer J.M., Chinn T.J.H. & Putnam A.E. (2013). Evaluation of Lateglacial temperatures in the Southern Alps of New Zealand based on glacier modelling at Irishman Stream, Ben Ohau Range. Quaternary Science Reviews 74, 160–169, DOI: 10.1016/j.quascirev.2012.09.013

Ehlers J., Gibbard, P. (2008). Extent and chronology of Quaternary glaciation. Episodes 31, 211–218, DOI: 10.18814/epiiugs/2008/v31i2/004

Grichuk V.P. (1989). The history of flora and vegetation of Russian Plain during the Pleistocene. Nauka Press, Moscow (in Russian)

Grigorieva G.V., & Filippov A.K. (1978). Late Palaeolithic site Peny. Soviet archaeology, 4, 280-300 (in Russian).

Gromov I.V., & Erbaeva V.A. (1995). Mammalian faunas of Russia and adjacent territories (Lagomorphs and Rodents). Zool. Inst. Press, S-Petersburg (in Russian)

Janossy D. 1986. Pleistocene Vertebrate Faunas of Hungary. Akademiai Kiado. Elsevier, Budapest- Amsterdam.

Lisiecki L.E., Raymo M.E. (2005). A Pliocene-Pleistocene stack of 57 globally distributed benthic δ18O records. Paleoceanography 20, 1–17, DOI: 10.1029/2004PA001071

Markova A.K. (1974). Data of teeth morphology of fossil steppe lemmings (Rodentia, Microtinae) in example of Dnieper River basin findings. Bull. Kom. Izuch. Chetv. Per. 41, 107-120 (in Russian.).

Markova A.K. (1982). Pleistocene rodents of the Russian Plain. Nauka Press, Moscow (in Russian).

Markova A.K. (1995). Rodent remains from the Late Palaeolithic site Yudinovo (Desna River basin). Cytology, 37 (7), 688 (in Russian).

Markova A.K. (2006). Evolution changes of Eastern European steppe lemmings Prolagurus-Lagurus and their significance for the stratigraphy. In: Late Cenozoic history of the northern part of arid zone. Rostov-na-Dony. Azov. South Scient. Center Press, 226-228 (in Russian).

Markova A.K. (2011). Small mammals from Palaeolithic sites of the Crimea. Quaternary International, 231, 22-27, DOI: 10.1016/j.quaint.2010.07.016

Markova A.K. (2017). European small mammal faunas of the second part of the Middle Pleistocene: species composition, distribution, correlations. Bull. Kom. Izuch. Chetver. Per., 75, 11-33 (in Russian).

Markova A., van Kolfschoten T., Bohncke S.J.P., Kosintsev P.A., Mol J., Puzachenko A.Yu., Simakova A.N., Smirnov N.G., Verpoorte A., & Golovachev I.V. (2019) Evolution of European ecosystems during Pleistocene – Holocene transition (24–8 kyr BP). GEOS Press, Moscow.

Markova A., & Puzachenko A. (2007). Late Pleistocene mammals of Northern Asia and Eastern Europe. Vertebrate records. In: Elias, S.A., (Ed.), Encyclopaedia of Quaternary Science. Elsevier B.V. P. 3158-3174.

Markova A.K., Smirnov N.G., Kozharinov A.V., Kazantseva N.E., Simakova A.N., & Kitaev L.M. (1995). Late Pleistocene distribution and diversity of mammals in Northern Eurasia (PALEOFAUNA database). Paleontologia i Evolucio 28-29, 5-143.

Nakagawa T., Tarasov P., Staff R., Bronk Ramsey C., Marshall M., Schlolaut G., Bryant C., Brauer A., Lamb H., Haraguchi T., Gotanda K., Kitaba I., Kitagawa H., Plicht J. van der, Yonenobu H., Omori T., Yokoyama Y., Tada R. & Yasuda Y. (2021). The spatio-temporal structure of the Lateglacial to early Holocene transition reconstructed from the pollen record of Lake Suigetsu and its precise correlation with other key global archives: Implications for palaeoclimatology and archaeology. Global and Planetary Change, 202, in print, DOI: 10.1016/j.gloplacha.2021.103493

Nenasheva G.I, 2013. Vegetation and climate of the Holocene intermountain basins of the Central Altai: monograph. Altaiski State University, Barnaul. (in Russian)

Patton H., Hubbard A., Andreassen K., Auriac A., Whitehouse P.L., Stroeven A.P., Shackleton C., Winsborrow M., Heyman J. & Hall A.M. (2017). Deglaciation of the Eurasian ice sheet complex. Quaternary Science Reviews, 169, 148–172, DOI: 10.1016/j.quascirev.2017.05.019

Ponomarev D., Puzachenko A. (2015). Evolution of occlusal shape of the first and second upper molars of Middle-Late Pleistocene collared lemmings (Dicrostonyx, Arvicolinae, Rodentia) in northeast European Russia. Boreas, 44(4), 741–759, DOI: 10.1111/bor.12131

Rasmussen S.O., Bigler M., Blockley S.P., Blunier T., Buchardt S.L., Clausen H.B., Cvijanovic I., Dahl-Jensen D., Johnsen S.J., Fischer H., Gkinis V., Guillevic M., Hoek W.Z., Lowe J.J., Pedro J.B., Popp T., Seierstad I.K., Steffensen J.P., Svensson A.M., Vallelonga P., Vinther B.M., Walker M.J.C., Wheatley J.J. & Winstrup, M. (2014). A stratigraphic framework for abrupt climatic changes during the Last Glacial period based on three synchronized Greenland ice-core records: Refining and extending the INTIMATE event stratigraphy. Quaternary Science Reviews, 106, 14–28, DOI: 10.1016/j.quascirev.2014.09.007

Rekovets L.I. (1985). Microtheriofauna from the Late Paleolithic sites of Desna - Dnieper basin. Naukova Dumka Press, Kiev (in Russian).

Rekovets L.I. (1994). Small mammals of the southern part of the Eastern Europe. Naukova Dumka Press, Kiev (in Russian).

Šeirienė V., Gastevičienė N., Luoto T.P., Gedminienė L. & Stančikaitė M. (2021). The Lateglacial and early Holocene climate variability and vegetation dynamics derived from chironomid and pollen records of Lieporiai palaeolake, North Lithuania. Quaternary International 605–606, 55–64, DOI: 10.1016/j.quaint.2020.12.017

Sheftel B.I., Makarova O.L., Artiushin I.V., Obolenskaia E.V., Burskaia V.O. & Glazov P.M. (2020). About the small mammal fauna of Bolshaia Zemlia tundra (Nenets Autonomous Okrug)]. Vest. Tomsk State Univ. Biology 50, 157-175 (in Russian).

Simakova A.N., & Puzachenko A. Yu. (2019). Paleovegetation of Europe during Pleistocene–Holocene transition (24–8 kyr BP).In: Markova A.K., Kolfschoten T. van, & Puzachenko A.Yu. (eds). Evolution of European ecosystems during Late Pleistocene – Holocene transition (24–8 kyr BP). GEOS Press, Moscow, 143-220.

Smirnov N.G. (1996). Small mammal diversity of Northern Urals during the Late Pleistocene and Holocene. In: Materials and studies of the history of modern Ural fauna. Yekaterinburg Press, Yekaterinburg, 39-83 (in Russian).

Svendsen J.I., Alexanderson H., Astakhov V.I., Demidov I., Dowdeswell J.A., Funder S., Gataullin V., Henriksen M., Hjort C., Houmark-Nielsen M., Hubberten H.W., Ingólfsson Ó., Jakobsson M., Kjær K.H., Larsen E., Lokrantz H., Lunkka J.P., Lysså A., Mangerud J., Matiouchkov A., Murray A., Möller P., Niessen F., Nikolskaya O., Polyak L., Saarnisto M., Sieger, C., Siegert M.J., Spielhagen R.F. & Stein R. (2004). Late Quaternary ice sheet history of northern Eurasia. Quaternary Science Reviews, 23, 1229–1271,. DOI: 10.1016/j.quascirev.2003.12.008

Terzea E. (1995). Mammalian events in the Quaternary of Romania and correlations with the climatic chronology of Western Europe. Acta zool. Cracoviensia 38, 109-120.

Topachevsky V.A. (1969). Fauna of USSR. V. III, No 3. Spalacidae. Leningrad, Nauka (in Russian)

Topachevsky V.A. (1975). Insectivores and rodents of Nogaisk Late Pliocene fauna. Naukova Dumka Press, Kiev (in Russian).

Višnjević V., Herman F. & Prasicek G. (2020). Climatic patterns over the European Alps during the LGM derived from inversion of the paleo-ice extent. Earth and Planetary Science Letters, 538, 116185, DOI: 10.1016/j.epsl.2020.116185

Velichko A.A. (Ed.) (2009). Paleoclimates and paleoenvironments of extra-tropical regions of the Northern Hemisphere. Late Pleistocene - Holocene. Atlas-monograph. GEOS Press, Moscow.

Velichko A.A., Faustova M.A., Pisareva V.V., Gribchenko Y.U.N., Sudakova N.G. & Lavrentiev N. V., (2011). Glaciations of the east european plain. Distribution and chronology. Developments in Quaternary Science 15, 337–359, DOI: 10.1016/B978-0-444-53447-7.00026-X

Vereshchagin N.K. (1979). Why the mammoths extinct. Nauka Press, Leningrad (in Russian).

RESEARCH PAPER

CHALLENGES IN REDUCING PHYTOTOXICITY OF METALS IN SOILS AFFECTED BY NON-FERROUS SMELTER OPERATIONS

Elvira A. Dovletyarova[1], Olga S. Fareeva[1], Ramilla A. Brykova[1], Mikhail M. Karpukhin[2], Ivan A. Smorkalov[3], Valeriya V. Gabechaya[4], Kooichi Vidal[5], Michael Komárek[6], Alexander Neaman[7,8,*]

[1]Department of Landscape Design and Sustainable Ecosystems, Peoples Friendship University of Russia (RUDN University), 6 Miklukho-Maklaya St., Moscow, 117198, Russian Federation

[2]Faculty of Soil Science, Lomonosov Moscow State University, Moscow, Russian Federation

[3]Institute of Plant and Animal Ecology, Ural Branch of the Russian Academy of Sciences, Ekaterinburg, Russian Federation

[4]Department of Ecology, Russian State Agrarian University - Moscow Timiryazev Agricultural Academy, Moscow, Russia

[5]Escuela de Agronomía, Pontificia Universidad Católica de Valparaíso, Quillota, Chile

[6]Department of Environmental Geosciences, Faculty of Environmental Sciences, Czech University of Life Sciences Prague, Prague, Czech Republic

[7]Laboratory of Bioresource Potential of Coastal Area, Institute for Advanced Studies, Sevastopol State University, Crimea, Russian Federation

[8]Centro Transdisciplinario de Estudios Ambientales y Desarrollo Humano Sostenible (CEAM), Universidad Austral de Chile, Valdivia, Chile

***Corresponding author:** alexander.neaman@gmail.com

Received: December 13th, 2021 / Accepted: February 15th, 2022 / Published: March 31st, 2022

https://DOI-10.24057/2071-9388-2021-141

ABSTRACT. Lime is one of the effective agents for reducing the phytoavailability of metals in contaminated acidic soils. However, previous studies have shown that lime alone cannot reduce metal phytotoxicity to the desired extent in such soils. The goal of this study was to evaluate the effect of different amendment combinations (lime with and without Fe- and/or Mn-based amendments) on plant growth. A sample of Histosol (0-5 cm) was collected around a Cu/Ni smelter near Monchegorsk, Murmansk region, exhibiting total Cu and Ni concentrations in the soil of 6418 and 2293 mg kg^{-1}, respectively. Likewise, a sample of forest litter (0-15 cm) was collected around a Cu smelter near Revda, Sverdlovsk region, exhibiting total Cu concentration in the soil of 5704 mg kg^{-1}. Fe-Mn oxides were sourced from ferromanganese nodules in the Gulf of Finland, and iron powder was used as a precursor for iron oxides. Perennial ryegrass was grown in pots for 21 days under controlled laboratory conditions. Two dolomite doses were tested: 5% w/w (giving a soil pH of 6.5) and 20% w/w (giving a soil pH of 7.4). Over-liming stunted plant growth; therefore, the dolomite dose was set at 5% in the further experiments of the study. Importantly, the addition of 0.5% and 1% of Fe-Mn-oxides or iron powder did not improve the efficacy of the lime amendment in promoting plant growth in the soils. Therefore, the issue of reducing plant exposure to metals remained unresolved in the soils under study.

KEYWORDS: heavy metals; phytoremediation; phytostabilization; Lolium perenne; phytotoxicity

CITATION: Dovletyarova E. A., Fareeva O. S., Brykova R. A., Karpukhin M. M., Smorkalov I. A., Gabechaya V. V., Vidal K., Komárek M., Neaman A. (2022). Challenges in Reducing Phytotoxicity of Metals in Soils Affected by Non-Ferrous Smelter Operations. Vol.15, № 1. Geography, Environment, Sustainability, p 112-121 https://DOI-10.24057/2071-9388-2021-141

ACKNOWLEDGEMENTS: The laboratory experiments of the present study were funded by the Russian Foundation for Basic Research (grant 20-54-26012) and the Czech Science Foundation - Grant Agency of the Czech Republic (grant 21-23794J). The writing of this article was supported by the Priority-2030 grant to Sevastopol State University (strategic project 3). The authors wish to thank Vojtěch Ettler, Denis A. Pankratov, Dmitry V. Morev and Alexander P. Zhikharev for assistance, and Irina P. Kremenetskaya for supplying soil from the Monchegorsk study area. The research team also acknowledges Andrei A. Tchourakov for editing the article. Finally, we wish to thank anonymous reviewers for their helpful comments.

"**Conflict of interests:** The authors reported no potential conflict of interest.

INTRODUCTION

Environmental issues associated with long-term operation of non-ferrous smelters are a global concern (e.g., Ettler 2016). Soil acidification caused by smelter emissions is known to increase metal solubility and mobility, resulting in higher metal toxicity in the soil (e.g., Ginocchio 2000, Korkina and Vorobeichik 2021). Note that what is referred to as "metals" or "potentially toxic metals" in this study was previously referred to as "heavy metals". However, the International Union of Pure and Applied Chemistry no longer recommends the use of the term "heavy metals" (Duffus 2002).

Polluted areas in the vicinity of non-ferrous metal smelters can act as secondary contamination sources (Luo et al. 2014). Indeed, due to the prolonged accumulation of pollutants and the deterioration of the soil cover, these areas lose their ability to bind metals and thus become uncontrolled sources of air and water pollution. One way to control metal mobility is to bind metals *in situ* by applying various additives to the soil to reduce the concentration of metals in the soil solution. Although this method does not eliminate metals from the soil, it does allow them to be converted into less soluble forms. The key criterion for evaluating the success of metal immobilization in soil is whether the toxic effects of metals on plants and soil organisms have been reduced (Lwin et al. 2018, Mahar et al. 2016).

A useful agent in reducing metal phytoavailability in acidic contaminated soils is lime (e.g., Pardo et al. 2018), which acts either by forming new solid phases – through precipitation or co-precipitation of metals – or by promoting metal adsorption on soil particles (e.g., Ma et al. 2006). For instance, lime was used in field trials at a rate of 2 t ha^{-1} to restore vegetation cover on soils in the vicinity of a Cu/Ni smelter on the Kola Peninsula, Russia (e.g., Ganicheva et al. 2004). However, our preliminary studies demonstrated that lime had not been sufficient to achieve a meaningful metal phytotoxicity reduction in soils from that site (Neaman et al. 2021, Tarasova et al. 2020). Specifically, we found that plants grown in the amended soils showed signs of metal phytotoxicity, suggesting that further experiments with combinations of multiple amendments would be required. Soil treatment with Fe- and/or Mn-based amendments has proven to be an effective technique for immobilizing metals and metalloids in contaminated soils (e.g., Komarek et al. 2013) due to the high adsorption capacity of iron oxide for potentially toxic metals (e.g., Cu, Zn, Pb, Cd) and metalloids (e.g., As) (e.g., Neaman et al. 2008, Neaman et al. 2004). Another effective method is to use iron oxide 'precursors' derived from iron powder (e.g., Kumpiene et al. 2019). As these zero-valent iron particles corrode in the soil, they produce iron oxides and hydroxides such as green rust, magnetite, ferrihydrite, hematite, and goethite (e.g., Tiberg et al. 2016).

This study was based on the hypothesis that the use of Fe- and/or Mn-based amendment additives could increase the efficacy of lime in promoting plant growth in the vicinity of non-ferrous smelters. The objective was therefore to determine the effect of different amendment combinations on plant growth in soils affected by long-term non-ferrous smelting operations. As a first step, we decided to test the selected amendments under laboratory conditions, as we have done in our previous studies (Neaman et al. 2021, Tarasova et al. 2020), before considering a field-scale investigation.

MATERIALS AND METHODS

Materials

The Soil 1 sample was taken in the industrial wasteland (67°55'70" N, 32°51'50" E) at a distance of 0.7 km from the copper-nickel (Cu/Ni) smelter located in the northern taiga subzone, near the town of Monchegorsk, Murmansk region, Russia (e.g., Slukovskaya et al. 2020) (Fig. 1). Hereafter, this smelter will be referred to as "the Cu/Ni smelter" or "the Monchegorsk site" for convenience. Peat eutrophic soil – Dystric Rheic Hemic Histosol (Toxic) (Slukovskaya et al. 2021) – was sampled from the depth of 0-5 cm. The soil was collected from 10 equidistant points of the total site area of 400 m^2. The composite soil sample was air-dried at a temperature of 20 ± 2 °C and sieved with a 1.25 mm mesh.

The Soil 2 sample was taken in fir-spruce (*Abies sibirica* and *Picea obovata*) forests at a distance of 1-3 km from the copper smelter (56°51'0.8" N 59°54'25.6" E), located in the southern taiga subzone, near the town of Revda, Sverdlovsk region, Russia (e.g., Dubrovina et al. 2021) (Fig. 1). Hereafter, this smelter will be referred to as "the Cu smelter" or "the Revda site" for convenience. The O soil horizon (hereafter "forest litter") (Dulya et al. 2019) was collected in 9 sampling plots of 25x25 m^2 at 10 random points within each plot. The

Fig. 1. Geographical locations of the study areas: (1) copper-nickel smelter located near the town of Monchegorsk, Murmansk region, and (2) copper smelter near the town of Revda, Sverdlovsk region

thickness of the litter was ~15 cm. The soils in the sampling plots are classified as Albic Retisols (Toxic), Stagnic Retisols (Toxic), and Skeletic Stagnic Retisols (Toxic) (Vorobeichik and Kaigorodova 2017). The litter samples were air-dried at room temperature and then homogenized. Coarse items (e.g., conifer cones) were thoroughly removed by hand.

Both soil samples were transferred to the laboratory of the RUDN University in Moscow. In our laboratory experiments, we also used uncontaminated eutrophic peat (Pelgorskoe brand, Russia). Hereafter, it will be referred to as "peat" for convenience. The pH of the peat was 4.0. When 10% dolomite was added to the peat, the pH increased to 6.2 ± 0.09. In addition, commercially available iron powder (<100 mm in size) with a minimal amount of admixture of Mn, Ni, and Cu (0.03%, 0.02%, and 0.003%, respectively) was used (Denis A. Pankratov, personal communication, unpublished results).

Finally, ferromanganese nodules (~24% Fe_2O_3 and ~14% MnO) from the Gulf of Finland were provided by the Olkat company, Russia. The industrial extraction of these nodules from marine shallow waters and processing is described by Zhamoida et al. (2017). The mineralogical composition (determined by X-ray diffraction analysis, PANalytical X'Pert Pro diffractometer) was dominated by goethite (FeOOH) and birnessite (nominal composition: $MnO_2 \cdot nH_2O$) with quartz, muscovite, and albite as other important components (Vojtěch Ettler, personal communication, unpublished results). The nodules were ground in mortar before being applied to the soil. Hereafter, the material resulting from the grinding process will be referred to as "Fe-Mn-oxides" for convenience.

Preliminary experiment on dolomite dosage

It can be argued that pH values >7 would be most appropriate for reducing metal uptake in the Monchegorsk histosol given the low concentrations of ammonium acetate-extractable metals at these pH values in that study area (e.g., Slukovskaya et al. 2018). However, ryegrass grows better in a slightly acidic pH environment (Spurway 1941). Therefore, a preliminary experiment was conducted to determine the appropriate dolomite doses to be used in the study. Two doses were tested: 5% w/w (giving a soil pH of 6.5) and 20% w/w (giving a soil pH of 7.4). The preliminary experiment showed that over-liming stunts plant growth (Fig. 2). Therefore, the dolomite dose was set at 5% in the further experiments of the study.

The higher dolomite dose lowered the foliar concentrations of Ni, Zn, and Cd, but had the opposite effect on the foliar concentrations of Cu and Co (Table 1). The fact that over-liming did not reduce Cu and Co uptake by ryegrass in our study is consistent with the results of other studies that investigated increased Cu solubility in alkaline soils with high dissolved organic carbon (e.g., Mondaca et al. 2015). We are inclined to think that Co uptake by ryegrass would show a similar trend, but future studies would be required to clarify this issue.

Treatments

The dosages of Fe-Mn-oxides and iron powder were based on our previous experiments (Goecke et al. 2011). The six experimental treatments performed in the present study were as follows:

Treatment 0: untreated soil;
Treatment 1: dolomite (5%);
Treatment 2: dolomite (5%) and Fe-Mn-oxides (0.5%);
Treatment 3: dolomite (5%) and Fe-Mn-oxides (1%);
Treatment 4: dolomite (5%) and iron powder (0.5%);
Treatment 5: dolomite (5%) and iron powder (1%).

Commercially available dolomitic lime (BHZ brand, Russia) was used. In all the treatments, multipurpose fertilizer (Fertika brand, Russia) was used according to the manufacturer's recommendations for grass species (0.4 g fertilizer per 1 kg of substrate). The fertilizer had the following composition of macro- and micronutrients: NH_4-N 6.6%, NO_3-N 4.4%, P_2O_5 12%, K_2O 26%, MgO 0.4%, S 0.7%, Ca 0.55%, Mn 0.16%, Cu 0.08%, B 0.09%, Fe 0.16%, Zn 0.09%, Mo 0.008%.

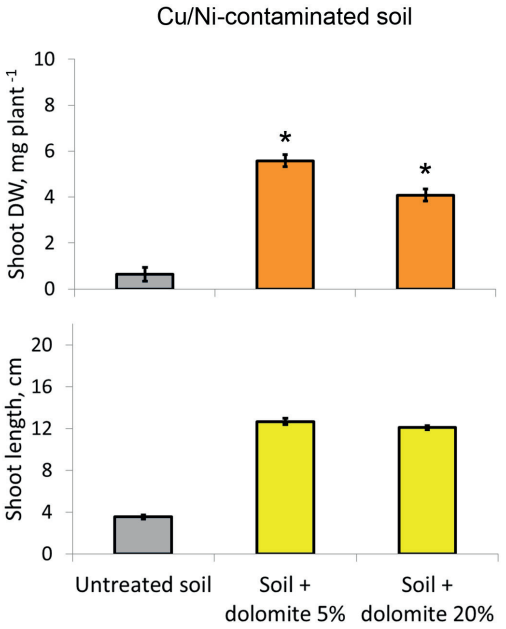

Fig. 2. Effect of different doses of dolomite (5% w/w and 20% w/w) on shoot dry weight (DW) and shoot length of ryegrass grown on Cu/Ni-contaminated soil (Histosol from Monchegorsk). Means and standard deviations are shown (n = 4). Untreated soil is also shown for comparison. Asterisks indicate a statistically significant difference between different doses of dolomite with respect to plant responses ($p < 0.05$). All-purpose fertilizer was added in all cases at a rate of 0.4 g fertilizer per 1 kg substrate

Table 1. Effect of different doses of dolomite (5% w/w and 20% w/w) on foliar metal concentrations in ryegrass grown on the Monchegorsk Histosol. The values of pH (in 0.01 N KNO^3) were 6.5 and 7.4, respectively. An asterisk indicates that the concentration of a particular metal is statistically higher in a given soil sample than in another soil sample ($p < 0.01$)

Metal	Foliar concentration, mg kg^{-1}	
	Dolomite 5%	Dolomite 20%
Cd	1.1±0.06*	0.62±0.12
Co	7.3±0.46	10±0.87*
Cu	47±17	130±7.5*
Ni	92±5.4*	74±4.3
Zn	149±7.4*	98±7.4

Peat, untreated and amended soils were wetted weekly and allowed to dry at room temperature (20-25 ºC). The weekly wetting-drying cycle continued for one month to allow sufficient time for the amendments to react in the soil. Four replicates were then used for plant bioassay, as detailed below.

Chemical characterization of the soils

Total elemental concentrations in soil and peat were determined by ICP-OES (Agilent, model 5110) after microwave digestion with a mixture of concentrated HNO3 and H_2O_2. Standard reference materials (Krasnozem and Chernozem, obtained from the Ecolan company, Russia) were used throughout the analysis, and the experimental values of the target metals were within 100 ± 20% of the certified values.

The exchangeable concentrations of Ca, Mg, Cu, Ni, Mn, Co, and Cd were also determined using ICP-OES. A solution of 0.01 M KNO_3 was used as extractant (soil/solution ratio of 1/25). This extractant is widely used for the extraction of exchangeable metals from metal-polluted soils (e.g., Almas et al. 2000, Luo et al. 2006, Moreno-Caselles et al. 2000, Perez-Esteban et al. 2013). Although chemically aggressive extractants, such as ammonium acetate buffer and 0.1 N HNO_3, are widely used (e.g., Slukovskaya et al. 2020), metal fractions extracted with chemically non-aggressive neutral salts are preferrable for assessing potential exposure of roots to metals in contaminated soils (e.g., Altimira et al. 2012, Kabata-Pendias 2004, McBride et al. 2009). The resulting suspension was shaken for 60 minutes and then filtered through ashless filter paper.

Soil pH was measured in the same extract of 0.01 M KNO_3 used for the determination of exchangeable metals. The approach of using the same extract for different purposes increases work efficiency and was used in our previous studies (e.g., Lillo-Robles et al. 2020). Furthermore, our previous study (Bustos et al. 2015) demonstrated a strong correlation (R^2 = 0.94) between pH values measured in KNO_3 extracts and those measured in soil solution obtained by Rhizons (Rhizosphere Research Products, Wageningen, Netherlands).

The organic matter content of the soil and commercial peat was estimated by loss-on-ignition at 600 °C. The following values were obtained: 87% for Soil 1 (Histosol from Monchegorsk), 62% for Soil 2 (forest litter from Revda), and 90% for commercial peat.

Plant bioassays

Plant bioassays were performed according to a standard protocol (ISO 11269-2 2012), as detailed in our previous studies (Neaman et al. 2021, Tarasova et al. 2020). Foliar elemental concentrations were determined after 21 days of growth by ICP-OES following a standard procedure of dry ashing at 600ºC and extraction of elements from the ash by 2 M HCl (Kalra 1998, Sadzawka et al. 2007). Four replicates were used for the foliar analysis. Standard reference materials (wheat, barley, rye, and peas, obtained from the Pryanishnikov All-Russian Scientific Research Institute of Agrochemistry) were used throughout the analysis, and the experimental values for the metals of interest were within 100 ± 20% of the certified values.

Statistical analysis

The effects of treatments on soil and plant responses were compared by one-way ANOVA; the Dunnett test was used for post-hoc comparisons ($p \leq 0.05$). Statistical analysis was performed using the R package DescTools (R Core Team 2021).

RESULTS AND DISCUSSION

Although both smelters have reduced their emissions in recent years (Eeva et al. 2012), there is so far no evidence that the metal content of the topsoil has decreased. In the soil from the Monchegorsk study area, the total concentrations of copper, nickel, cadmium, and cobalt were several times higher than the corresponding background concentrations (i.e., the concentrations of metals in the soil that has not been affected by anthropogenic influences) (Table 2). Copper and nickel were the main pollutants, with concentrations two orders of magnitude higher than the corresponding background levels reported in the Kashulina (2017) study. Copper and nickel are essential plant micronutrients (López and Magnitski 2011) but become toxic above a certain threshold.

It should be noted that ecotoxicological studies of metal toxicity in soil are usually based on the use of uncontaminated soils that have been progressively enriched with metals in the form of soluble salts. This approach is complicated by the difficulty of extrapolating laboratory results to actual soils exposed to decades of contamination. This is because metal toxicity depends, among other factors, on the residence time of the metals in the soil (e.g., Santa-Cruz et al. 2021b). Although many studies emphasize the importance of using actual anthropogenically contaminated soils for toxicity bioassays, the number of studies actually conducted based on this premise is relatively small.

In the soils from the Monchegorsk study area, the total concentrations of both copper and nickel exceeded the EC50 values (50% effective concentration) for phytotoxicity of metals of 987 mg kg^{-1} and 1710 mg kg^{-1}, respectively (Santa-Cruz et al. 2021a). Due to the inconsistent data on the comparative phytotoxicity of copper and nickel, and the lack of data on the phytotoxicity of cadmium and cobalt in actual anthropogenically contaminated soils (Santa-Cruz et al. 2021a), it is hard to pinpoint the exact cause of phytotoxicity in Soil 1 under study.

Meanwhile, the total concentrations of copper, zinc and cadmium in the soil from the Revda study area were several times higher than the corresponding background levels (Table 2). Copper was the main pollutant, with the concentration two orders of magnitude higher than the corresponding background reported in the study by Prudnikova et al. (2020).

Table 2. Total metal concentrations in the soils under study and in commercial peat. Background total metal concentrations in the study areas are also shown for comparison. All values are expressed in mg kg^{-1}

Metal	Soil 1	Background, Soil 1 (Kashulina 2017)	Soil 2	Background, Soil 2 (Prudnikova et al. 2020)	Peat
Cu	6418	12	5704	56	48
Ni	2293	18	57	-	6.5
Zn	82	48	2692	182	14
Cd	2.9	0.22	20	1.5	4.3
Co	77	7.4	19	-	1.8

The pH values of untreated soils were acidic (4.6 and 5.3, Monchegorsk and Revda, respectively, Table 3). Since acidic conditions make metals more soluble, thus increasing their availability (Lillo-Robles et al. 2020), we observed very high exchangeable metal concentrations in the untreated soils (Appendix A) and high metal concentrations in the shoots of *L. perenne* (Figs. 1 and 2, treatment 0). As a result, shoot length and biomass of *L. perenne* were severely inhibited in the untreated soil (Fig. 5).

In both soils, the dolomite treatments (i.e., treatments 1-5) resulted in higher pH values (Table 3) and thus lower exchangeable metal concentrations in the studied soils (Appendix A) and lower metal content in *L. perenne* shoots (Fig. 3 and 4), which was beneficial for plant growth (Fig. 5).

It is important to emphasize, however, that plant growth was slower in the dolomite-treated soil from Monchegorsk compared to the uncontaminated peat (Fig. 6A). This may be due to the fact that the metal toxicity remained high even after the dolomite treatment. Consistent with this argument, we found foliar Ni concentrations in L. perenne plants grown in Soil 1 to be above the toxicity threshold of 80 mg kg^{-1} (Table 4) for this species (Reuter and Robinson 1997). Likewise, foliar Co concentrations in L. perenne plants grown in Soil 1 were above the toxicity level for barley of 6 mg kg^{-1} (Davis et al. 1978). Thus, it is likely that Ni and Co had a toxic effect on plant growth in Soil 1 even after the dolomite treatment.

In Soil 2 treated with dolomite, foliar Zn concentration in *L. perenne* (329 mg kg^{-1}, Table 4) was higher than the lowest observed effective concentration of 221 mg kg^{-1} reported by Davis and Beckett (1978) for this species, but lower than the EC_{20} for foliar Zn concentration of 560 mg kg^{-1} reported by Smilde (1981). On the other hand, our previous study reported an EC_{50} (effective concentration 50%) value of 39 mg kg^{-1} for foliar concentration of Cu in *L. perenne* (Verdejo et al. 2015). In the present study, the foliar concentration of Cu in plants grown in Soil 2 after the dolomite treatment (Table 4) was higher than the reported EC_{50} value. Therefore, it is likely that Cu toxicity played a role in inhibiting plant growth in Soil 2 even after the dolomite treatment. Zinc toxicity is not expected in Soil 2 because zinc is known to exert an mitigating effect on copper phytotoxicity (e.g., Stuckey et al. 2021).

Table 3. The effect of treatments on soil pH determined in 0.01 M KNO_3 extract at soil/solution ratio of 1/25

Treatment	Code	pH in 0.01 M KNO_3	
		Soil 1	Soil 2
Untreated soil	0	4.6±0.04	5.3±0.08
Dolomite (5%)	1	6.5±0.05	6.2±0.13
Dolomite (5%) and Fe-Mn-oxides (0.5%)	2	6.5±0.08	6.1±0.04
Dolomite (5%) and Fe-Mn-oxides (1%)	3	6.5±0.10	6.2±0.21
Dolomite (5%) and iron powder (0.5%)	4	6.5±0.04	6.2±0.17
Dolomite (5%) and iron powder (1%)	5	6.4±0.07	6.3±0.02

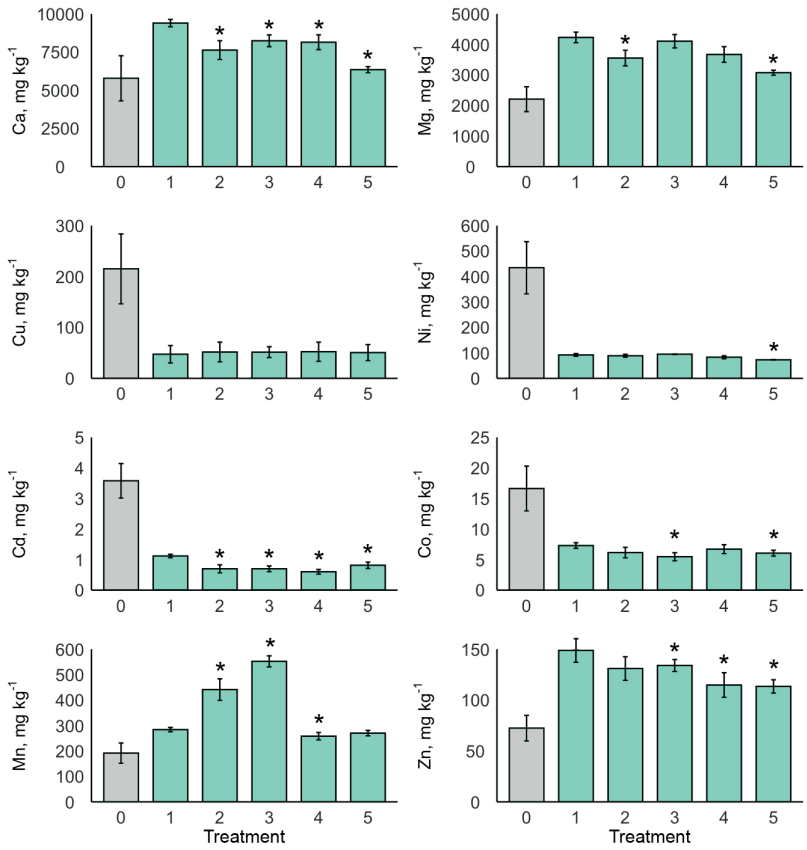

Fig. 3. Effect of treatment on the foliar concentrations of elements in ryegrass grown on Histosol from Monchegorsk, Kola Peninsula. An asterisk indicates a statistically significant difference between a particular treatment and Treatment 1 (Dunnet test, $p < 0.05$). Treatment 0 is shown but was not included in the statistical analysis

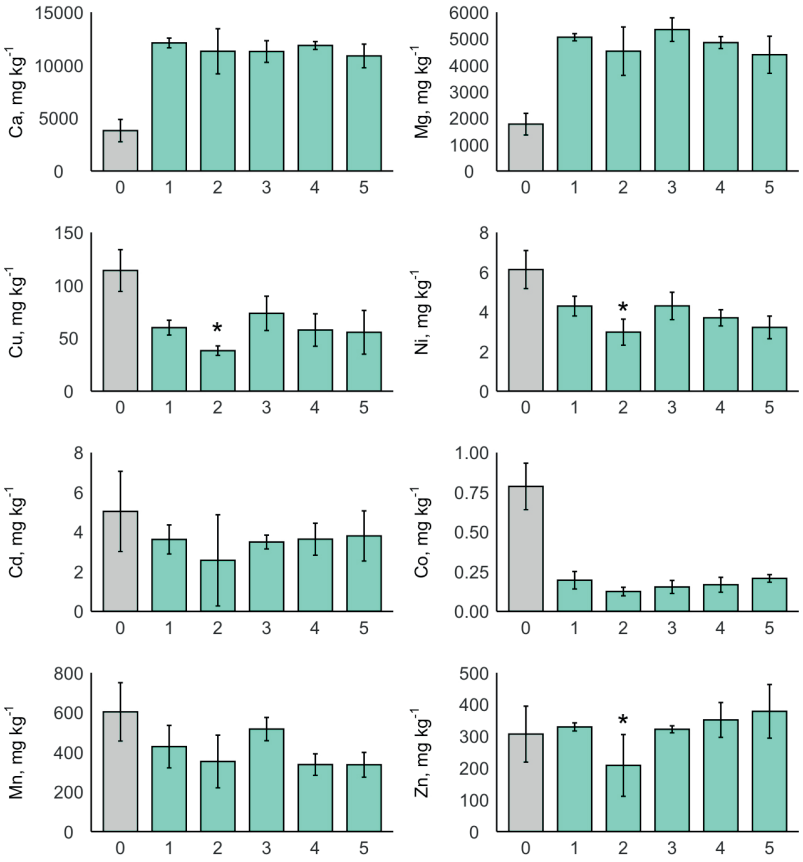

Fig. 4. Effect of treatment on the foliar concentrations of elements in ryegrass grown on forest litter from Revda. An asterisk indicates a statistically significant difference between a particular treatment and Treatment 1 (Dunnet test, p < 0.05). Treatment 0 is shown but was not included in the statistical analysis

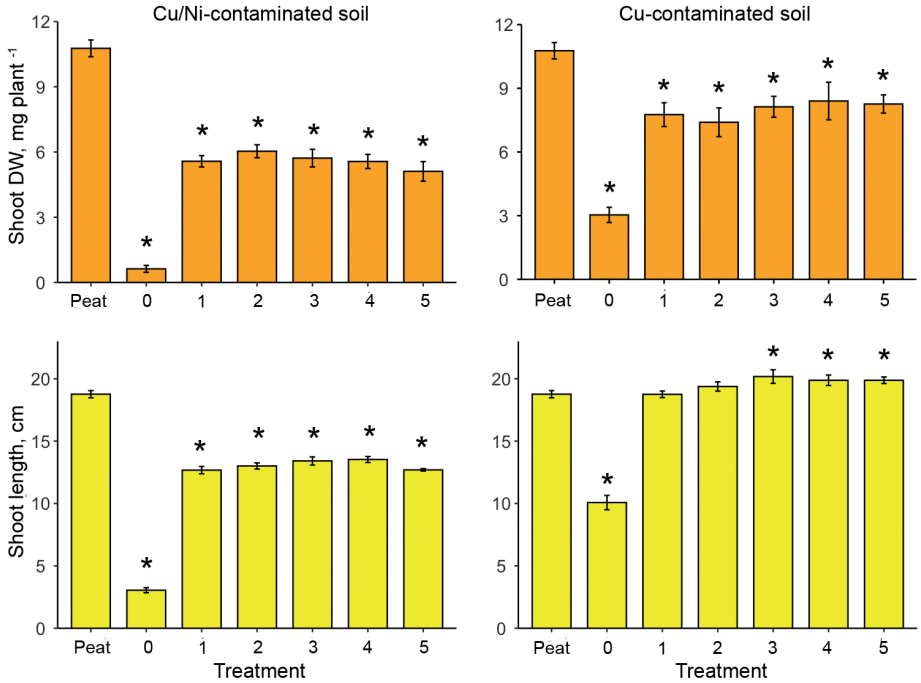

Fig. 5. Plant response to amendments. DW means dry weight. Cu/Ni-contaminated soil: Histosol from Monchegorsk; Cu-contaminated soil: forest litter from Revda). Average values and standard deviations are shown (n = 4). An asterisk indicates a statistically significant difference between a particular treatment and uncontaminated commercial peat (Dunnet test, p < 0.05). 0: untreated soil; 1: dolomite (5%); 2: dolomite (5%) and Fe-Mn-oxides (0.5%); 3: dolomite (5%) and Fe-Mn-oxides (1%); 4: dolomite (5%) and iron powder (0.5%); 5: dolomite (5%) and iron powder (1%). All-purpose fertilizer was added to all substrates, including commercial peat, at the rate of 0.4 g fertilizer per 1 kg substrate

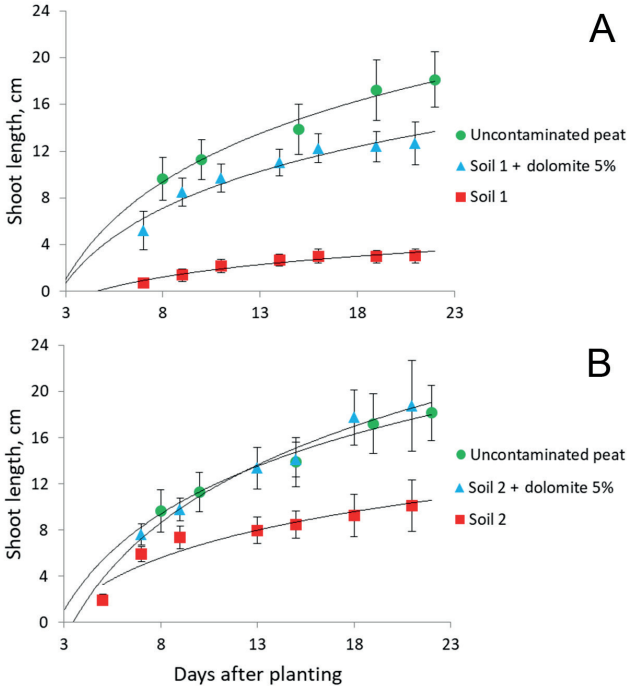

Fig. 6. Shoot length of *Lolium perenne* as a function of growth time in Soil 1 (A) and Soil 2 (B). Results are shown for untreated soil and dolomite-treated soil. Uncontaminated commercial peat is shown for comparison. The remainder of the treatments are not shown to simplify the figure and improve clarity and understanding

Table 4. Comparison of foliar metal concentrations in plants grown on soils treated with 5% dolomite. Means and standard deviations are shown (n = 4). Soil polluted with Cu and Ni corresponds to Histosol from Monchegorsk. Soil polluted with Cu corresponds to forest litter from Revda. An asterisk indicates that the concentration of a particular metal is statistically higher in a given soil sample than in another soil sample ($p < 0.01$). Toxicity threshold values for foliar concentrations of metals are also shown for comparison

Metal	Foliar metal concentrations, mg kg^{-1}		Toxicity threshold, mg kg^{-1}	Reference
	Cu/Ni-polluted soil	Cu-polluted soil		
Cu	47±17	60±7.0	39	Verdejo et al. (2015)
Ni	92±5.4*	4.3±0.5	80	Reuter and Robinson (1997)
Zn	149±8	329±13*	560	Smilde (1981)
Co	7.3±0.46*	0.2±0.05	6.0	Davis et al. (1978)
Cd	1.1±0.06	3.6±0.73*	15	Davis et al. (1978)

Finally, in our previous study (Goecke et al. 2011), treatment of contaminated soil with iron powder at 0.5% and 1% resulted in a significant reduction in copper solubility, which improved plant growth. In the present study, however, the difference between Treatment 1 (without Fe- and/or Mn-based amendments) and Treatments 2-5 (with Fe- and/or Mn-based amendments) was either not statistically significant ($p > 0.05$) or not substantial in terms of exchangeable metal concentrations in soil (Appendix A), metal concentrations in shoots (Fig. 3 and 4), and plant growth (Fig. 5). We are inclined to think that higher doses of Fe- and/or Mn-based amendments would improve the efficacy of the lime treatment in promoting plant growth in soils from the vicinity of non-ferrous smelters.

CONCLUSION

Many large metallurgical enterprises are located on the territory of Russia and the problem of soil pollution by emissions from such companies is therefore of particular concern to Russia. Therefore, the topic of the article is relevant and timely.

The addition of 0.5% and 1% of Fe-Mn-oxides or iron powder did not improve the efficacy of the lime amendment in promoting plant growth in soils from the vicinity of a Cu/Ni or Cu smelter. Thus, the challenge of reducing plant metal exposure remained unresolved in the soils studied. However, it is important to publish the results of unsuccessful studies, as negative results are also an important part of the scientific community's knowledge base.

In future studies, we plan to investigate other Fe- and/or Mn-based amendments, such as zero-valent iron nanoparticles, which have been proven to be effective metal sorbents (e.g., Mitzia et al. 2020). Likewise, higher application rates of iron amendments should be considered in future studies.

REFERENCES

Almas A.R., McBride M.B., and Singh B.R. (2000). Solubility and lability of cadmium and zinc in two soils treated with organic matter. Soil Science 165, 250-259, DOI: 10.1097/00010694-200003000-00007.

Altimira F., Yáñez C., Bravo G., González M., Rojas L., and Seeger M. (2012). Characterization of copper-resistant bacteria and bacterial communities from copper-polluted agricultural soils of central Chile. BMC Microbiology 12, 193, DOI: 10.1186/1471-2180-12-193

Bustos V., Mondaca P., Sauvé S., Gaete H., Celis-Diez J.L., and Neaman A. (2015). Thresholds of arsenic toxicity to Eisenia fetida in field-collected agricultural soils exposed to copper mining activities in Chile. Ecotoxicology and Environmental Safety 122, 448-454, DOI: 10.1016/j.ecoenv.2015.09.009.

Davis R.D., and Beckett P.H.T. (1978). Upper critical levels of toxic elements in plants. 2. Critical levels of copper in young barley, wheat, rape, lettuce and ryegrass, and of nickel and zinc in young barley and ryegrass. New Phytologist 80, 23–32, DOI: 10.1111/j.1469-8137.1978.tb02261.x

Davis R.D., Beckett P.H.T., and Wollan E. (1978). Critical levels of twenty potentially toxic elements in young spring barley. Plant and Soil 49, 395-408, DOI: 10.1007/BF02149747.

Dubrovina T.A., Losev A.A., Karpukhin M.M., Vorobeichik E.L., Dovletyarova E.A., Brykov V.A., Brykova R.A., Ginocchio R., Yáñez C., and Neaman A. (2021). Gypsum soil amendment in metal-polluted soils—an added environmental hazard. Chemosphere 281, 130889, DOI: 10.1016/j.chemosphere.2021.130889.

Duffus J.H. (2002). «Heavy metals» a meaningless term? (IUPAC Technical Report). Pure and Applied Chemistry 74, 793–807, DOI: 10.1351/pac200274050793

Dulya O.V., Bergman I.E., Kukarskih V.V., Vorobeichik E.L., Smirnov G.Y., and Mikryukov V.S. (2019). Pollution-induced slowdown of coarse woody debris decomposition differs between two coniferous tree species. Forest Ecology and Management 448, 312-320, DOI: 10.1016/j.foreco.2019.06.026.

Eeva T., Belskii E., Gilyazov A.S., and Kozlov M.V. (2012). Pollution impacts on bird population density and species diversity at four non-ferrous smelter sites. Biological Conservation 150, 33-41, DOI: 10.1016/j.biocon.2012.03.004.

Ettler V. (2016). Soil contamination near non-ferrous metal smelters: A review. Applied Geochemistry 64, 56-74, DOI: 10.1016/j.apgeochem.2015.09.020.

Ganicheva S.N., Lukina N.V., Kostina V.A., and Nikonov V.V. (2004). Technogenic degradation and demutation succession in coniferous forests of the Kola Peninsula. Lesovedenie 3, 57-67.

Ginocchio R. (2000). Effects of a copper smelter on a grassland community in the Puchuncaví Valley, Chile. Chemosphere 41, 15-23, DOI: 10.1016/S0045-6535(99)00385-9.

Goecke P., Ginocchio R., Mench M., and Neaman A. (2011). Amendments promote the development of Lolium perenne in soils affected by historical copper smelting operations. International Journal of Phytoremediation 13, 552-566, DOI: 10.1080/15226514.2010.495150.

ISO 11269-2 (2012). Soil quality - Determination of the effects of pollutants on soil flora - Part 2: Effects of chemicals on the emergence and growth of higher plants. Genève, Switzerland: International Organization for Standardization.

Kabata-Pendias A. (2004). Soil-plant transfer of trace elements - An environmental issue. Geoderma 122, 143-149, DOI: 10.1016/j.geoderma.2004.01.004.

Kalra Y.E. (1998). Handbook of Reference Methods for Plant Analysis. Boca Raton, FL, USA: Soil and Plant Analysis Council, CRC Press.

Kashulina G.M. (2017). Extreme pollution of soils by emissions of the copper-nickel industrial complex in the Kola Peninsula. Eurasian Soil Science 50, 837-849, DOI: 10.1134/s1064229317070031.

Komarek M., Vanek A., and Ettler V. (2013). Chemical stabilization of metals and arsenic in contaminated soils using oxides - A review. Environmental Pollution 172, 9-22, DOI: 10.1016/j.envpol.2012.07.045.

Korkina I.N., and Vorobeichik E.L. (2021). Non-typical degraded and regraded humus forms in metal-contaminated areas, or there and back again. Geoderma 404, DOI: 10.1016/j.geoderma.2021.115390.

Kumpiene J., Antelo J., Brannvall E., Carabante I., Ek K., Komárek M., Soderberg C., and Warell L. (2019). In situ chemical stabilization of trace element-contaminated soil - Field demonstrations and barriers to transition from laboratory to the field - A review. Applied Geochemistry 100, 335-351, DOI: 10.1016/j.apgeochem.2018.12.003.

Lillo-Robles F., Tapia-Gatica J., Díaz-Siefer P., Moya H., Celis-Diez J.L., Santa Cruz J., Ginocchio R., Sauvé S., Brykov V.A., and Neaman A. (2020). Which soil Cu pool governs phytotoxicity in field-collected soils contaminated by copper smelting activities in central Chile? Chemosphere 242, 125176, DOI: 10.1016/j.chemosphere.2019.125176.

López M.Á., and Magnitski S. (2011). Nickel: The last of the essential micronutrients. Agronomia Colombiana 29, 49-56.

Luo L.Q., Chu B.B., Liu Y., Wang X.F., Xu T., and Bo Y. (2014). Distribution, origin, and transformation of metal and metalloid pollution in vegetable fields, irrigation water, and aerosols near a Pb-Zn mine. Environmental Science and Pollution Research 21, 8242-8260, DOI: 10.1007/s11356-014-2744-8.

Luo X.-S., Zhou D.-M., Liu X.-H., and Wang Y.-J. (2006). Solid/solution partitioning and activity of heavy metals in the contaminated agricultural soils around a copper mine in eastern Nanjing city, China. Journal of Hazardous Materials A131, 19-27, DOI: 10.1016/j.jhazmat.2005.09.033.

Lwin C.S., Seo B.H., Kim H.U., Owens G., and Kim K.R. (2018). Application of soil amendments to contaminated soils for heavy metal immobilization and improved soil quality-a critical review. Soil Science and Plant Nutrition 64, 156-167, DOI: 10.1080/00380768.2018.1440938.

Ma Y., Lombi E., Oliver I.W., Nolan A.L., and McLaughlin M.J. (2006). Long-term aging of copper added to soils. Environmental Science & Technology 40, 6310-6317, DOI: 10.1021/es060306r.

Mahar A., Wang P., Ali A., Awasthi M.K., Lahori A.H., Wang Q., Li R.H., and Zhang Z.Q. (2016). Challenges and opportunities in the phytoremediation of heavy metals contaminated soils: A review. Ecotoxicology and Environmental Safety 126, 111-121, DOI: 10.1016/j.ecoenv.2015.12.023.

McBride M.B., Pitiranggon M., and Kim B. (2009). A comparison of tests for extractable copper and zinc in metal-spiked and field-contaminated soil. Soil Science 174, 439-444, DOI: 10.1097/SS.0b013e3181b66856.

Mitzia A., Vitkova M., and Komarek M. (2020). Assessment of biochar and/or nano zero-valent iron for the stabilisation of Zn, Pb and Cd: A temporal study of solid phase geochemistry under changing soil conditions. Chemosphere 242, DOI: 10.1016/j.chemosphere.2019.125248.

Mondaca P., Neaman A., Sauvé S., Salgado E., and Bravo M. (2015). Solubility, partitioning and activity of copper in contaminated soils in a semiarid zone. Journal of Plant Nutrition and Soil Science 178, 452-459, DOI: 10.1002/jpln.201400349.

Moreno-Caselles J., Moral R., Perez-Espinosa A., and Perez-Murcia M.D. (2000). Cadmium accumulation and distribution in cucumber plant. Journal of Plant Nutrition 23, 243-250, DOI: 10.1080/01904160009382011.

Neaman A., Martinez C.E., Trolard F., and Bourrie G. (2008). Trace element associations with Fe- and Mn-oxides in soil nodules: Comparison of selective dissolution with electron probe microanalysis. Applied Geochemistry 23, 778-782, DOI: 10.1016/j.apgeochem.2007.12.025.

Neaman A., Mouélé F., Trolard F., and Bourrié G. (2004). Improved methods for selective dissolution of Mn oxides: Applications for studying trace element associations. Applied Geochemistry 19, 973-979, DOI: 10.1016/j.apgeochem.2003.12.002.

Neaman A., Tapia-Pizarro F., Tarasova E., Brykov V., Brykova R., Slukovskaya M., Guzmán-Amado C., and Stuckey J.W. (2021). The challenge of reducing metal phytotoxicity in soils affected by historical nickel-copper smelting operations in the Kola Peninsula, Russia. AgroSur 49, 5-11, DOI: 10.4206/agrosur.2021.v49n1-02.

Pardo J., Mondaca P., Celis-Diez J.L., Ginocchio R., Navarro-Villarroel C., and Neaman A. (2018). Assessment of revegetation of an acidic metal(loid)-polluted soils six years after the incorporation of lime with and without compost. Geoderma 331, 81-86, DOI: 10.1016/j.geoderma.2018.06.018.

Perez-Esteban J., Escolastico C., Moliner A., and Masaguer A. (2013). Chemical speciation and mobilization of copper and zinc in naturally contaminated mine soils with citric and tartaric acids. Chemosphere 90, 276-283, DOI: 10.1016/j.chemosphere.2012.06.065.

Prudnikova E.V., Neaman A., Terekhova V.A., Karpukhin M.M., Vorobeichik E.L., Smorkalov I.A., Dovletyarova E.A., Navarro-Villarroel C., Ginocchio R., and Peñaloza P. (2020). Root elongation method for the quality assessment of metal-polluted soils: Whole soil or soil-water extract? Journal of Soil Science and Plant Nutrition 20, 2294-2303, DOI: 10.1007/s42729-020-00295-x.

R Core Team (2021). R: A language and environment for statistical computing. Vienna, Austria: R Foundation for Statistical Computing.

Reuter D., and Robinson J. (1997). Plant Analysis: an Interpretation Manual. CSIRO Publishing.

Sadzawka A., Carrasco M.A., Demanet R., Flores H., Grez R., Mora M.L., and Neaman A. (2007). Métodos de análisis de tejidos vegetales. Segunda Edición. Serie actas INIA Nº 40. Santiago, Chile: Instituto de Investigaciones Agropecuarias.

Santa-Cruz J., Peñaloza P., Korneykova M.V., and Neaman A. (2021a). Thresholds of metal and metalloid toxicity in field-collected anthropogenically contaminated soils: A review. Geography, Environment, Sustainability 14, 6-21, DOI: 10.24057/2071-9388-2021-023.

Santa-Cruz J., Vasenev I.I., Gaete H., Peñaloza P., Krutyakov Y.A., and Neaman A. (2021b). Metal ecotoxicity studies with spiked versus field-contaminated soils: Literature review, methodological shortcomings and research priorities. Russian Journal of Ecology 52, 478-484, DOI: 10.1134/S1067413621060126.

Slukovskaya M., Kremenetskaya I., Drogobuzhskaya S., Ivanova L., Mosendz I., and Novikov A. (2018). Serpentine mining wastes-materials for soil rehabilitation in Cu-Ni polluted wastelands. Soil Science 183, 141-149, DOI: 10.1097/SS.0000000000000236.

Slukovskaya M.V., Vasenev V.I., Ivashchenko K.V., Dolgikh A.V., Novikov A.I., Kremenetskaya I.P., Ivanova L.A., and Gubin S.V. (2020). Organic matter accumulation by alkaline-constructed soils in heavily metal-polluted area of Subarctic zone. Journal of Soils and Sediments, DOI: 10.1007/s11368-020-02666-4.

Slukovskaya M.V., Vasenev V.I., Ivashchenko K.V., Dolgikh A.V., Novikov A.I., Kremenetskaya I.P., Ivanova L.A., and Gubin S.V. (2021). Organic matter accumulation by alkaline-constructed soils in heavily metal-polluted area of Subarctic zone. Journal of Soils and Sediments 21, 2071-2088, DOI: 10.1007/s11368-020-02666-4.

Smilde K.W. (1981). Heavy-metal accumulation in crops grown on sewage sludge amended with metal salts. Plant and Soil 62, 3-14, DOI: 10.1007/bf02205020.

Spurway C.H. (1941). Soil reaction (pH) preferences of plants. Special Bulletin. Michigan Agricultural Experiment Station, 306.

Stuckey J.W., Mondaca P., and Guzmán-Amado C. (2021). Impact of mining contamination source on copper phytotoxicity in agricultural soils from central Chile. AgroSur 49, 21-27, DOI: 10.4206/agrosur.2021.v49n1-04.

Tarasova E., Drogobuzhskaya S., Tapia-Pizarro F., Morev D.V., Brykov V.A., Dovletyarova E.A., Slukovskaya M., Navarro-Villarroel C., Paltseva A.A., and Neaman A. (2020). Vermiculite-lizardite industrial wastes promote plant growth in a peat soil affected by a Cu/Ni smelter: a case study at the Kola Peninsula, Russia. Journal of Soil Science and Plant Nutrition 20, 1013-1018, DOI: 10.1007/s42729-020-00188-z.

Tiberg C., Kumpiene J., Gustafsson J.P., Marsz A., Persson I., Mench M., and Kleja D.B. (2016). Immobilization of Cu and As in two contaminated soils with zero-valent iron - Long-term performance and mechanisms. Applied Geochemistry 67, 144-152, DOI: 10.1016/j.apgeochem.2016.02.009.

Verdejo J., Ginocchio R., Sauvé S., Salgado E., and Neaman A. (2015). Thresholds of copper phytotoxicity in field-collected agricultural soils exposed to copper mining activities in Chile. Ecotoxicology and Environmental Safety 122, 171-177, DOI: 10.1016/j.ecoenv.2015.07.026.

Vorobeichik E.L., and Kaigorodova S.Y., 2017. Long-term dynamics of heavy metals in the upper horizons of soils in the region of a copper smelter impacts during the period of reduced emission. Eurasian Soil Science. 977-990.

Zhamoida V., Grigoriev A., Ryabchuk D., Evdokimenko A., Kotilainen A.T., Vallius H., and Kaskela A.M. (2017). Ferromanganese concretions of the eastern Gulf of Finland - Environmental role and effects of submarine mining. Journal of Marine Systems 172, 178-187, DOI: 10.1016/j.jmarsys.2017.03.009.

Appendix A. Effect of treatment on the concentration of exchangeable cations in Histosol from Monchegorsk (Soil 1) and forest litter from Revda (Soil 2). A 0.01 N KNO_3 solution with a soil/solution ratio of 1/25 was used for extraction.

Treatment	Ca_{exch}	Mg_{exch}	Cu_{exch}	Ni_{exch}	Zn_{exch}	Mn_{exch}	Co_{exch}	Cd_{exch}
	mg kg^{-1} of air-dry substrate							
Soil 1								
0	522±53	203±15	65±5	150±15	13±1.5	53±5.3	6±0.59	0.1±0.02
1	**1579±120**	**720±30**	**13±0.5**	**16±0.9**	**2±0.37**	**11±0.8**	**0.7±0.05**	**bdl**
2	1536±67	641±29*	13±1.0	15±0.6	2.1±0.44	41±1.8*	0.6±0.03	bdl
3	1534±33	681±11	12±0.9	16±0.6	4.8±3.31	57±1.8*	0.6±0.02*	bdl
4	1547±81	673±14	11±0.7*	14±0.5*	4.7±4.7	11±0.5	0.7±0.02	bdl
5	1496±124	640±49	11±1.5	14±1.1	3.8±5.85	11±1.0	0.7±0.06	bdl
Soil 2								
0	567±89	147±25	14±12	0.4±0.09	34±6.3	67±16	0.1±0.03	0.8±0.11
1	**1268±128**	**295±21**	**8.0±0.8**	**0.2±0.03**	**11±1.0**	**10±3.3**	**bdl**	**0.3±0.03**
2	1124±47	275±15	9.0±2.0	0.3±0.1	8.9±0.71	15±6.5	bdl	0.2±0.04
3	1238±15	324±5.0	8±0.7	0.2±0.02	8.4±0.07*	16±2.8	bdl	0.2±0.01*
4	1266±77	298±21	8±1.1	0.2±0.02	8.5±0.83	7.0±2.0	bdl	0.2±0.02
5	1151±26	282±6.0	8±1.9	0.2±0.03	7.6±0.56*	6.0±1.4	bdl	0.2±0.01*

An asterisk indicates a statistically significant difference compared to Treatment 1. Treatment 0 is shown but was not included in the statistical analysis. bdl means below the detection limit.

RESEARCH PAPER

CLIMATIC FACTOR IMPACT ON THE HEIGHT GROWTH OF LAPLAND PINE IN THE NORTHWESTERN RUSSIA

Elena N. Popova[1*], Anna E. Koukhta[2], Igor O. Popov[2]

[1]Institute of Geography of the Russian Academy of Sciences, Staromonetniy pereulok, 29, Moscow, 119017, Russia

[2]Yu.A. Izrael' Institute of Global Climate and Ecology, Glebovskaya str., 20b, Moscow, 107258, Russia

***Corresponding author:** en_popova@igras.ru

Received: May 15th, 2021 / Accepted: February 15th, 2022 / Published: March 31st, 2022

https://DOI-10.24057/2071-9388-2021-055

ABSTRACT. Lapland pine (*Pinus sylvestris* var. *lapponica Hartm.*) is a geographical and climatic ecotype and subspecies of *Pinus sylvestris* L. It is widespread in the north of Eurasia. Its height growth is interconnected with both climatic parameters and the state of the habitat of pine trees. Long-term data on height growth indices of Lapland pine from various humid biogeocenoses of three specially protected natural territories of Northwestern Russia were studied. Also, sixteen basic climatic parameters averaged over the growth period of the examined trees were calculated for these regions. The comparison of different climatic parameters and pine stand height growth in various biogeocenoses was made using cluster analysis. It was established that the mean daily average temperature in January (-9.4°C, -10.4°C, -16.1°C in the Kivach, Polar Circle and Pechora-Ilych Reserves respectively) and the amount of precipitation in spring and early summer periods have a primary influence on the cluster similarity of the Lapland pine height growth in Northwestern Russia. The similarity of soil and biocenotic conditions also influenced the similarity of Lapland pine height growth indices, but had a lower rank within the two main clusters distinguished by climatic values. Our studies showed that it is possible to identify the rank influence of the most significant climatic factors and biogeocenotic conditions on the pine height growth using cluster analysis.

KEYWORDS: Lapland pine, height growth, climatic factors, soils, cluster analysis

CITATION: Popova E. N., Koukhta A. E., Popov I. O. (2022). Climatic Factor Impact On the Height Growth Of Lapland Pine in The Northwestern Russia. Vol.15, № 1. Geography, Environment, Sustainability, p 122-129
https://DOI-10.24057/2071-9388-2021-055

ACKNOWLEDGEMENTS: The authors express their gratitude to the heads of the surveyed specially protected natural territories (Reserves) for their help and assistance in the fieldwork. The study was carried out in the framework of the state assignments of the Institute of Geography of the Russian Academy of Sciences no. AAAA-A19-119021990093-8 (FMGE-2019-0007) "Assessment of geographical, hydrological and biotic environmental changes and their effects for the development of a basis for stable environmental management" - data processing and analysis of the results, and AAAA-A19-119022190173-2 (FMGE-2019-0009) "Climate Change and Consequences for the Environment and Population Life and Activities on the Territory of Russia" – climate data analysis, and the themes of Roshydromet no. 3.2 for 2020–2024 "Monitoring of the Global Climate and the Climate of the Russian Federation and Its Regions Including the Arctic: Development and Modernization of Monitoring Technologies" - climate data processing, and no. AAAA-A20-120013190049-4 - data collection from Lapland pine stands.

"**Conflict of interests:** The authors reported no potential conflict of interest.

INTRODUCTION

Forest ecosystems play an important role in the life of our planet. They "provide ecological, economic, social and aesthetic services to natural systems and humanity" (Bonan 2008). Tree species are closely related both to macroecological conditions, including the climate of the regions in which they grow, and to microecological conditions, such as the soil, which nourishes and saturates them through the root system. The annual growth rate of pine depends on weather conditions (temperature and humidity), both current and over several previous years. This dependence is especially evident in extreme conditions of pine growth, including areas on the northern border of the range (Elagin, 1976; Rysin and Savelyeva, 2008).

The species *Pinus sylvestris* L. is characterised by a high degree of polymorphism, i.e. the presence of a wide variety of intraspecific forms (Pravdin 1964). The largest taxonomic ranks within this species are distinguished based on the geographical area of the individual population. The main forest-forming species of the Russian North European taiga territory is Lapland pine (*Pinus sylvestris* subsp. *lapponica Holmb.* or *Pinus sylvestris* var. *lapponica Hartm.*), one of the geographic subspecies of *Pinus sylvestris* L. (Plant List 2022; Gymnosperm DB 2022). This subspecies is widespread in Eurasia north of 61-62° N. This is a low plant with a maximum height of 20 m. There is also a wide variety of morphogenesis determined by the soil ecological conditions in the area of growth, which results in lower taxonomic ranks that stand out at the species level of *Pinus sylvestris* L. within the main subspecies. In particular, the swamp edaphic ecotype var. nana Pall., which grows in moist and waterlogged ecotopes (Pravdin 1964, Plant List 2022).

One of the main types of pine response to various environmental conditions is its linear growth (=height growth). Its variability is closely related to climatic factors and ecological conditions (Koukhta 2003; Chernogaeva and Kuhta 2018; Jansons et al. 2013a, b; Pozdnyakova et al. 2019; Zhou et al. 2019). The height growth of *Pinus sylvestris* L. in cold and moist regions is limited by the temperature in the previous summer and the length of the growing period (McCarroll et al. 2003; Pensa et al. 2005; Salminen and Jalkanen 2005). On the other hand, height growth of pine in southern regions is restricted by the amount of precipitation and available water, showing a positive correlation with summer precipitation and a negative correlation with summer temperature (Dobbertin et al. 2010; Mutke et al. 2003; Thabeet et al. 2009). Despite the importance of the linear growth indicators in studying various stands and their changes, the attention to it among research communities is much lower than to the radial growth of trees (Jansons et al. 2013a; Sánchez-Salguero et al. 2015; van der Maaten et al. 2017; Misi et al. 2019). Identifying the effects of each of these factors is a difficult but important task for understanding the relationships in the "climate-soil-plant" system in various biogeocenoses. Most often, correlation and regression analyzes are used to identify the relationship between environmental factors and linear growth. Cluster analysis stands out in multivariate statistical analysis, but it is rarely used for assessing the influence of ecological factors on plant trait changes. However, the advantage of the method is that it allows to compare qualitative and quantitative features and to build their classification systems (Gitis 2003).

The aim of this work was to assess the soil biocenosis and climatic characteristics of three different areas of Lapland pine growth, as well as to identify the relationships between individual soil and climatic parameters and the linear growth of this subspecies in the North European Russia using cluster analysis.

MATERIALS AND METHODS

Study area

Studies were carried out in three specially protected natural territories (SPNTs) located in Northern Russia: the Kivach state nature reserve (SNR) (KNR 2020), the Polar Circle state nature complex reserve (SNCR) of regional significance (BCNKC 2020), and the Pechora-Ilych state nature biosphere reserve (SNBR) (PISNBR 2020) (Fig. 1). According to the climatic classification of B.P. Alisov (1956), Polar Circle and Kivach Reserves are part of the northwestern subregion of the Atlantic-Arctic forest region of the temperate zone, and the Pechora-Ilych Reserve is located in the northeastern subregion of the same region, which has a more continental climate compared to the northwestern one (Fig. 1). The climate of investigated regions is characterized as cold and quite humid.

According to the geographical zoning of soils, all studied SPNTs are located in the European-West Siberian taiga forest region of podzolic and sod-podzolic soils of the Boreal belt (Dobrovol'skii and Urusevskaya 2004). In terms of vegetation zoning, all the studied protected areas belong to the Holarctic Boreal subkingdom, Circumboreal region (Voronov et al. 2002).

The Kivach SNR is located on the northwestern coast of Onega Lake in the southeastern region of the Baltic (Fennoscandinavian) crystalline shield. The territory of the reserve is characterized by a complex topography, formed as a result of tectonic and glacial processes. Ridge and hilly landforms here are interspersed by glacial lacustrine plains and swampy depressions (Fedorets et al. 2006). The variety of landforms determines the complexity of the soil cover. The territory corresponds to the Karelia province of alpha-humus podzols and bog soils of the middle taiga podzolic soils subzone (Dobrovol'skii and Urusevskaya 2004). The most biocenoses of the Kivach reserve are represented by

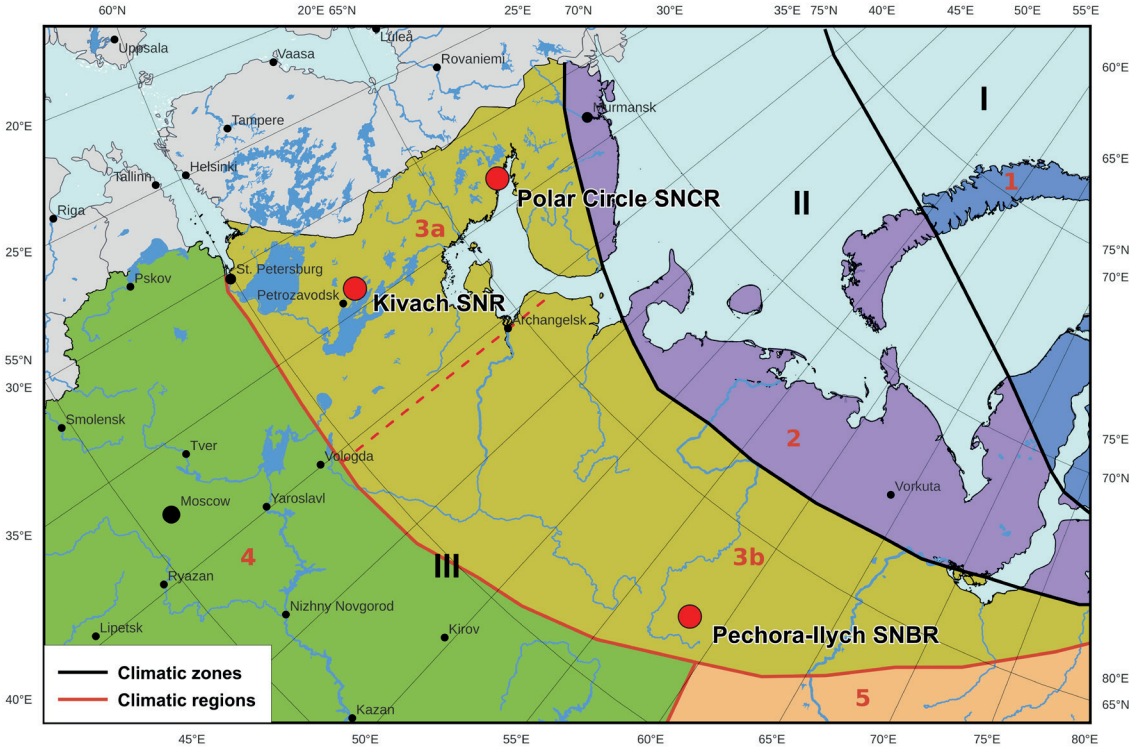

Fig. 1. Geographical location of studied territories: Climate zones: I – Arctic, II – Subarctic, III - Temperate. Climate regions: 1 – Atlantic arctic, 2 – Atlantic subarctic, 3 – Atlantic-Arctic forest (a - northwestern subregion, b - northeastern subregion), 4 – Atlantic-Continental forest, 5 - Continental forest West-Siberian. Borders of climate zones and regions are given according to the classification of B.P. Alisov (1956)

different pine forests (Fedorets et al. 2006). The territory is located on the border of the ranges of *Pinus sylvestris* L. subspecies *P. sylvestris* var. *sylvestris L.* and *Pinus sylvestris* var. *lapponica Hartm*.

The Polar Circle SNCR is located in the Loukhsky municipal district in the northern part of the Karelian Republic, on the northwest coast of the White Sea in the Kandalaksha Bay coastal zone. The region belongs to the Kola-Karelia province of alpha-humus podzols and bog soils of the northern taiga gley-podzolic and podzol soils subzones (Dobrovol'skii and Urusevskaya 2004). There are three main types of landscapes in the Polar Circle SNCR. The major part is occupied by the North-taiga East European lowland (57.6%). Other types of landscapes are represented by various swamps (6.2%) and marine areas (36.2%) (SPTsR 2020).

The Pechora-Ilych SNBR is located in the Komi Republic on the western slope of the Ural Mountains. Currently, it consists of two isolated sections located in the southwestern and eastern parts of the Upper Pechora and Ilych interfluve. The studies were carried out in the Yakshinsky (southwestern) site, which is bounded by a segment of the Pechora River between the mouths of its right and left bank tributaries of Polovinnaya and Krutaya. The reserve is part of the Onego-Vychegda province of podzolic and bog-podzolic soils of the middle taiga podzolic soils subzone (Dobrovol'skii and Urusevskaya 2004). Most of the reserve is occupied by coniferous forests. In depressions, there are raised and transitional sphagnum bogs (Degteva and Lapteva 2013). The dominant tree is Pinus sylvestris L. Similarly to the Kivach reserve, the Pechora-Ilych SNBR is located on the southern border of the Lapland pine and the northern border of Scots pine ranges (Pravdin 1964).

Stand data

We investigated the annual variability of the indexed linear growth of Lapland pine in humid ecotopes, which were distinguished according to the V.N. Sukachev classical typology (Sukachev 1972). The classification of soil for each examined area was carried out based on the following studies (Egorov et al. 1977; Degteva and Lapteva 2013; Fedorets et al. 2006). The object of our study was the swamp edaphic ecotype of Lapland pine, which is represented in fig. 2.

The studies spanned multiple years, lasting from 2000 to 2013. Measurements were conducted for undergrowth, young stand and maturing trees of Lapland pine. For unification, trees with similar morphological and age characteristics were selected. The height of measured trees was above 1 m and below 2.5 m. The age of registered undergrowth and maturing trees was 7-25 years. Stem internodes were measured on each tree, starting from the top (current year growth) and to the last clearly distinguishable one near the ground. The variability of the series of growths was estimated using standard deviation. The series of growths were indexed using the standard method adopted in dendrochronology by dividing the absolute values of each year's growth by a moving average over 5 years. A similar procedure was used to remove the age trend and obtain annual deviations from the course of growth. Then, the obtained values were averaged over the trial plots. The calculation technique is described in (Koukhta and Titkina 2005).

Climate data

For all three areas, we also calculated 16 climatic parameters that could affect the Lapland pine linear growth. The calculations were carried out based on daily resolution meteorological data, which included ground-based measurements of air temperature and precipitation on a network of Roshydromet international exchange hydrometeorological stations located in the areas of research (RSRIHI-WDC 2014). The values were averaged over the period 1991-2010, which coincides with the research period and the previous growing time of the examined trees. The calculated climatic parameters are:

Total annual precipitation (TAP): sum of precipitation for the year, mm;

Precipitation in spring (PSp): sum of precipitation for the period from March to May, mm;

Precipitation in April-June (PAJn): sum of precipitation for the period from April to June, mm;

Precipitation in July-September (PJlS): sum of precipitation for the period from July to September, mm;

Precipitation in the cold season (PCS): sum of precipitation from October to April, mm;

Precipitation in the growing season (PGS): sum of precipitation from May to September, mm;

Mean annual air temperature (MAAT): mean annual daily average air temperature, °C;

Fig. 2. The swamp edaphic ecotype of Lapland pine in a typical humid ecotope, the Polar Circle SNCR (Foto by A.E. Koukhta, unpublished)

Mean temperature in May (MTM): average daily temperature in May, °C;

Mean temperature in the warmest month (MTWM): average daily temperature in July, °C;

Mean temperature in the coldest month (MTCM): average daily temperature in January, °C;

Sum of active temperatures above 5°C (SAT>5°C) and above 10°C (SAT>10°C), °C×days (Equation 1):

$$T_a = \sum_{n=1}^{d} T_{n,>T_0} \quad (1)$$

where T_a is the annual sum of active temperatures (SAT), T_n is the average daily air temperature above the temperature threshold T_0 which in this work is 10°C for a time period d corresponding to the number of days in a year (Popova et al. 2017);

The number of days in a year with the daily average temperature above 5°C (NDY>5°C) and above 10°C (NDY>10°C), days;

The hydrothermal coefficient (HTC) of Selyaninov was calculated according to Equation 2:

$$HTC = \frac{r_n}{0.1\sum T_n} \quad (2)$$

where r_n is the sum of daily precipitation in the growing season (PGS) of the calendar year n; ΣT_n is the sum of the daily average active air temperatures with a threshold of 10°C for the same period of the year (May-September) (Selyaninov 1928);

The simplified aridity index (SAI) of Budyko was calculated according to Equation 3 (Sirotenko and Pavlova 2012):

$$SAI = \frac{0.18\sum T_{>10^0}}{r_{I-XII}} \quad (3)$$

where $\sum T_{>10^0}$ is the annual sum of active air temperatures above 10°C (SAT>10°C); r_{I-XII} is the annual amount of precipitation (TAP).

Statistical analyses

Generalized data for the entire observation period in individual sites of the three studied regions were compared using hierarchical cluster analysis with R function hclust (method "complete") using the OpenOffice.org Calc table processor.

The similarity of climatic conditions in different protected areas was also studied for individual climatic parameters using hierarchical cluster analysis and dendrograms, constructed using the SciPy package for the Python 3 programming language (Raschka, Mirjalili, 2017). The Euclidean distance (d) was used as a metric both in the case of linear growth of pine trees and for climatic parameters (equation 4):

$$d(p,q) = \sqrt{\sum_{i=1}^{n}(p_i - q_i)^2} \quad (4)$$

where p and q are the measured variables (i.e. values of a climatic parameter of two compared plots) and i indicates an individual measured value of the variable from a total number of n measurements.

RESULTS

Cluster analysis of the annual average values of the swamp ecotype of Lapland pine linear growth index variability in the three examined SPNTs for the entire observation period revealed a division of these indicators into two main clusters (Fig. 3). One of them includes values obtained from various test sites of the Polar Circle SNCR and the Kivach SNR, which belong to the northwestern subregion of the Atlantic-Arctic forest region of the Temperate zone, and the other includes values obtained from various test sites of Pechora-Ilych SNBR, which is part of the northeastern subregion of the same region. Thus, we see that climatic conditions, in general, have a more significant effect on the clustering of the selected indicators of linear growth.

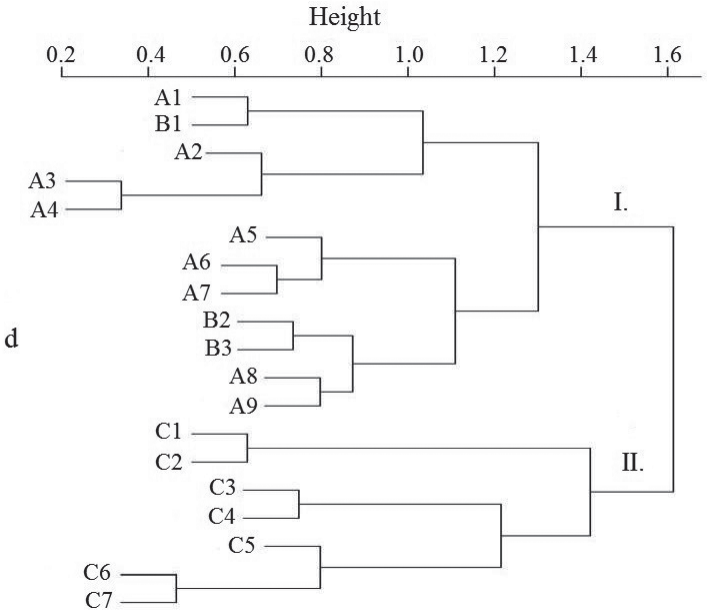

Fig. 3. Cluster analysis of the height growth index indicators of Lapland pine swamp ecotype in various environmental conditions of North European Russia, d is the Euclidean distance.
I. Northwest subregion of the Atlantic-Arctic forest region of the temperate zone. The Republic of Karelia. Kivach SNR: A1 – peat bog podzolic gleyed soil; A2, A3, A4 - transitional peat bog soil; A5, A6, A8, A9 - humus peat bog gleyed soil; A7 – peat bog gleyed soil. Polar Circle SNCR: B1 – peat bog podzolic soil; B2, B3 - humus peat bog gleyed soil. II. The northeastern subregion of the Atlantic-Arctic forest region of the temperate zone. The Komi Republic. Pechora-Ilych SNBR: C1, C2 – raised peat bog soil; C3, C4 – illuvial ferruginous gleyed podzol; C5 – transitional peat bog soil; C6, C7 – peat bog podzolic soil

Within these two main clusters, there is a similarity between the Lapland pine linear growth indices in test plots with similar soil conditions (Fig. 3). This indicates that the influence of the ecological niche, especially its edaphic component, also affects the linear growth of pine, but has a lower rank relative to the climate effect.

The next stage of our research was the identification of the climatic parameters that influenced the separation of the average annual variability values of the Lapland pine linear growth series into two different clusters. The calculated values of the selected climatic parameters averaged for the period 1991-2010 are given in Table 1. This period covers both the period of ground-based measurements of the linear growth of Lapland pine and the period of growth of this subspecies before the start of measurements, which is subsequently taken into account when conducting field observations.

Table 1. The values of climatic parameters of the studied SPNTs, averaged over the period 1991-2010

Climatic parameters (CP)	Values of CP in the studied regions		
	Polar Circle SNCR	Kivach SNR	Pechora-Ilych SNBR
TAP*, mm	523.2	604.1	634.3
PSp, mm	96.6	110.2	125.1
PAJn, mm	125.0	137.1	151.8
PJIS, mm	174.3	214.6	208.2
PGS, mm	263.6	319.4	336.3
PCS, mm	259.6	284.7	298.0
MAAT, °C	0.97	2.98	0.54
MTM,°C	4.4	7.9	8.1
MTWM, °C	14.1	16.65	17.4
MTCM, °C	-10.4	-9.4	-16.1
SAT>5°C, °C×days	1443	1958	1890
SAT>10°C, °C×days	1050	1583	1517
NDY>5°C, days	132-133	159	152-153
NDY>10°C, days	80	109-110	103
HTC	2.5	2.0	2.2
SAI	0.36	0.47	0.43

* The description of climatic parameters is given in the section "Climate data"

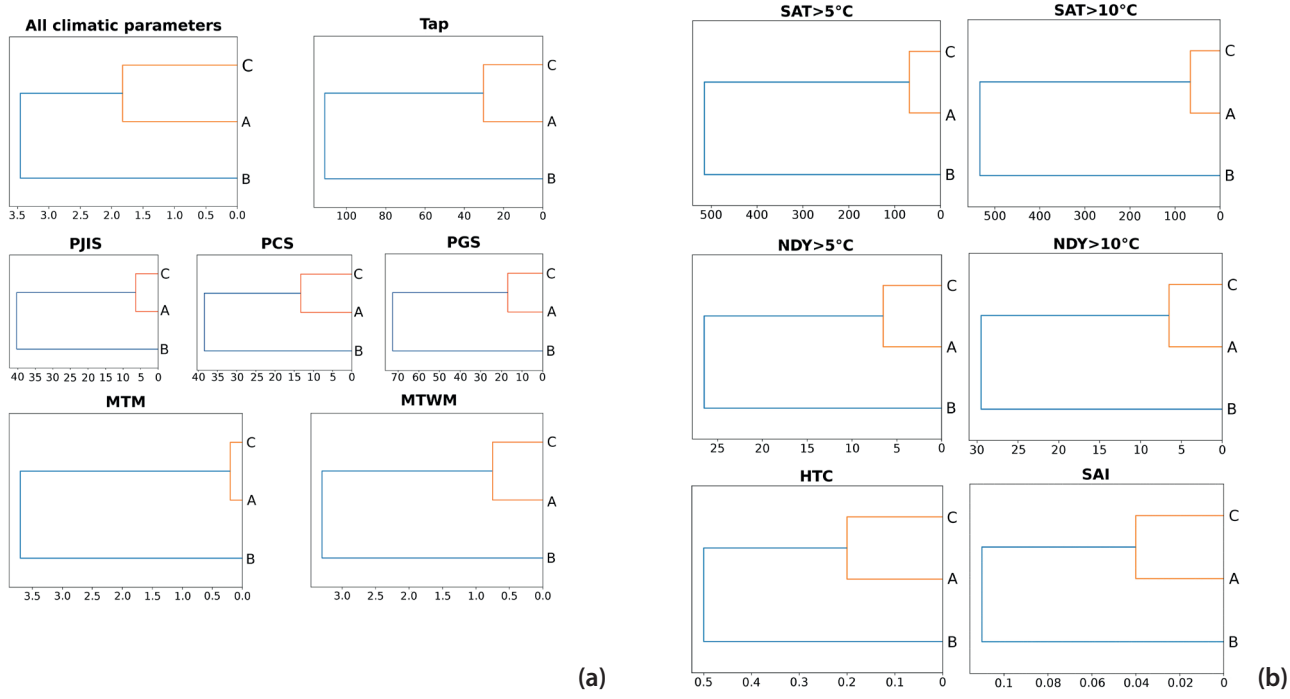

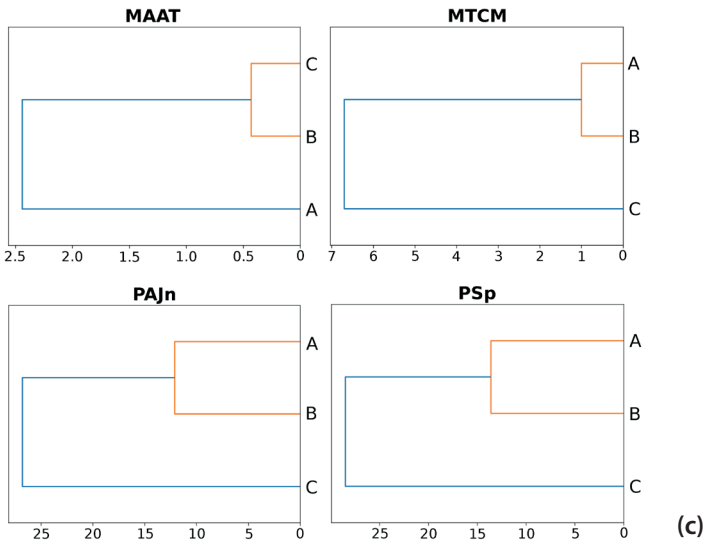

Fig. 4. Cluster analysis of the climatic parameters in the three studied SPNTs, averaged over the period 1991-2010: a) all climatic parameters, TAP, PJlS, PCS, PGS, MTM, MTWM; b) SAT>5°C, SAT>10°C, NDY>5°C, NDY>10°C, HTC, SAI; c) MAAT, MTCM, PSp, PAJn. Study sites: A - Kivach SNR, B - Polar Circle SNCR, C – Pechora-Ilych SNBR. The horizontal axis indicates Euclidean distance

After calculating the climatic parameters presented in table 1, we also performed a cluster analysis to identify similarities between the three studied SPNTs using both all climatic parameters values combined and each of them separately (Fig. 4a-c).

The results of clustering of all climatic parameters showed that the Kivach SNR and the Pechora-Ilych SNBR were the most similar across the entire set of values (Fig. 4a). The same results were obtained for most of the other climatic parameters (Fig. 4b).

However, when conducting a cluster analysis by the climatic parameter MAAT, the Polar Circle SNCR and the Pechora-Ilych SNBR turned out to be the closest (Fig. 4c). This indicator brings the more northern (Polar Circle SNCR) and more continental (Pechora-Ilych SNBR) regions closer together.

According to the climatic parameters MTCM, PSp and PAJn, the greatest similarities were found for the territories of the Kivach SNR and the Polar Circle SNCR (Fig. 4c). The cluster analysis also showed a greatest similarity in the values of the average annual variability of the Lapland pine height growth series in these surveyed SPNTs (Fig 3). Obviously, these climatic parameters have a decisive influence on the magnitude of the indexed height growth of the studied pine subspecies.

DISCUSSION

Pine height growth takes place in spring and in the first half of summer. Previously, it was shown that in Karelia, in the middle taiga region, an intensive linear growth of pine trees begins in the first half of May, reaches a maximum in mid-June and completely stops in August (Kishchenko 2019). The amount of precipitation in this period can have both a positive (in case of insufficient moisture) and a negative (in case of excessive moisture) effect on the linear growth of *Pinus sylvestris* L. (Koukhta and Titkina 2005; Pozdnyakova et al. 2019). A significant negative correlation between the precipitation in May-July and height growth indices of Scots pine were found for humid biotopes of the northern regions (Pozdnyakova et al. 2019). The same results were obtained while examining the forest pine biotopes of the Baltic region with a cool humid Atlantic-Continental European climate (Janson et al. 2013b). The reason for this phenomenon is that in waterlogged biogeocenoses, an increased amount of precipitation causes water stress in pine trees and a decrease in the internode growth rate, while also contributing to a deterioration in the quality of the established buds' renewal (Pozdnyakova et al. 2019).

MTCM is also of great importance to the vegetation of the northern regions, so its influence on the growth of Lapland pine in height is quite obvious. The negative influence of MTCM on the growth of *Pinus sylvestris* L.was also noted in the studies on the relationship between climatic factors and the height growth of pine stands in Siberia (Nikolaeva and Savchuk 2008; Shestakova et al. 2017) and the mountain regions of Spain (Sánchez-Salguero et al. 2015). However, for these regions (forest-steppe regions of Siberia and the Mediterranean climate territories of Spain), a decrease in the height growth of the examined pines was also observed with an increase in the aridity of the growing season, while the correlation with precipitation was positive.

Depending on the growing conditions, the set of climatic factors influencing the growth of *Pinus sylvestris* L.is different. In previous studies, using correlation analysis, it was found that the height growth of pine stands in Penza region decreased with increasing temperature during the growing season and increased with an increase in the amount of precipitation in the current growing season (Koukhta and Titkina 2005). When studying pine stands of the Mongolian pine (*Pinus sylvestris* L. var. *mongolica*) in three northern regions of China, it was found that the height growth of pine trees generally increased with increasing average monthly temperature in May and the amount of precipitation from October to April, and decreased with increasing precipitation in the previous growing season (Zhou et al. 2019). Also, a significant positive correlation of the height growth indices of *Pinus sylvestris* L. with May temperatures was noted by scientists conducting studies in Latvia (Janson et al. 2013b). According to our data, the May temperature did not have a significant effect on the cluster similarity of the height growth of Lapland pine in the conditions of the northern Russian protected areas. The patterns obtained are consistent with the results of previous studies, in which it was shown that the limiting factor in most habitats of boreal biogeocenoses of North European Russia is the lack or excess of precipitation, and not the temperature of the growing season (Chernogaeva and Kuhta 2018).

A relationship between the average monthly temperature of January and the growth of pine trees in the territory of northern and southern Karelia, which are located within the same climatic subregion, was found. Earlier, D.E. Rumyantsev (2004) established a significant negative correlation between pine growth and the average monthly temperature in December of the previous year (r up to -0.54), which he chose as the coldest winter period. In our study, January was taken as the coldest month of the year based on long-term meteorological data. These observations can be considered similar.

CONCLUSIONS

Our studies showed that cluster analysis can be used to identify the rank influence of climatic conditions on the Lapland pine height growth. Also, it can be used to reveal the most significant climatic factors for a given geographical subspecies. According to our results, the most significant impact on the annual variability of the Lapland pine height growth was caused by precipitation in spring and early summer, as well as the average daily mean temperature in January. A significant effect of the average January temperature on the height growth indicators of Lapland pine was revealed in our research.

The results obtained from the cluster analysis are preliminary and show directions for further more detailed observations and studies, particularly for identifying the mechanisms determining the response of height growth increments of pine stands to various climatic parameters.

REFERENCES

Alisov B.P. (1956). Climate of the USSR. Publishing house of Moscow University, Moscow (in Russian).

BCNKC (2020). The Basin Council of North Karelian Coast. Non-Profit Corp. [online] Available at: https://www.kareliacoast.org. [Accessed 18 Mar. 2020].

Bonan G.B. (2008). Forests and climate change: Forcings, feedbacks, and the climate benefits of forests. Science 320(5882),1444–1449, DOI: 10.1126/science.1155121.

Chernogaeva G.M. and Kuhta A.E. (2018). The Response of Boreal Forest Stands to Recent Climate Change in the North of the European Part of Russia. Russian Meteorology and Hydrology, 43(6), 418-424, DOI: 10.3103/S1068373918060109.

Degteva S.V. and Lapteva E.M. (eds) (2013). Soils and soil cover of the Pechora-Ilych Reserve (Northern Urals). Syktyvkar, ISBN:978-5-89606-513-5 (in Russian).

Dobbertin M., Eilmann B., Bleuler P., Giuggiola A., Graf-Pannatier E., Landolt W., Schleppi P., Rigling A. (2010). Effect of irrigation on needle morphology, shoot and stem growth in a drought-exposed Pinus sylvestris forest. Tree Physiol., 30, 346–360. DOI: 10.1093/treephys/tpp123.

Dobrovol'skii G.V. and Urusevskaya I.S. (2004). Soil geography. Second Edition. Publishing house of Moscow University, Moscow ISBN:5-211-04481-9, KolosC, Moscow ISBN:5-9532-0254-7 (in Russian).

Egorov V.V., Fridland V.M., Ivanova E.N., Rozov N.N., Nosin V.A., Friev T.A. (1977). Classification and diagnostics of soils in the USSR. Kolos, Moscow (in Russian).

Elagin I.N. (1976). Seasonal development of pine forests. Nauka, Novosibirsk (in Russian).

Fedorets N.G., Morozova R.M., Bakhmet O.N., Solodovnikov A.N. (2006). Soils and soil cover of the Kivach reserve. Proceedings of the Karelian Scientific Center of the Russian Academy of Sciences, Petrozavodsk 10, 131-152 (in Russian with English summary).

Gitis L. (2003). Statistical classification and cluster analysis. Publishing House of Moscow State Mining University, Moscow ISBN:5-7418-0010-6 (in Russian).

Gymnosperm DB (2022). The Gymnosperm Database. [online] Available at: https://www.conifers.org/pi/Pinus_sylvestris.php. [Accessed 4 Jan. 2022].

Jansons A., Matisons R., Baumanis I., Purina L. (2013a). Effect of climatic factors on height increment of Scots pine in experimental plantation in Kalsnava, Latvia. Forest Ecology and Management, 306, 185–191. DOI: 10.1016/j.foreco.2013.06.039.

Jansons A., Matisons R., Lībiete-Zālīte Z., Baders E., Rieksts-Riekstinëš R. (2013b). Relationships of height growth of lodgepole pine (Pinus contorta var. latifolia) and Scots pine (Pinus sylvestris) with climatic factors in Zvirgzde, Latvia. Baltic Forestry, 19(2), 236–244.

Kishchenko I.T. (2019). Seasonal formation of aboveground phytomass of middle-aged pine stands of various types of forest in the middle taiga. Lesovedenie (Forestry), 1, 19-28 (in Russian with English summary), DOI: 10.1134/S002411481901008X.

KNR (2020). Kivach Nature Reserve. Official Website. [online] Available at: https://zapkivach.ru. [Accessed 20 Mar. 2020].

Koukhta A.E. (2003). Linear growth of trees as an indicator of the state of the environment. Siberian ecological journal, 6, 767-771 (in Russian with English summary).

Koukhta A.E. and Titkina S.N. (2005). Climatogenic variations in linear increment of Scots pine juvenile plants in model stands in the Penza region. Problems of ecological monitoring and modeling of ecosystems, 20, 251-261 (in Russian with English summary).

McCarroll D., Jalkanen R., Hicks S., Tuovinen M., Gagen M., Pawellek F., Eckstein D., Schmitt U., Autio J., Heikkinen O. (2003). Multiproxy dendroclimatology: a pilot study in northern Finland. Holocene, 13, 829–838, DOI: 10.1191/0959683603hl668rp.

Misi D., Puchałka R., Pearson C., Robertson I., Koprowski M. (2019). Differences in the Climate-Growth Relationship of Scots Pine: A Case Study from Poland and Hungary. Forests, 243(10), 1-12, DOI: 10.3390/f10030243.

Mutke S., Gordo J., Climent J., Gil L. (2003). Shoot growth and phenology modelling of grafted Stone pine (Pinus pinea L.) in Inner Spain. Ann. For. Sci., 60, 527–537, DOI: 10.1051/forest:2003046.

Nikolaeva S.A. and Savchuk D.A. (2008). Climatogenic response of pine trees in the south of the Tomsk region. J. of the Siberian Federal University, Biology, 1(4), 400-413 (in Russian with English summary).

Pensa M., Salminen H., Jalkanen R. (2005). A 250-year-long height-increment chronology for Pinus sylvestris at the northern coniferous timberline: a novel tool for reconstructing past summer temperatures? Dendrochronologia, 22, 75–81, DOI: 10.1016/j.dendro.2005.02.005.

PISNBR (2020). Pechora-Ilych State Nature Biosphere Reserve. Official Website. [online] Available at: https://www.pechora-reserve.ru. [Accessed 22 Mar. 2020].

Plant List (2022). The Plant List. [online] Available at: http://www.theplantlist.org. [Accessed 4 Jan. 2022].

Popova E.N., Yasyukevich V.V., Popov I.O. (2017). On the correct use of cumulative applied climate indices for studying biological objects. Russian Meteorology and Hydrology, 42(10), 661–664, DOI: 10.3103/S1068373917100053.

Pozdnyakova E.A., Volkova G.L., Koukhta A.E. (2019). Variability of Scots pine linear increment in different types of biotopes of the European part of Russia. Lesnoy Vestnik (Forestry bulletin), 23(2), 61–69 (in Russian with English summary), DOI: 10.18698/2542-1468-2019-2-61-69.

Pravdin L.F. (1964). Pinus sylvestris. Variability, intraspecific taxonomy and selection. Nauka, Moscow (in Russian).

Raschka S. and Mirjalili V. (2017). Python Machine Learning - Second Edition. Packt Publishing Ltd. ISBN:9781787125933.

RSRIHI-WDC (2014). All Russian Research Institute of Hydrometeorological Information - World Data Center. Official Website. [online] Available at: http://www.meteo.ru. [Accessed 10 Feb 2014].

Rumyantsev D.E. (2004). Diagnostics of the growth features of pine and spruce in South Karelia using dendrochronological methods. Dissertation.... candidate of biological sciences, Moscow State Forest University, Moscow (in Russian).

Rysin L.P. and Savelyeva L.I. (2008). Pine forests of Russia. Partnership of scientific publications "KMK", Moscow, ISBN:978-5-87317-512-3 (in Russian).

Salminen H. and Jalkanen R. (2005). Modelling the effect of temperature on height increment of Scots pine at high latitudes. Silva Fennica, 39, 497–508. Available at: http://www.metla.fi/silvafennica/full/sf39/sf394497.pdf. [Accessed 10 Apr. 2020].

Sánchez-Salguero R., Camarero J.J., Hevia A., Madrigal-González J., Linares J.C., Ballesteros-Canovas J.A., Sánchez-Miranda A., Alfaro-Sánchez R. (2015). What drives growth of Scots pine in continental Mediterranean climates: Drought, low temperatures or both? Agric. For. Meteorol., 206, 151–162, DOI: 10.1016/j.agrformet.2015.03.004.

Selyaninov G.T. (1928). On agricultural assessment of climate. Works on agricultural meteorology. Issue 20, 169-178 (in Russian).

Shestakova T.A., Voltas J., Saurer M., Siegwolf R.T.W., Kirdyanov A.V. (2017). Warming effects on Pinus sylvestris in the cold–dry Siberian forest–steppe: positive or negative balance of trade? Forests, 8(12), 1-21, DOI: 10.3390/f8120490.

Sirotenko O.D. and Pavlova V.N. (2012). Methods for assessing the impact of climate change on agricultural productivity. In: Semenov S.M., Popova E.N., Trifonova-Yakovleva A.M., Yasukevich V.V. (eds). Methods for assessment of climate change consequences for physical and biological systems, Roshydromet, Moscow, pp. 165-189. ISBN:978-5-904206-10-9 (in Russian).

SPTsR (2020). Specially protected territories of Russia. Official Website. [online] Available at: http://oopt.aari.ru. [Accessed 20 Aug. 2020] (in Russian).

Sukachev V.N. (1972). Selected works in three volumes. In: Lavrenko E.M. (ed). Vol. 1: Fundamentals of forest typology and biogeocenology. Nauka, Leningrad (in Russian).

Thabeet A., Vennetier M., Gadbin-Henry C., Dendelle N., Roux M., Caraglio Y., Vila B. (2009). Response of Pinus sylvestris L. to recent climatic events in the French Mediterranean region. Trees – Structure and Function, 23, 843–853, DOI: 10.1007/s00468-009-0326-z.

van der Maaten E., Mehl A., Wilmking M., van der Maaten-Theunissen M. (2017). Tapping the tree-ring archive for studying effects of resin extraction on the growth and climate sensitivity of Scots pine. Forest ecosystems, 4(7), 1-7, DOI: 10.1186/s40663-017-0096-9.

Voronov A.G., Drozdov N.N., Krivolutsky D.A., Myalo E.G. (2002). Biogeography with the basics of ecology. Publishing house of Moscow State University, Moscow, ISBN:5-211-04664-1, Publishing house «Higher school», Moscow ISBN:5-06-004341-X (in Russian).

Zhou Y., Lei Z., Zhou F., Han Y., Yu D., Zhang Y. (2019). Impact of climate factors on height growth of Pinus sylvestris var. mongolica. PloS ONE, 14(3), e0213509, DOI: 10.1371/journal.pone.0213509.

RESEARCH PAPER

ASSESSING THE SPATIOTEMPORAL URBAN GREEN COVER CHANGES AND THEIR IMPACT ON LAND SURFACE TEMPERATURE AND URBAN HEAT ISLAND IN LAHORE (PAKISTAN)

M. Jabbar*[1], M.M. Yusoff[1]
[1]University of Malaya, 50603 Kuala Lumpur, Malaysia
***Corresponding author:** Jabbar.lhr@gmail.com
Received: January 12th, 2021 / Accepted: February 15th, 2022 / Published: March 31st, 2022
https://DOI-10.24057/2071-9388-2021-005

ABSTRACT. Urban vegetation has a decisive role in sustaining homogeneous Land Surface Temperature (LST) in a built-up environment. However, urban areas are facing rapid changes in land use/land cover (LULC) over the last few decades as green cover is being replaced by built-up structures. Consequently, LST is increasing and urban heat island (UHI) effects are expanding. In this context, this study was organized to assess urban green cover changes in Lahore and their impact on LST and UHI effects. For this, climate data was collected from the Pakistan Meteorological Department and Landsat images were acquired from Earth Explorer. LULC and LST maps were generated for 1990, 2000, 2010, and 2020 in ArcGIS 10.8. Also, Normalized Difference Vegetation Index (NDVI) and Normalized Difference Built-up Index (NDBI) were computed to analyze the effects of vegetation and built-up areas on LST and UHI. The study found that over the last three decades, built-up area increased 113.85% by removing 392.78 km^2 of green cover in the study area. Similarly, a rapid expansion of the high LST range and UHI effects was found towards the eastern and southern parts of the study area. Moreover, a negative correlation was found between LST and NDVI, whereas the correlation between LST and NDBI was found to be positive. Therefore, it was concluded that the continuation of green cover reduction is highly damaging because this might render the city more fragile ecologically. So, the study calls the attention of the responsible authorities for suitable measures against continuous green cover loss in the study area.

KEYWORDS: Land Surface Temperature; Land Use/Land Cover Changes; Urban Heat Island; Urban Green Cover; Normalized Difference Vegetation Index

CITATION: Jabbar M., Yusoff M. M. (2022). Assessing The Spatiotemporal Urban Green Cover Changes and Their Impact on Land Surface Temperature and Urban Heat Island in Lahore (Pakistan). Vol.15, № 1. Geography, Environment, Sustainability, p 122-140 https://DOI-10.24057/2071-9388-2021-005

ACKNOWLEDGEMENTS: *The author (Muhammad Jabbar) gratefully appreciates the support and supervision of the co-author (Dr. Mariney Mohd Yusoff) and the efforts of reviewers and editors in converting this piece of research into a successful scientific research paper.*

Conflict of interests: The authors reported no potential conflict of interest.

INTRODUCTION

Human life is strongly dependent on a suitable natural environment and cannot properly function without it. A balanced natural environment that exists on the earth makes it a suitable planet for living. However, human activities are continuously damaging the state of the natural environment. Urban green cover is significant for urban structure because it affects human life in many ways; for instance, urban green spaces stimulate better physical, psychological, and mental health and provide clean air for breathing. Besides the potential to reduce city temperature, the urban green cover offers healthy spaces for running, jogging, and walking. Urban green cover provides an appropriate environment for recreational and physical activities along with opportunities for social interaction (*WHO | Urban Green Spaces,* n.d.). Urban greenness is a well-recognized element of socio-economic and environmental benefits. Physical, psychological, and emotional relaxation are all provided by urban green areas (Mensah et al. 2016).

Rapid urbanization and climate change created several challenges for urban residents. Rapid urbanization damages the urban environment, making it difficult to live in (Habitat, 2016). These rapid urban changes include the transformation of natural green places into impermeable surfaces, which increase Land Surface Temperature (land skin temperature that is derived from solar radiation) and Urban Heat Island (the region with a greater temperature than the surrounding environment) by shifting energy or radiation into the near-surface layer of the atmosphere (Aflaki et al. 2017; Forman, 2016; Oke, 1982). These Land Use / Land Cover (LULC) changes adversely affect the urban air quality and homogeneity of land surface temperature. The change of green cover into built-up spaces results in the emergence

and expansion of urban heat islands (Yu et al. 2018). Similarly, urban heat island negatively affects the urban environment as it aggravates air quality and increases energy and water consumption, which also has adverse effects on human and environmental health (Gunawardena et al. 2017; Varentsov et al. 2019; Wibowo et al. 2020; Zhang et al. 2017; Zhou et al. 2017). On the other side, urban vegetation reduces temperature, minimizes UHI effects, enhances air quality, conserves soil, reduces noise pollution, and cuts down wind speed (Lou et al. 2017). Urban green cover helps to mitigate climate change effects and provides a suitable environment for human and environmental well-being (Jabbar et al. 2021; Krellenberg et al. 2014).

All land cover types have distinct radiation and energy absorption capacities; therefore, it is crucial to consider them when modifying the physical properties of the earth's surface (Koko et al. 2021; Wang et al. 2017). Land cover modification disrupts the energy exchange pattern in the near-surface layer of the atmosphere. As a result, land use/land cover changes can significantly modify urban microclimate (Abuloye et al. 2015; Koko et al. 2021; Palafox-Juárez et al. 2021). Urban land cover modification particularly leads to high land surface temperature, which affects the thermal properties of the near-surface layer of the atmosphere. (Abuloye et al. 2015; Alavipanah et al. 2015; Jiang et al. 2015; Palafox-Juárez et al. 2021). Therefore, LST is recommended as an essential gauge for examining the earth heat balance or solar radiation budget. LST is a helpful indicator for identifying human-environment interaction because it regulates the bio-physical system of the earth (Kaplan et al. 2018; Palafox-Juárez et al. 2021).

Land use/land cover changes are a chief driver of environmental changes at the spatiotemporal scale (Mishra et al. 2014). LULC change detection is used to identify its temporal variation and helps to manage natural resources. Moreover, it provides valuable data on current land cover and a platform for future land use planning. Therefore, the assessment of LULC changes is a significant source of information for urban land use planning and sustainable development of the city (Naeem et al. 2018; Yasin et al. 2019). In the recent decade, it has been observed that urban areas are expanding rapidly, especially in the developing world, and this trend is accompanied by significant changes in urban land cover settings, especially in the urban green cover (Fu & Weng 2016; Yasin et al. 2019). Therefore, it is important to assess urban green cover changes at a spatiotemporal scale and their effect on land surface temperature and urban heat island (Konstantinov et al. 2015).

Various studies have found that LULC changes are a major cause of the urban green cover reduction, and this reduction is rapidly increasing in developing countries (El-Hattab et al. 2018; Koko et al. 2021; Palafox-Juárez et al. 2021; Ramaiah et al. 2020). Such a pattern of LULC change is highly significant because it affects land surface temperature. Because of this, it is crucial to examine the relationship between LULC changes and their effect on LST and UHI for urban planning and development. Furthermore, studies on the relationships between LULC changes and LST might be instrumental in an urban environment in the context of climate change (Mohamed, 2021). Deng et al. (2016), Jiang et al. (2015), Koko et al. (2021), and Palafox-Juárez et al. (2021) suggested that land surface temperature is a significant predictor of urban heat islands; therefore, an assessment of urban heat island can be made based on land surface temperature and NDVI data.

Lahore metropolitan is famed as a city of gardens. It is located in Pakistan, in a highly fertile area of the Upper Indus alluvial plain. Lahore is an economic hub of Pakistan and functions as a dry port for the whole country. This makes it an attractive place for living, which also leads to significant and rapid LULC changes (Shirazi & Kazmi 2016). The rapid development of built-up areas instead of green-covered land is damaging the ecosystem of the study area, converting it from a highly suitable place for living to an unsuitable one. The negligent behaviour of the management regarding the implementation of environmental guidelines in built-up areas and lack of accurate data are the main causes of environmental issues. Therefore, the assessment of urban green cover changes is necessary to identify the right pulse of land modification in the study area and overcome future environmental consequences. Under these considerations, this study was arranged to assess the urban green cover changes in Lahore and their effect on land surface temperature and urban heat island.

MATERIAL AND METHODS

The Study Area

Lahore is the second largest metropolitan area in Pakistan by population and the capital city of Punjab, which is the most populated province. It is located in the northeastern part of the province and extends from 31° 15′ 0″ N to 31° 45′ 0″ N and from 74° 01′0″ E to 74° 39′0″ E. According to the census report of 2017, the study area has 11,126,285 inhabitants. It covers an area of 1772 km^2 and has an average population density of 6278.94/km^2 (https://pwd.punjab.gov.pk/). Geographically, the study area is mostly located in the Upper Indus plain, particularly in the alluvial plain of the Ravi river, one of the Indus river tributaries.

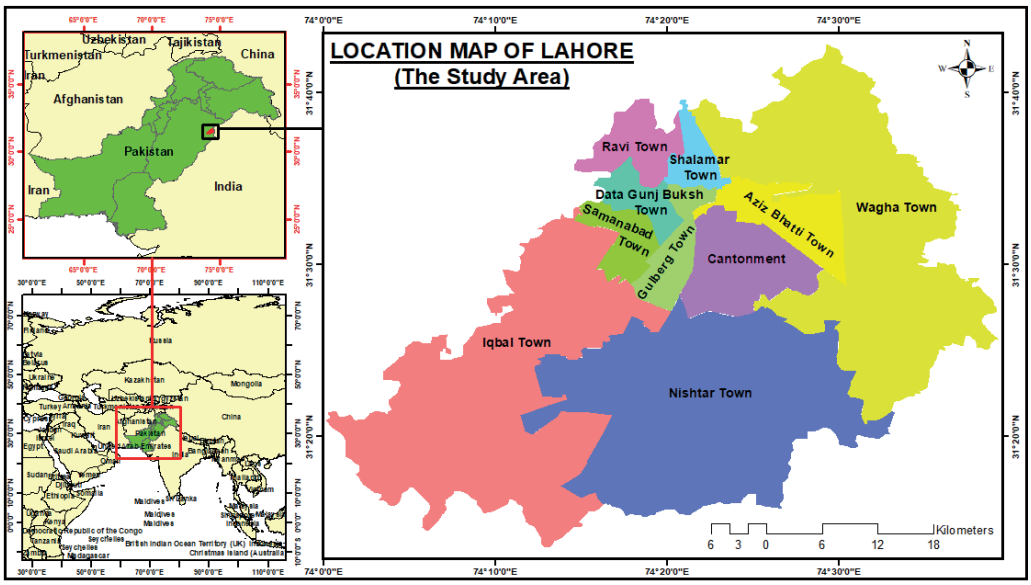

Fig. 1. Location of the Study Area

Climate of the Study Area

The study area is located in a semi-arid region characterized by five seasons: (i) Foggy Winter (from mid-November to mid-February with some western depression rainfall), (ii) Mild Spring (from mid-February to mid-May, (iii) Warm and Hot Summer (from mid-May to end-June with dust and rainy storms), (iv) Rainy Monsoon (from July to mid-September), and (v) Dry Autumn (from mid-September to mid-November). June is the hottest, July is the wettest, and January is the coldest month in the study area. The maximum recorded temperature is 48.3^{0}C and the minimum is -2.2^{0}C (National Oceanic and Atmospheric Administration; Pakistan Meteorological Department).

The annual minimum temperature, which is presented in figure 3, varies from -2.2°C to 4°C. The temperature of -2.2°C was observed in the study area in 1996, 2006, and 2008, while 4°C was recorded in 2016. Regarding the change in the annual minimum temperature, the trendline shows a 0.4°C increase (0.5°C to 0.9°C) based on data for the last thirty years (1990 to 2019).

The annual maximum temperature in the study area, which is presented in figure 4, varies between 44°C and 48.8°C. The highest temperature (48.8°C) was observed in the study

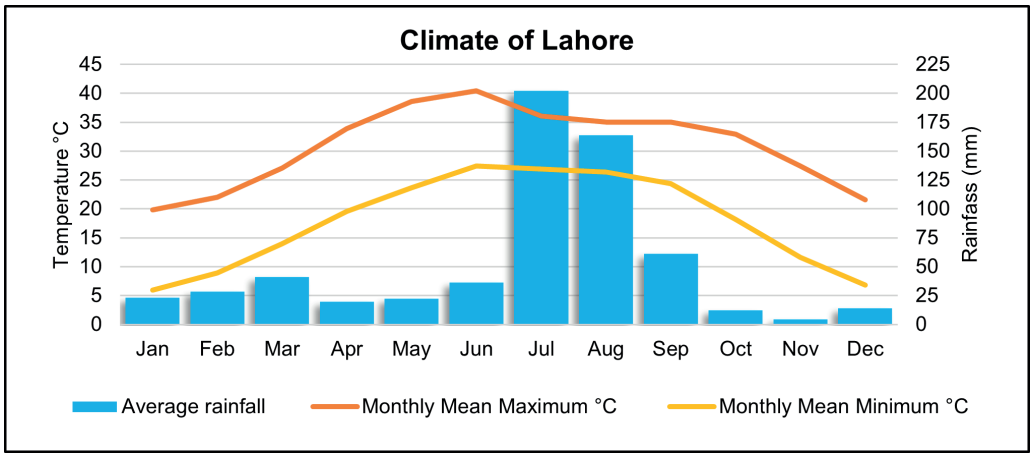

Fig. 2. Climate of the Study Area

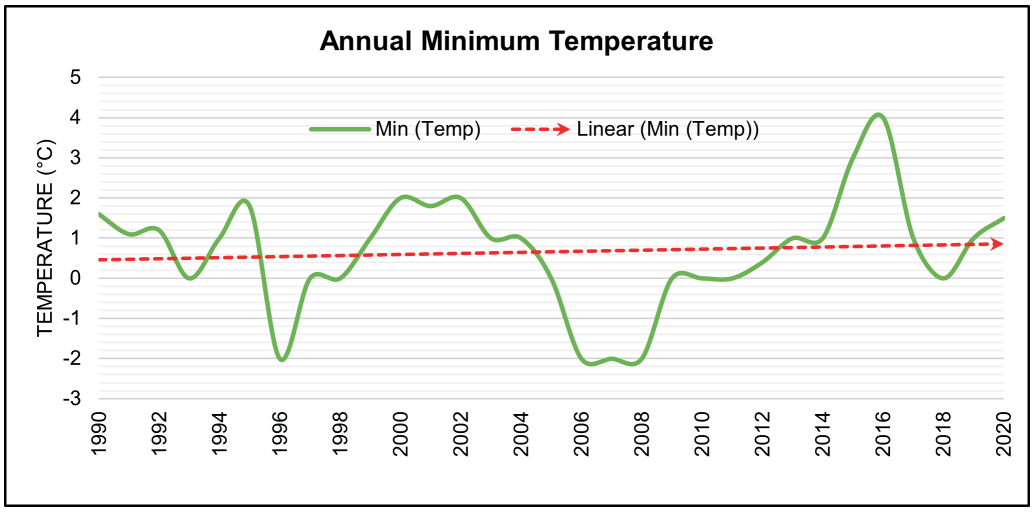

Fig. 3. Annual Minimum Temperature in the Study Area

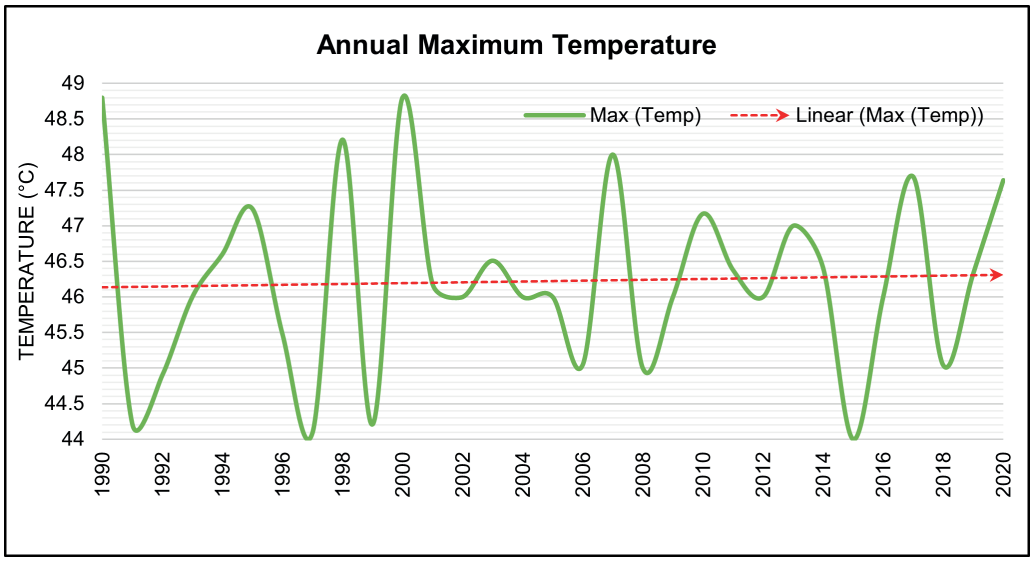

Fig. 4. Annual Maximum Temperature in the Study Area

area in 1990 and 2000. The trendline obtained from the analysis of changes in the annual maximum temperature shows an increase of 0.2°C. So, it was found that both annual minimum and maximum temperatures have increased in the study area.

Data Acquisition and Preparation

The study was based on Landsat images, which were acquired from Earth Explorer (https://earthexplorer.usgs.gov/) for the Path/Row 149/38. Spring was selected for the analysis as it is the most suitable season for LULC classification. The images were acquired for 16 March 1990, 19 March 2000, 7 March 2010, and 18 March 2020 according to the availability and clear weather conditions. All the acquired images had a resolution of 30 meters and are presented in table 1. During data preparation, the study area was extracted from the images by applying "extract by mask" tool in ArcGIS 10.8 after band composition.

LULC Classification

The study was based on Anderson's Image Classification System (Level-I), which is used by the United States Geological Survey (USGS) in the LULC datasets. The study area was classified into five major land cover classes: (i) Forest Land, (ii) Agricultural Land, (iii) Barren Land, (iv) Built-up Area, and (v) Water Bodies. The Supervised Image Classification technique was applied for the classification. This Landsat image classification technique is characterized by the highest accuracy of the assessment (Barman et al. 2016; Iqbal & Iqbal 2018). After obtaining the classified images, the reclassification process was applied to clean misclassified cells using the cleanup tool. Then the classified image results were enhanced by removing the small isolated regions and smoothing class boundaries. After getting the final classified images, raster data was converted into polygons. Then the polygons were dissolved according to their class, and the area of each class was calculated by applying the geometry in the attribute table. This procedure was repeated for the classification of all the images.

Accuracy Assessment

For the accuracy assessment, 450 random reference points were generated using Supervised Image Classifiers in ArcGIS. After that, the confusion (error) matrix and kappa statistics were calculated. Omission and Commission errors were also computed. Omission errors occur when a class pixel is included in other classes, while Commission error occurs when the system assigns pixels of a class that does not belong to this class. Moreover, the user's and producer's accuracy were calculated in the study.

The following equations were used during the accuracy assessment process:

$$\text{Produser's Accuracy (\%)} = \left(\frac{X_{kk}}{X_{kk}}\right) X100 \quad (1)$$

$$\text{User's Accuracy (\%)} = \left(\frac{X_{kk}}{X_{k+}}\right) X100\% \quad (2)$$

$$\text{Overall Accuracy } (OA) = \frac{1}{N}\sum_{k=1}^{\gamma} n_i \quad (3)$$

$$\text{Kappa - coefficient } (k) = \frac{N\sum_{k=1}^{r} X_{kk} - \sum_{k=1}^{r}\left(X_{k+} \odot X_{+k}\right)}{N^2 - \sum_{k=1}^{r}\left(X_{k+} \odot X_{+k}\right)} \quad (4)$$

In these equations, N = Total No. of pixels, r = No. of classes, X_{kk} = Total pixels in a row, X_{k+} = Total samples in a row, and X_{+k} = Total samples in the column in the error matrix.

LULC Change Detection

A post-classification comparison technique was applied to detect the change between two classified images. All four self-classified images were used for the LULC change detection. The change (C) in land cover classes was calculated by applying equation 5.

Table 1. Detail of Landsat Images used in the study

Years	Satellite	Sensor	Path/Row	Resolution (m)	Acquisition Day
1990	Landsat-5	TM	149/38	30	16-03-1990
2000	Landsat-7	ETM	149/38	30	19-03-2000
2010	Landsat-7	ETM	149/38	30	07-03-2010
2020	Landsat-8	OLI	149/38	30	18-03-2020

Table 2. Accuracy of Classified Images

Class Name	1990		2000		2010		2020	
	U/A	P/A	U/A	P/A	U/A	P/A	U/A	P/A
Forest Land	84.48%	81.67%	89.66%	86.67%	89.47%	85.00%	91.38%	88.33%
Agricultural Land	90.65%	88.18%	92.73%	92.73%	92.04%	94.55%	93.75%	95.45%
Barren Land	89.83%	88.33%	90.00%	90.00%	86.89%	88.33%	93.10%	90.00%
Built-up Area	83.08%	90.00%	90.16%	91.67%	88.14%	86.67%	90.32%	93.33%
Water Bodies	90.91%	100%	100%	100%	100%	100%	100%	100%
	OA = 87.67%		OA = 91.00%		OA = 90.00%		OA = 92.67%	
	KC = 0.82		KC = 0.87		KC = 0.85		KC = 0.90	

Note: U/A = User's Accuracy, P/A = Producer's, O/A = Overall Accuracy, K/C = Kappa-coefficient

$$C_i = L_i - B_i \quad (5)$$

In the next step, the percentage of land cover changes (C %) was calculated using equation 6.

$$Pi = (Li - Bi) / BiX100 \quad (6)$$

Where *i* stands for No. of classes in the image, *Ci* represents the magnitude of changes in a class "*i*", and *Pi* represents the percentage of change in classes.

Extraction of LST

Landsat 5 & 7

Land surface temperature was extracted using band 6 for Landsat 5 and 7, according to Chen et al. (2002). Firstly, digital numbers (DNs) of band 6 were converted into radiation luminance using equation 7. In this equation, QCALMIN is equal to 1, QCALMAX is equal to 255, QCAL stands for DN, whereas LMAX and LMIN are equal to 1 and 255, respectively.

$$\text{Radiance} = \frac{LMAX - LMIN}{QCALMAX - QCALMIN}(QCAL - QCALMIN) + LMIN \quad (7)$$

Secondly, LST in Kelvin was calculated using equation 8.

$$T = \frac{K2}{In(K1/L\gamma + 1)} \quad (8)$$

Lastly, temperature values in Kelvin (A) were converted into dse5regrees Celsius (B) using equation 9.

$$B = A - 273.15 \quad (9)$$

Landsat 8

For the Landsat 8 image, land surface temperature was extracted using the following Metadata values: 0.10000 for Radiance add bands 10 & 11, 0.0003342 for Radiance Mult Band 10 & 11, 774.8853 for K1 constant band 10, 1321.0789 for K2, 480.8883 for K1 constant band 11, and 1201.1442 for K2.

By using the above values, LST was calculated from Landsat 8 in five stages:

(i) Thermal Infra-Red Digital Numbers were converted into TOA (Top of Atmosphere) spectral Radiance using equation 10.

$$L\lambda = ML \times QCAL + AL \quad (10)$$

(ii) Spectral radiance data were converted into TOA brightness temperature using equation 11.

$$BT = K2 / In(k1/L\lambda + 1) - 272.15 \quad (11)$$

(iii) NDVI values were calculated using equation 12.

$$NDVI = NIR - RED / NIR + RED \quad (12)$$

(iv) Average Land Surface Emissivity (LSE) was determined using equations 13 and 14, in which PV is the proportion of vegetation, and E is Land Surface Emissivity.

$$PV = (NDVImax - NDVImin / NDVImax + NDVImin) \wedge 2 \quad (13)$$

$$E = 0.004 * PV + 0.986 \quad (14)$$

(v) LST was calculated using equation 15.

$$LST = (BT/1) + W * (BT/14380) * In(E) \quad (15)$$

After generating the LST maps, the areas of each LST range were calculated in QGIS 3.14.

Quantification of NDVI, NDBI, and UHI

NDVI was quantified using equation 12, whereas for NDBI equation 16 was applied.

$$NDBI = (SWIR - NIR) / (SWIR + NIR) \quad (16)$$

After that, the relationships of LST with NDVI and NDBI were analyzed using Fishnet Polygons, and then the data from LST, NDVI, and NDBI maps were extracted.

UHI was quantified in ArcGIS 10.8 using equation 17 based on LST maps of 1990 and 2020.

$$UHI = (Ts - Tm) / SD \quad (17)$$

Two UHI profiles were calculated: (i) North to South and (ii) West to East, creating the polylines in both directions using Stack Profiles.

RESULTS

Land Use/Land Covers Changes

Land use/land cover changes in the study area were detected using Landsat images of 1990, 2000, 2010, and 2020, as shown in figure 5. The figure shows that the study area has faced rapid LULC changes in the last three decades. In 1990, the study area had 23.41% of Forest Land, 48.03% of Agricultural Land, 11.18% of Barren Land, 16.17% of Built-up Area, and 1.21% Water Bodies. However, after ten years, in 2000, the distribution in the study area changed to 17.30% of Forest Land, 46.09% of Agricultural land, 14.38% of Barren Land, 21.38% of Built-up Area, and 0.83% of Water Bodies. Consequently, the share of Forest Land in the study area decreased over this decade (1990 to 2000) by 6.11%, Agricultural Land decreased by 1.94%, while Barren Land and Built-up Area increased by 3.20% and 5.21%, respectively, the share of Water Bodies also decreased by 0.38%.

After assessing the LULC changes from 1990 to 2000, LULC for 2010 was analyzed. It was found that in this year, the study area had 14.79% of Forest Land, 42.18% of Agricultural Land, 16.59% of Barren Land, 25.73% of Built-up Area, and 0.69% of Water Bodies. As a result, in the decade from 2000 to 2010, the share of Forest Land and Agricultural Land in the study area further decreased by 2.51% and 3.91%, respectively, while Barren Land increased by 2.21%, Built-up Area increased by 4.35%, and Water Bodies decreased by 0.14%.

In order to analyze LULC changes over three decades (1990 to 2020), LULC was also detected for 2020. It was found that in the final year, the study area had 11.97% of Forest Land, 37.31% of Agricultural Land, 15.29% of Barren Land, 34.58% of Built-up Area, and 0.85% of Water Bodies. As a result, in the third decade (2010 to 2020) the share of Forest Land, Agricultural Land and Barren Land decreased by 2.82%, 4.87% and 1.30%, respectively, while Built-up Area increased by 8.85%, and Water Bodies increased by 0.16% in.

As expected, it was found that in the last three decades (1990 to 2020), the share of Forest Land decreased by 11.44% (from 23.41% to 11.97%), Agricultural Land decreased by 10.72% (from 48.03% to 37.31%), and Water Bodies decreased by 0.36% (from 1.21% to 0.85%). On the other side, the area of Barren Land and Built-up Area increased during the last three decades by 4.11% (from 11.18% to 15.29%), and 18.41% (from 16.17% to 34.58%), respectively. Finally, it was confirmed that a rapid increase in Built-up Area occurred along with a swift decrease in Forest Land, which is the main concern of the study as it directly affects LST and UHI. All the details of land use/land cover changes are given in figure 5.

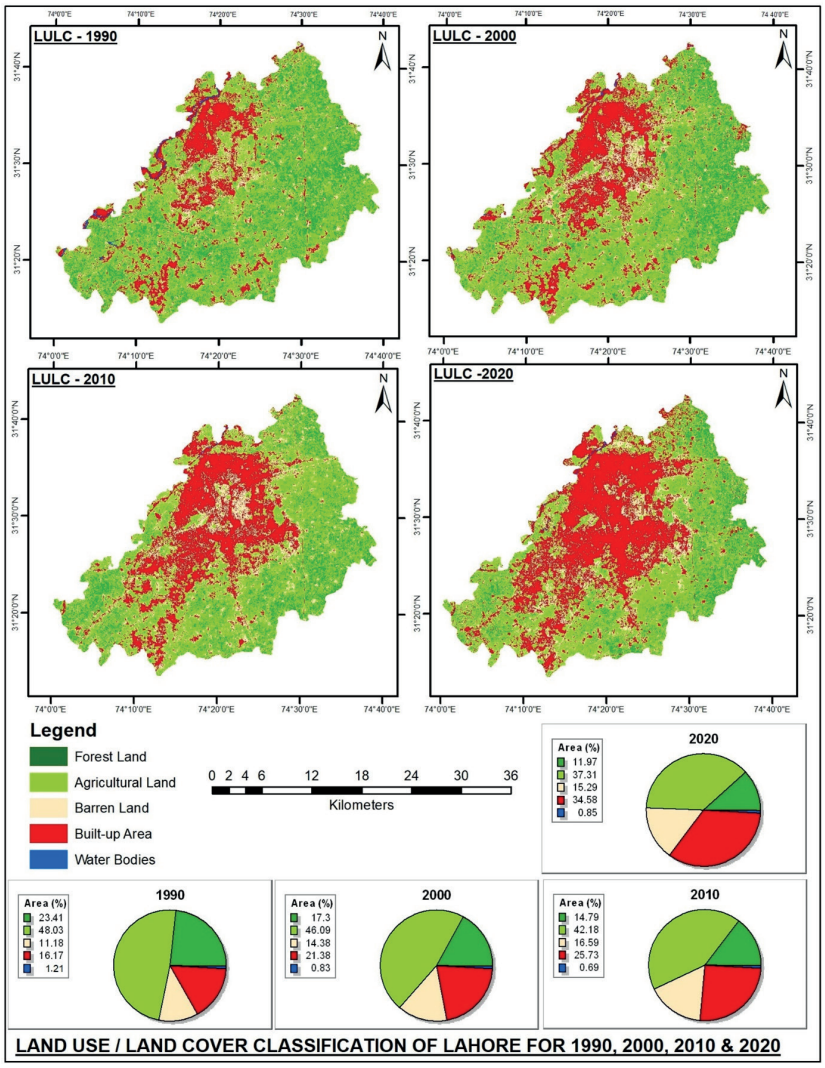

Fig. 5. Land Use/Land Cover Classification of the Study Area

Changes in Land Cover Area

After assessing the LULC changes over three decades (1990 to 2020), it was found that the decrease in area corresponded only to green and blue land cover types whereas the area of built-up and barren land increased. Figure 6 shows the overall increase and decrease in area of different land cover types. It can be seen that the area of Forest Land, Agricultural Land, and Water Bodies lost 202.72 km^2 (11.44%), 189.96 km^2 (10.72%), and 6.38 km^2 (0.36%), whereas Barren Land and Built-up Area gained 72.83 km^2 (4.11%) and 326.23 km^2 (18.41%) respectively.

Changes in Land Surface Temperature

The change of green cover into built-up environment was found to be a significant cause of LST increase and UHI development in various studies (Amani-Beni et al. 2019;

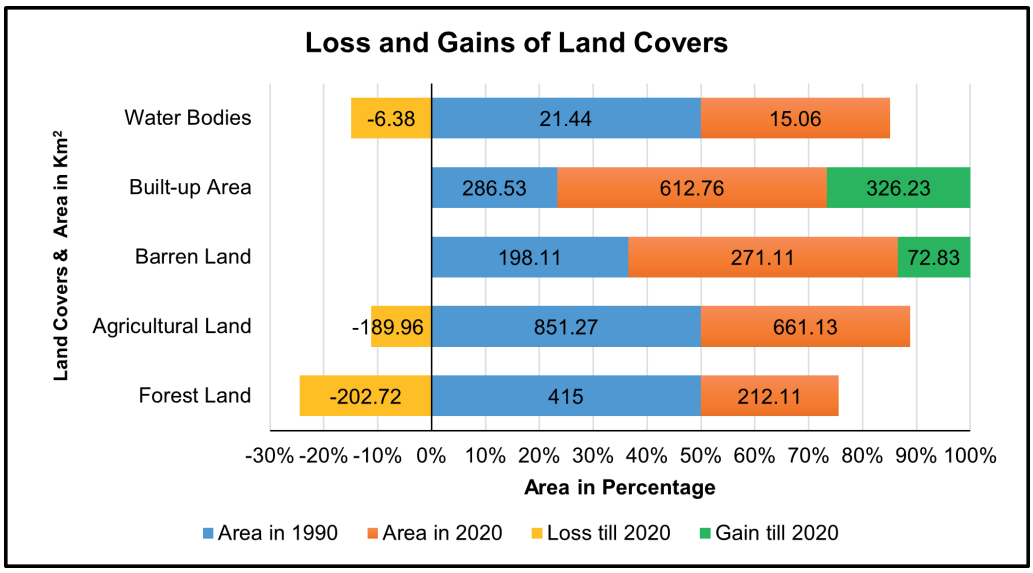

Fig. 6. Loss and Gains of Land Covers from 1990 to 2020

Wan Mohd Jaafar et al. 2020; Yu et al. 2018). Therefore, LST was also computed for the study area. It is shown in figure 07, which presents seven land surface temperature ranges; (i) 14°C - 21°C, (ii) 21°C - 22°C, (iii) 22°C - 23°C, (iv) 23°C - 24°C, (v) 24°C - 25°C, (vi) 25°C - 26°C, and (vii) 26°C - 32°C for 1990, 2000, 2010, and 2020.

The comparison of these LST ranges showed that the area under the first LST range (14°C - 21°C) amounted to 0.20% of the total area in 1990, 8.31% in 2000, 2.29% in 2010 and 6.68% in 2020, so a slight overall area expansion was found for this range. Similarly, an increase was found in the area under the second LST range (21°C - 22°C) as it stood at 11.60% in 1990, 26.56% in 2000, 37.39% in 2010, and 20.44% in 2020. The area under the third LST range (22°C - 23°C) reduced as it amounted to 29.12% in 1990, 20.20% in 2000, 20.66% in 2010, and 19.27% in 2020. For the fourth LST range (23°C - 24°C), a significant expansion was found with the area changing from 36.73% in 1990, to 13.54% in 2000, 16.48% in 2010, and 8.74% in 2020. Similarly, a slight expansion was found for the fifth LST range (24°C - 25°C) as its area accounted for 17.94% of the total area in 1990, 19.90% in 2000, 8.25% in 2010, and 20.38% in 2020. A considerable expansion was found for the sixth LST range (25°C - 26°C). Its area changed from 3.23% in 1990, to 8.84% in 2000, 10.42% in 2010, and 14.12% in 2020. Almost similar results were found for the seventh and last LST range (26°C - 32°C). The area under this range amounted to 0.55% in 1990, 2.02% in 2000, 1.87% in 2010 and 9.73% in 2020. The results of the LST comparison show that the ranges with the highest land surface temperature (sixth and seventh) expanded sharply and constantly, which represents a considerable change in the land surface temperature of the study area.

Correlation of LST with NDVI and NDBI

The correlation of LST with NDVI and NDBI is shown in figure 8. A negative relationship was found between LST and NDVI, whereas between LST and NDBI it was positive. According to these relationships, higher NDVI leads to lower LST, and lower NDVI leads to higher LST. A 5°C decrease in LST corresponds to the increase of NDVI by 0.5. On the other hand, a positive relationship between LST and NDBI means that LST increases with NDBI increase and decreases with the decreasing NDBI. The trendline shows that more than 5°C increase in LST corresponds to an increase of NDBI from -0.35 to 0.1. From these results, it is clear that LST decreases with increasing NDVI and decreasing NDBI. Similarly, LST increases with decreasing NDVI and increasing NDBI. This correlation proves that urban green cover may contribute to a 5°C LST decrease and can help to maintain thermal homogeneousness in cities.

Urban Heat Island

Urban Heat Island effects are commonly found in urban areas, especially in developing countries like Pakistan. These effects become broader and more severe with the

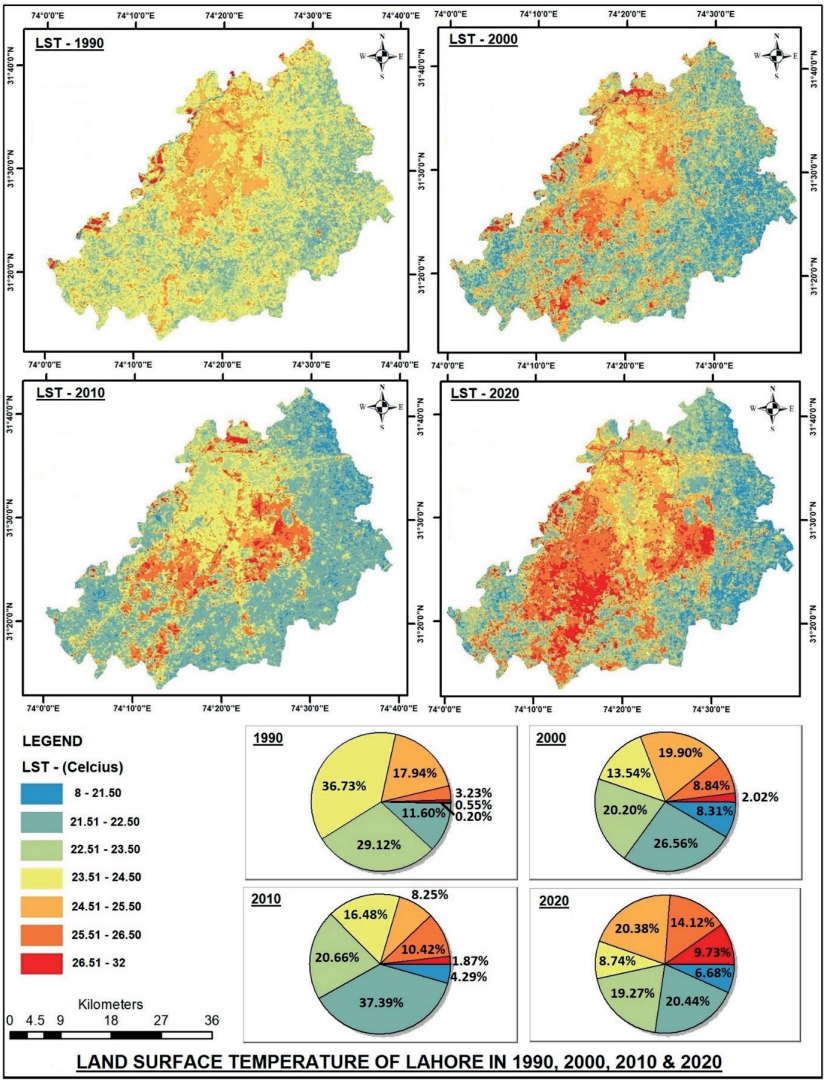

Fig. 7. Changes in Land Surface Temperature in the Study Area

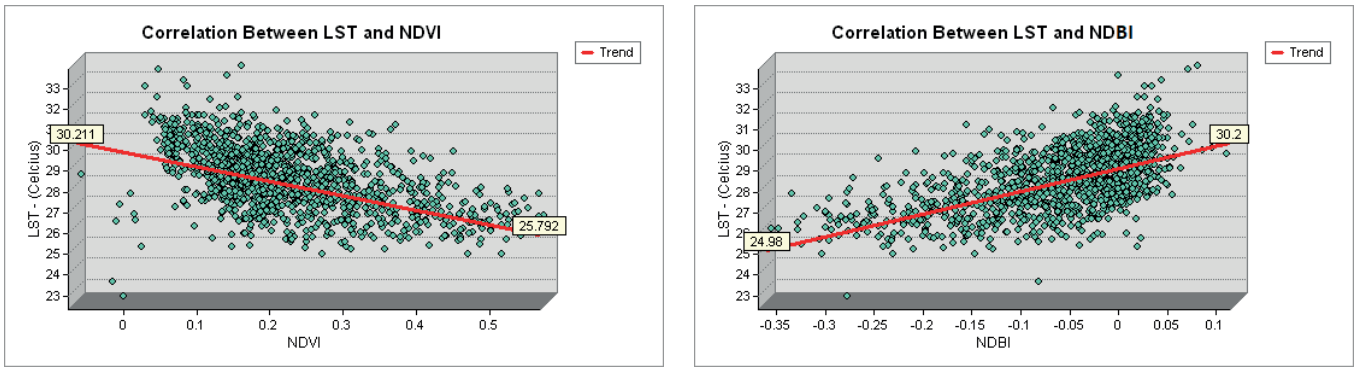

Fig. 8. Correlation of LST with NDVI and NDBI

expansion of urban built-up areas. In this context, the UHI of Lahore was analyzed for the years 1990 and 2020. Figure 9 shows the UHI profiles of the study area in which 1990-(A) and 2020-(A) display North to South profiles, whereas 1990-(B) and 2020-(B) show West to East profiles. The comparison of these UHI profiles is presented below.

UHI-1990-(A) shows LST fluctuations from 19°C to 27°C. A decreasing trend can be found between 20,000 and 32,500 meters as LST drops from 23°C to 19°C. After that, LST increases again reaching 23°C. The low LST area consists of green cover, which confirms the negative relation between green cover and LST. This profile is compared to UHI-2020-(A), which presents LST along the same axis. The UHI-2020-(A) shows high LST from 5,000 to 8,000 meters and from 19,000 meters to the end of the study area. Between 8,000 and 19,000 meters, LST is more or less constant, which is similar to UHI-1990-(A). This UHI comparison shows an LST increase in UHI-2020-(A) where green cover was replaced with built-up area (19,000 to 38,000 meters). This demonstrates an evident expansion of UHI due to the removal of green cover.

UHI-1990-(B) and UHI-2020-(B) represent West to East UHI profiles of the study area. UHI-1990-(B) shows LST around 21 to 22°C from 1,000 to 5,000 meters, but after that, it fluctuates around 23°C from 5,000 to 22,000 meters. Next, a decreasing trend was found from 22,000 to 26,000 meters as LST drops from 23°C to 20°C. After that, LST is almost constant between 26,000 and 41,000 meters. For UHI-2020-(B) an increasing trend was found between 5,000 and 20,000 meters where LST changes from 27 to 29°C, while in UHI-1900-(B) it was 23°C. Similarly, higher LST was found from 25,000 to 40,000 meters. Overall, the high LST area in 2020 was found from 5,000 to 40,000 meters, while in 1990 it spanned from 5,000 to 21,000 meters, which suggests that UHI has expanded by almost 19,000 meters in the last thirty years. So, after comparing UHI profiles from north to south and from west to east for the years 1990 and 2020, there is an evident indication of UHI expansion with the built-up area increase.

DISCUSSION

The effect of Land Use/Land Cover changes is not limited to Land Surface Temperature as they also affect air temperature. In this study, it was found that LST and UHI effects increased with the replacement of green cover by built-up area. Also, an increasing trend was found for the annual maximum and minimum (air) temperature in the study area. Similar results were found in various other studies. Yang et al. (2013) conducted a study in Anhui Province of China and found that annual mean maximum and minimum temperature increased by 0.407, 0.383, and 0.432°C per decade from 1970 to 2008 due to LULC changes (Yang et al. 2013). So, the results of this study support the assertion that the study area has become warmer due to the loss of urban green cover and rapid growth of built-up area. The impact of LULC changes on air temperature was also analyzed in other studies. A regional study on East Asia projected an 0.14°C air temperature increase between 2030 to 2060 due to LULC changes (Niu et al. 2019). It was shown that air temperature also increases along with LST due to the urban expansion and removal of urban green cover. LULC changes led to the increase in air temperature in Beijing–Tianjin–Hebei. The conversion of cropland into built-up area was found to be the most significant factor, causing an 0.36°C/decade increase in air temperature,

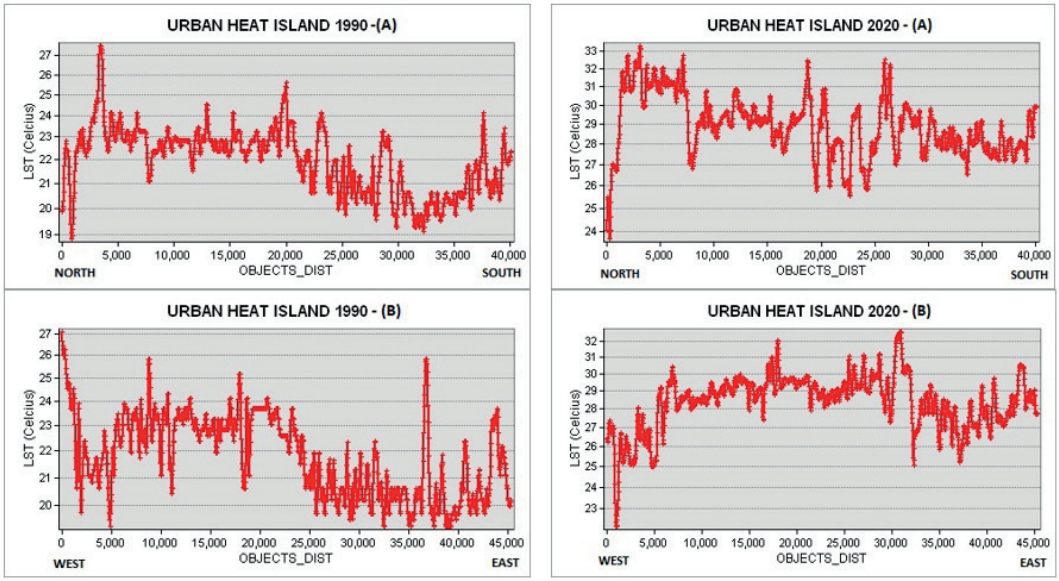

Fig. 9. Comparison of the Urban Heat Island in 1990 and 2020

while the changes from grassland to built-up area led to an 0.306°C/decade increase (Li et al. 2018, p.). Similarly, built-up land in the study area is expanding due to the removal of Forest and Agricultural Land, which leads to increasing air and land surface temperature trend. So, the results of this study support the statement that urban green cover works as a ventilator that maintains urban temperature and reduces UHI effects.

From the comparison of LST profiles (i) UHI-1990-A and UHI-2020-A and (ii) UHI-1990-B and UHI-2020-B, it was found that UHI effects expanded in the study area towards its southern and eastern parts. The area of moderate LST range has also shifted towards high LST, for example, 26°C - 32°C (the highest) LST range covered only 0.20% of the total area in 1990 , while in 2020 it amounted to 9.73%. It means that the area of the maximum temperature zone has significantly increased and the UHI effect expanded with the decrease in green cover and increase in built-up area. Similar findings were given by Forman (2016), stating that rapid modification of green spaces into impermeable surfaces increases the reflection of solar radiation energy into the near-surface layer of the atmosphere. Also, Yu et al. (2017) concluded that built-up area expansion is a significant cause of the UHI development (Yu et al. 2018). UHI has several adverse effects on the urban environment, including the increase in energy consumption and water usage (Gunawardena et al. 2017; Zhang et al. 2017; Zhou et al. 2017). The expansion of UHI in the study area will also result in higher energy and water usage, which will ultimately lead to higher LST and air temperature. Therefore, the study highlights that the loss of green cover enhances extreme environmental issues like harsh UHI effects and high LST, especially during summer.

The study area is located in a semi-arid region, which means that the amount of natural vegetation is already lower than required. Under these circumstances, green cover in the study area becomes even more valuable. In contrast, the results show a significant decrease in the urban green cover area (Forest Land and Agricultural Land). The green cover in the study area is shrinking, whereas built-up area is expanding rapidly. In the last three decades, the study area lost 1/3 of its green area, which was replaced by impermeable surfaces as built-up area increased more than 100%. These changes are severe because the decrease of green cover still continues without any restriction.

The study also analyzed relationships of LST with NDVI and NDBI to recognize the actual effects of vegetation and built-up area on LST and UHI. The results (figure 08) show that LST is negatively correlated with NDVI. High NDVI leads to lower LST and reduces the UHI effects, whereas low NDVI causes LST increase and enhances the UHI effects. On the other side, the relationship between LST and NDBI was found to be positive, indicating that expansion of built-up area leads to the expansion of UHI and higher LST. In all study areas, the decrease in NDVI comes with a decrease in plant cover and an increase in the natural environment changes. According to the findings, vegetation regions and areas outside built-up sites have greater NDVI and lower LST. Low LST was found in regions with dense natural plant cover and gardens as well as in fields of dense agricultural vegetation with high NDVI values. Vegetation helps to reduce LST through evapotranspiration (Grover & Singh, 2015; Palafox-Juárez et al. 2021). These findings also correspond with similar studies based on Landsat data analysis (Guo et al. 2019; Kaplan et al. 2018; Tran et al. 2017). The matter is more threatening because the built-up land cover is still expanding towards the remaining green area, increasing the area of dark surfaces in the city, which causes an increase in air and land surface temperature. With increasing land surface and air temperature, the UHI effects will be more severe in the future. The study area is also located in a semi-arid region and faces extreme temperatures up to 48°C in the summer season, as well as more than 50°C feels like temperature in wet summer. In these circumstances, the availability of green spaces in highly built-up areas is needed because they work like a ventilator and decrease the temperature by almost 5°C.

CONCLUSION AND SUGGESTIONS

The study analyzed urban green cover reduction in Lahore due to LULC changes and found its significant effects on LST and UHI expansion. It was found that the study area is continuously losing its green cover due to rapid urban expansion. LULC changes have demolished a significant part of urban green cover, whereas built-up areas and barren land have spread over 50% of the total area without any planning and violating environmental guidelines. Rapid urban expansion has led to a large-scale increase in the area of dark surfaces in the city, which is accelerating land surface temperature increase and enhancing the UHI effects. The trends of increasing air temperature and LST are attracting extreme climatic events towards the study area. The expansion of built-up area in place of agricultural and forest land has led to the green cover removal, which expanded high LST and UHI effects towards the eastern and southern parts of the study area.

The continuation of the found LULC change trend is extremely sensitive for the ecosystem and ecological structure of the study area. These changes might render the city more ecologically fragile, particularly the areas that could be transformed into built-up regions in the future. So, more studies are needed to evaluate vegetation cover required for a sustainable environment of the city and mitigation of global climate change effects at the micro-level. Moreover, studies are required to convert the high heated built-up land into sustainable and thermally homogeneous areas by using modern technologies like green walls, green roofs, and vertical gardens. Finally, the study calls the attention of the management to mitigate or minimize the adverse effects of LULC changes by limiting the loss of green cover and increasing the number of green spaces in densely populated urban areas, which would help to reduce LST and UHI effects in the city.

REFERENCES

Abuloye, A., Popoola, K., Adewale, A., Vera, O., & Nicholas, E. (2015). Assessment of Daytime Surface Urban Heat Island in Onitsha, Nigeria, DOI: 10.13140/RG.2.1.5117.5765.

Aflaki A., Mirnezhad M., Ghaffarianhoseini A., Ghaffarianhoseini A., Omrany H., Wang Z.-H., & Akbari H. (2017). Urban heat island mitigation strategies: A state-of-the-art review on Kuala Lumpur, Singapore and Hong Kong. Cities, 62, 131–145.

Alavipanah S., Wegmann M., Qureshi S., Weng Q., & Koellner T. (2015). The Role of Vegetation in Mitigating Urban Land Surface Temperatures: A Case Study of Munich, Germany during the Warm Season. Sustainability, 7(4), 4689–4706. https://doi.org/10.3390/su7044689

Amani-Beni M., Zhang B., Xie G.-D., & Shi Y. (2019). Impacts of urban green landscape patterns on land surface temperature: Evidence from the adjacent area of Olympic Forest Park of Beijing, China. Sustainability, 11(2), 513.

Barman T., Ghongade R., & Ratnaparkhi A. (2016). Rough set based segmentation and classification model for ECG. 2016 Conference on Advances in Signal Processing (CASP), 18–23.

Deng X., Li, Z., & Gibson J. (2016). A review on trade-off analysis of ecosystem services for sustainable land-use management. Journal of Geographical Sciences, 26(7), 953–968.

El-Hattab M., S.m. A., & G.e. L. (2018). Monitoring and assessment of urban heat islands over the Southern region of Cairo Governorate, Egypt. The Egyptian Journal of Remote Sensing and Space Science, 21(3), 311–323, DOI: /10.1016/j.ejrs.2017.08.008.

Forman R. T. (2016). Urban ecology principles: Are urban ecology and natural area ecology really different? Landscape Ecology, 31(8), 1653–1662.

Fu P., & Weng Q. (2016). A time series analysis of urbanization induced land use and land cover change and its impact on land surface temperature with Landsat imagery. Remote Sensing of Environment, 175, 205–214.

Grover A., & Singh R. B. (2015). Analysis of Urban Heat Island (UHI) in Relation to Normalized Difference Vegetation Index (NDVI): A Comparative Study of Delhi and Mumbai. Environments, 2(2), 125–138, DOI:10.3390/environments2020125.

Gunawardena K. R., Wells M. J., & Kershaw T. (2017). Utilising green and bluespace to mitigate urban heat island intensity. Science of the Total Environment, 584, 1040–1055.

Guo G., Wu Z., & Chen Y. (2019). Complex mechanisms linking land surface temperature to greenspace spatial patterns: Evidence from four southeastern Chinese cities. Science of The Total Environment, 674, 77–87.

Iqbal M. Z., & Iqbal M. J. (2018). Land use detection using remote sensing and gis (A case study of Rawalpindi Division). American Journal of Remote Sensing, 6(1), 39–51.

Jabbar M., Yusoff M. M., & Shafie A. (2021). Assessing the role of urban green spaces for human well-being: A systematic review. GeoJournal, DOI:10.1007/s10708-021-10474-7.

Jiang Y., Fu, P., & Weng Q. (2015). Assessing the Impacts of Urbanization-Associated Land Use/Cover Change on Land Surface Temperature and Surface Moisture: A Case Study in the Midwestern United States. Remote Sensing, 7(4), 4880–4898. https://doi.org/10.3390/rs70404880

Kaplan G., Avdan U., & Avdan Z. Y. (2018). Urban Heat Island Analysis Using the Landsat 8 Satellite Data: A Case Study in Skopje, Macedonia. Proceedings, 2(7), 358, DOI:10.3390/ecrs-2-05171.

Koko A. F., Yue W., Abubakar G. A., Alabsi A. A. N., & Hamed R. (2021). Spatiotemporal Influence of Land Use/Land Cover Change Dynamics on Surface Urban Heat Island: A Case Study of Abuja Metropolis, Nigeria. ISPRS International Journal of Geo-Information, 10(5), 272, DOI: 10.3390/ijgi10050272.

Konstantinov P. I., Grishchenko M. Y., & Varentsov M. I. (2015). Mapping urban heat islands of arctic cities using combined data on field measurements and satellite images based on the example of the city of Apatity (Murmansk Oblast). Izvestiya, Atmospheric and Oceanic Physics, 51(9), 992–998, DOI: 10.1134/S000143381509011X.

Krellenberg K., Welz J., & Reyes-Päcke S. (2014). Urban green areas and their potential for social interaction–A case study of a socio-economically mixed neighbourhood in Santiago de Chile. Habitat International, 44, 11–21, DOI: 10.1016/j.habitatint.2014.04.004.

Li J., Zheng X., Zhang C., & Chen Y. (2018). Impact of land-use and land-cover change on meteorology in the Beijing–Tianjin–Hebei Region from 1990 to 2010. Sustainability, 10(1), 176.

Lou H., Yang S., Zhao C., Wang Z., Liu X., Shi L., Wu L., Hao F., & Cai M. (2017). Combining multi-source data to explore a mechanism for the effects of micrometeorological elements on nutrient variations in paddy land water. Paddy and Water Environment, 15(3), 513–524, DOI: 10.1007/s10333-016-0568-5.

MAHMOUDZADEH H. (2007). Digital change detection using remotely sensed data for monitoring green space destruction in Tabriz.

Mensah C. A., Andres L., Perera U., & Roji A. (2016). Enhancing quality of life through the lens of green spaces: A systematic review approach. International Journal of Wellbeing, 6(1), 142–163, DOI: 10.5502/ijw.v6i1.445.

Mishra V. N., Rai P. K., & Mohan K. (2014). Prediction of land use changes based on land change modeler (LCM) using remote sensing: A case study of Muzaffarpur (Bihar), India. Journal of the Geographical Institute» Jovan Cvijic», SASA, 64(1), 111–127.

Mohamed M. A. (2021). Spatiotemporal Impacts of Urban Land Use/Land Cover Changes on Land Surface Temperature: A Comparative Study of Damascus and Aleppo (Syria). Atmosphere, 12(8), 1037, DOI: 10.3390/atmos12081037.

Naeem M. A., Armutlulu A., Imtiaz Q., Donat F., Schäublin R., Kierzkowska A., & Müller C. R. (2018). Optimization of the structural characteristics of CaO and its effective stabilization yield high-capacity CO_2 sorbents. Nature Communications, 9(1), 1–11.

National Oceanic and Atmospheric Administration. (n.d.). Retrieved 5 October 2020, from https://www.noaa.gov/

Niu X., Tang J., Wang S., & Fu C. (2019). Impact of future land use and land cover change on temperature projections over East Asia. Climate Dynamics, 52(11), 6475–6490, DOI: 10.1007/s00382-018-4525-4.

Oke T. R. (1982). The energetic basis of the urban heat island. Quarterly Journal of the Royal Meteorological Society, 108(455), 1–24.

Pakistan Meteorological Department PMD. (n.d.). Retrieved 5 October 2020, from http://www.pmd.gov.pk/index-old.html

Palafox-Juárez E. B., López-Martínez J. O., Hernández-Stefanoni J. L., & Hernández-Nuñez H. (2021). Impact of Urban Land-Cover Changes on the Spatial-Temporal Land Surface Temperature in a Tropical City of Mexico. ISPRS International Journal of Geo-Information, 10(2), 76, DOI: 10.3390/ijgi10020076.

Ramaiah M., Avtar R., & Rahman M. M. (2020). Land Cover Influences on LST in Two Proposed Smart Cities of India: Comparative Analysis Using Spectral Indices. Land, 9(9), 292, DOI: 10.3390/land9090292.

Shirazi S. A. (n.d.). Temporal Analysis of Land Use and Land Cover Changes in Lahore-Pakistan. 13(1), 20.

Shirazi S. A., & Kazmi J. H. (2016). Analysis of socio-environmental impacts of the loss of urban trees and vegetation in Lahore, Pakistan: A review of public perception. Ecological Processes, 5(1), 1–12.

Tran D. X., Pla F., Latorre-Carmona P., Myint S. W., Caetano M., & Kieu H. V. (2017). Characterizing the relationship between land use land cover change and land surface temperature. ISPRS Journal of Photogrammetry and Remote Sensing, 124, 119–132, DOI: 10.1016/j.isprsjprs.2017.01.001.

Varentsov M. I., Grishchenko M. Y., & Wouters H. (2019). Simultaneous assessment of the summer urban heat island in Moscow megacity based on in situ observations, thermal satellite images and mesoscale modeling. GEOGRAPHY, ENVIRONMENT, SUSTAINABILITY, 12(4), 74–95, DOI: 10.24057/2071-9388-2019-10.

Wan Mohd Jaafar W. S., Abdul Maulud K. N., Muhmad Kamarulzaman A. M., Raihan A., Md Sah S., Ahmad A., Saad S. N. M., Mohd Azmi A. T., Jusoh Syukri N. K. A., & Razzaq Khan W. (2020). The influence of deforestation on land surface temperature—A case study of Perak and Kedah, Malaysia. Forests, 11(6), 670.

Wang H., Zhang Y., Tsou J. Y., & Li Y. (2017). Surface Urban Heat Island Analysis of Shanghai (China) Based on the Change of Land Use and Land Cover. Sustainability, 9(9), 1538, DOI: 10.3390/su9091538.

WHO | Urban green spaces. (n.d.). WHO; World Health Organization. Retrieved 27 April 2020, from http://www.who.int/sustainable-development/cities/health-risks/urban-green-space/en/

Wibowo A., Yusoff M. M., Adura T. A., & Zaini L. H. (2020). Spatial model of air surface temperature using Landsat 8 TIRS. IOP Conference Series: Earth and Environmental Science, 500(1), 012009.

Yang Y.-J., Wu B.-W., Shi C., Zhang J.-H., Li Y.-B., Tang W.-A., Wen H.-Y., Zhang H.-Q., & Shi T. (2013). Impacts of Urbanization and Station-relocation on Surface Air Temperature Series in Anhui Province, China. Pure and Applied Geophysics, 170(11), 1969–1983, DOI: 10.1007/s00024-012-0619-9.

Yasin M. Y., Yusof M., & Nisfariza M. N. (2019). Urban sprawl assessment using time-series lulc and NDVI variation: A case study of Sepang, Malaysia. Applied Ecology and Environmental Research, 17(3), 5583–5602.

Yu Z., Guo X., Zeng Y., Koga M., & Vejre, H. (2018). Variations in land surface temperature and cooling efficiency of green space in rapid urbanization: The case of Fuzhou city, China. Urban Forestry & Urban Greening, 29, 113–121.

Zhang L., Tan P. Y., & Diehl J. A. (2017). A conceptual framework for studying urban green spaces effects on health. Journal of Urban Ecology, 3(1), DOI: 10.1093/jue/jux015.

Zhou W., Wang J., & Cadenasso M. L. (2017). Effects of the spatial configuration of trees on urban heat mitigation: A comparative study. Remote Sensing of Environment, 195, 1–12.

RESEARCH PAPER

MAPPING ECOSYSTEM SERVICES OF FOREST STANDS: CASE STUDY OF MAAMORA, MOROCCO

Abdelkader Benabou[1,2], Said Moukrim[1] , Said Laaribya[3*], Abderrahman Aafi[4], Aissa Chkhichekh[5], Tayeb El Maadidi[2], Ahmed El Aboudi[1]

[1]Mohammed V University, Faculty of Sciences. Rabat, Morocco.
[2]Ministerial Department of Water and Forestry, Rabat, Morocco.
[3]Ibn Tofail University Laboratory of territories, environment, and development Kenitra, Morocco.
[4]National Forestry School of Engineers, Sale, Morocco.
[5]Royal Technical Institute of Water and Forestry, Sale, Morocco.
***Corresponding author:** said.laaribya1@uit.ac.ma
Received: April 26th, 2021 / Accepted: February 15th, 2022 / Published: March 31st, 2022
https://DOI-10.24057/2071-9388-2021-047

ABSTRACT. The concept of ecosystem services (ES) is increasingly used to analyze the relationships and interactions between humans and nature. Understanding the ecosystem services' flow and the ecosystems' capacity to generate these services is an essential element in considering the sustainability of ecosystem uses and the development of ecosystem accounts. For such purpose, we conduct spatially explicit analyses of nine ecosystem services in the Maamora forest, Morocco. The ecosystem services included are timber and industry wood harvest, firewood harvest, cork gathering, forage production, acorn gathering, forest carbon storage, and recreational hiking. Results make it possible to distinguish between the forest capacity to provide ecosystem services from their current use (demand) and assess them quantitatively. It came out that both capacity and flow differ in spatial extent as well as in quantity. Distinguishing capacity and flow of ES also provided an estimate of over-or under-utilization of services, and offer the possibility to map the ecosystem service provision hotspots (SPA) and degraded SPHs. The respective assessment of capacity and flux in a space-explicit manner can therefore support the monitoring of the forest ecosystem use sustainability.

KEYWORDS: assessment, ecosystem accounting, monitoring, spatial analyses, sustainability

CITATION: Benabou A., Moukrim S., Laaribya S., Aafi A., Chkhichekh A., El Maadidi A., EL Aboudi A. (2022). Mapping Ecosystem Services of Forest Stands: Case Study of Maamora, Morocco. Vol.15, № 1. Geography, Environment, Sustainability, p 141-149
https://DOI-10.24057/2071-9388-2021-047

Conflict of interests: The authors reported no potential conflict of interest.

INTRODUCTION

Ecosystem services (ES) are increasingly used as a concept for analyzing the relationships and interactions between humans and nature. It can also be referred to as a framework to support decision-making for sustainable natural resources' management, emerging from the scientific field to be serving the policy and operational domains in recent years (Plieninger and Bieling 2013). They are defined as the contributions that ecosystems make to human well-being, and result from the interaction of biotic and abiotic processes (MEA 2005). This concept emergence resulted in the development of ecosystem accounting The latter is considered as a new approach in ecology for the environmental assessment through measuring ecosystems and ecosystem service flows under human activities.

In Morocco, the national accounting sytem, which is based on branches, does not consider the multiple contributions of the forestry sector to the economy, particularly non-timber products and services. This contribution is rather incorporated into the 'Agriculture, Forestry and Fishing' branch. This explains why the economic role of forest ecosystems is still insufficiently highlighted (El Mokaddem 2016).

Spatial mapping of both ecosystem provision of ES and their current use by societies is a key feature of ecosystem services (Schröter et al. 2014). Mapping multiple ecosystem services has become an important scientific endeavor (Bryan et al. 2011, Turner et al. 2016). However, the number of ecosystem services considered in studies remains low and the validation of results is rarely performed (Seppelt et al. 2011).

Taking into consideration recent experiences of ES mapping in North Africa, this study aims at mapping the provisioning capacity and the multiple ecosystem services' use flow of the Maamora forest. It is also intended to assess this approach's relevance in designing and implementing innovative forest ecosystem management plans that best conciliate between the user populations' pressing needs and the natural resource sustainability requirements (Laaribya et al. 2021).

Area of study

The Maamora forest is located in Northwestern Morocco close to the Atlantic Ocean (Fig. 1). It is subdivided into five cantons, three of which (A, B, and C) will be concerned by this study. The topography is flat. The geological formations are primarily Pliocene to Pleistocene marine deposits (Aafi et al. 2005a), with sandy soils overlying a clay substrate. They are classified as aerosols according to the WRB nomenclature (FAO/IUSS 2006).

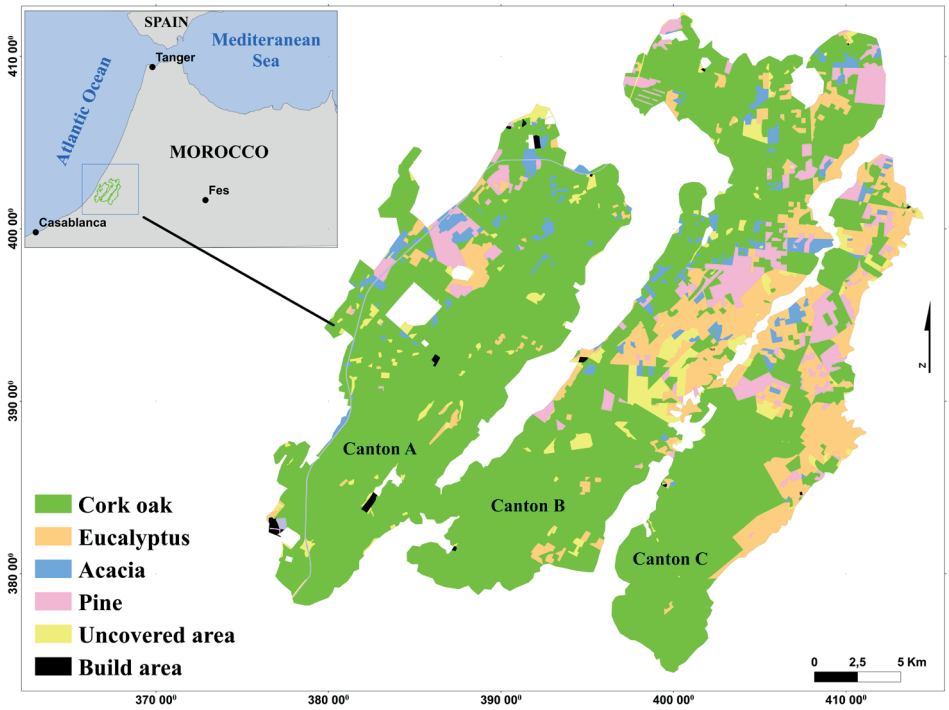

Fig. 1. Forest stand type map

The study area is dominatd by a Mediterranean climate with a dry season generally begining in late April or early May and extending through October (Aafi et al. 2005a). The spatial distribution of forest cover is illustrated by the stand type map (Fig. 1). It shows that more than 75 % of the study area is made out of natural stands of cork oak (*Quercus suber* L.), endemic species of the Mediterranean-Atlantic. The other stands are based on exotic species such as: *Eucalyptus camaldulensis* D., *Eucalyptus cladocalyx* F., *Eucalyptus gomphocéphalla* DC., *Eucalyptus gradnis* W., *Acacia molicima* D., *Acacia cyclops* A., *Pinus canariensis* C., *Pinus pinea* L., *Pinus radiata* D., *Pinus pinaster* Aiton., and *Pinus halipensis* Mill.

MATERIALS AND METHODS

This study is intended to develop spatial maps of some ecosystem services in the study area by distinguishing the capacity of their production by forest ecosystems as well as their flow. It is also sought to produce maps of spatial balance between capacity and flow for two ecosystem services taken as examples. Furthermore, it will provide tables of both capacity and flow accounting by ecosystem and at the level of each territorial unit. Such tables will serve as as a first draft of the ecosystem accounting drawing up.

Ecosystem Services' choice

This assessment emcompasses ecosystem services coming out of interviews lead with the Department of Water and Forestry officials and representatives of the few rural communes and NGOs. Similarly, the choice was oriented to step the guidelines of the International Common Classification of Ecosystem Services, covering a range of ecosystem services representing categories of provisioning and regulation, as well as cultural ones (Chan et al. 2012, Fagerholm et al. 2012).

The list of selected ecosystem services and assessment indicators in the study area are showens in Table 1.

The indicators used (Table 1) for the spatial assessment of ecosystem service capacity and flow provide relevant, reliable, and accurate measures (Burkhard et al. 2012). These measures generally correspond to annual averages per hectare. The reference year is that of 2016 as it corresponds to the new Maamora forest management plan launching (DEF 2015).

Spatial units

The spatial units taken as the basic unit for determining the average values of ecosystem services were defined taking into consideration the recommendations of the SEEA (System of Environmental-Economic Accounting). Such system, undeniably allows for the human and institutional dimensions in the establishment of ecosystem spatial accounting. Thus, two spatial units are to be distinguished:

- The administrative units are defined according to the division of the territorial communes. It benefit from the revenues generated by the forest products' valorization.
- The traditional grazing units for livestock and Firewood harvesting rights are quite granted to the user tribes.

Spatial models of ecosystem service capacities and flow patterns

Considering the collected data sets, the spatial mapping was based on distinct spatial models according to the selected indicators (Schröter et al. 2014) as indicated in Table 1. The used data are from the stand types' map

Table 1. List of selected ecosystem services and assessment indicators

Section	Supply					Control	Cultural Activity
Ecosystem services	Forage (grazing)	Lumber and industrial wood	Firewood	Cork	Acorns	Carbon storage	Recreational hiking density
Indicators	SLU·ha^{-1}	m^3·ha^{-1}	stere·ha^{-1}	stere·ha^{-1}	t·year^{-1}	mg·ha^{-1}	km·km^{-2}

Note: SLU is Standard Livestock Unit.

established as part of the Maamora Forest management study (DEF 2015). It is carried out, after determining the useful area, based on preliminary interpretations; stratification criteria; choice of symbols; delineations of strata; verification of strata in the field; final interpretation; drafting of the map and cutting into parcels.
The area of forest stands scheduled for harvesting is showed in Table 2.

The data sources used in this study are as follows:

- The cutting program was established in the framework of the Maamora Forest management study (DEF 2015). This plan defines the annual program.
- The average annual area of the programmed forest area was calculated by species and/or type of silvicultural operation, as well as by administrative unit (Tab.2).
- The average yields of forestry cuts. Knowing that they vary significantly depending on the species, its age, as well as the considered type of silvicultural and harvesting operation, their yields were estimated based on the analysis of data from auctions conducted between 2004 and 2014.
- The results of the research conducted on (i) carbon storage in forest stands in the Maamora, (ii) Firewood removals, (iii) grazing, (iv) recreation and leisure.
- Socio-economic data from the general population census.
- Forest tracks were assimilated to hiking trails. Their plots were used for both the capacity maps' development and the recreation trails' ecosystem service.

Spatial Balances of Ecosystem Services

The balances were created for two services: Firewood and livestock grazing. These services are the major constraints faced by forest managers in relation with the realization and success of forest ecosystem restoration, recovery, and enhancement projects.

This type of spatial map makes it possible to delimit as precisely as possible the strong pressure prone areas regarding a given service, or those with unused production potential by measuring the involved quantities using appropriate indicators.

RESULTS

Harvesting of lumber and industrial wood

The analysis of the capacity (Fig. 2a) and flow (Fig. 3a) maps of the ecosystem service of the lumber and industrial wood harvest show high spatial variability. The high spots of this service are almost localized in the eastern parts of the two cantons B and C of the Maamora Forest. The scattered patches' form is rather observed in canton A.

This situation is explained by the spatial distribution of artificial stands, particularly Eucalyptus plantations, which contribute up to 96 % of this ecosystem service's production capacity, estimated at 302,607m^3 (Table 3). These plantations were mostly located in the eastern parts of the Maamora subject to human pressure, climate severity, and capricious edaphic conditions (Dahmani 2006, Laaribya et al. 2013).

This spatial variability also characterizes the levels of its supply capacity; it thus rises, according to the zones, from 0.1–1.5 m^3·ha^{-1}·yr^{-1} to more than 43 m^3·ha^{-1}·yr^{-1}. This difference is directly related to the planted stands' type and the planned cuts' nature during the management period under consideration (Table 2). It is also influenced by the effects of the new management objectives' implementation set to convert artificial woodlands in areas of regeneration and recovery of the cork oak's natural stands.

The flow map (Fig. 3a) remains largely comparable to that of capacity (Fig. 2a), given the implementation rates of previous management plans. It vary significantly depending on the stands'types as well as on the failure to take into account the illegal cutting phenomenon of Eucalyptus wood poles that is obvious in certain forest areas. Such situation results in a flow of this service set at 224,515 m^3·yr^{-1} on the scale of this study.

Thus, the achievements' analysis of the cited above management plans reveals that the intervention program concerning pine stands is the most well respected with a success rate of nearly 85 %, followed by that of Eucalyptus with 75 %, and lastly Acacia-based plantations with barely 42 %.

Firewood harvesting

The capacity map for the ecosystem service of harvesting Firewood shows a clear distinction between the southern and northern parts of the study area (Fig. 2b). The former area has a capacity of little more than 0.5 stere·ha^{-1}·yr^{-1}, while the latter has higher levels with up to 41 steres·ha^{-1}·yr^{-1}, in some places. This high spatial variability in this service capacity is the result of the cover heterogeneity of the artificial forest stands as previously mentioned.

The supply capacity levels of this service are also impacted by the recommended conducting rules for these series of cork oak. The realization of regeneration operations was done only by whole plot under cover of trees, considering the total absence of regeneration either by stump sprouting or by natural seedlings. The silvicultural maintenance operations (Table 2) in the form of depressing, pruning, formation pruning, and thinning are also defined for young stands of the cork oak.

The flow map of these services (Fig. 3b) was also established by applying the same implementation rates of the previous management plans except for the cork oak series. It is noted a solemn commitment on the part of the forestry administration officials to meet the challenge of the reconstitution and restoration of the Maamora original ecosystem, through a strict application of the dedicated silvicultural conducting rules by capitalizing on past failure experiences. This will raise the contributing share of these natural stands in this service flow to nearly 58 %, followed by plantations of Eucalyptus with 28 %.

Firewood harvesting by local populations was also taken into consideration when mapping this service flow. Considered as the primary beneficiaries, they have the right, as enshrined in the current forestry law, to collect dead wood lying around to satisfy their domestic needs for heating and cooking. However, these uses have evolved and have been, over the years, transformed into almost

Table 2. Area of forest stands scheduled for harvesting

Types of forest cutting	Silvicultural cuts			Regeneration and maintenance of cork oak stands				Cork harvest
	Pine	Acacia	Eucalyptus	A	B	C	Total	
Area, ha	6867	2624	10,965	8286	2021	3126	13,433	89,343

Note: A – area to be regenerated on 1st pass; B – area to be maintained on 1st pass; C– area to be regenerated on 2nd pass.

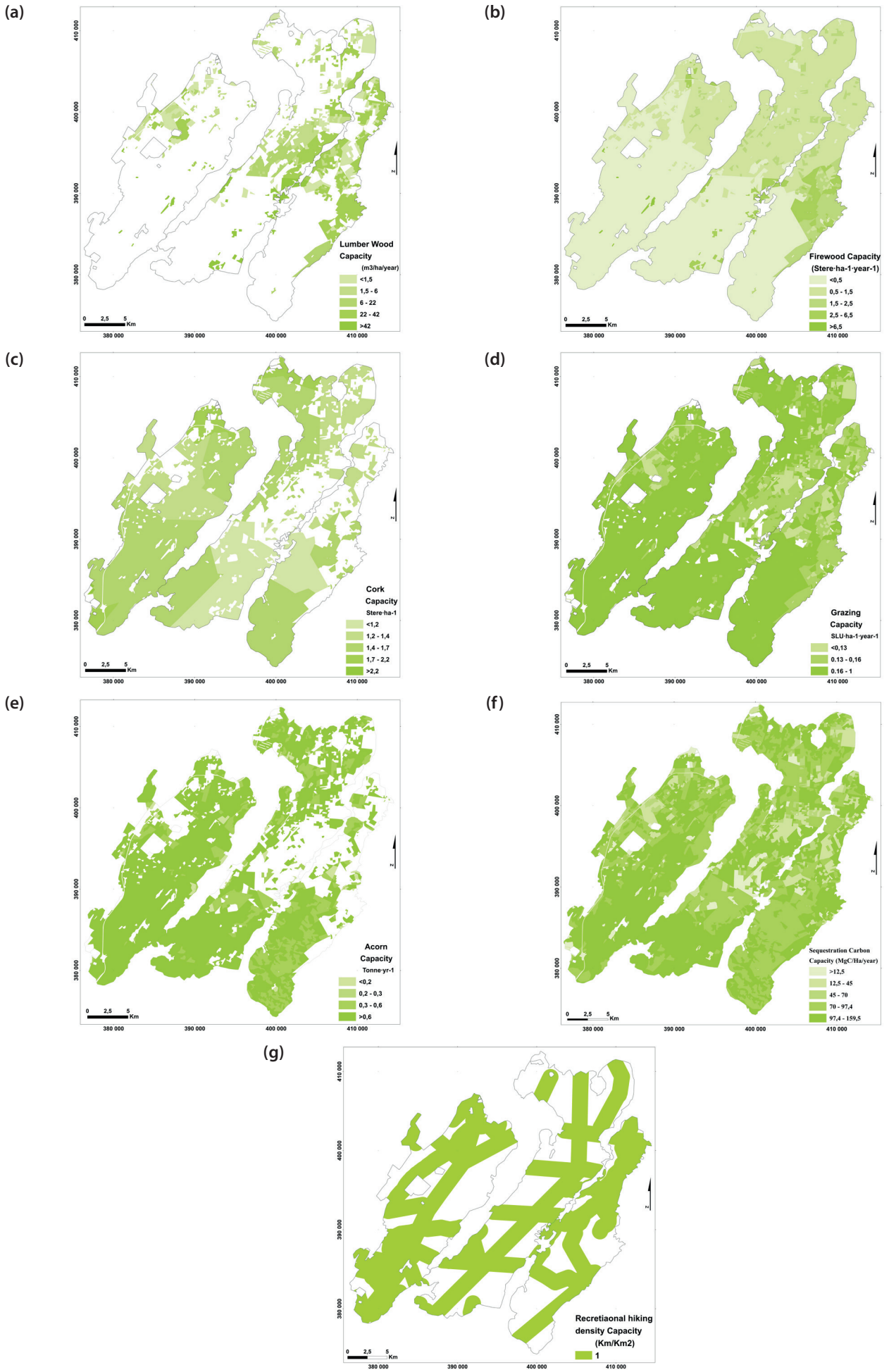

Fig. 2. Maps of the ecosystem services capacity: 2.a) Lumber and industrial wood harvest, 2.b) Firewood harvest, 2.c) Cork harvest, 2.d) Forage production, 2.e) Acorn gathering, 2.f) Carbon storage, 2.g) Recreational hikin

generalized criminal practices, in search of new financial resources to improve their standard of living through direct sale to the nearest urban centers, whether it be raw firewood or transformed into charcoal wood.

This uses' mutation is mainly due to the vertiginous bordering urban zones' sprawl and the subsequent needs' increase in terms of woody fuels used in the functioning of the bread ovens, the brick factories, the Moorish baths, the pressings and others (Bendaanoun 1996, Hemmich 2003). Thus, the firewood flow varies very significantly spatially without a particular noticeable trend. It is estimated at less than 1.4 stere^{-1}ha^{-1}·yr^{-1} particularly in the southeastern part of the study area and can reach the threshold of 160 stere^{-1}ha^{-1}·yr^{-1} in its eastern part, where a large population is concentrated within rural settlements which are considered as black spots in terms of wood cutting offenses (Aafi 2007).

That explain the hight level of flow wich represent more than three times of the supply capacity estimated at 49,816 steres·yr^{-1}, wich is an average of overharvesting rate equal to 1.66 steres·ha-1·yr^{-1} (Table 3). Moreover, referring to the results of the spatial balance map (Fig. 4a), this deficit rate varies significantly between communes, ranging from 1 to more than 4 steres·ha^{-1}·yr^{-1}.

Cork harvesting

The spatially explicit maps of cork harvesting capacity and service flow (Fig. 2c and 3c) accurately reflect the condition and structure of cork oak stands, the history of past harvests, which are set at 5 with a 9-year rotation, and the regeneration efforts of this natural species undertaken in recent years by the forestry administration.

The western parts containing the most preserved stands show the highest capacity levels, reaching up to 6.4 steres·ha^{-1}·yr^{-1} in their northern and southern extremities. However, the eastern portions show low capacities of only 1.1 stere·ha^{-1}·yr^{-1}, particularly in its highly disaggregated northern areas. The latter are classified in high proportion in the regeneration management group.

This spatial heterogeneity in this service provision, estimated on average at more than 77,261 steres·yr^{-1}, could have been more pronounced if the stands' density factor was taken into consideration, instead of being assessed solely based on average production yields of reproductive cork and male cork estimated respectively at 8.36 and 0.28 steres·ha^{-1} throughout the study area (Hammoudi 2002, DEF 2015).

The yields' diversity remains very much influenced by the still young age of the regeneration perimeters carried out under the conversion programs of the old artificial plantations. These plots, covering nearly 15 % of the surface area of cork oak stands, will only be partially affected by the cork harvesting program during the current management period. (Hammoudi 2002, DEF 2015).

The flow map of these ecosystem service (Fig.3c) was established on the basis of the implementation rate of previous cork harvest programs. This rate is estimated at 96%, which shows the importance given to this sector.
Although this ecosystem service flow is subject to better control and regulated organization through two stages with a separation between the operation of exploitation and sale, Moroccan cork production remains poorly valorized. It is mainly destined for export, with varying degrees of transformation (raw, semi-worked and worked cork) (Hammoudi 2002).

Forage

The forage production capacity map (Fig. 2d) accurately expresses the equilibrium pastoral load that determines the small livestock units' number that a grazing area can support without compromising its sustainability. It illustrates the potential for forage production, which is highly differentiated between the natural and artificial stands in the study area.

This potential is estimated at 300 Forage Unit (FU)·ha^{-1}·yr^{-1} for cork oak stands (FU: Forage Unit), 50 FU·ha^{-1}·yr^{-1} for hardwood reforestation, and 40 FU·ha^{-1}·yr^{-1} for softwood plantations (Laaribya et al. 2013, 2021; DEF 2015). Knowing that these average yields vary significantly from one year to another depending on the recorded rainfall volume. They are also highly sensitive to the nature of soils, density, and structure of stands (M'hirit et al. 1995, Benabid 2000, Aafi et al. 2005a).

Based solely on the stand types' map, the capacity map produced in this way broadly follows a northwest-southeast gradient, with a near-dominance of the capacity threshold of 1 Standard Livestock Unit (SLU)·ha^{-1}·yr^{-1}, delivered by the cork oak-based areas of different density classes. These forests' stands provide more than 95 % of the average annual capacity of this service, estimated at 54,941 SLU.

The flow map (Fig. 3d) provides information on the real pastoral load, defined as the load imposed on the grazing, evaluated annually at 178,303 SLU (Table 3). Since this is an ecosystem service whose flow is defined as a right of use recognized by the riparian populations, organized into traditional tribes delimiting 5 spatially distinct pastoral parks, this map shows a variation in flow levels that is very perceptible at the territorial level.

Thus, the map of spatial balance (Fig. 4.b) shows a positive balance of 0.4 SLU·ha^{-1}·yr^{-1}, recorded at the level of

Table 3. Accounting tables for ecosystem services

Peuplement	Firewood harvesting (Stere/year)		Harvesting of timber and industrial wood (m^3/year)		Forage (SLU/year)		Cork Harvesting (Stere/year)		Carbon storage (MgC)	Acorn gathering (Tonne/year)
	Capacity	Flow	Capacity	Flow	Capacity	Flow	Capacity	Flow	Capacity	Capacity
Acacia	4 526	12 234	4 464	1 857	402	546			168 872	
Eucalyptus	13 744	46 627	292 729	218 083	1 543	4 325			1 430 545	
Pin	3 369	9 453	5 415	4 576	600	1 421			202 331	
Chêne-liège	28 177	99 463			52 396	172 011	77 261	74 170	6 869 864	34 487
Vide									33 078	
Total	49 816	167 777	302 607	224 515	54 941	178 303	77 261	74 170	8 704 689	34 487

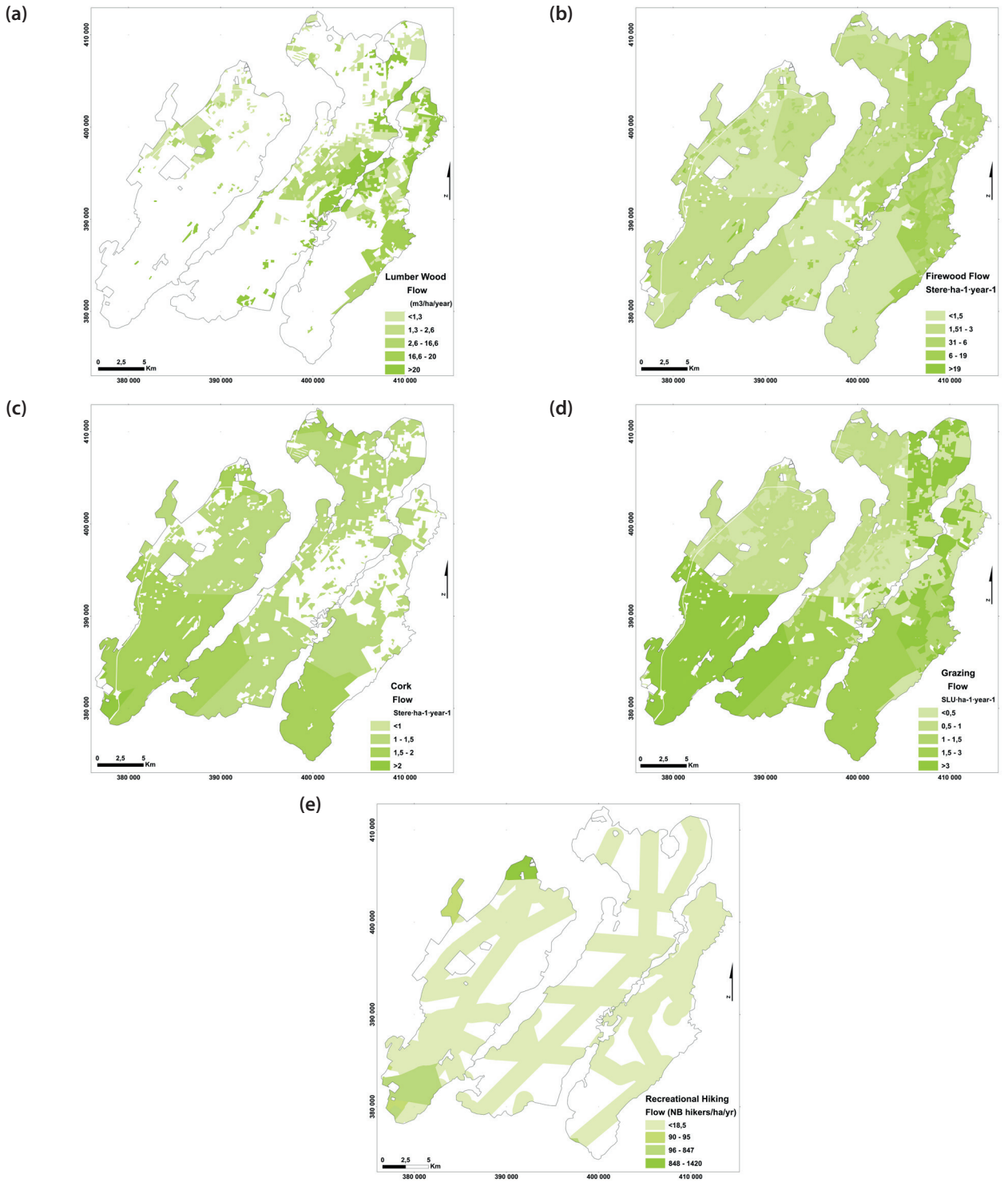

Fig. 3. Maps of the ecosystem services flow: 3.a) Lumber and industrial wood harvest, 3.b) Firewood harvest, 3.c) Cork harvest, 3.d) Forage production, 3.e) Recreational hiking

the pastoral park of Ameur-Haouzia, while it is negative in the other four parks with overgrazing rates ranging from 0.6 to over 3 SLU·ha^{-1}·yr^{-1}.

This observed variability between the different pastoral parks is also the expression of the related differences in terms of the number and composition of the herd, the extent of irrigated and rural agricultural areas, as well as the mode of herd management, supplementation in fodder units used by households as well as their standard of living (DEF 2015). It is known that supplements only contribute up to 25 % of the herd's needs in fodder units, and nearly 8 % for useful agricultural areas (UAA) dominated by high value-added crops such as arboriculture to the detriment of high-balance cereal crops forage.

Thus, the flow levels vary from less than 0.4 SLU·ha^{-1}·yr^{-1} in a few terroirs in the northeast, to nearly 6 SLU·ha^{-1}·yr^{-1}, mainly in the terroir located southwest of the study area.

Acorn gathering

The acorn production capacity map of the cork oak (Fig. 2e) highlights a clear territorial variability, with a distinction between the eastern and western parts. It shows capacity levels ranging from less than 0.1 t·ha^{-1}·yr^{-1} to more than 0.7 t·ha^{-1}·yr^{-1}. Which reprsents an average annual capacity of 34,487 tons.

This substantial territorial heterogeneity is the result of considering the density criterion in the evaluation. Thus, if an average production yield of a cork oak tree was

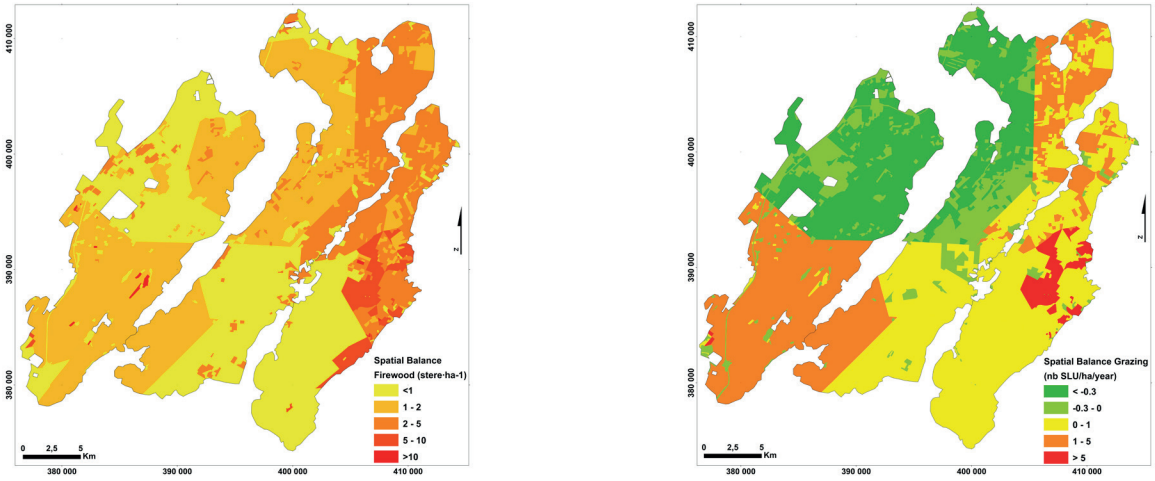

Fig. 4. Ecosystem services spatial balances: 4.a) Firewood harvesting, 4.b) Forage production

estimated at 6 kg·tree^{-1}·yr^{-1}, the number of trees retained by density classes is estimated at 250 tree·ha^{-1} for the dense class, 150 tree·ha^{-1} for the medium dense class, 75 tree·ha^{-1} for the light class and 25 tree·ha^{-1} for the sparse class (Aafi 2005b, DEF 2015).

The flow map of this ecosystem product has been considered identical to the capacity map since all the acorns produced are assumed to be consumed in full. Thus, its flow is mainly ensured by the local populations who are almost systematically involved in the acorn collection activity, either for self-consumption or for marketing.

In recent years, it is observed that acorn harvesting is used to harvest as many acorns as possible at an early stage, not only in times of shortage to feed livestock, but rather to maximize the profits generated from sales in urban centers.

Carbon storage

The map of the carbon storage capacity (Fig. 2f) shows a very marked spatial variability, from less than 12.5 MgC·ha^{-1}·yr^{-1} in some isolated and very bare areas, to more than 100 MgC/ha/yr in the parts covered by dense stands of the cork oak, contributing to 79 % of the annual average capacity estimated at 8.7 Tons of Carbon (Table 3). This variability reflects the heterogeneous distribution of forest cover, especially since the assessment was based on both the types and densities of stands.

Capacity varies significantly, depending on the density classes, from 65 to 237 MgC·ha^{-1}, with a mean value of 121 MgC·ha^{-1}, concentrated mainly at the level of the soil and tree biomass with nearly 51 % and 47 % of the total carbon stock respectively (Oubrahim et al. 2015). For the Eucalyptus stands, an average yield was fixed at 154.55 MgC·ha^{-1}, considering the dense class dominance for more than 93 % of the covered area and whose carbon stocks fluctuate according to the compartments, depending on the number of their rotations (Boulmane et al. 2017). This average value was also retained for Acacia stands and reduced by 50 % for resinous forests' stands.

The flow map was considered similar to the capacity map, knowing that the carbon flows released by the rural user populations remain very low as compared to the stored quantities by the forest ecosystems. Nevertheless, given that the Maamora forest is located between three large cities in Morocco with a very high urban density and a declared ambition to develop the industrial sector, a more thorough study, taking into consideration the final users of this ecosystem service, would be useful to better measure the major environmental role of this ecosystem in carbon storage at a regional or even national and global spatial scale.

Recreational hiking

The ecosystem service capacity map for recreational hiking (Fig. 2g) simply reflects the trail network, which is made up of both hiking trails and main trails. These trails are taken as territorial boundaries between municipalities or as boundaries between the main management groups that divide the Maamora forest stands.

It is only at the level of the five (5) dedicated recreational sites where it is noted a high density of trail network created as part of recreational development projects to accommodate the public (CRF 2011, El Mokaddem 2016). Outside of these natural areas, there is a strong capacity for recreational hiking; the capacity to provide this service remains almost equal, over an area exceeding 43,000 ha, or nearly 60 % of the area of the study area.

This ecosystem service's flow (Fig. 3e) shows that it is delivered to village hikers along spatial corridors as delineated and defined by the grid network of forest roads. However, it is also delivered within the five recreational sites created within the study area to accommodate a high proportion of urban visitors. Thus, flow levels are highly variable. They range from less than 5 hikers·ha-1 to nearly 500 hikers·ha-1 on weekend days in the spring and summer seasons. This high frequentation is recorded mainly at the recreational sites located in the northern and southern extremities of the western part of the study area. These high ratios greatly reflect the pressure of visitors coming from the main metropolises: Rabat, Salé and Kenitra, frequenting those sites being accessible through the main national roads (CRF 2011, Laaribya et al. 2013, El Mokaddem 2016).

DISCUSSIONS

The application of the ecosystem services mapping approach as a tool for sustainable management of forest ecosystems was based based upon seven ecosystem. The latter are intimately linked to the management objectives assigned to the Mamora Forest by its management plan, as well as to the commitments made by the country in the framework of the Convention on Biological Diversity and the Aichi targets (DEF 2015, CBD 1992). This choice also takes into consideration the multiple, sometimes contradictory, expectations of the different actors involved in defining the future of this natural area (DEF, 2015, Laaribya & al., 2021), known for its particular characteristics in terms of structure, health and physiology, as well as the fragility of its physical environment (García-Nieto & al. 2015).

In this regard, it is important to specify that the management study of the Mamora forest was carried out according to approaches based on the participation and adhesion of the riparian user populations, as well as of all the local actors involved in its management so as to guarantee a better valorization of the forest resources and to improve their contribution in the local economic development efforts (DEF 2015). The main management objectives assigned to the forest of Mamora aim its suberaie rehabilitation to ensure its sustainability, while improving its functions of reproduction cork and fodder units' production, and of neighboring towns' protection against wind erosion.

The sustainable management of forest areas inevitably implies taking into account their production capacities in terms of goods and services, often competitive, with regard to the various users and actors concerned. This requires compromises to be made on the temporal and spatial levels by the different users, including in particular (i) users with rights to harvest dead wood and to graze their livestock within well-defined territories, (ii) the territorial communes benefiting from revenues resulting in particular from the forest products' sale such as cork, timber and industrial wood, as well as firewood, (iii) the companies in charge of forestry work (iv) manufacturers involved in the activities of the forest products' valorization to various degrees, (v) hikers interested in leisure and recreation activities, (vi) neighboring urban populations in search of a clean environment, as well as the international community urging more conservation of nature and biodiversity for better adaptation and mitigation of the climate change phenomenon (DEF 2015, Maes & al. 2018).

Based on the above, the mapping of ecosystem services by distinguishing the capacity of their production and the flow of their provision, constitutes a better tool for assessing both the bio-physiological characteristics of forest ecosystems, as well as the impacts induced on the different user groups concerned by each or a group of forest ecosystems. Spatial identification of service provision hotspots (SPHs) and degraded areas can better inform decision-makers on how to implement rational, sustainable, and equitable forest resource management. Understanding the flow of ecosystem services and the capacity of ecosystems to generate these services is an essential element for understanding the sustainability of ecosystem use as well as developing ecosystem accounts (Palomo et al. 2012, Schröter 2014).

In this sense, the spatial balances created between the capacity and flow of ecosystem services are of particular interest in this regard. They allow a fine and precise analysis of the ecosystem services' use sustainability , as in the case of firewood production or cattle grazing taken as an example in our study. This corroborates the results obtained in several studies conducted in this area (Schröter et al., 2014, Burkhard et al, 2012; Nedkov et al. 2012). Similarly, the ecosystem services' accounting table for both capacity and flow (Table 3) can be a first step towards establishing environmental or ecosystem accounting (SEEA-EAA 2012, Schröter et al., 2014). It displays information that is as relevant as it is reliable for establishing sustainable management of forest ecosystem. In fact, this type of table can be constructed according to different possible spatial units (territorial communes, pastoral park, tribal terroir, etc.). This makes it possible to show the differences observed between the intrinsic potential of forest ecosystems to provide ecosystem services and the current levels of their use.

The use of these tools that support the implementation of an ecosystem accounting system as well as of the ecosystem service mapping approach, by distinguishing between capacities and flows, are fully in line with the guidelines advocated by both the SEEA and the TEEB (SEEA-EAA 2012, TEEB 2010).

This work's ES mapping results can support sustainable management of natural resources and spatial planning. They can also be applied to the development of nature-based solutions for social and economic challenges as well as in environmental education to share information about the importance of ecosystems for ES delivery and to promote choices supporting the sustainable use of those precious ecosystems. It's based on a better understinging of the interactions between land management, ecological processes and ecosystem service provision. Indicators can help to better understand these interactions and provide information for policy-makers to prioritize land management interventions (Geneletti & al. 2020, van Oudenhoven et al. 2012).

CONCLUSIONS

Spatial mapping of ecosystem services is a new approach to forest ecosystem assessment and analysis. It provides a better understanding of the complexity of attributes, uses, and direct and ultimate beneficiaries of multiple and diverse ecosystem services.

Based primarily on the stand type map and management plan for the Maamora Forest (DEF 2015), the produced spatially explicit ES maps are of great value in presenting the assessment results of the capacities and flows of each ecosystem service. This way of quantification and specialization is a new technique for guiding natural area management decisions towards more spatial and territorial equity and trade-offs in pursuit of forest resource conservation and enhancement goals.

Spatial balance maps and ecosystem accounting tables at different reference spatial units contribute greatly to this perspective. The determination of hotspots and cold ones, as well as the easy comparison between territories, by type of ecosystem service, can only offer managers and stakeholders the necessary information to make decisions in a clear and documented way. Such decisions should be defined based on a compromise between the range of ecosystem services of forest ecosystems, and between their different direct and final beneficiaries.

REFERENCES

Aafi A. (2007). Etude de la diversité floristique de l'écosystème de Chêne-liège de la forêt de la Maamora. Thèse de Doctorat D'Etat Es-Sc., Institut Agronomique et Vétérinaire Hassan II, Rabat, Maroc, 190 p. [in French].

Aafi A., Achhal El Kadmiri A., Benabid A., Rouchdi M. (2005a). Richesse et diversité floristique de la subéraie de la Mamora (Maroc). Acta Botanica Malacitana 30: 127–138. Available at: http://www.bioveg.uma.es/abm/volumenes/vol30/08.mamora.pdf.

Aafi A., Achhal El Kadmiri A., Benabid A., Rouchdi M. (2005b). Utilisation des images satellitaires SPOT pour la cartographie des types de peuplements de la forêt de la Mamora (Maroc). Revue Française de Photogrammétrie et Télédétection 178 (2): 30–35.

Benabid A. (2000). Flore et écosystèmes du Maroc: Evaluation et préservation de la biodiversité. Ibis Press, Paris, France. 359 p.

Bendaanoun M. (1996). La Maâmora un patrimoine national vital pour l'avenir de Salé et de la région. Journée d'étude 'Sauvons la Maâmora', Ecole National Forestière d'Ingénieurs, Salé. 30 p.

Boulmane M., Oubrahim H., Halim M., Bakker M.R., Augusto L. (2017). The potential of Eucalyptus plantations to restore degraded soils in semi-arid Morocco (NW Africa). Annals of Forest Science 74, 57, DOI: 10.1007/s13595-017-0652-z

Bryan B.A., Raymond C.M., Crossman N.D., King D. (2011). Comparing spatially explicit ecological and social values for natural areas to identify effective conservation strategies. Conservation Biology 25(1): 172–181.

Burkhard B., Kroll F., Nedkov S., Muller F. (2012). Mapping ecosystem service supply, demand and budgets. Ecological Indicators 21: 17–29.

CBD, 1992.Convention on Biological Diversity. United Nations.

Chan K.M.A., Satterfield T., Goldstein J. (2012). Rethinking ecosystem services to better address and navigate cultural values. Ecological Economics 74: 8–18.

CRF (Centre de Recherche Forestière) (2011). Etude relative aux attentes sociales vis à vis de la forêt marocaine, Forestry Research Center, Ministerial Department of Water and Forests, Rabat, Morocco: 10–29.

Dahmani J. (2006). Etude de la régénération naturelle et artificielle du Chêne-liège (Quercus suber L.) dans les forêts de la Mamora et de Témara. Thèse de Doctorat d'Etat, Faculté des Sciences, Université Ibn Tofaïl, Kénitra, Maroc, 138 p.

DEF (Département ministériel des Eaux et Forêts) (2015). Management plan of the Maamora forest, Morocco. Ministerial Department of Water and Forests, Kenitra, Morocco. 206 p.

El Mokaddem A. (2016). Estimation of the economic and social value of the services provided by Mediterranean forest ecosystems: Mamora forest, Morocco. Plan Bleu, Valbonne. 85 p. Available at: https://planbleu.org/sites/default/files/publications/rapport_foret_maroc_c2_6oct2016.pdf

Fagerholm N., Käyhkö N., Ndumbaro F., Khamis M. (2012). Community stakeholders' knowledge in landscape assessments – mapping indicators for landscape services. Ecological Indicators 18: 421–433.

FAO/IUSS (2006). IUSS Working Group WRB World Reference Base for Soil Resources 2006: a Framework for International Classification, Correlation and Communication. 2nd edition. World Soil Resources Reports no. 103. Food and Agriculture Organization of the United Nations, Rome. Italy. 128 p.

García-Nieto A., Quintas-Soriano C., García-Llorente M., Palomo I., Montes C., & Martín-López B. (2015) Collaborative mapping of ecosystem services: The role of stakeholders´ profiles. Ecosystem Services 13: 141152, DOI: 10.1016/j.ecoser.2014.11.006

Geneletti D., Esmail B. A., Cortinovis C., Arany I., Balzan M., van Beukering P. J., & Burkhard B. (2020). Ecosystem services mapping and assessment for policy-and decision-making: Lessons learned from a comparative analysis of European case studies. One Ecosystem 5: e53111, DOI: 10.3897/oneeco.5.e53111

Hammoudi A. (2002). Suberaie and landscape biodiversity. Vivexpo conference, Institut Méditerannène de Liège, France, 5 p. Available at: http://www.vivexpo.org/foire/images/Abdelaziz%20Hammoudi.pdf

Hemmich H. (2003). Evaluation des activités anthropozoogènes exercées dans la Maâmora occidentale et processus de gestion durable. Mémoire de 3ème cycle ENFI, Salé. 89 p.

Laaribya S., Alaoui A., Ayan S., Benabou A., Labbaci A., Ouhaddou H., Bijou M. (2021). Prediction by maximum entropy of potential habitat of the cork oak (Quercus suber L.) in Maamora Forest, Morocco. Forestist. 7 p., DOI: 10.5152/forestist.2021.20059

Laaribya S., Alaoui A., Gmira N., Gmira N. (2014). Contribution to the assessment of pastoral pressure in the Maâmora forest. Forest routes and overgrazing. Nature et Technologie C- Sciences de l'Environnement 10: 39–50.

M'hirit O., Benzyane M., Naggar M. (1995). L'Aménagement sylvopastoral. Actes de l'atelier sur le sylvo-pastoralisme- ENFI (Maroc), 25–28 Octobre 1995. Annales de la Recherche Forestière au Maroc. Rabat: 20–35.

Maes J, Teller A, Erhard M, Grizzetti B, Barredo JI, Paracchini ML, Condé S, Somma F, Orgiazzi A, Jones A, Zulian A, Petersen JE, Marquardt D, Kovacevic V, Abdul Malak D, Marin AI, Czúcz B, Mauri A, Loffler P, Bastrup-Birk A, Biala K, Christiansen T, Werner B. 2018. Mapping and Assessment of Ecosystems and their Services: An analytical framework for ecosystem condition. Publications office of the European Union, Luxembourg.

MEA (Millennium Ecosystem Assessment) (2005). Ecosystems and Human Well-Being: Synthesis. Island Press, Washington, DC. 64 p.

Oubrahim H., Boulmane M., Bakker M.R., Augusto L., Halim M. 2015. Carbon storage in degraded cork oak (Quercus suber) forests on flat lowlands in Morocco. iForest 9: 125–137, DOI: 10.3832 / ifor1364-008

van Oudenhoven A.P.E., Petz K., Alkemade R., Heina L., de Groot R. S. (2012). Framework for systematic indicator selection to assess effects of land management on ecosystem services. Ecological Indicators 21 (2012) 110–122. doi:10.1016/j.ecolind.2012.01.012

Palomo I., Martıin- Lopez B., Potschin M., Haines-Young R., Montes C. 2012. National Parks, buffer zones and surrounding lands: Mapping ecosystem service flows. Ecosystem Services, 13 p., DOI: 10.1016/j.ecoser.2012.09.001

Plieninger T., Bieling C. (2013). Resilience and the Cultural Landscape: Understanding and Managing Change in Human-Shaped Environments. Cambridge University Press, Cambridge. Landscape Ecol 28: 1841–1843, DOI:10.1007/s10980-013-9922-9

Schröter M., Bartonb D.N., Remmea R.P., Heina L. (2014). Accounting for capacity and flow of ecosystem services: A conceptual model and a case study for Telemark, Norway. Ecological Indicators. Volume 36, Pages 539-551, DOI: 10.1016/j.ecolind. 2013.09.018.

SEEA-EEA, 2012. System of Environmental-Economic Accounting 2012: Experimental Ecosystem Accounting. http://unstats.un.org/unsd/envaccounting/eea_white_cover.pdf

Seppelt R., Dormann C.F., Eppink F.V., Lautenbach S., Schmidt S. (2011). A quantitative review of ecosystem service studies: approaches, shortcomings and the road ahead. Journal of Applied Ecology 48: 630–636, DOI: 10.1111/j.1365-2664.2010.01952.x

TEEB, (2010). The Economics of Ecosystems and Biodiversity: Ecological and economic foundation. Earthscan, Cambridge.

Turner K.G., Andersonc S., Gonzales-Chang M., Costanza R., Courvillef S., Dalgaarda T., Dominati E., Kubiszewski I, Ogilvye S., Porfirio L., Ratna N., Sandhui H., Suttonc P.C., Svenning J.C., Turner G.M., Varennes Y.D., Voinov Y., Wratten S. 2016. A review of methods, data, and models to assess changes in the value of ecosystem services from land degradation and restoration. Ecological Modeling 319: 190–207.

RESEARCH PAPER

ENVIRONMENTAL CONSEQUENCES OF THE CAPITAL RELOCATION IN THE REPUBLIC OF KAZAKHSTAN

Natalia A. Koldobskaya
Candidate of Geographical Science, Department of Economic and Social Geography of Russia, Lomonosov Moscow State University, 119991, Russian Federation, Moscow, GSP-1, Leninskie gory, Faculty of Geography
***Corresponding author:** koldobskaya@gmail.com
Received: September 25th, 2021 / Accepted: February 15th, 2022 / Published: March 31st, 2022
https://DOI-10.24057/2071-9388-2021-110

ABSTRACT. The large-scale socio-economic and political changes that have taken place in the post-Soviet space since the early 1990s have led to cardinal transformations of the economy and settlement in the former Soviet republics. The purpose of the study is to identify patterns and main features of the transformation of the environmental situation in the old and new capitals of the Republic of Kazakhstan. The subject of this article is the ecological transformation in former and modern capitals of the Republic of Kazakhstan, which was affected not only by post-Soviet changes but also by the transfer of capital functions from Almaty to Nur-Sultan.

For a comprehensive analysis of the situation, the state of atmospheric air, water, soil and green spaces were considered. Quantitative calculations and qualitative assessment of the ecological situation showed that the environmental situation of both cities in 2020 was very similar, but the environmental state transformation index does not reach the level of Almaty due to the higher self-cleaning potential of the city and a newer and, accordingly, more environmentally friendly traffic flow. In two cities over the past 20 years, we registered a negative trend in impact level on water sources: a decrease in water consumption in Almaty by 45%, in Nur-Sultan by 27% since 2000. Modernization of plumbing and sewerage systems can reduce water leaks and improve wastewater transport to wastewater treatment plants. In 1998–2020, the environmental situation in Nur-Sultan changed much faster than in Almaty due to the low base effect and the transfer of capital functions because of the emissions from motor transport. However, for Almaty and Nur-Sultan, it can be concluded that the environmental situation by 2020 had been deteriorating much faster than it improved after the collapse of the USSR.

KEYWORDS: air pollution, solid wastes, integrated analysis, environmental conditions, environmental quality, Nur-Sultan, Almaty

CITATION: Koldobskaya N. A. (2022). Environmental Consequences Of the Capital Relocation In the Republic Of Kazakhstan. Vol.15, № 1. Geography, Environment, Sustainability, p 150-158 https://DOI-10.24057/2071-9388-2021-110

ACKNOWLEDGEMENTS: This research was performed according to the Development program of the Interdisciplinary Scientific and Educational School of Lomonosov Moscow State University «Future Planet and Global Environmental Change».

Conflict of interests: The authors reported no potential conflict of interest.

INTRODUCTION

After gaining independence, the Republic of Kazakhstan has seen significant political and socio-economic changes. One of the examples of these transformations is the transfer of the capital from Almaty to Nur-Sultan (former Astana). The transfer of capital changed the economic structure of the cities (Zimmerman 2010), their demographic situation, and, accordingly, this led to dynamic changes in the environmental situation (ES) in the cities.

The most visible environmental impacts are due to innovations and technical progress. Changes in economic and urban planning conditions, population, economy, and transport development changed anthropogenic impact on the urban environment (Tarkhov 2010; Mukhamedzhanov 2011).

The relevance of studying environmental consequences of changes in the ecological situation of capital cities is preconditioned by the fact that the capitals are distinguished by the fastest rate of change in the quality of the urban environment – after the adoption of the capital status, the population in Nur-Sultan increased by 295% from 1997 to 2020; in Almaty, this indicator increased by 64%, which both, directly and indirectly, increases the anthropogenic load. The share of Almaty and Nur-Sultan in the total impact on atmospheric air of Kazakhstan in 1997–2020 was 2.3–4.0%, the total contribution of the two cities to the accumulation of municipal waste in Kazakhstan is 31% (for 2020) (Statistics agency…2021).

To identify and analyze these consequences, it is important to assess changes in the nature and structure of anthropogenic impact on the environmental components (air, water and soil). In addition to analyzing key factors, it is necessary to conduct a comprehensive assessment of the transformation of the environmental situation.

The purpose of the study was to identify and analyze the environmental consequences of the transfer of capital functions using the case of the Republic of Kazakhstan.

Current studies of the topic

Capitals are a specific class of cities (most often significant). They are the centers of life in general, economics, science, and accelerated technological progress (Gottman 1990; Lappo 1997; Hirschhausen 2001).

The transfer of the capital is a unique phenomenon in the history of post-Soviet states caused by specific reasons (Treivish 2009; Rachmawati 2021). Soon after the collapse of the USSR in 1997, Tselinograd received the official status of the capital and was renamed into Astana and then into Nur-Sultan (Akimat website… 2021).

The transfer of the capital was due to the influence of various factors (Aksenov 2006; Kovacs 1999). Because of the negative reasons, the following can be distinguished:

1. Natural and ecological factors

Almaty is located in a seismic hazard zone – in a mountainous area with tectonic faults and sometimes destructive mudflows. Also, the location in the foothill basin negatively affects the environment. Temperature inversion and city relief contribute to the excessive accumulation of pollutants within the city. These factors do not correspond to the environment required to perform the capital's functions. From the environmental point of view, these factors negatively affect the life quality of the city's population. On the other hand, Nur-Sultan is located on a plain, which contributes to the removal of emissions outside the city limits and, in general, improved self-cleaning potential of the atmosphere (Walter 2021).

2. Socio-economic and environmental

According to the former President of the Republic of Kazakhstan, the transfer of the capital was scheduled after gaining independence. First of all, this was due to the geopolitical position of Nur-Sultan (Astana), its crucial strategic location in the center of the Eurasian continent, which makes the new capital a geopolitically important and economically beneficial cultural and national communication, transport hub, and a specific transit bridge between Europe and Asia (Kaufmann 2018).

The population of Almaty is growing rapidly. This is the reason for several environmental problems: air pollution due to increased anthropogenic impact, increased pollution of water resources, soil cover, etc. Another acute problem in Almaty is the lack of territory for constructing residential buildings due to the constantly growing population. The city of Almaty is located in the foothills, limiting the city's expansion in space (Akhmetzhanova and Spanov 2001).

On the other hand, the location of Almaty in the south of Kazakhstan near the Chinese border can be attributed to foreign policy factors – the Almaty region borders on the Xinjiang Uygur Autonomous Region of China with an unabated national Uyghur independence movement (Smirnyagin 2011). Also, until 1998, the problem of joint borders between China and Kazakhstan and the problem of water shortage remained unresolved (Water resources…2021). In the event of a conflict, the southern borders of the republic remain vulnerable (Didko 2001).

The positive reasons mainly relate to the advantages of the new capital, Nur-Sultan. Positive reasons include the following (Rossman 2012):

1. Striving to consummate a regional ethnic-demographic balance, inspirational migration from labor-surplus southern regions to industrially developed northern cities, involving the Kazakh population in industrial and agricultural production in central and northern Kazakhstan. Five regions were disbanded, and the regions with the largest share of the Russian-speaking residents were unified with the regions with the largest share of the Kazakh population. By 2010, the number of residents in the capital exceeded 700 thousand people, most of whom were representatives of the titular nation – ethnic Kazakhs (65%). In 1989, Kazakhs made up only 18% of the city's population.

2. The transfer of the capital to the country's geographic center, along with administrative transformations, also contributed to strengthening the state's territorial integrity, attracting investment, accelerating economic recovery of the region and development of the infrastructure of the new capital (Bhavna 1999; Ghalib 2021).

3. The need for geopolitical use of the middle position of the republic between Europe and Asia and the possibility of overcoming the one-sided distribution of production forces across the state's territory (Raimov 1971; Shatz 1992).

MATERIALS AND METHODS

To assess the ecological situation in cities we used statistical, historical, comparative-descriptive, and linear scaling methods. They allowed calculating the complex ecological transformation index.

Urban environmental studies based on works of specialists, textbooks on geo-urban studies, encyclopedias of Almaty and Nur-Sultan, and capital studies by foreign political scientists and researchers.

The work used national statistical compilations, bulletin archives, Internet resources of the Committee on Statistics, comprehensive reports on the state of air quality in the cities of Nur-Sultan and Almaty, reports on the state of the environment by independent experts, yearbooks of the national meteorological service Kazhydromet; encyclopedic reference books and literary sources.

RESULTS AND DISCUSSION

Selection of priority components for a comprehensive index in the environmental impact of the capital cities transfer

The ecological consequences of the transfer of capital functions are expressed in the transformation of the environmental situation.

The transformation of the ecological situation is a complex and multidirectional process with both positive and negative tendencies. It represents a change in the parameters and consequences of the impact (factors), both anthropogenic and natural.

To study changes in the ecological situation, several groups of indicators can be distinguished. They are presented in Table 1. To calculate the complex index, the absolute and relative indicators of anthropogenic impact on the atmosphere, water sources, and the city's population, both a source of a negative impact and its recipient, were selected.

Absolute scores show the magnitude of the impact (Lawrence and Roderick 1997), while relative scores reflect the difference in effects relative to the population or city area.

The anthropogenic impact on the environment is described not only by the indicators presented in the table. In each block, it is impossible to analyze some important sources of pollution due to the lack of information data. This is because the regional statistical bulletins of Kazakhstan do not consider indicators such as emissions from mobile sources, water intake volumes, and amount of wastewater received without treatment. Also, we are lacking data on other types of pollution (noise, radiation, biological).

Methodology for calculating the complex index of the ecological situation transformation

To study the environmental consequences of the transfer of the capital from Almaty to Nur-Sultan using a complex index, it is

Table 1. Indicators of the ecological situation transformation

Index	Peculiarities	Index unit
A. Impact and air quality		
A1. Emission from stationary sources	All businesses in the city to varying degrees affect the atmospheric air, the most significant contribution of emissions from stationary sources is made by combined heat and power energy enterprises. Emissions are an absolute indicator that reflects the extent of pollution.	emission volumes (thousand tons/year)
A2. Air quality index (AQI)	AQI is a complex indicator that reflects how many times the total air pollution by five substances exceeds the permissible value.	The Air Quality Index is the sum of exceeding the permissible concentrations by the average annual concentrations based on measurement of particulate matter ($PM_{2.5}$ and PM_{10}), ozone (O_3), nitrogen dioxide (NO_2), sulfur dioxide (SO_2), and carbon monoxide (CO) emissions
A3. Level of motorization	With the development of road transport, the negative impact on the atmosphere increases. Emissions from mobile sources are «low», poorly dispersed due to building density combined with a small area of green space (Slashchev and Iskakov 2012). The use of the motorization growth indicator for comparing Nur-Sultan and Almaty is quite correct, since the area of the cities and the density of the street and road network are similar, and the indicator deals with an equal network density since vehicle emissions depend not only on traffic intensity, but also on the kind of transport (Abilov at al. 2021). The number of cars is a proxy indicator, it would be more correct to take into account vehicle emissions, but such data are not available for a significant part of the study period.	number of cars / 1000 inhabitants
B. Impact on water sources		
B1. Water consumption	The volume of water consumption is a relative indicator. It reflects the impact on water sources and characterizes the population's water supply (Sources of water supply… 2021). The total volume of all water consumption was taken into account.	thousand cubic meters / per 1 inhabitant
B2. Wastewater volume	Uncontrolled wastewater discharge reduces the self-cleaning capacity of water ecosystems and leads to the ecological disadvantages of the primary water sources of the cities. Wastewater volume is an absolute indicator.	thousand cubic meters / per 1 inhabitant
C. Waste management		
C1. Volumes of accumulation of toxic waste (TW) from industrial enterprises.	Annual volumes of incoming maintenance exceed the permissible accumulation rates. Large volumes of accumulated toxic waste from industrial plants require high storage safety. Incorrect disposal of TW can cause a severe impact on the environment, and if it enters the atmosphere in larger volumes, it can cause an environmental disaster.	tons
C2. Municipal solid waste (MSW) accumulation volumes	The increase in the volume of MSW leads to the problem of overloaded landfills and, accordingly, increases the number of unauthorized landfills. Spontaneous dumps harm the soil and cause organoleptic discomfort for residents living near the landfill.	tons
D. Population		
D1. Population	The population is an absolute indicator that reflects the scale of anthropogenic impact. This indicator indirectly or directly affects the level of water consumption, the formation of MSW, and the level of motorization.	thousand people
E. Green zones		
E1. Area of green space within the city limits	Changing the area of green spaces affects not only the ecological situation but also the comfort of living in the city.	% of green areas in the total area of the city

important to determine the time interval, with a corresponding single set of indicators that will help characterize the changes. The capital status was transferred in 1997; therefore, to reflect the change in the ecological situation in two cities, the period from 1988 to 2020 was chosen.

This period can be divided into three nominal periods:

1. Pre- transfer period – from 1988 to 1998,
2. Post-transfer period – from 1998 to 2008,
3. Current period – from 2008 to 2020.

The National Statistical Committee has mainly produced regional statistics since 2000. The website of the hydrometeorological service of the Republic of Kazakhstan provides an archive only since 2015. All the calculations are based on data (Environment in the countries… 2001–2020; Environmental protection….1989; National Air Quality…1997; Nur-Sultan industry website…2021; Statistics agency…2021; Ten years of the Commonwealth…. 2021).

Based on the available data of articles and studies in the field of city ecology and official statistics, which contains only some indicators of atmospheric air pollution, we built a comparative table with the following indicators:

Because the developed system of indicators for assessing changes in the ecological situation includes many indicators with different dimensions (Bityukova and Borovikov 2018), the data are normalized using the linear scaling formula (1):

$$A_i = \frac{x_i - x_{\min}}{x_{\max} - x_{\min}} \quad (1)$$

where *i* is an indicator;

X_i –the value of the indicator for the yth year;

X_{max} and X_{min} – maximum and minimum values of indicators in two cities; Ai – normalized indicator (indicator index).

The linear scaling method helps to display the values of each indicator in the range from *0* (at $X_i = X_{min}$) to 1 (at $X_i = X_{max}$), keeping all the proportions between the individual values.

Calculating the complex index of changes in an environmental situation when transferring capital functions from 1988 to 2020.

To normalize indicators of different dimensions, we applied a linear scaling formula. Each indicator was calculated for the period from 1988 to 2020. The results of data calculations are presented in Table 3.

In order to take into account all groups of indicators, the scores for each group are summed up. Differences are more accurately taken into account for individual indicators when summing up the dynamics of natural growth (decrease) in the complex index of changes in the ES, and each indicator is monitored within the boundaries of stable (reference) points (fig.1).

Table 2. Comparative characteristics of Almaty and Nur-Sultan by several indicators directly or indirectly affecting the ecological situation

Index	Year	Almaty	Nur-Sultan
Emissions from stationary sources (thousand tons)	1998	16.2	41.5
	2020	43.0	56.4
AQI	1998	9.8	1.3
	2020	7	7
Traffic flow (cars / 1,000 inhabitants)	1998	188	134
	2020	242	234
Population, thousand people	1998	1117	300.5
	2020	1802	1032
The area of green spaces within the city limits, ha	1998	4.414	2.903
	2020	2.612	4.186
City area located in an unfavorable ecological zone (%)	1998	50	10
	2020	80	50

Table 3. Normalization of indicators from 1988 to 2020 for Almaty and Nur-Sultan according to the linear scaling formula

		Index	Year	Almaty	Nur-Sultan
A	A1	Emissions from stationary sources	1988	0.44	1.00
			1998	0.03	0.37
			2008	0.00	0.40
			2020	0.40	0.60
	A2	AQI	1988	0.68	0.00
			1998	0.75	0.03
			2008	1.00	0.61
			2020	0.51	0.52

A	A3	Traffic flow	1988	0.62	0.00
			1998	0.44	0.20
			2008	1.00	0.65
			2020	0.67	0.64
B	B1	Water consumption	1988	0.32	0.00
			1998	0.54	0.34
			2008	0.81	0.78
			2020	1.00	0.94
	B2	Wastewater volume	1988	0.39	0.00
			1998	0.62	0.49
			2008	1.00	0.73
			2020	0.87	0.84
C	C1	Volumes of accumulation of toxic waste (TW) from industrial enterprises.	1988	0.89	0.00
			1998	1.00	0.19
			2008	0.48	0.24
			2020	0.51	0.32
	C2	Municipal solid waste (MSW) accumulation volumes	1988	0.54	0.28
			1998	0.65	0.49
			2008	0.76	0.71
			2020	1.00	0.94
D	D1	Population	1988	0.50	0.00
			1998	0.55	0.03
			2008	0.23	0.23
			2020	1.00	0.50
E	E1	The area of green spaces within the city limits	1988	0.43	0.61
			1998	0.49	0.92
			2008	0.00	0.61
			2020	1.00	0.55

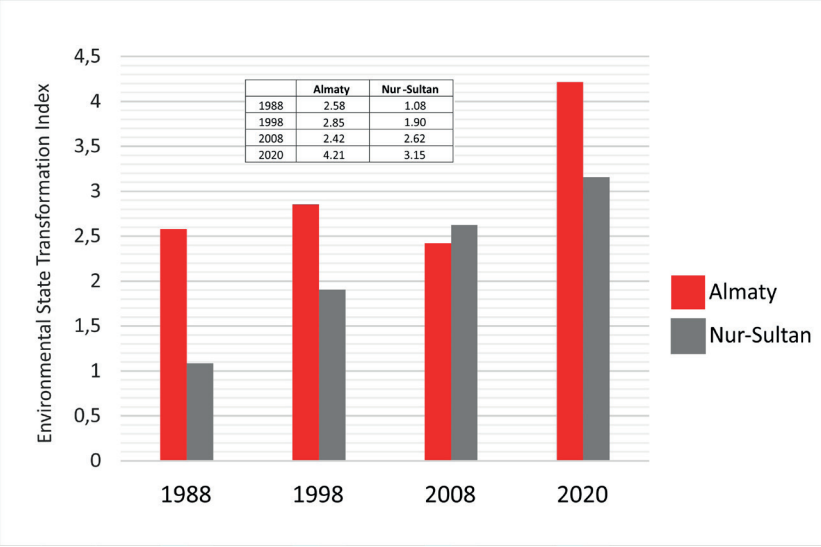

Fig. 1. Environmental State Transformation Index for three time periods: from 1988 to 1998, from 1998 to 2008, and from 2008 to 2020

This graph reveals some similarities and differences in the change in the ES of Almaty and Nur-Sultan:

1. In the period from 1988 to 1998, after the collapse of the USSR, the impact in two cities was decreasing. This is due to the restructuring of the economy and the closure of some industrial enterprises (Almaty cotton mill, Almaty house-building plant). In the first years of independence, in connection with the transition to a market economy and market relations, all sectors of the national economy were in crisis. As a result, in 1991-1996, production was significantly reduced. The reduction in production volume was: in the chemical and petrochemical industry - 71%, in light industry - 84%, in the woodworking industry - 76%, in mechanical engineering and metalworking - 64%, in construction - 82%, in electricity generation - 30%, ferrous metallurgy - 30%, non-ferrous metallurgy -28%, fuel production -40%. It was necessary to solve the following tasks: restructuring the economy, its reorientation to modern science-intensive technological industries; creating a socially oriented market (Toksambaeva and Bazarbaeva 2017). The transformation index in the former capital is 2.2 times higher than in Nur-Sultan.

During the Soviet period, Almaty was one of the largest industrial centers of Kazakhstan. A high employment rate increased the population and, accordingly, the level of motorization (Koldobskaya 2014).

The implications of the transfer of metropolitan functions are highlighted in the graph for the period from 1998 to 2008. The new capital is characterized by a sharp threefold deterioration in the ES; the reason for this is an increase in the impact on all four indicators, in particular, on AQI, which changed from 0.03 to 0.61.

The growth of the indicator in both cities is due to the development of the economy of Kazakhstan, an increase in investment flows, and, accordingly, an increase in the population. The ES has moderately deteriorated over the past 12 years (from 2008 to 2020) in both cities. The values of the transformation index in Alma-Ata and Nur-Sultan are associated with the deteriorating environmental situation in all respects. In Almaty, the largest contribution to the deterioration is made by an increase in the population, and in Nur-Sultan, due to the rise in the level of motorization and the volume of emissions from stationary sources of pollution.

Calculation of the complex transformation index of the ES from 2000 to 2020

Table 4 analyzes in more detail the environmental consequences of the transfer of the capital city presenting the complex index.

Official statistics on the impact on water sources and waste management have been taken into account only since 2000. Therefore, the study takes time intervals from 2000 to 2008 and 2008 to 2020.

After summing up the indicators by cities, we calculated the complex indices presented them in Figure 2:

Table 4. Normalization of indicators according to the linear scaling formula for Almaty and Nur-Sultan from 2000 to 2020

		Index	Year	Almaty	Nur-Sultan
A	A1	Emissions from stationary sources	2000	0.00	0.77
			2008	0.02	0.71
			2020	0.69	1.00
	A2	AQI	2000	0.75	0.00
			2008	1.00	0.58
			2020	0.49	0.48
	A3	Traffic flow	2000	0.28	0.00
			2008	1.00	0.61
			2020	0.65	0.61
B	B1	Water consumption	2000	1.00	0.26
			2008	0.94	0.09
			2020	0.23	0.00
	B2	Wastewater volume	2000	1.00	0.00
			2008	0.86	0.08
			2020	0.87	0.38
	B3	Total area equipped with a sewerage system	2000	1.00	0.94
			2008	0.88	0.39
			2020	0.10	0.00
C	C1	Accumulation of TW	2000	0.02	1.00
			2020	0.05	0.98
	C2	MSW accumulation	2008	1.00	0.00
			2020	0.99	0.79

D	D1	Population	2000	0.53	0.00
			2008	0.66	0.16
			2020	1.00	0.46
E	E1	Area of green space within the city limits	2000	0.45	0.85
			2008	0.28	0.78
			2020	1.00	1.25

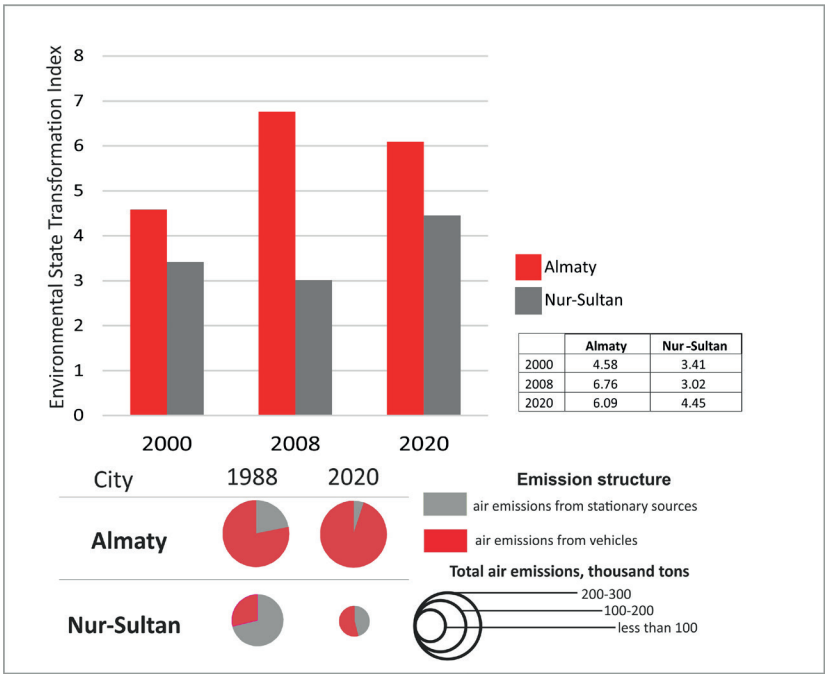

Fig. 2. Environmental State Transformation Index for three periods: from 1988 to 1998, from 1998 to 2008, and from 2008 to 2020

This graph shows the differences in the transformation of the ES:

1. In the period from 2000 to 2008 – the first decade after the transfer of capital functions there was a stabilization of the impact level, which is typical for the new capital (RK news portal, 2021). This is due to a decrease in the impact in Block B – indicators of effects on water sources and C – waste management. An increase in the area of the city equipped with a sewer network resulted in a wastewater decrease. For block C we note a decrease in MSW. The annual increase in the volume of municipal waste in the city exceeds the acceptable standards by an average of 125 kg/person per year; many spontaneous dumps are emerging (about 160 in 2020). However, we registered an increase in a set of atmosphere impact indicators. The transfer of the capital to Nur-Sultan accelerated the development of the infrastructure on the left bank with a new administrative center of the capital. This prompted the construction industry and transport infrastructure (New interchanges of Almaty 2021); respectively, the number of motor vehicles increased.

For the city of Almaty, the ES is deteriorating; this is due to an increase in indicators for each of the blocks, in particular, the population is growing, and the impact on the atmosphere is increasing, including the level of motorization and AQI.

2. From 2008 to 2020, the ES transformation index in two cities is changing.

For the city of Nur-Sultan, we registered an increased impact on the atmosphere and the growing pollutant emissions. A feature of Nur-Sultan and Almaty is the preservation and sometimes the development of low-rise buildings. Moreover, Almaty is largely gas-fueled, whereas Nur-Sultan is coal-fueled. Moreover, in Nur-Sultan, there are quarters of old buildings left from Tselinograd, summer cottages, which are quickly demolished, there are new cottage quarters, which are also demolished. In Nur-Sultan these quarters undergo significant transformations, whereas in Almaty, they are quite stable. In 2017 population reached 1 million inhabitants, and the volume of MSW generation increased accordingly. In terms of the number of cars per person, the new capital has caught up with Almaty. At the same time, the impact on water sources decreases, which is associated with a reduction in water consumption due to the introduction of water metering devices, and the area of the territory, which is equipped with a sewer network, also increases.

For Almaty, we registered a slight decrease in the composite index by 0.4. This is also mainly due to a reduction of the impact on water sources: the level of water consumption is decreasing, the area equipped with a sewerage system is increasing. The population has increased significantly (by 36% compared to 2008). The level of MSW accumulation increased accordingly. At the same time, the population's motorization level has changed insignificantly, and the AQI has decreased.

CONCLUSIONS

The ecological consequences of the transfer of the capital city are qualitative and quantitative changes in the factors, components, and interaction of anthropogenic influence and the self-cleaning potential of the environment. Together with the physical and geographical

factors of the formation of the ES in Almaty and Nur-Sultan, these consequences have a multidirectional nature and their characteristics. With the acquisition of the independence of Kazakhstan, the capital status was transferred to the city of Nur-Sultan. Urbanization of the new capital is accelerating. The redirection of migration flows has sharply increased the population of Nur-Sultan and slowed down the rate of population growth in the old capital from 1999 to 2001. During this period, the migration growth of the population of Almaty is 35% lower than the city of Nur-Sultan.

On the analysis of the complex index of the ecological situation transformation and the peculiarities of the development of the two capitals of Kazakhstan from 1988 to 2020 allowed for the following conclusions:

1. The Almaty city has many inherited factors of influence: the city's population already in 1998 was more than 1 million, the presence of industrial enterprises left after the collapse of the USSR. Almaty, due to the lack of opportunities for spatial expansion due to the city's location in the foothill basin and an increase in the population and traffic flow, has seen a moderate deterioration in the environmental situation.

2. Nur-Sultan underwent a sharp change in the environmental situation due to an increase in the population and the level of motorization.

The ecological situation of the two cities in 2020 is almost equivalent, but the ES transformation index does not reach the level of Almaty due to the higher self-cleaning potential of the city and a newer and, accordingly, more environmentally friendly traffic fleet.

3. Over the past 20 years the two cities registered a positive trend in the impact on water sources: in Almaty water consumption decreased by 45% and in Nur-Sultan it decreased by 27%. Modernization of plumbing and sewerage systems can reduce water leaks and improve wastewater transport to wastewater treatment plants.

4. From 1998 to 2020 the environmental situation in Nur-Sultan changed much faster than in Almaty due to the low base effect and the transfer of capital functions if emissions from motor transport are not resolved. The transformation index of the former capital is 2.2 times higher than in Nur-Sultan.

5. Nur-Sultan will increase its impact on the Akmola region due to the development of the agglomeration, pollution from motor transport will increase every year, but t the environmental situation will not reach the level of Almaty due to the higher self-cleaning potential of the city and a newer and, accordingly, more environmentally friendly transport infrastructure. In addition, Almaty is an established million-plus city, and its planning structure was formed in previous years with a view to a significantly lower level of motorization, while Nur-Sultan is an actively developing and expanding city with modern and future needs.

However, for both cities, it can be concluded that by 2020 the environmental situation has been deteriorating much faster than it improved after the collapse of the USSR.

REFERENCES

Abilov A., Anzorova M., Bityukova V., Makhrova A., Khojikov A. and Yaskevich V. (2021). Planning structure as a road traffic pollution differentiation factor: a case study of Nur-Sultan. Geography, Environment, Sustainability, 14(3), 6–13.

Akhmetzhanova G. and Spanov M. (2001). From Beijing to Astana: the history of the transfer of capitals. Astana: Institute of Development of Kazakhstan, 204. (in Russian).

Akimat website of Nur-Sultan city. Available at: www.akorda.kz/ru/legal_acts/decrees/ob-izmenenii-granic-goroda-astany [Accessed 13 June 2021].

Aksenov K, Brade I., and Bondarchuk E. (2006). Transformational and post-transformational urban space of Leningrad: SPb: Helikon Plus, 184 (in Russian with English summary).

Bityukova V. and Borovikov M. (2018). Transformation of environmental conditions in large former soviet countries: a regional analysis. IOP Conference Series: Earth and Environmental Science, 012051 (1)–012051.

Bhavna D. (1999). Kazakhstan. Ethnicity, language, and power, 283.

Didko E. (2001). Migration in Kazakhstan at the turn of the XXI century: main trends and prospects Alma-Ata, 42–48.

Environment in the countries of the Commonwealth of Independent States for 2001, 2006, 2012,2018 Moscow: Interstate Statistical Committee of the CIS, 2013, 2018, 2020.

Environmental protection and rational use of natural resources in the USSR (1989). Moscow, State Committee of the USSR on Statistics, Finance, and Statistics. 175. (in Russian).

Ghalib H., El-Khorazaty M. and Serag Ye. (2021). New capital cities as tools of development and nation-building: Review of Astana and Egypt's new administrative capital city. Ain Shams Engineering Journal, 12(3), 3405-3409.

Gottman J. (1990). Capital Cities. Since Megalopolis. The Urban Writings of Jean Gottman. Baltimore: Johns Hopkins Press, Ch. 3, 63–82.

Hirschhausen C. von. (2001). The Process and the End of Systemic Transformation – A Survey of Central/Eastern Europe and the former Soviet Union in the 1990s. Tagung der Deutschen Gesellschaft fur Osteuropakunde, Fachgruppe Wirtschaftswissenschaften. – Berlin: German Institute for Economic Research.

Kaufmann D, and Tobias A. (2018). Strategies of Cities in Globalized Interurban Competition: The Locational Policies Framework. Urban Studies, 55(12), 2703-2720.

Koldobskaya N. (2014). Research of transformation of the environmental situation with the help of integral indexes and rating (on the example of the capitals of post-Soviet countries). Regional study, 3 (45), 84–91. (in Russian with English summary).

Kovacs Z. (1999). Cities from the state–socialism to global capitalism: GeoJournal, 1–6.

Lappo G. (1997). Geography of cities. Moscow, Vlados, 480. (in Russian).

Lawrence I. and Roderick J. (1997). Better Understanding our Cities: the role of urban indicators, 94.

Mukhamedzhanov A. (2011). Comparative analysis of the impact of road transport on the environmental situation in Astana and Almaty. Environmental problems and sustainable development of the Republic of Kazakhstan, research of students, undergraduates, and graduates. Astana: Kazakhstan Branch of Lomonosov Moscow State University, 47–57. (in Russian).

National Air Quality and Emissions Trends Report (1997). U.S. EPA, 198.

New interchanges of Almaty. Official Internet resource of the city of Almaty. Available at http://almaty.gov.kz/page.php/admin/upload/images/images/page.php?page_id=9&lang=1&news_id=12353 [Accessed 12 July 2021].

Nur-Sultan industry website. Available at: www.astana2050.kz/ru/predpriyatiya-astany/mashinostroenie-astany. [Accessed 13 June 2021].

Rachmawati R., Haryono E., Ghiffari R., Reinhart H., Permatasari F. and Rohmah A. (2021). Best Practices of Capital City Relocation in Various Countries: Literature Review. E3S Web of Conferences. 325.

Raimov T. (1971). Capitals as an object of economic and geographical research., 32. (in Russian).

RK news portal. Available at: www.google.kz/amp/s/tengrinews.kz/kazakhstan_news/226-dney-otopitelnyiy-sezon-zavershilsya-v-astane-343946/amp/ [Accessed 12 June 2021].

Rossman V. (2012). Capital Cities. Their diversity, patterns of development, and movement. Moscow: Gaidar Publishing House, 352. (in Russian).

Shatz R. (1992). Path dependence and privatization strategies in East-Central Europe // East European Politics and Societies, 4, 351–392.

Slashchev V.and Iskakov U. (2012). Eco structures of Kazakhstan. Alma-Ata: Rauan, 295. (in Russian).

Smirnyagin L.V. (2011). Zoning of society: methods and algorithms. Social geography: diversity and unity. Moscow-Smolensk, 55–82. (in Russian).

Sources of water supply in Almaty. Available at: https://365info.kz/2015/04/voda-v-almaty-odna-iz-luchshix-v-kazaxstane-ekspert-almatysu [Accessed 12 June 2021].

Statistics agency of the Republic of Kazakhstan. Available at: http://www.stat.kz [Accessed 18 June 2021].

Tarkhov S. (2010). Transport and geographical position of the capital cities. Geography of world development. Ed. 2. Collection of scientific papers. Moscow, IG RAS, 2010, 207–227. (in Russian).

Ten Years of the Commonwealth of Independent States (1991–2000): Statistical collection, Moscow, Interstate Statistical Committee of the CIS, 2001, 800.

Toksambaeva A. and Bazarbaeva L. (2017). Economic development of Kazakhstan over the years of independence. Issues of Economics and Management, 1 (8), 62–64. (in Russian with English summary).

Treivish A. (2009). City, region, country, and world. Moscow: New chronograph, 372 (in Russian).

Walter T. (2021). Urban Greening for New Capital Cities. A Meta Review. Frontiers in Sustainable Cities. 3, 1-12

Water resources of Almaty. Available at: https://almatysu.kz/?page_id=542&lang=ru. [Accessed 19 June 2021].

Zimmerman H. (2010). Do Different Types of capital cities make a difference for economic dynamism? Environment and Planning. Government and Policy, 28, 761–767.

ges.rgo.ru/jour/

ISSN 2542-1565 (Online)